DNA methylation and histone modification dynamics in neurons in aging and Alzheimer's disease

by

Andrew James Phipps

B.MedRes & Biotech (Hons)

Wicking Dementia Research and Education Centre

College of Health and Medicine

Submitted in fulfilment of the requirements for the Degree Doctor of Philosophy

(Medical Sciences)

University of Tasmania

February, 2019

Copyright Statement

This thesis contains no material which has been accepted for a degree or diploma by the University or any other institution, except by way of background information duly acknowledged in the thesis, and to the best of my knowledge and belief no material previously published or written by another person except where due acknowledgement is made in the text of the thesis, nor does the thesis contain any material that infringes copyright.

Andrew James Phipps

21/2/2019

Statement of Authority of Access

The publishers of the papers comprising Chapter 3 hold the copyright for that content, and access to the material should be sought from the respective journal. The remaining content of this thesis may be made available for loan and limited copying in accordance with the *Copyright Act 1968*.

Andrew James Phipps

21/2/2019

Statement of Co-Authorship

The following people and institutions contributed to the publication of work undertaken as part of this thesis:

Candidate -- Andrew James Phipps, Wicking Dementia Research and Education Centre
Author 1 -- Andrew James Phipps, Wicking Dementia Research and Education Centre
Author 2 -- James C. Vickers, Wicking Dementia Research and Education Centre, University of Tasmania
Author 3 -- Phillippa C. Taberlay, College of Health and Medicine, University of Tasmania
Author 4 -- Adele Woodhouse, Wicking Dementia Research and Education Centre, University of Tasmania

Contribution of work by co-authors for each paper:

Publication entitled: Neurofilament-labelled pyramidal neurons and astrocytes are deficient in DNA methylation marks in Alzheimer's disease - Located in Chapter 3

Andrew J. Phipps, James C. Vickers, Phillippa C. Taberlay, Adele Woodhouse, (2016). Neurofilament-labeled pyramidal neurons and astrocytes are deficient in DNA methylation marks in Alzheimer's disease. *Neurobiology of Aging,* 45, 30-42. DOI: 10.1016/j.neurobiolaging.2016.05.003.

Author contributions:
Candidate/Author 1 was the primary author and performed all experiments and analysis, contributed to data interpretation and performed the manuscript preparation (85%). Author 2 contributed to data interpretation and manuscript editing (5%). Authors 3 (5%) and 4 (5%) developed experimental rationale and design and aided with data interpretation and editing of the manuscript.

We the undersigned agree with the above stated "proportion of work undertaken" for each of the above published (or submitted) peer-reviewed manuscripts contributing to this thesis:

We, the undersigned, endorse the above stated contribution of work undertaken for each of the published (or submitted) peer-reviewed manuscripts contributing to this thesis:

Signed:	_____	_____	_____
	Andrew James Phipps Candidate Wicking Dementia Research and Education Centre, College of Health and Medicine University of Tasmania	Dr Adele Woodhouse Primary Supervisor Wicking Dementia Research and Education Centre, College of Health and Medicine University of Tasmania	Prof Ben Canny Head of School College of Health and Medicine University of Tasmania
Date:	13/02/2019	13/02/2019	21/02/2019

Statement of ethical conduct

The research associated with this thesis abides by the international and Australian codes on human and animal experimentation, the guidelines by the Australian Government's Office of the Gene Technology Regulator and the rulings of the Safety, Ethics and Institutional Biosafety Committees of the University of Tasmania.

Andrew James Phipps

21/2/2019

Abstract

The epigenome dynamically regulates chromatin structure to control cellular function and homeostasis in a highly specific fashion and mediates the complex interaction between the DNA and our environment. Epigenetic mechanisms such as DNA methylation and post-translational histone modifications contribute to the maintenance of cellular structure, identity, and plasticity in a cell type specific manner. Despite the key role epigenetics has in the regulation of the genome, there have been relatively few studies that have characterised the epigenome in neurons, neither in the healthy aging brain nor in neurodegenerative disease. Alzheimer's disease (AD) is a terminal progressive neurodegenerative disorder. While familial mutations account for approximately 10% of cases, the cause of 90% of AD cases is unknown. In the absence of highly penetrant risk alleles, epigenetics is well poised to contribute to the pathogenesis and progression of AD, but this role is yet to be fully explored. The research in this thesis has characterised DNA methylation in post-mortem human AD brains in a cell type specific manner, and is the first to characterise key histone modifications in neurons across a time-course of healthy aging, and across a time-course in a model of AD.

Firstly, global DNA methylation (5mC) and hydroxymethylation (5hmC) levels were assessed in neuronal and glial cell types in the inferior temporal gyrus of human AD cases and age-matched controls. Neurofilament (NF)-labelled pyramidal neurons, known to be vulnerable to AD pathology were deficient in extranuclear 5mC in AD cases compared to controls. This work also demonstrated that fewer astrocytes exhibited nuclear 5mC and 5hmC marks in AD cases compared to controls. However, there were no alterations in global levels of 5mC and 5hmC in disease-resistant calretinin-interneurons or microglia in AD. Furthermore, no alteration in the density of 5mC or 5hmC labelled nuclei was detected in near-plaque versus plaque-free regions in late-AD cases. 5mC and 5hmC were present in a high proportion of neurofibrillary tangles, suggesting no loss of DNA methylation marks in tangle bearing neurons. This demonstrated that global epigenetic dysregulation may be occurring in astrocytes and NF-positive pyramidal neurons in AD.

Histone modifications aid in the regulation and compaction of DNA into chromatin. The second part of this PhD study was the first to characterise H3K27ac and H3K4me3 markers of active enhancer and promoter elements, using chromatin immunoprecipitation and next-generation sequencing (ChIP-seq) in neurons from the forebrain of C57/BL6 mice at 3, 6, 12, and 24 months of age (n=5 per genotype). H3K27ac marking was enriched in young neurons

at 3 months of age and old neurons at 24 months of age at a range of genomic regulatory regions including promoters proximal to transcriptional start sites, CpG islands around transcriptional start sites, enhancers distal to transcriptional start sites, and at known cortical super enhancers. H3K4me3 was also enriched at promoters in neurons at 3, 12, and 24 months of age, and at enhancers at 3 months of age. Gene ontology analysis predicted that H3K27ac and H3K4me3 aid in the regulation of neuronal processes including synaptic plasticity, ion channel binding, transporter activity, calcium channel activity and cellular metabolic processes. These data also point towards a partial recapitulation of a juvenile-like epigenetic state in late aging and demonstrate the dynamic nature of the histone landscape in neurons in the aging brain.

APP/PS1 AD mice closely recapitulate the pathology present in human early-AD cases, including beta-amyloid plaque deposition, neuritic dystrophy and plaque-associated synapse loss. APP/PS1 mice allow for the examination of the earliest pre-pathology epigenetic changes that occur in AD, as well as measurement across a time course of disease progression. The third part of this PhD thesis used neuronal nuclei from the forebrain of APP/PS1 mice and age-matched wild-type control mice (n=5 per genotype) at 3, 6 and 12 months of age that were subject to ChIP-seq using antibodies detecting H3K27ac and H3K4me3. These data identified enrichment of H3K27ac marking at the transcriptional start site and at cortical super enhancers, but depletion from enhancers, in neurons prior to pathology onset in APP/PS1 mice. H3K4me3 marking was also enriched at the transcriptional start site in neurons prior to pathology onset, and in pathology rich cases in APP/PS1 mice. Gene ontology analysis predicted that key neuronal specific pathways were disrupted early in AD. These included pathways involved in synaptic plasticity, membrane depolarisation and protein localisation, as well as pathways involved in cellular maintenance. Both H3K27ac and H3K4me3 marking evolved over time in APP/PS1 neurons. In addition, these data point towards a partial recapitulation of a juvenile-like epigenetic state epigenome in pathology rich neurons, with numerous H3K27ac and H3K4me3 marked sites shared between 3 and 12 months of age and the results have also identified several novel genes and pathways yet to be investigated in AD.

In summary, the data presented here show the complex nature of the neuronal epigenome and its dynamic response to neuropathology. The neuronal epigenome undergoes dramatic change in early adulthood and undergoes a partial recapitulation of a juvenile-like epigenetic state in late aging. The epigenome undergoes cell-type specific global loss of DNA methylation, occurring in both NF+ pyramidal neurons and astrocytes in AD. Furthermore, the neuronal epigenome is dysregulated prior to pathology onset in AD mice, and major restructuring of the

histone landscape occurs with dense AD pathology. Taken together, the data presented within this thesis demonstrate the evolution of the neuronal epigenome in aging, and dysregulation of both DNA methylation and histone modifications in AD.

Acknowledgements

I would first and foremost like to thank my supervisors Dr Adele Woodhouse, Dr Phillippa Taberlay and Prof James Vickers for their patience, enthusiasm, generosity, support, guidance and friendship throughout my PhD. I could not have completed this journey without their support, and I am forever grateful for their guidance through my PhD.

Thank you to Mr Graeme McCormack and Mr Justin Dittmann for their technical support and guidance while I was optimising the many protocols for this project. A special thanks to Dr Terry Pinfold from the University of Tasmania and Dr Kate Giles, Dr Eric Lam and Mr Rob Salomon from the Garvan Institute of Medical Research for their support with flow cytometry, and for being welcoming and accommodating during my time at Garvan. I would also like to thank the animal care staff and the CFF for their assistance with animal work. Thanks also to Mr Aidan Bindoff, Professor Michael Charleston and Prof Mark Robinson for their assistance with bioinformatics and programming while I jumped head first into the analysis of ChIP-seq data.

To the members of the Wicking Dementia Research and Education Centre, you have all become like a second family to me and provided so much encouragement and friendship throughout this journey and made it truly enjoyable. I have learnt so much from all of you. I would also like to show my utmost appreciation to all my friends and family for their continued support, love, patience and friendship throughout the highs and lows of my PhD.

Finally, this project could not have happened without the funding and support from the JO and JR Wicking Trust (Equity Trustees), Dementia Australia Research Foundation, Yulgilbar Foundation, and the Judith Jane Mason & Harold Stannett Williams Memorial Foundation (ANZ Masons).

Contents

Common Abbreviations

AD	Alzheimer's disease
APP	Amyloid protein precursor
ApoE	Apoliopoprotein E
Aβ	Amyloid beta
BACE	Beta secretase
CBP	Calcium binding protein
CpG	Cytosine guanine dinucleotides
CrBP	Creb binding protein
CREB	Cyclic-AMP response binding protein
DN	Dystrophic neurite
DNA	Deoxyribonucleic acid
DNMT	DNA methyltransferase
EGR1	Early-growth-response protein 1
FACS	Fluorescence activated cell sorting
IBA1	Ionised calcium-binding adapter 1
LOAD	Late-onset AD
LTD	Long-term depression
LTP	long-term potentiation
MAPT	Microtubule associated protein tau
MCI	Mild cognitive impairment
MFG	Middle frontal gyrus
MTG	Middle temporal gyrus
NF+	Neurofilament positive
NeuN	Neuronal nuclei antibody
NFT	Neurofibrillary tangle
NT	Neuropil threads
NMDA	N-methyl-D-aspartate
PS1	Presenilin 1
PS2	Presenilin 2
TET	Ten eleven translocase
5mC	5-methylcytosine
5hmC	5-hydroxymethylcytosine

Chapter 1: Introduction

Introduction

1.1 Dementia and Alzheimer's disease

Dementia is a syndrome that covers a range of neurological disorders, including frontotemporal lobar dementia, dementia with Lewy bodies and Alzheimer's disease. These disorders manifest as progressive cognitive decline and memory loss. Since its discovery by Alois Alzheimer in 1906, Alzheimer's disease (AD) has been identified as the most common form of dementia, accounting for more than 70% of all dementias, with an estimated 46.8 million people living with dementia globally (Alzheimer's Disease International, 2015). Alzheimer's disease is a terminal, progressive, neurodegenerative disorder, that represents a large financial and socioeconomic burden, with dementia expenditure in Australia increasing to an estimated $14.67 billion per annum in 2017 (Brown, Hansnata, & La, 2017).

Although AD develops and progresses differently in each person living with dementia, there are general similarities that can be used for diagnosis of the disease. Common clinical symptoms for AD include cognitive impairment, memory loss, changes to emotion, and changes in sensory perception (Förstl & Kurz, 1999), each reflecting underlying pathological changes in the brain. The pathological hallmarks of AD include extracellular beta-amyloid plaques (Aβ), intraneuronal neurofibrillary tangles (NFTs) of microtubule associated protein tau, aberrant neuronal processes of neurofilaments, scaffolding or signalling proteins termed dystrophic neurites (DNs), and neuropil threads (NTs), which are aggregates of tau and ubiquitin (Braak & Braak, 1991; G. Perry et al., 1991) (Figure 1.1). Widespread cortical atrophy, neuronal and synaptic loss are also observed in late-stage AD cases (Braak & Braak, 1991; Brun & Englund, 1981; P. R. Hof, Cox, & Morrison, 1990; L. F. Lue, Brachova, Civin, & Rogers, 1996; Mitew, Kirkcaldie, Dickson, & Vickers, 2013b; Terry et al., 1991). There are a number of familial, dominantly inherited genetic alleles that contribute to the early onset of AD (EOAD), which leads to clinical symptoms prior to 65 years of age and a more aggressive phenotype when compared with late-onset AD (LOAD) (Chartier-Harlin et al., 1991; van Duijn et al., 1994). The key pathological features of AD consist of accumulations of abnormal insoluble protein aggregates within the brain, however, the driving mechanisms for disease onset and progression remains elusive.

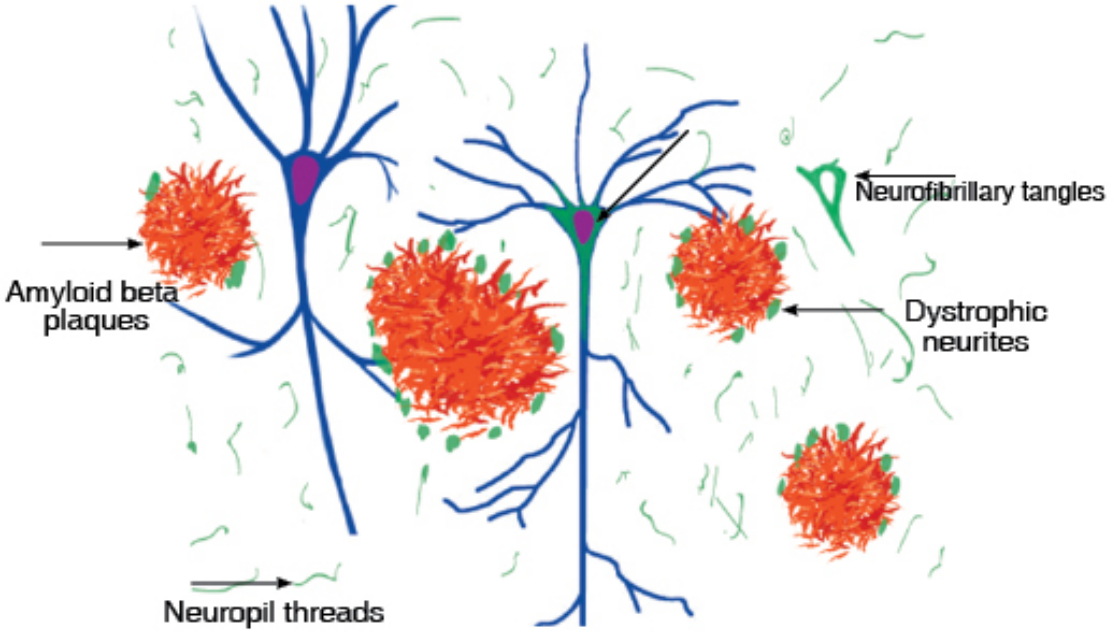

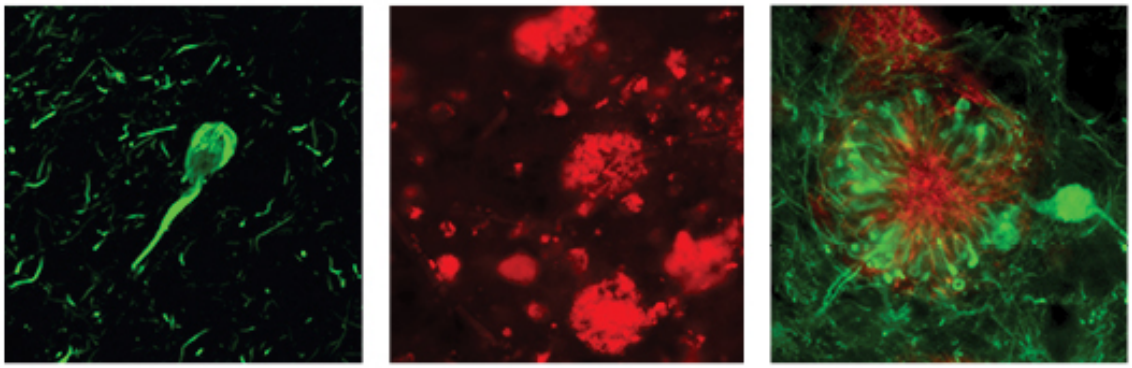

Neurofibrillary tangles | Amyloid beta plaques | Dystrophic neurites

Figure 1.1: Common Alzheimer's disease pathology

Schematic of the pathology characteristic of AD. Extracellular Aβ plaques (orange), intracellular NFTs (green) in excitatory neurons (blue). Tau and ubiquitin pathology accumulate in the extracellular space as dystrophic neurites (green around plaques) proximal to Aβ plaques, and neuropil threads. Insoluble NFT pathology persists as ghost tangles (green, hollow) after the neuron has deteriorated, some of which are engulfed by astrocytes. Images depicting neurofibrillary tangles (left, green), Aβ plaques (middle, red), and dystrophic neurites surrounding Aβ plaques (right, green).

1.2 Beta amyloid production, processing & the 'amyloid cascade hypothesis'

The major constituent of the insoluble protein aggregates in AD is from the amyloid beta (Aβ) protein. Aβ is formed as a product from the processing and cleavage of the amyloid precursor protein (APP), which is a membrane bound protein with roles in neuronal survival, neurite outgrowth and in signal transduction (review: (Dawkins & Small, 2014)). Proteolytic cleavage of APP is accomplished by two pathways: APP is cleaved by α-secretase and γ-secretase complexes, generating sAPPα and P3 fragment. Amyloid precursor protein can also be cleaved by β-secretase (BACE) in the extracellular domain (n terminus) generating sAPPβ (Vassar et al., 1999). The sAPPβ fragment is then cleaved by the γ-secretase complex to generate Aβ 1-40 and 1-42, which are prone to aggregation and lead to the formation of plaques (review: (Rajendran & Annaert, 2012; Thinakaran & Koo, 2008)). Early onset AD (EOAD) is associated with mutations in the presenilin protein genes (*PS1, PS2*) and *APP* genes; highly penetrant autosomal dominant mutations which lead to increased generation of Aβ 1-40 and 1-42 and contribute to plaque accumulation in AD (review:(Czech, Tremp, & Pradier, 2000)). These mutations form the basis of many *in vivo* models of AD (De Strooper et al., 1998; Scheuner et al., 1996). Increased Aβ 1-40 and 1-42 also lead to a rise of soluble, oligomeric Aβ within the brain (James P. Cleary et al., 2004; C. A. McLean et al., 1999). Studies have implicated oligomeric Aβ to cause much of the toxicity and synaptic loss seen in AD, rather than fibrillar plaques (James P Cleary et al., 2005; Koffie et al., 2009a; C. A. McLean et al., 1999). Dystrophic neurites (DN) are another common pathology formed from inclusions of neurofilament processes, APP, ubiquitin, and tau, and can aggregate to form neuritic plaques (Tracey C. Dickson, King, McCormack, & Vickers, 1999; Mitew et al., 2013b; J. C. Vickers et al., 1996; Adele Woodhouse, James C. Vickers, Paul A. Adlard, & Tracey C. Dickson, 2009).

The 'amyloid cascade hypothesis' posits that the accumulation of Aβ acts as the driving mechanism for AD onset and progression, likely through an imbalance between Aβ production and clearance, with intracellular changes in tau, neuronal loss and vascular damage occurring as a secondary consequence (J. A. Hardy & Higgins, 1992). The clearest evidence in support of the amyloid cascade hypothesis is that genetic mutations in genes associated with EOAD are all involved in APP processing, including APP (Citron et al., 1992; Goate et al., 1991), S182/PS1 (Sherrington et al., 1995), PS2 (Levy-Lahad et al., 1995), and the ApoE ε4 mutation (Strittmatter et al., 1993), all of which have been established as autosomal dominant risk factors for AD (review: (Czech et al., 2000)). Indeed, some studies have identified stronger correlations between Aβ peptides (including soluble $A\beta_{40,42}$) cognitive decline, and synaptic

alterations, rather than Aβ deposits (L.-F. Lue et al., 1999; Näslund, Haroutunian, Mohs, & et al., 2000) (review:(Selkoe, 2008)). While it has also been shown that mutations in *APP* are protective against AD (Jonsson et al., 2012). Neuritic plaque load has also been shown to be associated with the severity of cognitive impairments in AD (Cummings & Cotman, 1995). Strong support for the amyloid cascade hypothesis is also present within Down syndrome. The genetic basis of Down syndrome is trisomy of chromosome 21, which is the chromosome containing the *APP* gene (Kang et al., 1987; St George-Hyslop et al., 1987). Subsequent over-expression of proteins on chromosome 21 results in accumulation of Aβ pathology consistent between AD and Down syndrome (Masters et al., 1985). While the Aβ hypothesis provides a strong framework for the onset and progression of AD there are several concerns worth noting, including that Aβ deposits do not correlate with the rate of cognitive decline (Berg, McKeel, Jr, Miller, & et al., 1998). Amyloid beta plaques have also been observed in patients with no cognitive impairment (Crystal et al., 1988), though this may be due to individuals having a higher cognitive reserve (review: (J. Hardy, 2002)). In the absence of Aβ driving disease pathogenesis, studies have developed an alternative hypothesis of tau driving AD based neurodegeneration.

1.3 Tau hypothesis and Neurofibrillary Tangles

The tau hypothesis stipulates that mutations altering the composition or function of tau lead to abnormal phosphorylation of the protein. The key component of the NFT aggregates observed in AD is paired helical filaments of hyperphosphorylated tau, usually present in the soma of some subsets of excitatory neurons (Grundke-Iqbal et al., 1986). The protein accumulation and cellular dysfunction leads to the development of Aβ plaques as a downstream consequence. Tau is a microtubule-associated protein that is well established in the development and stability of microtubules (Cleveland, Hwo, & Kirschner, 1977; Weingarten, Lockwood, Hwo, & Kirschner, 1975). The microtubule-associated protein tau (MAPT) gene is alternatively spliced to form tissue and cell-type specific isoforms (Goedert, Spillantini, Jakes, Rutherford, & Crowther, 1989). Studies have identified loss of tau to increase Aβ autophagy and deposition *in vivo* (Lonskaya, Hebron, Chen, Schachter, & Moussa, 2014). While other studies have shown a reduction in tau improves cognitive outcome in APP expressing mice with a Aβ burden, and reduces excitotoxicity in those models (Roberson et al., 2007). Studies have shown tau accumulation and NFTs to correlate with progressive cognitive decline in AD (Arriagada,

Growdon, Hedley-Whyte, & Hyman, 1992; Berg et al., 1998; M. E. Murray et al., 2015). Recently, positron-emission tomography imaging of tau in human temporal lobe correlated with cognitive decline and AD severity (Brier et al., 2016).

Tau-mediated neurodegeneration in AD has been hypothesised to occur because of either a toxic gain-of-function, or because of a loss of normal function of the tau protein, leading to cell loss and subsequent clinical symptoms. Hyperphosphorylation of tau leads to tau aggregating in the form of NFTs. Neurofibrillary tangles prevent the normal transport of vesicles, leading to a toxic loss of function and detachment of tau molecules from microtubules. This causes an overall compromise of normal axonal transport (review:(Ballatore, Lee, & Trojanowski, 2007)). Despite progress in detection of AD and longitudinal studies of disease progression, correlations between amyloidosis, tauopathies and AD clinical symptoms are contradictory and the underlying cascade of events that leads to AD onset and subsequent neurodegeneration remain unknown (Berg et al., 1998).

1.4 Neuropathological stages of Alzheimer's disease

Extracellular Aβ plaques and intraneuronal NFTs accumulate throughout AD progression and can be characterised into several stages (Braak & Braak, 1991). The most widely accepted classification has been produced by Braak & Braak (1991), who characterised plaque and NFT formation in post-mortem AD tissue (Braak & Braak, 1991). Braak & Braak (1991) detected inter-individual differences in plaque formation and distribution that were highly variable, but could be characterised into three stages as follows: In the first stage (A) low density Aβ deposits are present in basal areas of the frontal, temporal and occipital cortices, with some deposition in the presubiculum and entorhinal cortex, however no Aβ deposits are present in the hippocampus. In stage (B), there is an increased density of Aβ in the neocortex, with mild deposition in the hippocampal formation and relatively little involvement of the of primary sensory and motor cortex. Aβ deposition accumulates in cortical layers V and VI of in the basal parts of the frontal, temporal and occipital cortical regions, while layers II/III contain fewer plaques than V and VI but feature more densely packed cores. In the final, and most severe stage (C) neocortical areas exhibit dense packed Aβ with moderate amyloid deposition of primary neocortical areas, that are mainly localised in layer II, III and V (Braak & Braak, 1991). Another major study has utilised positron-emission tomography to confirm amyloid deposition through AD progression in living participants, confirming Aβ progression to start in the

temporobasal cortices, then spreading through association areas of the neocortex, and finally through primary sensory, motor cortex and medial temporal lobe and striatum (Grothe et al., 2017). The hippocampus contains limited amyloid pathology early in disease (stage A), but has limited Aβ accumulations by stage B, and is fully involved by stage C. Striatum and other subcortical structures gradually accumulate Aβ pathology, however substantia nigra and pars compacta rarely show Aβ deposits.

Braak & Braak (1991) were also able to produce a pathological classification of AD based on intracellular NFT pathology, and six stages were established for classification: Stage I: Very few NFTs are detected in cortical areas, with only limited accumulations in excitatory projection neurons in regions between the entorhinal cortex and the temporal cortex (termed 'trans-entorhinal cortex') (Braak & Braak, 1985, 1991). Stage II: The trans-entorhinal cortex exhibits numerous NFTs. NFTs begin to accumulate in the CA1 hippocampal sub-region. Stage III: NFTs progress through the entorhinal cortex, with numerous dendrites containing NTs. Few NFTs are present in the basal frontal, temporal and occipital cortex in layers II/III and V. Ghost NFTs are present in the trans-entorhinal region. Stage IV: NFTs are widely dispersed throughout the CA1 region of the hippocampus, while still only having mild isocortical involvement. Stage V: Ghost tangles can be found in pre-α projection neurons, and numerous NFTs are seen in all regions of the hippocampus. In stage V, the occipital and temporal neocortex is affected by NFT pathology, however there is resistance in the occipital and temporal neocortices, Stage VI: In stage VI, NFTs are more pronounced, wide accumulations of ghost tangles are present within the entorhinal pre-α subregion. Ghost NFTs may also be degraded and glial populations are present at the site of debris. The CA1 region of hippocampus has severe loss of neuronal cells, and vast NT presence. The major distinguishing feature of stage VI is that isocortical regions are severely affected with dense NT formations, ghost tangles and glial formations (Braak & Braak, 1991).

Another method for staging AD was established in 1989 which included psychological assessment from mild cognitive impairment (MCI) through to post-mortem analysis. The Consortium to Establish a Registry for Alzheimer's disease (CERAD) includes a battery of 17 clinical and neuropsychological assessments including the Mini-Mental State Examination, measurements of episodic memory, and immediate and delayed recall for assessment of clinically diagnosed AD, often followed by post-mortem analysis of plaque load and tangle pathology (Moms et al., 1989).

The use of pathological and clinical staging allows for measurement of disease progression, allowing for study of the healthy, preclinical, MCI, and late-stage AD. However, as the first pathological changes in AD can occur up to 17 years prior to clinical symptoms, it is difficult to identify mechanistic changes occurring during the onset and early progression of AD (Rodriguez-Vieitez et al., 2016).

1.5 Transgenic models of Alzheimer's disease

Despite current research with post-mortem human tissue, it is not possible to detect the first changes associated with disease onset and there is difficulty identifying changes that occur in the earliest stages of AD progression using post-mortem human tissue. Thus, several key murine models have been developed to investigate the onset and mechanisms of early AD pathology progression. These transgenic AD models are based on human familial AD mutations in *App*, *Ps1/Ps2* and *Mapt*, some of which are detailed below:

Tg2576 – The Tg2576 is an over-expression of the Swedish mutation KM670/671 familial APP gene (APPswe) (Lys670-Met, Met671-Leu), driven by a hamster prion protein promoter (hPRP) vector, with expression present throughout the CNS (Hsiao et al., 1996). This model expresses APP with 5-fold increase compared to endogenous mouse APP, and a 14-fold increase Aβ 1-40/1-42, has behavioural deficits in spatial learning and working memory by 9-10 months, and plaque deposition at 11 months of age. (Elder, Gama Sosa, & De Gasperi, 2010; Hsiao et al., 1996). There is no tau pathology or overt neuronal loss present in this model, though synaptic deficits have been noted

APP22/23 – This mouse model is based on over-expression of mutant human APPswe leading to Aβ deposition in the neocortex by 6 months of age (Sturchler-Pierrat et al., 1997). Key differences between APP22/23 and the Tg2576 is the promoter used for driving over-expression, with APP22/23 utilising the *Thy1* promoter to drive over-expression, which is a neuronal house-keeping gene. This model exhibited cognitive impairment in spatial memory from 3 months of age (P. H. Kelly et al., 2003; Van Dam et al., 2003), with neuronal loss reported in adult mice from 12 months of age (Calhoun et al., 1998).

APP/PS1 – This model is based on the C57/BL6 background harbouring familial AD mutations: human APPswe (KM670/671NL or K595N/M596L APP695swe mutations depending on strain) and PS1 (L166P/dE9) under the *Thy1* or mouse *Pnrp* promoter

(Jankowsky et al., 2004; Spanopoulou, Giguere, & Grosveld, 1991). Plaque deposition begins from 6 months of age, with dense plaque deposition by 12 months of age (Garcia-Alloza et al., 2006; Jankowsky et al., 2004)). Global neuronal loss is not observed, with only limited neuronal loss occurring at 8 months of age (Radde et al., 2006). Studies have reported cognitive deficits in spatial awareness and memory with the Morris water maze by 6 months (Gallagher, Minogue, & Lynch, 2013; Serneels et al., 2009). Studies have shown increased levels of tau in the CSF of APP/PS1 mice, and tau labelled neuritic accumulations, but no NFT accumulation (Maia et al., 2013; Radde et al., 2006). Synaptic loss occurs for Vglut-1, VGAT, and GAD65 immunopositive boutons in 12-month APP/PS1 mice, closely recapitulating human disease (Mitew, Kirkcaldie, Dickson, & Vickers, 2013a). Synaptic loss has also been reported to occur in dendritic spines with proximity to Aβ plaques at 3 months of age from *in vivo* live imaging (Bittner et al., 2012).

5xFAD – A subsequent model has been developed based around the APPswe KM670/671NL and Ps1 (M146L), but also incorporating 3 more familial AD mutations: App I716V, App V717I and PS1 L286V. This model has a more aggressive pathogenic phenotype, with interneuronal accumulations of Aβ observed by 1.5 months of age, and plaque deposition detected by 2 months of age (Oakley et al., 2006). This model also features synaptic loss and neuronal loss by 6 months, however no NFT formation occurs in this model (Oakley et al., 2006).

HTau – Murine models have been developed of human tau accumulation, featuring multiple isoforms of non-mutated human tau. Key pathology includes age dependent accumulation tau, resulting in the redistribution and hyperphosphorylation of tau in cell bodies and dendrites of the hippocampus and cortex (Andorfer et al., 2003; Maeda et al., 2016). Intraneuronal accumulations of hyperphosphorylated tau were present between 3-5 months of age, particularly in the hippocampus, with NFT formation evident by 15 months of age (Andorfer et al., 2003). Spatial learning and memory deficits were observed at 12 months of age, measured by novel object recognition, and Morris water maze (Polydoro, Acker, Duff, Castillo, & Davies, 2009).

Tau P301S – This model develops NFT-like pathology due to the expression of a transgene of mutant human tau, driven by a mouse prion protein promoter (Allen et al., 2002; Yoshiyama et al., 2007). NFTs were reported in hippocampus, neocortex and entorhinal cortex at 4 months of age, and synaptic loss and gliosis have been observed in the hippocampus by 3

months. Cortical atrophy (loss of up to 25%) and hippocampal atrophy of (loss of 45%) has been observed at 12 months of age, with neuronal loss starting at 3 months of age (Hampton et al., 2010; Yoshiyama et al., 2007).

Knock in AD mice (App^{NL} and App^{NLF}, App^{NLGF}) – More recently, genetic knock-in AD mice have been established in an attempt to minimise the artefact generation that feature in genetic over-expression models, that often result in disruption of endogenous gene expression, and over-express other APP products as well as Aβ (Saito, Matsuba, Yamazaki, Hashimoto, & Saido, 2016). Knock in AD mouse models expressed mutant human App (Swedish KM670/671 in App^{NL}, and Swedish KM670/671 with beyreuther/Iberian mutations I716F in App^{NLF}), which increase both the expression of Aβ and increase the proportion of $Aβ_{1-42}$ in comparison to $Aβ_{1-40}$ (Takashi Saito et al., 2014). The App^{NLF} model generated Aβ plaques in the cortex by 6 months that also exhibited immunoreactivity for activated astrocytes and microglia (Takashi Saito et al., 2014). App^{NLF} mice also exhibited memory loss at 18 months. App^{NLGF} mice exhibited Aβ plaque accumulation at 2 months of age, and greater microglial and astrocyte activity (Takashi Saito et al., 2014).

Triple transgenic models have also been developed to provide more comprehensive disease modelling, recapitulating Aβ deposition and tau accumulation together. These models allow for the investigation of the complex interactions between amyloid and tau neuropathology and subsequent degeneration.

3xTG – This overexpression model features three key human familial AD mutations, including the APPswe KM670 Swedish, MAPT P0311, and the PS1 M146V, driven by Thy1.2 promoter (Oddo et al., 2003). It is one of the most widely studied triple transgenic models, featuring Aβ plaque and NFT pathology. Intracellular accumulations of tau have been reported by 3-4 months within the neocortex and hippocampus, that were often accompanied by synaptic loss, Aβ deposition by 6 months of age, and NFT pathology was present in the hippocampus by 12 months (Oddo et al., 2003). Cognitive deficits in long term retention occurred by 4 months (Billings, Oddo, Green, McGaugh, & LaFerla, 2005), while spatial learning and working memory deficits were observed at 7 months of age (Oddo et al., 2003).

Animal models of AD have been very successful in identifying the key impacts of disease pathology in the cortex. Studies have been able to identify the impact of amyloid and tau deposition on the surrounding neuropil and study potential therapeutic targets in a model of the disease (B. Zhang et al., 2012). Many of the AD mouse models closely recapitulate the

pathologies seen in human AD, including neuronal and plaque associated DN pathology of post-mortem human preclinical AD (A. Woodhouse, J. C. Vickers, P. A. Adlard, & T. C. Dickson, 2009), and synaptic loss similar to human AD (Mitew et al., 2013a). The use of these models allows for examination of the earliest physiological changes as a result of Aβ or tau deposition in the cortex. The initial effects of AD pathology are currently impossible to study in post-mortem human tissue, as it is not possible to identify the earliest stages of AD, where cortical changes are occurring more than 17 years prior to the onset of clinical symptoms (Rodriguez-Vieitez et al., 2016).

Despite the success of the transgenic mouse models of AD there are some limitations that need to be considered when using them for research. Limitations of these models include the dependency on over-expression of familial AD associated mutations, which can generate phenotypes unrelated to the disease, and due to the lifespan of rodents, these are not models of the time-frame of human AD. Many of the transgenic models do not feature all pathologies of human AD, including substantial neuronal loss (Irizarry, McNamara, Fedorchak, Hsiao, & Hyman, 1997; Irizarry, Soriano, et al., 1997), and only few models exhibit NFT like pathology (Elder et al., 2010).

1.6 Cell type specific vulnerability in Alzheimer's disease

The brain consists of a wide range of cell types, each with specialised functions to allow for normal homeostasis and proper function. Pioneering work by Santiago Ramón y Cajal (1852-1934) provided the framework for modern neuroscience, illustrating the anatomical landscape of the brain. Cajal (1909) utilised the Golgi staining method to present the first histological images of the brain, illustrating that the brain is made up of individual neurons, rather than a global network as hypothesised in the reticular theory (Cajal, 1909) (review: (de Castro, López-Mascaraque, & De Carlos, 2007; López-Muñoz, Boya, & Alamo, 2006)). Broadly, these cells can be split into two main classes: neurons – classically thought of as the functional cells of the brain; and glial cells – the supporting cells in the brain. There are a range of neuronal subtypes including excitatory neurons and interneurons. Excitatory neurons generate a positive charge in response to stimuli, generating an action potential to transmit to post-synaptic neurons. Interneurons can be both excitatory or inhibitory, maintaining or limiting the excitatory state of surrounding neurons within the network (Figure 1.2).

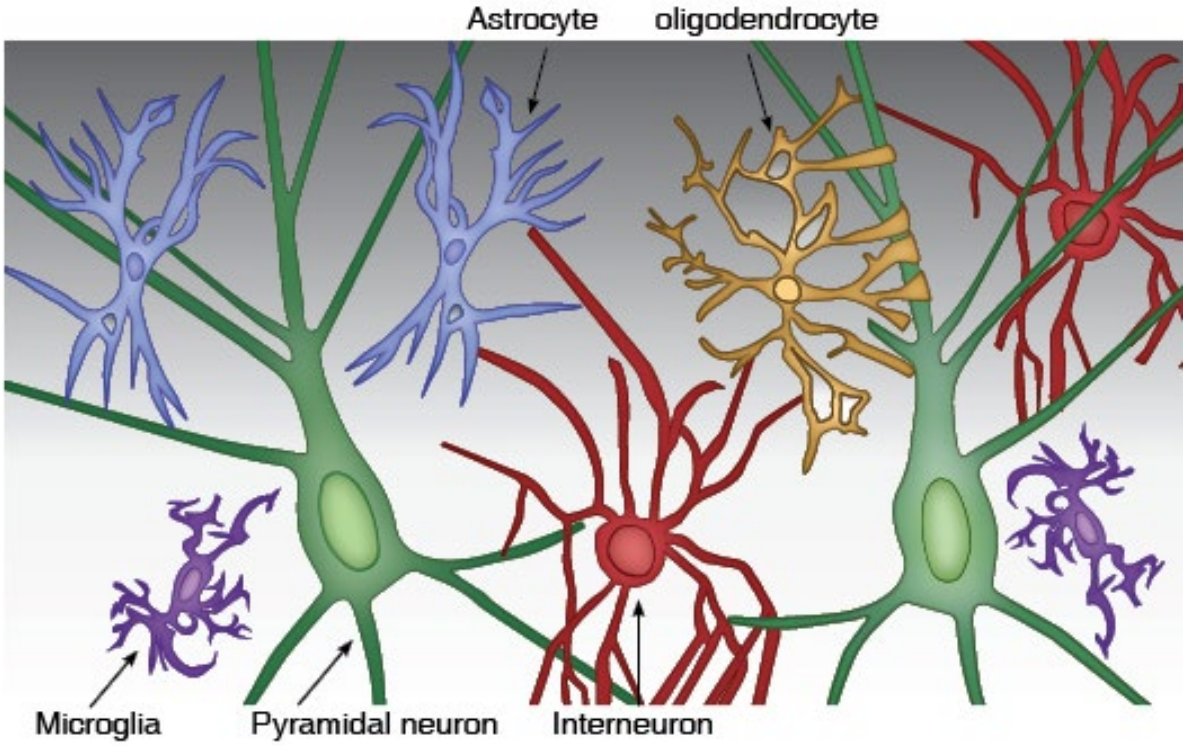
Astrocyte
oligodendrocyte
Microglia
Pyramidal neuron
Interneuron

Figure 1.2: Cell types of the brain

Schematic showing pyramidal neurons (green), interneurons (red), oligodendrocytes (yellow), microglia (purple), and astrocytes (blue) in the brain. Pyramidal neurons have been shown to be selectively vulnerable to AD pathology, whereas interneurons have been shown to be resistant to AD pathology. Microglia and astrocytes respond to AD pathology and promote the phagocytosis of AB. Each of these cells will have a different epigenetic and transcriptional profile.

A vast network of glial cells support and maintain homeostasis within the brain. Microglia act as resident macrophages and are the main immune cell type in the brain. Microglia feature highly ramified, motile processes that survey the local environment for CNS damage, dynamically interacting with neurons and astrocytes. Microglia clear metabolic and cellular debris from the surrounding extracellular space, and can mobilise to initiate a localised pro-inflammatory state in response to homeostatic imbalance and injury, promoting phagocytosis and apoptotic pathways (Khandelwal, Herman, & Moussa, 2011; Nimmerjahn, Kirchhoff, & Helmchen, 2005). Astrocytes are star-like glial cells identified by Cajal (1909) that also play a role in maintenance of homeostasis in the brain alongside microglia (Cajal, 1909). Astrocytes maintain and remove cellular and synaptic debris and they also have functional roles in synaptic plasticity and neuronal activity (Araque, Parpura, Sanzgiri, & Haydon, 1999) (review:(Perea, Navarrete, & Araque, 2009)). Astrocytes are capable of long range Ca^{2+} signalling from mechanical stimulation and in response to synaptic transmission (Araque et al., 1999; Charles, Merrill, Dirksen, & Sanderson, 1991).

Neuronal cells exhibit differential vulnerability to AD pathology. Analysis of neuronal cell loss and synaptic loss in AD brains has shown a subset of pyramidal neurons containing neurofilament-triplet proteins (NF+) to be selectively vulnerable to AD pathology. Neurofilament positive pyramidal neurons residing in cortical layers II/III and V in the prefrontal and temporal cortex, and in the CA1 and CA3 regions of the hippocampus, have all been shown to be vulnerable to AD pathology (P. R. Hof et al., 1990; Patrick R. Hof & Morrison, 1990; Koffie et al., 2009b; Thangavel, Sahu, Van Hoesen, & Zaheer, 2009; J. C. Vickers et al., 1994). Neurofilaments are the structural and functional unit of the neuronal cytoskeleton that assist in maintaining the morphology of neurons. Combinations of neurofilament light, medium and heavy heteropolymers form elastic cores to assist normal cellular function including axonal transport and synaptic plasticity (reviews: (M. K. Lee & Cleveland, 1996; J. C. Vickers, Kirkcaldie, Phipps, & King, 2016)). Dysregulation of the neuronal cytoskeleton is frequently seen in neurodegenerative diseases, including AD, Parkinson's disease, and Lewy body dementia. It has been suggested that NF+ pyramidal neurons may be particularly susceptible to AD pathology due alterations in calcium buffering, long range projections, metabolic stress, and to the loss or hyperphosphorylation of cytoskeletal proteins such as tau to be key to the cell-type specific vulnerability (P. R. Hof et al., 1990; Patrick R. Hof & Morrison, 1990; Morrison et al., 1987; Parodi et al., 2010; Thangavel et al., 2009).

In contrast, studies have indicated that a subset of calcium binding protein (CBP) interneurons expressing calretinin are resistant to excitotoxicity and to AD pathology (Fonseca & Soriano, 1995; P. R. Hof, Nimchinsky, Celio, Bouras, & Morrison, 1993; Lukas & Jones, 1994; Sampson, Morrison, & Vickers, 1997). While, other research has shown parvalbumin and calretinin interneuron loss in the hippocampus of knock-in APP/PS1 mouse models and the dentate gyrus of post-mortem human AD cases (Takahashi et al., 2010). Interneurons expressing gamma-aminobutyric acid (GABA) are also implicated in the hippocampus of Tg2576 mice (review: (Y. Li et al., 2016)). Calretinin immunopositive interneurons show lower dystrophic neurite accumulation than neurofilament positive neurons in plaque dense regions in transgenic AD mice, and in post-mortem inferior temporal gyrus of AD cases (Mitew et al., 2013b). Indeed, Mitew et al., (2013) determined that NF+ DN pathology, but not calretinin associated DNs, correlated with Aβ load, and plaque size in post-mortem human tissue and in APP/PS1 or Tg2576 mice (Mitew et al., 2013b). It has been suggested that interneurons have an enhanced ability to process calcium, and are resistant to oxidative damage (Pike & Cotman, 1995). It is also possible that calretinin interneurons are resistant to physical damage from Aβ plaques, or feature a strengthened ability for structural and functional remodelling in comparison to NF+ pyramidal neurons (Blizzard et al., 2011; Mitew et al., 2013b).

Neuroinflammation is also a commonly accepted hallmark of AD, however it is not known whether the neuroinflammation is acting as a protective mechanism, or is detrimental to neurodegeneration (L. F. Lue et al., 1996) (review: (Mosher & Wyss-Coray, 2014)). In AD, microglia undergo phenotypic changes to become amoeboid, and have been identified surrounding dense-core Aβ plaques, from early stages of AD pathogenesis (Bornemann et al., 2001; Itagaki, McGeer, Akiyama, Zhu, & Selkoe, 1989; Sasaki, Yamaguchi, Ogawa, Sugihara, & Nakazato, 1997). Surface receptors including TLRs, and a range of immune related genes including *Cd36*, *Cd47*, *Clu*, *Cr1*, *Cxcr2, Tgf-β*, *Trem2* and *Mcp-1* are expressed in microglia surrounding Aβ plaques, however, the pathway for microglial activation is unknown (Bamberger, Harris, McDonald, Husemann, & Landreth, 2003; Karch & Goate, 2015; Reed-Geaghan, Savage, Hise, & Landreth, 2009). Recently, studies utilising single-cell transcriptomics have identified sub-populations of microglia that reacted to AD pathology, via TREM2 dependent and independent pathways (Keren-Shaul et al., 2017). Activated astrocytes have also been shown to surround Aβ plaques alongside microglial activation, and bind and degrade Aβ and dysfunctional synaptic dystrophies (T. Wyss-Coray et al., 2003).

It has been recently hypothesised that astrocytic dysfunction leads to the accumulation of dystrophic neurites and presynaptic protein aggregations *in vivo* (Gomez-Arboledas et al., 2018).

1.7 Genetics, Environment and Alzheimer's disease

Individual risk for sporadic AD is determined by both genetic and environmental factors; it is a multifactorial disease. There are multiple physiologic and molecular pathways altered during the progression of AD. The ApoE ε4 allele has been implicated in AD, attributable for up to 60% of late-onset AD cases, making it the strongest genetic risk factor for late onset AD (Ashford, 2004; Strittmatter et al., 1993). Apolipoprotein E ε4 is known to regulate lipid transport and is primarily produced in the liver, however its role in the brain is less well understood. Studies have shown that carriers of the ApoE ε4 allele have more abundant Aβ plaques than non-carriers (Kok et al., 2009). It has been hypothesised that the ApoE protein has roles in APP membrane insertion, processing and Aβ clearance (Corder et al., 1993; Tokuda et al., 2000), and the ε2 allele has been shown to be protective against AD (Tokuda et al., 2000). APOE ε4 has also been shown to downregulate cleavage and secretion of a key neurotrophin in the brain; brain derived neurotrophic factor (BDNF) *in vitro*, while ApoE ε2 and ε3 increased BDNF secretion (Sen, Nelson, & Alkon, 2017). In the healthy brain, BDNF has been implicated in long-term potentiation (LTP), synaptogenesis, and memory formation (review:(Bramham & Messaoudi, 2005)), and BDNF mRNA is downregulated in transgenic models of AD (Peng et al., 2009), and in post-mortem AD (Phillips et al., 1991). Other risk alleles have been implicated in late-onset AD including Clu, Picalm, Bin1, Cr1, Abca7 and Cd33, but have a low prevalence in AD (Bamberger et al., 2003; Hu et al., 2011; Karch & Goate, 2015; Lambert et al., 2009; Reed-Geaghan et al., 2009). Many of the alleles implicated in AD are associated with endocytosis of synaptic vesicles (review: (Ridge, Ebbert, & Kauwe, 2013)). Despite numerous genetic risk factors for AD, their penetrance and prevalence do not account for the total number of AD cases seen today, which implicates other external risk factors in the development of AD.

Environmental factors have also been implicated as a key contributor for AD development and may account for the cause of late-onset AD. Some examples of environmental risk factors for developing sporadic AD include cardiovascular health, diet, obesity and diabetes, traumatic brain injury, trace metal levels and heavy metal exposure, vitamin B, and education level/cognitive reserve.

Cardiovascular health – Cardiovascular health has been implicated in AD. Studies have shown regular physical activity (exercise equal to or greater than walking more than three times a week) to reduce the risk of AD in people aged 65 and older (Laurin, Verreault, Lindsay, MacPherson, & Rockwood, 2001). Subsequently, studies have correlated obesity and diabetes (type II) with altered risk of AD (W. L. Xu et al., 2011); being underweight, or overweight between the ages of 30-45 led to increased risk of AD in one study (Beydoun et al., 2008), however other studies have shown higher body-mass-index to correlate with lower risk of AD (Atti et al., 2008).

Diet – Lifestyle factors like diet have been shown to impact AD. A Mediterranean influenced diet has been associated with reduced risk of AD, as opposed to western style diets (M. C. Morris et al., 2015; Scarmeas, Stern, Tang, Mayeux, & Luchsinger, 2006). Excessive consumption of alcohol has been linked with increased risk of dementia, potentially due to neurotoxic effects in later life, but moderate consumption of alcohol is thought to be protective against dementia (Anttila et al., 2004).

Traumatic Brain Injury – Epidemiological studies and meta-analysis have identified a history of head injury to increase the risk for Alzheimer's disease (Fleminger, Oliver, Lovestone, Rabe-Hesketh, & Giora, 2003; Mortimer et al., 1991). Head injury occurring in later life, or more severe head injury with periods of loss of consciousness or memory loss have been shown to also increase risk for AD. Some studies have implicated repeat head injury with more severe or earlier onset of AD (Plassman et al., 2000).

Metal Homeostasis – An imbalance in metal homeostasis is seen in AD, potentially due to changes in redox-activity leading to cytotoxicity. A concentration of trace metals, including zinc, copper, and iron has been identified in the core of Aβ plaques, and surrounding neuropil of the amygdala (Lovell, Robertson, Teesdale, Campbell, & Markesbery, 1998). In particular, zinc and iron is highly concentrated in the core of plaques and surrounding neuropil (Connor, Menzies, St Martin, & Mufson, 1992; Lovell et al., 1998), and a disruption in iron homeostasis has been observed in post-mortem AD cases (Connor, Snyder, Beard, Fine, & Mufson, 1992). Studies have identified significantly decreased levels of DNMT1 and MeCP2, and significantly increased Ser 396, 235 phosphorylated tau mRNA and protein in C57/BL6 mice exposed to environmental lead (Bihaqi, Bahmani, Adem, & Zawia, 2014; Eid, Bihaqi, Renehan, & Zawia, 2016). It has been suggested that an imbalance in environmental exposure to trace metals can increase the risk for AD, though the mechanism is poorly understood, but might indicate a role

of oxidative stress in AD pathogenesis (review: (George Perry, Cash, Srinivas, & Smith, 2002; Peters, Connor, & Meadowcroft, 2015)).

Vitamin B – Vitamin B deficiency is thought to alter Aβ production, with longitudinal studies showing that folate deficiency increases the risk of AD (Ho et al., 2003; H. X. Wang et al., 2001). Vitamin b deficiency has also led to changes in PS1, BACE and APP gene expression (Andrea Fuso et al., 2008).

Education/cognitive reserve – Education level and occupation, or social/leisure activities that promote neuronal activity and consolidate cortical connections are thought to delay the onset of AD (Brayne et al., 2010; Karp et al., 2009; Stern et al., 1994). There is often a discrepancy between observed neuropathology and functional deficits seen in AD, which is thought to be due to a cognitive reserve generated from occupational and educational level (Barulli & Stern, 2013). Genetics may also influence the base level of cognitive reserve (Ward et al., 2017).

In the absence of genetic mutations, epigenetic factors may link environmental risk in the onset and development of AD.

Epigenetics

1.8 Regulation of transcription

Described by Waddington in 1942, the term epigenetics was defined as a change in phenotype without change in genotype (Waddington, 1942a, 1942b). There have been numerous studies of the role of epigenetics, chromatin structure and gene regulation since 1942 through to today (Britten & Davidson, 1969; Kornberg, 1974) (review: (Allis & Jenuwein, 2016)). Epigenetics has since been refined to describe changes to the DNA environment, or changes to transcription, without directly altering the DNA sequence. Regulation of the DNA by epigenetic modifications such as DNA methylation and histone modifications allows for complex interaction between the environment and the DNA by regulating chromatin structure (review: (Allis & Jenuwein, 2016)). Appropriate packaging of the DNA in the nucleus is essential for proper gene expression. DNA is packaged with equal mass of proteins (histones) into chromatin (Kornberg, 1974). Repeating units of DNA and histones (~146bp DNA wrapped 1.65 times around a histone octamer) form nucleosome subunits (Carter, 1978; Kornberg,

1974), which interact with linker DNA to form euchromatin or heterochromatin (Figure 1.3) (Carter, 1978; Luger, Mader, Richmond, Sargent, & Richmond, 1997; McGhee & Felsenfeld, 1980; Mirsky & Silverman, 1972; Olins & Olins, 1974; Waddington, 1942a). Epigenetic modifications such as histone modifications and DNA methylation allows for the modification of chromatin structure by altering nucleosome positioning and their affinity to compact, thus increasing or decreasing accessibility to the DNA (Figure 1.3). The presence of densely packed nucleosome subunits and heterochromatin limits the binding of transcriptional machinery to promoter sequences and the initiation of transcription at the transcriptional start sites (TSS). This occurs in a highly regulated, cell-type specific and gene specific fashion. Thus, epigenetic processes allow cells to be genetically homogeneous, but structurally and functionally heterogeneous (Ryan Lister et al., 2013; Maruyama et al., 2011; Mo et al., 2015; Stedman & Stedman, 1950) (review: (Rudolf Jaenisch & Adrian Bird, 2003)).

The two most commonly studied epigenetic modifications are DNA methylation (Bird, Taggart, Frommer, Miller, & Macleod, 1985; Holliday & Pugh, 1975; Hotchkiss, 1948; Razin & Riggs, 1980), and post-translational histone modifications (Vincent G. Allfrey & Mirsky, 1964; Britten & Davidson, 1969; N. D. Heintzman et al., 2009; Nathaniel D. Heintzman et al., 2007; S. A. Morris et al., 2007; Stedman & Stedman, 1950) (Figure 1.3). Epigenetic modifications alter the accessibility for determining whether regions of chromatin will generally be active (euchromatin) or repressed (heterochromatin) (Heitz, 1928). Epigenetic control of cis-regulatory elements including promoters and enhancers also alter the chromatin accessibility for transcriptional machinery to bind and initiate gene transcription (Banerji, Olson, & Schaffner, 1983; Banerji, Rusconi, & Schaffner, 1981) (review: (Andersson, 2015)). Next-generation sequencing technologies, the ability to sequence rare populations of cells, and even single-cell analysis has improved our understanding of the complexity of epigenetic regulation within cell types and between individual cells (Ryan Lister et al., 2013; R. Lister et al., 2009; Luo et al., 2017; Meissner et al., 2008; Mo et al., 2015). Epigenetic processes are now being implicated in neurodegenerative diseases as potential mechanisms for disease onset and progression.

1.9 DNA Methylation

DNA methylation is the most widely studied epigenetic modification. Chemical modifications to DNA were hypothesised by Avery & McCarty (1944), and Hotchkiss (1948) (Avery,

Macleod, & McCarty, 1944; Hotchkiss, 1948). The role of DNA methylation in gene regulation and differentiation was hypothesised independently by Holliday, and Riggs in 1975, with the discovery of its roles in repression and subsequently the identification of cytosine-guanine dinucleotide (CpG islands) and shores occurring shortly after (Bird et al., 1985; Holliday & Pugh, 1975; P. A. Jones & Taylor, 1980; Razin & Riggs, 1980). In mammalian species, DNA methylation involves the addition of methyl groups at CpG sites (5-methylcytosine – 5mC), by DNA methyltransferases (DNMTs) (L. Chen et al., 1991; Klimasauskas, Kumar, Roberts, & Cheng, 1994; Okano, Bell, Haber, & Li, 1999). These CpG sites are often found in clusters, called CpG islands (typically unmethylated), and the distribution of methylation across CpG islands can regulate transcription. However, methylation can also accumulate in non-CpG sites (Guo et al., 2013; Ryan Lister et al., 2013; Ramsahoye et al., 2000). Methylation of CpG islands at TSS is generally associated with repression and subsequent gene silencing, by preventing transcription factor access to DNA (Antequera, Boyes, & Bird, 1990; Watt & Molloy, 1988). Thus, heavily methylated CpG islands often co-localise with heterochromatin and are inhibitory to transcription (Choy et al., 2010; Razin & Riggs, 1980)(review: (J. Y. Lee & Lee, 2012; Suzuki & Bird, 2008)). CpG islands are often present at promoter regions (with as many as 50-60% of promoters contain CpG islands), but can also be observed within gene bodies and in intergenic regions resulting different (often permissive) transcriptional profiles (Ioshikhes & Zhang, 2000; Jjingo, Conley, Yi, Lunyak, & Jordan, 2012). However distal regulatory elements are generally less methylated than promoters, and are CpG poor regions (~30% of distal elements are methylated) (Stadler et al., 2011). Interestingly, DNA methylation has also been identified to occur at non-CpG dinucleotides (CC, CA, CT), which accounts for up to approximately 0.02% of all methylated cytosines, and was first described in the plant genome (Lindroth et al., 2001) with DNMT3A/B both involved in the maintenance of non-CpG sites (reviews: (R. Jaenisch & A. Bird, 2003; Peter A. Jones, 2012; Peter A. Jones & Liang, 2009)). However non-CpG methylation may regulate neuronal differentiation and function (Ryan Lister et al., 2013). It should be noted that association of DNA methylation and silencing is not always absolute. A recent study has shown that DNA methylation may not be enough to silence gene promoter elements in human MCF7 cells (Ford et al., 2017).

Conversely, the removal of 5mC allows for permissive, or stimulated gene expression, and can be achieved through passive or active mechanisms. Passive demethylation occurs through depletion during replication, with DNMTs withholding methylation on selected bases. A key pathway of active demethylation involves ten-eleven-translocase proteins (TET) (Ito et al.,

2010; Tahiliani et al., 2009). In mammalian species, TET proteins catalyse the conversion of 5mC to 5-hydroxymethylcytosine (5hmC), which is a marker of active demethylation and is associated with gene transcription (Ito et al., 2010; Tahiliani et al., 2009). Proteins can bind to methylated genomic regions and regulate transcription. Methyl-CpG-binding proteins (MeCP) bind to 5mC and particularly 5hmC, and can act to enhance or repress transcription (Lewis et al., 1992; Mellen, Ayata, Dewell, Kriaucionis, & Heintz, 2012). Methyl-CpG-binding proteins are involved in many different aspects of gene regulation. They can facilitate interaction between DNA methylation and other chromatin modifiers, and are also involved in processing mRNA, alternative splicing, x-inactivation, gene imprinting, and limits 5hmC labelling within gene bodies (Cheng et al., 2017; X. Nan et al., 1998). Interestingly, methyl-CpG-binding proteins are highly expressed in the brain and regulate neuronal chromatin structure (Skene et al., 2010).

The function of DNA methylation requires understanding of the distribution of DNA methylation across the genome: the sum of methylated regions across promoter, enhancer and gene bodies, and unmethylated regions, or CpG shores. Recent advances in bisulphite treatment of DNA and next-generation sequencing (whole genome bisulphite sequencing; WGBS) has allowed for single base resolution of 5mC across the genome (R. Lister et al., 2009). Techniques have also advanced to include nucleosome positioning with simultaneous methylation sequencing of the same strand of DNA. Nucleosome occupancy with next generation sequencing (NOMe-seq) allows for simultaneous measurement of methylation and nucleosome positioning and has been adapted for single cell analysis (T. K. Kelly et al., 2012; Phillippa C. Taberlay, Statham, Kelly, Clark, & Jones, 2014, Pott, et al., 2017). Utilising these advances in technology, sequencing of cell populations and single cells has been accomplished, showing that DNA methylation is both tissue and cell-type specific (R. Lister et al., 2009; Luo et al., 2017; Mendizabal & Yi, 2016; Mo et al., 2015).

1.10 Histone modifications

Post-translational modifications to the histone N-terminus tail domain were first described by Allfrey et al., (1964), and it was hypothesised that acetylation and methylation play a role in the regulation of RNA synthesis (V. G. Allfrey, Faulkner, & Mirsky, 1964). It is now known that a core octamer of histone proteins (two copies each of H2A, H2B, H3, and H4) forms nucleosomes, which act as the dynamic building blocks of chromatin (Luger et al., 1997), while

histone H1 binds to the outside of the histone octamer aiding in structural stabilisation (Finch & Klug, 1976; Thoma & Koller, 1977) (Figure 1.3). The modifications on the tail domains of the histone proteins can alter charge, binding affinity and facilitate chromatin restructuring through interaction with other nucleosomes, and the recruitment of chromatin remodelling enzymes resulting in changes to gene expression (Hong, Schroth, Matthews, Yau, & Bradbury, 1993). Post-translational histone modifications are now documented to include methylation, acetylation, phosphorylation and ubiquitination, where methylation and acetylation have been most widely studied; however, there are more than 100 possible known histone modifications that can modify chromatin structure on lysine and arginine residues (M. Tan et al., 2011). Histone modification nomenclature is denoted by histone number, followed by residue and modification; for example, histone 3 lysine 9 can be acetylated (H3K9ac), or methylated H3K9me3. These modifications do not occur in isolation, with combinations of histone modifications working together to adapt nucleosome structure and regulate gene expression. Histone modifications alter the access for transcriptional machinery to regulatory elements such as the TSS, promoters and enhancer elements. A histone code hypothesis has been postulated, in which the combination of post-translational histone modifications and overall profile of the nucleosome structure lead to diverse biological outcomes (Dion, Altschuler, Wu, & Rando, 2005; Jenuwein & Allis, 2001) (reviews: (Bannister & Kouzarides, 2011; Kouzarides, 2007; Zentner & Henikoff, 2013)).

Histone modifications are actively catalysed by a suite of enzymes including histone methyltransferases and acetyltransferases and can be actively removed with demethylases and deacetylases. The first histone lysine methyltransferases (HKMT) to be discovered were the SUV39H1 and SUV39H2 complexes, responsible for methylation of lysine residues on histone H3 (Aagaard et al., 1999; O'Carroll et al., 2000). In 1996, Brownwell and colleagues identified the functional role for histone acetyltransferases (HATs) and histone deacetylases (HDACs), which act as a switch for transcriptional regulation (Brownell et al., 1996). There is now a wide range of known methyltransferases/demethylases and acetylases/deacetylases, each modifying specific histone modification substrates (Allis et al., 2007). One of the many effects of modifying histones is to allow for nucleosome remodelling and alternative splicing. Transcriptional activity is dependent on nucleosome positioning, which changes through active (ATP-dependent) pathways. The SWI/SNF nucleosome remodelling complex was found to regulate chromatin structure, and subsequently transcription, in 1992 (Hirschhorn, Brown, Clark, & Winston, 1992). The SWI/SNF complex removes histones from DNA by nucleosome

disassembly, or by transferring histone octamers to another position on the DNA (Hirschhorn et al., 1992; Whitehouse et al., 1999).

Single nucleosome resolution mapping of histone methylation and acetylation was first accomplished with chromatin immunoprecipitation on microarrays (ChIP-chip), giving the first analysis of histone distribution across the genome (C. L. Liu et al., 2005). However, advances in the use of next-generation technology for chromatin immunoprecipitation and next-generation sequencing (ChIP-seq) has allowed for modification specific analysis at a high resolution across the genome (Johnson, Mortazavi, Myers, & Wold, 2007; Robertson et al., 2007; Schmid & Bucher, 2007). Limitations of ChIP-seq protocols include the large sample size required and antibody quality limitations. Adaptations to the ChIP-seq protocol have allowed for higher resolution mapping, indexing and multiplexing of rare samples and low cell number (van Galen et al. 2015), and protocols have been developed for single cell ChIP-seq experiments to reveal cellular heterogeneity for the epigenome (Rotem et al., 2015). High sensitivity and specificity antibodies to transcription factors and histone modifications have improved the quality and resolution of ChIP-seq experiments (Kidder, Hu, & Zhao, 2011).

Histone acetylation:

Histone acetylation was first described by Allfrey and colleagues in 1964 (V. G. Allfrey et al., 1964; Vincent G. Allfrey & Mirsky, 1964). Histones have a positive ionic charge, which is weakened through the addition of acetyl groups, subsequently reduces the attraction between histones and DNA, and increasing access for transcription factors to bind to DNA open reading frame (Hong et al., 1993). This function plays a vital role in the maintenance of DNA integrity, with early studies finding loss of histone H4, or replacement of the lysine residue leading to cell cycle defects in G2 and M phase (Megee, Morgan, & Smith, 1995). Acetyl groups are added to histone tails by HATs, a class of enzymes that catalyse the transfer of acetyl groups from acetyl-CoA to lysine on the N-terminus of histone proteins (Belikoff, Wong, & Alberts, 1980; Kleff, Andrulis, Anderson, & Sternglanz, 1995) (review: (Zentner & Henikoff, 2013)). Histone deacetylases transfer acetyl groups from acetylated histone proteins to coenzyme-A (CoA), producing a more condensed chromatin state (Taunton, Hassig, & Schreiber, 1996).

Histone acetylation is generally associated with active chromatin and is permissive to gene expression. H3K9ac is highly correlated with active promoters, and is often found around TSS, and may recruit elongation complexes for transcription (Gates et al., 2017). While H3K27ac is a modification that marks active from poised enhancers, is also present around transcriptional

start sites of active genes and may have a role in the elongation of transcription (Creyghton et al., 2010a). Morris and colleagues (2007) determined H3K36ac to be located at the promoters of RNA polymerase II (RNA pol II) transcribed genes (S. A. Morris et al., 2007). To further illustrate the regulatory control histone modifications have on gene expression, Shogren-Knaak et al., (2006) showed that H3K16ac inhibited the compaction of chromatin fibres, demonstrating the control that histone modifications have over higher order chromatin structure and subsequent gene expression (Shogren-Knaak et al., 2006b). Distal regulatory elements also aid in the regulation of transcription. Broad regions involved in the trans-regulation of genes are usually identified by enrichment of H3K27ac, and have been defined as putative super enhancers (Khan & Zhang, 2016; Pott & Lieb, 2014). Super enhancers are genomic regulatory regions that are responsible for cellular identity (Hnisz et al., 2013; Whyte et al., 2013). Only a small percentage of super enhancers have been identified through initiatives like the Super Enhancer Database (Khan & Zhang, 2016), however the functional role of many super enhancer regions remains to be elucidated.

Histone methylation:

Histone methylation can occur to both lysine and arginine residues of the N-terminus residues. Histone methyltransferase enzymes can recognise and bind lysine and arginine residues and catalyse the addition of one, two or three (mono-, di- or tri-) methyl groups to the N-terminus tail of histone residues. Unlike histone acetylation, the addition of methyl groups does not alter the charge of the histone DNA complex in the nucleosome. H3K4me1 marking at the TSS has been shown to be associated with the promoters of actively transcribed genes (Barski et al., 2007; B. E. Bernstein et al., 2005; Nathaniel D. Heintzman et al., 2007). While H3K4me1 marking present outside of promoter regions is associated with functional enhancers (Nathaniel D. Heintzman et al., 2007). Histone 3 lysine 4 methylation can also act as an initiator for downstream histone acetylation (Z. Wang et al., 2009). One of the most comprehensively studied histone methylation marks is histone 3 lysine 4 tri-methyl (H3K4me3), which has been shown to mark transcriptional start sites of active genes (B. E. Bernstein et al., 2005; Nathaniel D. Heintzman et al., 2007; Santos-Rosa et al., 2002). Studies have also identified interactions between demethylation complexes and H3K4me3, where they couple (including both chromo- and bromo- domains) to the N-terminus of tri-methylated histones and initiate chromatin remodelling (Huang, Fang, Bedford, Zhang, & Xu, 2006; Wysocka et al., 2006). H3K27me3 is a marker of repressive chromatin and inactive gene promoters (Barski et al., 2007; P. C.

Taberlay et al., 2011; Young et al., 2011). Polycomb repressive complex 2, containing EZH2 add methyl groups to histone residues such as H3K27 (Cao et al., 2002; Ferrari et al., 2014). The co-localisation of H3K4me3 and H3K27me3 marking indicate bivalent chromatin domains (Azuara et al., 2006; B. E. Bernstein et al., 2006). This has been implicated in higher global chromatin structure by facilitating interactions with chromatin and transcription factors, and by interacting with chromatin assembly and remodelling complexes to regulate chromatin compaction (Shogren-Knaak et al., 2006a; Blosser, 2009 #973; Zhou & Grummt, 2005). Histone modifications both influence and are influenced by the histone modification signature of neighbouring nucleosomes and protein complexes that are recruited to DNA (Fischle et al., 2005)(reviews: (Kouzarides, 2007).

Histone and DNA methylation interactions:

To aid appropriate gene transcription, regions of the genome are partitioned into accessible euchromatin and dense compact heterochromatin. A growing body of evidence supports cross talk between DNA methylation and histone modifications (Hisashi Tamaru & Selker, 2001; H. Tamaru et al., 2003). Mutations in genes encoding histone methyltransferases have been associated with reduced DNA methylation (Hisashi Tamaru & Selker, 2001; H. Tamaru et al., 2003), and subsequent studies have identified DNMT domains and co-binding proteins (SIN3A, UHRF1, MeCP2) that bind to histone modifications (Dhayalan et al., 2010; Q. Zhao et al., 2016). Functional mapping of DNA methylation and histone modifications has identified prerequisites for the establishment of DNA methylation. The addition of H3K9me1 by Suv39hp1 is required to recruit Dnmt3b for subsequent DNA methylation in mammalian species (Lehnertz et al., 2003). Another key example of the interactions occurring between histone modifications and DNA methylation is during differentiation when *de-novo* methylation is happening within the embryo. Histone methylation on lysine 4 such as H3K4me1/2/3 act as mediators for the establishment of *de-novo* methylation in the embryo during development, preventing DNA methyltransferase 3L (DNMT3L) from binding and recruiting DNMT3A and DNMT3b (Jia, Jurkowska, Zhang, Jeltsch, & Cheng, 2007; Ooi et al., 2007).

DNA methylation silences transcription by changing nucleosome structure and subsequent formation of heterochromatin. In 1998, two studies identified a role for methyl CpG-binding protein 2 (MeCP2) in the regulation of chromatin structure through interactions with DNA

methylation and histone modifications (P. L. Jones et al., 1998; Xinsheng Nan et al., 1998). These studies showed that the MeCP2 complex recruited the HDAC/SIN3A co-repressors to remove histone acetylation and lead to transcriptional silencing and heterochromatin formation (P. L. Jones et al., 1998; Xinsheng Nan et al., 1998). SIN3A acts as a scaffolding protein for HDACs and other transcriptional regulators to bind target promotors (Yi Zhang, Iratni, Erdjument-Bromage, Tempst, & Reinberg, 1997). Recruitment of HDAC/SIN3A complex by MeCP2 was specific to methylated DNA located in a nucleosome, rather than CpG or site specific recruitment (Fuks et al., 2003; P. L. Jones et al., 1998). It has also been shown that MeCP2 can drive methylation of H3K9, regulate learning and memory formation, and is associated with Rett syndrome and other neurological disorders (Ambigapathy, Zheng, & Keifer, 2015; Amir et al., 1999; Fuks et al., 2003). These examples demonstrate the complexity and interaction between DNA methylation and histone modifications, establishing the need to integrate the research on each form of epigenetic modification (reviews: (Cedar & Bergman, 2009; Du, Johnson, Jacobsen, & Patel, 2015)).

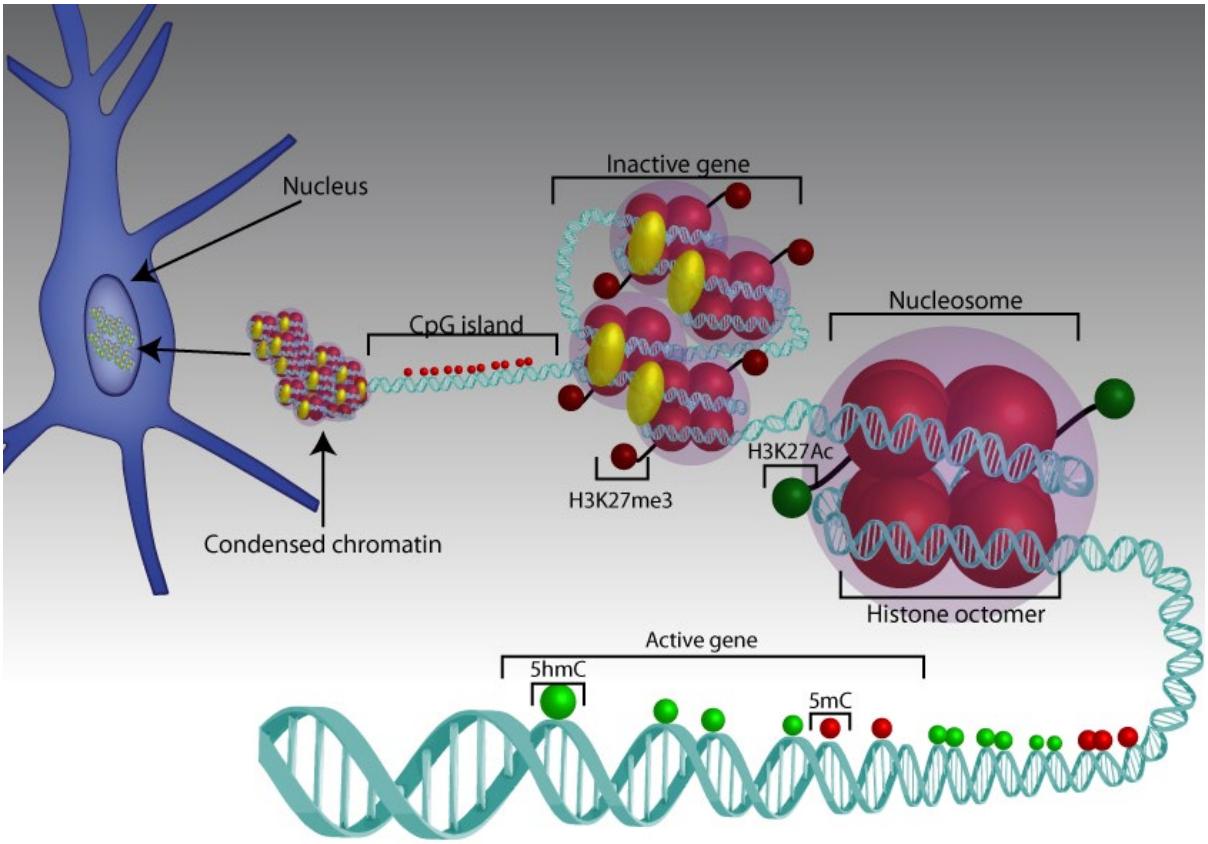
Nucleus
Inactive gene
CpG island
Nucleosome
H3K27Ac
H3K27me3
Condensed chromatin
Histone octomer
Active gene
5hmC
5mC

Figure 1.3: Regulation of chromatin structure through epigenetic modifications

Dynamic regulation of the genome through epigenetic mechanisms including DNA methylation (5mC: red – repressive; 5hmC: green – permissive), post-translational histone modifications (eg:H3K4me3 - active, H3K27ac – permissive; H3K27me3 – repressive), and subsequent changes to nucleosome positioning. Each of these result in changes to chromatin structure and access for transcriptional machinery to promoters and initiate transcription.

Epigenetics in the brain

1.11 Dynamic epigenetic regulation in the brain

The study of epigenetics in the brain has recently expanded, demonstrating epigenetic regulation plays key roles in neural development, the formation of memory, synaptic plasticity, axonal pathfinding, aging and AD (Ambigapathy et al., 2015; Calfa et al., 2012; Fischer, Sananbenesi, Wang, Dobbin, & Tsai, 2007a; Ryan Lister et al., 2013; Mo et al., 2015). Understanding the role of epigenetic regulation in the healthy developing and aging brain is essential to understand how disease will dysregulate the system.

The epigenome is highly specific in neurons of the developing brain

Distinct sub-types of excitatory and inhibitory neurons communicate in intricate networks to govern higher thought processes, emotion and behaviour. Neuronal diversity is associated with differences in synaptic plasticity, electrophysiological properties, and morphology. This is accomplished partially through epigenetic regulation of gene expression in stem-cells as they differentiate into neurons (Ryan Lister et al., 2013). Neural progenitor cells (NPCs) generate terminally differentiated cells in a distinct order, with key signalling pathways activated during gestation and post-birth to promote neural development; for example, platelet derived growth factor and Wnt signalling drive neural differentiation in the mammalian cortex (Erlandsson, Enarsson, & Forsberg-Nilsson, 2001; Y. Hirabayashi et al., 2004) (reviews: (Yusuke Hirabayashi & Gotoh, 2005; Molyneaux, Arlotta, Menezes, & Macklis, 2007)). Neural progenitor cells also give rise to oligodendrocytes and astrocytes through activation of alternative signalling pathways (including the STAT3/JAK cascades for intracellular signalling) (Magistri et al., 2016; Raff, Miller, & Noble, 1983; Yanagisawa et al., 2000). Studies have shown that histone modifications (H3K9me3) and DNA methylation are involved in the regulation of cellular differentiation from neural progenitor cells into astrocytes and neurons (Singh, Shiue, Schomberg, & Zhou, 2009; Takizawa et al., 2001; S.-L. Tan et al., 2012). For example, Kraus, et al., (2016) measured core epigenetic modifiers of DNA methylation (including *Dnmt1, Dnmt3a, Dnmt3b, Tet1, Tet2, Tet3*, and *Apobec1-3*) across an early life time-course in the frontal cortex and cerebellum of C57/BL6 mice, ranging from postnatal day 0, 7, 15, 30 to 120, utilising immunohistochemistry (T. F. J. Kraus et al., 2016). This study observed the percentage of 5hmC positive cells in the frontal cortex to significantly

increase through post-natal development to adulthood, however 5mC remained consistent with age (T. F. J. Kraus et al., 2016). Similar to other studies, methylation was more abundant in neuronal cells compared to non-neuronal cells of the brain (T. F. Kraus, Guibourt, & Kretzschmar, 2015; T. F. J. Kraus et al., 2016; Ryan Lister et al., 2013; Wagner et al., 2015). The cellular outcomes of neural progenitor cells are associated with diverse epigenetic landscapes, which are established early in development (Ryan Lister et al., 2013; Mo et al., 2015).

Initial difficulties in the isolation of neuronal nuclei have limited cell-type specific epigenetic analysis in the brain. Jiang and colleagues (2008) developed new methods utilising the FOX-3 transcription factor (NeuN - (Kee K. Kim, Robert S. Adelstein, & Sachiyo Kawamoto, 2009; R. J. Mullen, C. R. Buck, & A. M. Smith, 1992)), which is present in the vast majority of neuronal nuclei, to assess the default epigenetic landscape for mammalian neuronal cells with flow cytometry (Jiang, Matevossian, Huang, Straubhaar, & Akbarian, 2008). Neuronal nuclei isolated with this technique were shown to maintain nucleosomes and chromatin structure compared to unsorted nuclei, making the method of isolation ideal for epigenetic based NGS protocols (Jiang et al., 2008). More recently, Lister et al., (2013) isolated neuronal and glial cell populations from mouse and human frontal cortex at four time-points representing embryonic, juvenile, adolescent and adult ages, and performed whole genome bisulphite sequencing (WGBS) and ChIP-seq. This study found that non-CG specific methylation accumulated throughout the genome in neurons across age, but not in glial populations across life (Ryan Lister et al., 2013). Key timepoints for non-CG methylation occurred alongside synaptogenesis and synaptic pruning in a highly conserved fashion between mouse and human brain (Ryan Lister et al., 2013).

The epigenome defines cell-type specificity

To date there is no standard ‘reference epigenome’, as epigenetics regulates gene transcription in a cell type specific manner; however, consortiums are working to establish a framework and database of the epigenome (The, 2012). Recent studies have concentrated on identifying distinct epigenetic patterns of neuronal sub-types (Alexey Kozlenkov et al., 2016; Mo et al., 2015). To address the lack of cell-type specific maps of the neuronal epigenome, a seminal study by Mo et al., (2015) isolated and separated Camk2a fast acting excitatory neurons, parvalbumin interneurons, and vasoactive-intestinal peptide expressing interneurons from the

neocortex of transgenic mice, and performed WGBS, ChIP-seq, ATAC-seq (measuring chromatin accessibility), and RNA-seq on the isolated populations (Mo et al., 2015). This study demonstrated that DNA methylation, in particular non-CpG methylation to be highly specific to particular neuronal subtypes, with almost half of all differentially methylated regions were hypomethylated in excitatory neurons, and cell-type specific transcription factors and promoter regions contained low levels of methylation (Mo et al., 2015) Only 13.4% of ATAC-seq peaks shared across parvalbumin, Camk2a and VIP neurons (Mo et al., 2015).

The advent of single-cell sequencing has demonstrated that the epigenome and transcriptome are highly cell-type specific (Buenrostro et al., 2015; Clark et al., 2017; Farlik et al., 2015; Islam et al., 2014; Pott, 2017; Smallwood et al., 2014). Single-cell RNA-seq experiments and unsupervised clustering based on sequence similarity (t-distributed stochastic neighbour embedding) have allowed for the molecular identification of seven distinct sub-types of pyramidal neurons and glial cells within the somatosensory cortex and hippocampus of mouse, with layer 5 pyramidal neurons clustering into two distinct sub-types (Zeisel et al., 2015). The application of single-cell WGBS in the brain has also resulted in the identification of new neuronal cell-types. Luo, et al., (2017) utilised single-cell WGBS in 8-week mouse and human (25 years) frontal cortex to sequence over 6000 methylomes from single cells (Luo et al., 2017). By utilising t-SNE based clustering analysis, Luo identified novel parvalbumin expressing inhibitory neuron and layer 6 excitatory neuron subtypes; and showed inhibitory neurons have conserved regulatory regions across species in comparison to excitatory neurons (Luo et al., 2017). A key difficulty with single-cell WGBS is achieving high coverage and sequencing depth from a single cell. The single-cell WGBS study from Luo et al., (2017) achieved 5% coverage of the reference genome from a single cell, with approximately 1.55 million mapped reads per cell (Luo et al., 2017). This is further supported by mRNA profiling of excitatory/inhibitory neuronal subtypes and glial populations in the CNS, showing significant translational diversity between neuronal sub-types (Doyle et al., 2008).

Several studies have also highlighted the importance for brain region specific analysis when studying epigenetics (Davies et al., 2012; Rizzardi et al., 2017). Techniques such as MeDIP-seq and HumanMethylation450K arrays in human brain have shown region specific differences in methylation between the visual cortex, entorhinal cortex, superior temporal cortex, cerebellum, pons and blood (Davies et al., 2012; Hernandez et al., 2011). One study has demonstrated that the methylation status of the frontal and temporal cortex to be similar, but both dissimilar to cerebellum when measured with HumanMethylation 27 arrays (Hernandez

et al., 2011). Whereas studies in post-mortem schizophrenic brain have shown region and loci specific differences of methylation in dorsolateral prefrontal cortex and hippocampus (Alelú-Paz et al., 2016; Viana et al., 2016). Differentially hydroxymethylated regions also exist between hippocampus and cerebellum in murine models (Szulwach et al., 2011). However, all studies of 5hmC to date have discovered region specific differences in mixed cell populations and haven't investigated cell-type specific epigenetic landscapes.

Epigenetics, memory and synaptic plasticity

Synaptogenesis, long-term potentiation and long-term depression are essential for learning and memory. Synapses form between neurons allowing for communication throughout the brain. The formation, maintenance, extinction and dynamic regulation of synapses (synaptic plasticity) occurs throughout life. These processes require changes to gene expression and appropriate regulation of chromatin structure to assist in the formation of memories (Dickey et al., 2003). Initial studies of the epigenetic regulation of memory formation demonstrated chromatin-level regulation of learning and memory in a learned taste aversion paradigm (Swank & Sweatt, 2001). Swank, et al., (2001) showed that mitogen-activated protein kinase activity regulated histone acetyltransferases in the insular cortex during long-term memory formation (Swank & Sweatt, 2001).

To date, numerous studies have reported changes in the epigenetic states of specific signalling pathways or genes associated with learning and memory. Methylation maintenance molecules are essential for synaptic plasticity, learning and memory (Feng et al., 2010b; Levenson et al., 2006). Studies have demonstrated that experience dependent plasticity in the brain correlates with a changing methylation landscape around genes involved in synaptic plasticity (Leighton et al., 2018; X. Li et al., 2014; Widagdo et al., 2016). For example, neuronal activity has been shown to alter genome-wide expression of epigenetic regulators for DNA maintenance and repair *in vitro* (for example the *Ing1* pathway) (Leighton et al., 2018). While other studies have shown upregulation of transcriptional regulators *Egr1* and *Fos* mRNA in the ventral tegmental area *in vivo* after auditory associated reward learning, associated with decreased promoter methylation of *Egr1*, but increased gene body methylation for *Egr1* and *Fos* (Day et al., 2013). Other transcriptional regulators such as *Tet*3, which mediates the deposition of 5hmC, has been shown to accumulate around genes associated with synaptic plasticity in the prefrontal cortex and hippocampus during learning and behavioural adaptation (X. Li et al., 2014; Widagdo et

al., 2016). DNA methyltransferases have also been implicated in the regulation of synaptic plasticity. Conditional knockdown of *Dnmt1* and *Dnmt3a* postnatally in post-mitotic neurons have led to long term deficits in LTP and long-term depression (LTD), hippocampal atrophy, and cognitive dysfunction (Feng et al., 2010b). *In vitro* studies have shown the *Gadd45* gene to rapidly demethylate in response to synchronised therapeutic stimulus or in response to exercise based neuronal stimulation (Guo et al., 2011; Ma et al., 2009). Similarly, studies have also shown histone modifications to be important for memory consolidation and retention in mice (Pavlopoulos et al., 2013; Peleg et al., 2010). Much of the research into synaptic plasticity and epigenetics has centred around brain derived neurotrophic factor (*BDNF). BDNF* is a key gene in the regulation of synaptic plasticity and has been implicated in memory formation. Neuronal depolarisation has been shown to reduce CpG methylation around the *Bdnf* gene promoter *in vitro,* regulated by a complex of MeCP2/HDAC/SIN3a (Martinowich et al., 2003). While histone acetylation at *Bdnf* gene promoters in the mouse prefrontal cortex is associated with consolidation of long-term memory (Bredy et al., 2007; Lubin, Roth, & Sweatt, 2008). In summary, epigenetic regulation of memory formation and retention, and underlying changes to synaptic plasticity correlate with changes to the epigenome.

1.12 Epigenetics in the aging brain

Aging is widely accepted as the leading risk factor associated with AD (review: (Ghosh, Agarwal, & Haggerty, 2011; Yankner, 2000)); however, AD is not a normal part of cognitive aging. Epigenetics has an established role in synaptic plasticity, long term potentiation and depression, and memory formation; however, there have been few studies of the epigenome in the aging brain. The transcriptional profile of genes involved in synaptic plasticity and memory formation are altered in the aging brain, which occur alongside significant DNA damage in promoter regions in neural and glial cells (Tao Lu et al., 2004; Soreq et al., 2017). Epigenetic changes may be the cause of underlying cognitive impairment occurring in the aging brain.

DNA methylation in the aging brain

Cortical aging has been associated with a variety of methylation states. Genome-wide studies have illustrated a complex landscape of both accumulation of DNA methylation in the aging brain (Ryan Lister et al., 2013; Yu et al., 2012), hypomethylation in the aging brain (Christensen et al., 2009; Penner et al., 2011), while other studies have shown both hyper- and hypomethylation in the aging brain (Bakulski et al., 2012). An epigenome wide association study utilising HumanMethylation27 Beadchip arrays identified 2,227 genes differentially methylated with aging in the mid-frontal gyrus of the post-mortem human prefrontal cortex, with ~50% of sites hypermethylated and ~50% of sites hypomethylated with increasing age (Bakulski et al., 2012). Other genome-wide array based studies have identified correlations between aging and increased methylation at CpG islands in the frontal and temporal cortex noting that dramatic changes to methylation occur early in life and are stabilised through aging (Hernandez et al., 2011; Numata et al., 2012). Non-CpG methylation also accumulates in neurons throughout later life (Ryan Lister et al., 2013; Szulwach et al., 2011). Interestingly, cortical CpG methylation has been shown to predominantly accumulate throughout life, in genomic regions separate from non-CpG methylation (Ryan Lister et al., 2013; Yu et al., 2012). While non-CpG methylation also accumulates in the cortex throughout later life (Ryan Lister et al., 2013; Szulwach et al., 2011). Studies using bead based arrays have observed age related hypomethylation for CpGs around *Igf2, Hdac5, Ercc1* and *Myod1* loci; specifically and an age related decrease in *Arc* promoter methylation in the CA1 region of the hippocampus, and increased *Arc* promoter methylation in the dentate gyrus of aged (24+ months) rats (Christensen et al., 2009; Penner et al., 2011). Studies in murine models have shown accumulation of 5hmC

in neuronal cells during development that is conserved through aging in cerebellum and hippocampus, while others have shown an increase of 5hmC in dopaminergic neurons in the aging substantia nigra (H. Chen, Dzitoyeva, & Manev, 2012; Fasolino, Liu, Wang, & Zhou, 2017).The different results reported by these studies may be due to different sampling and molecular techniques, brain regions examined and cellular heterogeneity within the samples analysed (Davies et al., 2012; Ryan Lister et al., 2013; Mo et al., 2015).

While there have been some genome-wide DNA methylation studies in the aging brain, many studies have focused on candidate pathways or genes of interest in the aging brain. For instance, quantitative PCR-based studies of DNA methylation across age in neuronal nuclei from the anterior and lateral temporal lobe from human cases have shown increased DNA methylation in promoter CpG islands of *PGR, SYK* and *HOXA1* genes, but decreased methylation in *S100A2* with age (Siegmund et al., 2007). The study also found 8 loci in whole brain homogenate to have increased methylation with aging, including *GABRA2, GAD1, HOXA1, NEUROD1, NEUROD2, PGR, STK11*, and *SYK* (Siegmund et al., 2007). Another study of post-mortem human parietal cortex reported that CpGs of the *Tau* promoter were hypomethylated with increasing age (Tohgi et al., 1999). However, mass spectrometry analysis of DNA methylation binding sites in the post-mortem human prefrontal cortex have shown no significant aging related changes in promoter CpG sites for *APP, NCSTN, BACE*, *SIN3A* and *DNMT1*, but detected a negative drift in promoter methylation for *APOE* and *PS1* with increasing age (S.-C. Wang, Oelze, & Schumacher, 2008).

Histone modifications in the aging brain

There have been few studies of histone modifications in the aging brain. Much of the literature is not in agreement regarding the role of histone modifications in the aging brain. Likely, a complex combination of enrichment and depletion of histone modifications occurs through aging (Benito et al., 2015; Cheung et al., 2010; Nativio et al., 2018; Peleg et al., 2010; Rodrigues, Souza, Ghiraldini, Mello, & Moraes, 2014). Indeed, one study has identified histone modifications to be dynamic in the developing brain, but stabilise through aging (Shulha, Cheung, Guo, Akbarian, & Weng, 2013). Animal models allow for the study of a time-course of histone modification changes in aging in a controlled environment that is difficult to mirror with post-mortem human tissue. Cognitive aging results in a global loss of H3K9me3 and gain in H3K9ac in the cortex of Balb/c mice, indicative of increased euchromatin and transcriptional

activity with aging (Rodrigues et al., 2014). Depletion of H3K9 methylation has been correlated with the decreased expression of BDNF from aged hippocampal and cortical neuronal cultures (Walker, LaFerla, Oddo, & Brewer, 2013). While other studies have shown no difference in H3K9ac, H3K14ac, H4K5ac, H4K8ac, and H4K16ac in 16 month old hippocampal neurons from the C57/BL6 mice compared to 3 month old littermates, there was an age associated depletion of H4K12ac (localises to promoters/intron-exon boundaries and correlates with gene expression in neurons (Benito et al., 2015)), which suggests a reduction in transcription and subsequent loss of memory consolidation in aged animals (Peleg et al., 2010). When measured with ChIP-seq, H4K12ac was depleted from 20 month old CA1 hippocampal neurons compared to 3 month old counterparts in a murine model (Benito et al., 2015). H4K12ac depletion in aged neurons was associated with dysregulation of RNA metabolic process, splicing, apoptosis and autophagic cell death when measured with RNA-seq (Benito et al., 2015).

There have been few studies of the aging brain in post-mortem human tissue. These studies have identified a complex pattern of enrichment and depletion in the aging brain. A ChIP-seq study of neurons (NeuN+ FACS) in the human prefrontal cortex in 11 samples from 0.5-14 and 68-69 years investigated H3K4me3 alterations with age (Cheung et al., 2010). Analysis of 3 samples less than 1 year old with 3 samples greater than 60 years of age showed 589 sites of enrichment present in infant, but not aged samples, and 101 peaks were unique to the aged samples (Cheung et al., 2010). In accordance with previous literature, another genome-wide study in post-mortem prefrontal cortex has identified rapid developmental changes to H3K4me3 at 1157 loci in neurons at sites pertaining to neuronal development, synaptogenesis, and intracellular signalling, but few changes to adult or aging neurons (Shulha et al., 2013). A recent study highlighted the importance for genome wide histone modification analysis in the aging brain. Nativio et al. (2018) performed ChIP-seq for H4K16ac (associated with promoter activation) in young and aged temporal lobe with mixed neuron and glial cell populations. The study utilised ChIP-seq and identified an increase in H4K16ac in aged individuals compared to younger cognitively healthy controls (Nativio et al., 2018). Gene ontology analysis showed that the top genes associated with aging were within pathways associated with respiration processing, insulin stimulus and the inflammatory response (Nativio et al., 2018). Alongside studies characterising histone modifications in the aging brain, others have trialled histone deacetylase inhibitors (HDACi) as a potential treatment to improve memory performance in

the aging brain (Dagnas, Guillou, Prévôt, & Mons, 2013; Pavlopoulos et al., 2013; Peleg et al., 2010; Walker et al., 2013).

Epigenetics in Alzheimer's disease

A wide range of evidence exists to support the notion of epigenetic dysregulation in AD. Recently studies have identified epigenetic alterations present in post-mortem AD cases and in AD mouse models, which provide support for epigenetic dysregulation in AD, however it is not known whether epigenetic dysregulation causes AD, or is a downstream consequence of the disease. Indeed, seminal studies of epigenetics in AD identified changes to DNA methylation that occur in tandem with neuritic plaque load and Braak staging, occurring at some of the earliest detectable stages of the disease (P. L. De Jager et al., 2014; Lunnon et al., 2014).

Several methods have been utilised for assessing epigenetic modifications in AD. Many studies have investigated global levels of DNA methylation and histone modifications with immunohistochemistry or various blotting techniques to determine total protein or methylation levels (A. I. Bernstein et al., 2016; Bradley-Whitman & Lovell, 2013; Coppieters et al., 2013; Lashley et al., 2014; D. Mastroeni et al., 2015; D. Mastroeni et al., 2010; Narayan, Lill, Faull, Curtis, & Dragunow, 2015). Others have used next generation sequencing to identify changes at a base-pair resolution, through genome-wide association studies, WGBS, or ChIP-seq (Benito et al., 2015; P. L. De Jager et al., 2014; Gjoneska et al., 2015; Lunnon et al., 2014). Coordinated changes in DNA methylation and histone modifications may explain the dysfunction seen in AD.

1.13 DNA methylation in Alzheimer's disease

DNA methylation is the most widely studied epigenetic modification in AD. Global DNA methylation is altered through the progression of AD, however the results of current research have not been in agreeance as to the nature of change occurring in AD (Table 1.1). Some studies have shown global hypermethylation (Bradley-Whitman & Lovell, 2013; Coppieters et al., 2013; Lardenoije et al., 2018), while others have reported global hypomethylation in AD (Chouliaras et al., 2013; A. Fuso, Seminara, Cavallaro, D'Anselmi, & Scarpa, 2005; D.

Mastroeni et al., 2010; S.-C. Wang et al., 2008; West, Lee, & Maroun, 1995) (Table 1.1). Indeed, other studies have not found any change to global DNA methylation in AD (Lashley et al., 2014). For example, immunohistochemistry and dot-blot based analysis have detected an increase in global 5mC, 5hmC and TET1 intensity in the middle-frontal gyrus, middle-temporal gyrus and hippocampus of late-onset AD cases compared to age-matched controls (Bradley-Whitman & Lovell, 2013; Coppieters et al., 2013). While a study of the post-mortem human hippocampus with immunohistochemistry presented a decrease of 5mC in CA1 and CA3 hippocampal subregions and a decrease of 5hmC in the dentate gyrus and CA3 region of the hippocampus in AD cases (Chouliaras et al., 2013). However, other research has shown no change in 5mC and 5hmC in the entorhinal cortex of post-mortem AD brains when measured with immunohistochemistry and ELISA (Lashley et al., 2014). DNA methylation has also been identified in the cytoplasm of AD middle frontal gyrus and middle temporal gyrus, but has not been quantified (Coppieters et al., 2013; D. Mastroeni et al., 2015).

Table 1.1: DNA methylation alterations in Alzheimer's disease

Author (year)	Methodology	Tissue source	Key findings
Bradley-Whitman, et al., (2013)	Immunohistochemistry and western blot	Human hippocampus/ parahippocampal gyrus, cerebellum	Increased levels of TET1, 5mC and 5hmC in the hippocampus of preclincal and late stage AD compared to control cases
Chouliaras, et al., (2013)	Immunohistochemistry	Human hippocampus	Decreased 5mC in glia but not neurons in hippocampal CA3, decreased 5mC intensity in neurons and glia in hippocampal CA1 in AD vs control. 5hmC decreased in neurons and glia in dentate gyrus, and in glia of CA3, but not CA1 in AD vs control cases.
Coppieters, et al., (2013)	Immunohistochemistry	Human MFG and MTG	No difference in 5mC or 5hmC immunolabelling in neurons, astrocytes or microglia in the MFG or MTG between AD and control cases
Lashley, et al., (2014)	Immunohistochemistry and ELISA	Human entorhinal cortex	No difference in 5mC or 5hmC immunolabelling in neurons in entorhinal cortex of control and AD cases, confirmed with ELISA
Mastroeni, et al., (2010)	Immunohistochemistry	Human EC	Decrease in 5mC labelled neurons in the EC of AD cases compared to controls
Sanchez-Mut, et al., (2013)	Illumina VeraCode CG DNA methylation	Homogenised human FC & Mouse brains	DNA hypermethylation associated silencing of 3 target genes: TBXA2R, SORBS3 and SPTBN4 in AD compared to control
Siegmund, et al., (2007)	5' methylation status of 50 genes of CNS growth and development	Human TC	*S100A2* hypomethylated in AD, *SORBS3* hypermethylated in AD
Bernstein, et al., (2016)	MeDIP, RNA-seq (analysis only)	Human PFC, *Drosophila*	5hmC differentially methylated in PFC of AD cases. 5431 sites hyper-hydroxymethylated, 2170 hypo-hydroxymethylated, genes identified to be differentially hydroxymethylated in post-mortem AD were confirmed in fly model
Rao, et al (2012)	Methylation CpG qPCR, RNA qPCR	Human FC	Both hypermethylation and hypomethylation in AD cases compared to control and preclinical. Hypermethylation of Bdnf and Nf-κβ gene promoter, hypomethylation of Cox-2 gene promoter, but no other changes to methylation in sites investigated.
Bakulski, et al., (2012)	HumanMethylation 27, RNAseq	Human FC	Hypomethylation of *TMEM59*, *PS1* and *PS2*, transcriptional changes in *TMEM59*, and no differences for *APOE*, *BACE1*, *BDNF*, *BIN1*, *PICALM* and *TOMM40* in AD samples. No global difference in DNA methylation between AD samples and controls
De Jager, et al., (2014)	HumanMethylation 450K	Human PFC	Correlation between DNA methylation and neuritic plaque load. Changes occur early in AD progression
Gasparoni, et al., (2018)	HumanMethylation 450k	FC and TC (bulk), occipital cortex (FACS NeuN)	Braak staging associated DMRs in neurons and glia in AD, including *HOXA3, APP* and *ADAM17*
Lunnon, et al., (2014)	HumanMethylation 450K	Human entorhinal cortex, PFC, STG	*ANK1* hypermethylation correlates with Braak staging and neuritic plaque load in EC, STG and PFC, but not in cerebellum
Chibnik, et al., (2015)	HumanMethylation 450K	Human dorsolateral PFC	CpG hypermethylation was associated with neuritic plaque load in AD (including including Bin1, Clu, ABCA7, Ms4a6a, and Apoe). Hypermethylated SNP risk loci correlated with increased neuritic plaque load in AD
Smith, et al., (2016)	HumanMethylation 450K, Pyrosequencing	Human STG	Trem2 promoter methylation increased in 3 separate cohorts of AD, and correlated with Braak staging
Sanchez-Mut, et al (2014)	Genome wide DNA methylation study	Human hippocampus	DUSP22, CLDN15, QSCN6 enriched in AD hippocampus compared to control. Linear correlation between DNA methylation of Dusp22 and plaque load
Sanchez-mut, et al., (2016)	Bisulphite sequencing genome wide	Human dorsolateral PFC	DNA methylation changes are common across neurodegenerative disease including AD, Parkinson's disease, FTD, and Lewy body dementia. Neurodegenerative diseases have shared sites that are hypo- and hypermethylated
Tohgi, et al., (1999)	Bisulfite sequencing, PCR and sequencing	Human cerebral cortex	Age associated global hypomethylation, but transcription factor binding site (SP1) specific hypermethylation in AD vs control cases
West, et al., (1995)	Southern blot	Human cortex	APP gene hypomethylated in AD cortex, but not age matched controls
Zhao, et al., (2017)	Genome wide 5hmC sequencing	Human dorsolateral PFC	Differentially hydroxymethylated regions to correlate with neuritic plaques. Differentially methylated regions associated with cellular and synaptic activity 203 hyper-5mC, 118 hypo-5mC
Zilller, et al., (2013)	Genome-wide bisulfite sequencing	Various human tissue including AD cortex	12408 differentially methylated AD CpGs overlapped with developmental methylation landscape

FC – frontal cortex, TC – temporal cortex, PFC – prefrontal cortex, MFG – middle frontal gyrus, MTG – middle temporal gyrus, STG – superior temporal gyrus, EC – entorhinal cortex

With the advent of next generation sequencing, it is now possible to measure CpG site specific changes in DNA methylation with arrays or at a genome-wide level. However, many previous genome-wide association studies (450k/HumanMethylation) and whole-genome bisulphite sequencing studies have presented contradictory results. Some studies have shown a mix of hypomethylation and hypermethylation in AD compared to control cases (Bakulski et al., 2012; Rao, Keleshian, Klein, & Rapoport, 2012; Sanchez-Mut et al., 2016), while others have detected predominately hypomethylation (Watson et al., 2016), and others have reported hypermethylation in the AD brain (Chibnik et al., 2015; P. L. De Jager et al., 2014; Lunnon et al., 2014; Siegmund et al., 2007; M. J. Ziller et al., 2013). Bakulski, et al. (2012) performed genome wide DNA methylation analysis of a heterogenous cell population from human frontal cortex using the HumanMethylation27 array. This study identified 948 CpGs to be differentially methylated in late-onset AD, including hypomethylation of *TMEM59, PS1* and *PS2* with associated transcriptional changes in *TMEM59*, but no differences in methylation or transcriptomics for *APOE, BACE, BDNF, BIN1, PICALM* and *TOMM40* in AD samples (Bakulski et al., 2012). The difference in global coverage of DNA methylation between late-onset AD cases and cognitively normal controls was within 2.9% of each other, regions of chromosome 3 were hypomethylated, and chromosome 10 and 17 were hypermethylated in AD compared to control (Bakulski et al., 2012). Lunnon, et al., (2014) utilised HumanMethylation450 array and bisulphite pyrosequencing in the post-mortem entorhinal cortex, superior temporal gyrus, and prefrontal cortex of AD cases and age-matched controls to identify AD associated differentially methylated loci. This study identified hypermethylation of *ANK1, PCBD1, SLC15A4, SIRT6, MEST, MLST8, ZNF512,* and *TMX4* in AD cases (Lunnon et al., 2014). Early research using WGBS in the frontal cortex of two severe AD cases reported that more than 60% of known ENCODE transcription factor binding sites showed high levels of methylation in the AD cases compare to age-matched controls (M. J. Ziller et al., 2013). In particular, AD samples had DMRs within regions of non-conserved genomic regions as well as intergenic regions compared to controls (M. J. Ziller et al., 2013). More recently, genome-wide analysis of hypermethylated CpG regions identified correlations of H3K4me3 and H3K27me3 marked promoters with known AD loci including *CLU, DIP2C, FRMD4A, HLA-DRB1, HLA-DQB1, CTNNA2,* and *KLK7* (Watson et al., 2016). A recent study has highlighted the importance of cell sorting to identify AD related changes in DNA methylation in neurons. Gasparoni and colleagues sorted human neuronal and glial nuclei from the occipital cortex and assessed DNA methylation alterations in AD using the HumanMethylation 450k array (Gasparoni et al., 2018). This study demonstrated that isolated neurons and glia were

hypomethylated (60% of differentially methylated CpGs) in AD cases compared to controls (Gasparoni et al., 2018). Interestingly, neurons and glia had different methylation profiles that dynamically progressed with increasing Braak stage of AD cases (Gasparoni et al., 2018). Gene ontology analysis demonstrated that differential methylation was occurring at pathways for neurological processes including synaptic transmission, neurotransmitter levels and neuron projection morphogenesis (Gasparoni et al., 2018). The changes to DNA methylation in AD may also be shared across other dementias, with one study utilising WGBS to identify a core set of genes being differentially methylated across AD, Parkinson's disease, and Lewy body dementia (Sanchez-Mut et al., 2016).

DNA hydroxymethylation has also been implicated in AD, however techniques have only recently been developed to measure it at a genome-wide level. There have been two studies that have performed genome-wide sequencing of 5hmC in post-mortem human AD brain (A. I. Bernstein et al., 2016; J. Zhao et al., 2017). Bernstein, et al., (2016) identified a range of 5hmC DMRs to be enriched at intergenic regions of the prefrontal cortex of 10 post-mortem AD samples, with a mix of both hypo-hydroxymethylation and hyper-hydroxymethylation (A. I. Bernstein et al., 2016). Gene ontology analysis demonstrated significant enrichment in pathways of cell polarity, synaptic activity and cellular maintenance, and differentially hydroxymethylated regions included AD associated single nucleotide polymorphisms such as *ANK1, MAPK1, BIN1* and *CAMK1D* (A. I. Bernstein et al., 2016). This study tested gene loci from the findings of the human data to follow up in *Drosophila*, showing the genes associated with 5hmC DMRs to alter tau-associated neurotoxicity (A. I. Bernstein et al., 2016). Additionally, genome wide analysis of 5hmC in the post-mortem human dorsolateral prefrontal cortex has shown global enrichment in exons, introns, TSS and promoter regions but global loss at intergenic regions of AD cases (J. Zhao et al., 2017).

Some studies have concentrated on characterising DNA methylation in brain specific or disease specific loci, predominantly at genes involved in memory formation and familial AD risk loci. These studies show gene specific hypermethylation of genes associated with synaptic plasticity (Rao et al., 2012), and generally hypomethylation at AD risk loci (S.-C. Wang et al., 2008; West et al., 1995). An early study of DNA methylation in AD showed the *APP* locus to be hypomethylated in in the AD brain with Southern blot (West et al., 1995). Mass spectrometry analysis of DNA methylation binding sites in the human prefrontal cortex detected a loss in promoter methylation for *APOE* and *PS1* in AD samples (S.-C. Wang et al., 2008). Gene and transcript specific analysis of *Bdnf*, *Creb, Synaptophysin, Cox-2* and *Nf-κβ* through qPCR

analysis showed hypermethylation of CpGs in the *BDNF* and *NF-κβ* gene promoters, and hypomethylation of CpGs in the *COX-2* gene promoter in frontal cortex of post-mortem AD cases (Rao et al., 2012). Moreover, a study of DNA methylation of 50 genes related to CNS growth and development of the anterior temporal cortex (including a subset analysis of neuronal nuclei for 10 genes) has identified hypomethylation of *S100a2* and increased methylation of *Sorbs3* in AD (Siegmund et al., 2007).

Among the most convincing evidence for epigenetics being critical to the progression of AD lies in the correlations between epigenetic data and AD pathology. Multiple studies have correlated loss of DNA methylation with Braak staging or neuritic plaque load, while others have reported positive correlations between DNA methylation and increased pathology load. The different cortical regions, fixation strategy, and methods of analysis may have led to inconsistent results between studies (Table 1.1). For instance, Coppieters et al., (2013), reported positive correlations between Aβ, tau and ubiquitin (dystrophic neurite) loads and both 5mC and 5hmC intensity in AD. However, Chouliaras, et al., (2013) described negative correlations between global 5mC and 5hmC levels and Aβ plaque load in the hippocampus, but did not observe any correlation with NFT load (Chouliaras et al., 2013). Recently, a study in the 3xTG and APP/PS1 mice and primate models of AD, and observed negative correlations between global levels of 5mC, 5hmC and DNMT3A and plaque load in dentate gyrus and CA3 region of the hippocampus in APP/PS1 and 3xTg AD models (Lardenoije et al., 2018). One seminal study correlated DNA methylation with pathological staging in AD (P. L. De Jager et al., 2014). De Jager, et al., (2014) performed DNA methylation analysis of a large suite of samples from the prefrontal cortex of two major post-mortem studies (totalling over: 2700 samples), and a replicate study of 117 individuals. This study used InfiniumHumanMethylation450 array to show that DNA methylation at a set of genes, including *Bin1*, *Abca7, Ank1, Cdh23, Dip2a, Rhbdf2, Rpl13,* and *Serpinf1/2,* correlated with neuritic plaque load; and that DNA methylation alterations were present early in AD progression (P. L. De Jager et al., 2014). A follow up study using HumanMethylation 450k arrays confirmed that hypermethylation of a range of CpGs including *BIN1, CLU, ABCA7, MS4A6A,* and *APOE* correlated with increased neuritic plaque load in human AD prefrontal cortex (Chibnik et al., 2015). Other studies have shown linear correlations between DNA methylation of the *DUSP22, ANK1* and *TREM2* genes and neuritic plaque load, and Braak staging in the superior temporal gyrus (Lunnon et al., 2014; Sanchez-Mut et al., 2014; Smith et al., 2016). Differential hydroxymethylation correlated with neuritic plaque load in the human

dorsolateral prefrontal cortex at genomic sites associated with cellular and synaptic activity (including *DUSP22*, *SYN2*, *ATXN1*, and *APC2*) (J. Zhao et al., 2017). Furthermore, four differentially hyroxymethylated sites, *ABAT*, *CAMK1D*, *HTRA3*, and *LRRN1,* also correlated with NFTs, in the human dorsolateral prefrontal cortex (J. Zhao et al., 2017). Interestingly, data suggests that the correlations between DNA methylation at certain sites and pathology load may also be cell type specific. Recent research indicates that different loci exhibited DNA methylation that changed in tandem with Braak staging in neurons (e.g. *HOXA3, APP* and *ADAM17*) compared to glia (*ANK1*) in the human occipital cortex (Gasparoni et al., 2018).

1.14 Histone modifications in Alzheimer's disease

Histone acetylation and methylation are dysregulated in AD, however there have been few studies to that performed genome-wide analysis of histone modifications to ascertain the molecular underpinnings of AD (Benito et al., 2015; Gjoneska et al., 2015; A. Kozlenkov et al., 2014).

Studies of global histone modifications utilising immunohistochemistry or blotting are not in agreeance, demonstrating either enrichment or depletion of various histone modifications in AD (Table 1.2) (Francis et al., 2009; D. Mastroeni et al., 2015; Narayan et al., 2015). Francis, et al., (2009) demonstrated that APP/PS1 mice performed worse in fear conditioning than WT controls, and identified that after fear conditioning there is a global loss of histone H4 in the hippocampus of 3-4-month-old APP/PS1 mice compared to WT control mice (Francis et al., 2009). In contrast, total H3, H4, H3ac and H4ac are enriched in neurons of the middle-temporal gyrus of post-mortem AD brains, and correlate GFAP, tau and Aβ load (Narayan et al., 2015). Mastroeni, et al., (2015) performed immunohistochemical analysis of H3K4me3 marking. This study observed that intracellular changes in H3K4me3 to occurred early in AD progression by correlating with Braak staging, and showed a shift in the intracellular location of H3K4me3 from the nucleus to the soma of neurons (D. Mastroeni et al., 2015).

Alongside changes to histone modifications, research has also illustrated that HDACs are enriched as a result of AD pathogenesis *in vivo* (Table 1.2) (Govindarajan et al., 2013; Graff et al., 2012). In particular, HDAC2 was increased in neurons of the CA1 hippocampus in an AD-like mouse model (Graff et al., 2012). Furthermore 8-month transgenic APP/PS1-21 mice recover cognitive deficits to wild-type levels after knocking out HDAC6 (Govindarajan et al.,

2013). Another study has identified AD risk loci, including *ApoE €4,* to induce nuclear translocation of HDACs in the hippocampus of C57/BL6 mice resulting in a reduction of BDNF expression. However, mice exposed to *ApoE €3* increased histone acetylation within the nucleus and upregulated BDNF (Sen, Nelson, & Alkon, 2015). Subsequently, a number of studies have investigated the use of HDACi in AD to improve behavioral outcomes in animal models of the disease (Francis et al., 2009; Govindarajan et al., 2013; Kilgore et al., 2009; Vecsey et al., 2007). Histone deacetylase inhibitors have been shown to increase learning and memory performance in a contextual fear paradigm using 6-month APP/PS1 transgenic mice (Kilgore et al., 2009). Additionally, treatment with HDACi prior to a fear conditioning paradigm restored histone H4 in the APP/PS1 mice, rescued behavioral performance and improved long-term potentiation in hippocampal slice recordings (Francis et al., 2009).

There have been five studies investigating histone modifications in AD at a genome-wide scale (Table 1.2) (Benito et al., 2015; Gjoneska et al., 2015; Klein et al., 2019; Marzi et al., 2018; Nativio et al., 2018). The limited literature that is available regarding histone modifications in AD points towards depletion of certain histone modifications at putative enhancers and promoters associated with synaptic plasticity along with enrichment at immune response genes (Gjoneska et al., 2015), and genome-wide depletion of H4K16ac and H4K12ac (both indicative of transcriptional activity) at transcriptional start sites (TSS) (Benito et al., 2015; Nativio et al., 2018). An early ChIP-seq study by Gjoneska, et al., (2015) was a significant advance for the field at the time, performing ChIP-seq and RNA-seq of hippocampal homogenate in CK-p25 inducible neurodegeneration mouse model measuring H3K4me1, H3K4me3, H3K9me3, H3K27me3, H3K27ac, H3K36me3 and H4K20me1 (Gjoneska et al., 2015). The CKp25 mouse model accumulates plaques rapidly with dense accumulation 6 weeks after induction of p25. There was widespread downregulation of genes involved in synaptic plasticity by 6 weeks post p25 induction, and widespread enrichment of H3K4me1 and H3K27ac at both promoters and enhancers for genes associated with immune activity and stimuli response, that was present at pre-symptomatic timepoints (2 weeks post-induction of p25) (Gjoneska et al., 2015). Interestingly, Gjoneska noted only a small number of peaks were present for polycomb-repressed regions labelled by H3K27me3 (Gjoneska et al., 2015). A seminal study by Benito and colleagues (2015) used a combination of FACS and ChIP-seq in 3-month and 20-month APP/PS1-21 mice to analyse histone modifications in neurons from the hippocampus. The authors report that Aβ plaque accumulation resulted in both depletion of H4K12ac and transcriptional loss of genes associated with synaptic plasticity (Benito et al., 2015). This loss

of synaptic plasticity associated transcripts occurred in conjunction with impaired synaptic function, inflammation, and behavioral deficits in APP/PS1 mice (Benito et al., 2015). Histone deacetylase inhibitor (SAHA) administration was able to alleviate behavioral deficits and reduce inflammation and partially restore H4K12ac marking in neurons but not glia (Benito et al., 2015). However, SAHA did not reduce plaque load in 20-month-old APP/PS1 mice (Benito et al., 2015). Nativio, et al., (2018) has demonstrated genome-wide depletion of H4K16ac from the post-mortem human lateral temporal lobe compared to age-matched controls (Nativio et al., 2018). This study also characterized age associated epigenetic changes as well as disease related changes and correlated H4K16ac marking with pathology load, leading to the identification of three separate classes of change in H4K16ac marking; age-regulated, age-dysregulated and age-independent changes, many of which overlapped AD-associated quantitative trait loci curated from previous genome-wide association studies, with 143 age-regulated, 231 age-dysregulated and 220 disease specific overlaps (Nativio et al., 2018). A recent genome-wide study of H3K27ac (active enhancers; indicative of activation) identified 4162 sites of differential enrichment between post-mortem entorhinal cortex from AD cases and age-matched control cases (Marzi et al., 2018). H3K27ac was increased in promoter and enhancer regions of genes associated with AD, including *Mapt*, *App*, *Ps1*, and *Ps2* (Marzi et al., 2018). In accordance with other recent literature, genome-wide analysis of H3K9ac (indicative of activation) with ChIP-seq in the prefrontal cortex of post-mortem AD cases have shown that tau, but not Aβ correlates with altered H3K9ac profile at promoters and enhancers (Klein et al., 2019). This study detected 5990 differentially H3K9ac marked sites leading to transcriptional changes in AD measured by RNA-seq (Klein et al., 2019). While the knowledge of the histone modifications in AD is expanding, further research is required to generate comprehensive multilayered epigenetic maps, particularly in specific cell types in AD.

Table 1.2: Histone modifications, HAT and HDAC in Alzheimer's disease

Author (year)	Methodology	Tissue source	Key findings
Benito, et al., (2015)	FACS/ChIP-seq RNA-seq	Hippocampal neurons APP/PS1-21 mice	Loss of H4K12ac in neurons of hippocampus. Associated with impaired synaptic function, increased inflammation
Francis, et al., (2009)	Western blotting, patch clamp	APP/PS1 mouse hippocampus	Global loss of histone H4 in APP/PS1 mice. HDACi improved histone acetylation and improved behavioural deficits and long-term potentiation
Gjoneska, et al., (2015)	ChIP-seq/RNA-seq	CKp25 mouse hippocampus	Changes to histone landscape at promoters and enhancers. Increased transcription of genes associated with immune response, decreased expression genes associated with synaptic plasticity.
Govindarajan, et al., (2013)	qPCR, immunoblot, immunohistochemistry	APP/PS1-21 with HDAC6 KO Hippocampal culture	HDAC6 KO restores behavioural deficits in APP/PS1-21 mice
Graff, et al., (2012)	Immunohistochemistry, Western blot	CKp25 mouse CA1 hippocampus	HDAC2 increased in neuronal nuclei of CA1 hippocampus of AD mice
Hendrickx, et al., (2014)	ChIP-qPCR, qRT-PCR,	APP mice prefrontal cortex and hippocampus	APP+ mice have decreased histone H4, APP- mice showed increased H4K5ac and H4K12ac at the same promoters. APP- mice have reduced capability to learn, and associated hypoacetylation
Klein, et al., (2019)	ChIP-seq, RNA-seq	Human prefrontal cortex	Tau, but not Aβ, correlates with altered H3K9ac profile and leads to transcriptional
Koldamova, et al., (2014)	ChIP-seq	APP23 mouse pooled forebrain	EGR1 correlates with histone methylation and acetylation. Total levels of EGR1 were reduced in APP23 mice when compared to WT controls. Depletion in AD risk loci: *Picalm, Ps2, App*
Marzi, et al., (2018)	ChIP-seq	Human entorhinal cortex	4162 H3K27ac marked sites differentially enriched in AD: 35% were enriched for H3K27ac marking, while 65% were depleted for H3K27ac marking. H3K27ac associated with Aβ and tau pathology.
Mastroeni, et al., (2015)	Immunohistochemistry, Western blot	Human middle temporal gyrus, hippocampus, midbrain	H3K4me3 labelling moves from nucleus to cytoplasm in – correlates with Braak staging
Narayan, et al., (2015)	Immunohistochemistry	Human inferior temporal gyrus	Correlations between total histone H3, total histone H4, H3ac and H4ac with GFAP, tau and Aβ load, hyperacetylation of neurons labelled with NeuN
Nativio et al., (2018)	ChIP-seq	Human lateral temporal lobe	AD associated loss of H4K16ac, associated with dysregulation of REST, programmed cell death and immune response. i

1.15 Limitations and challenges of current epigenetic approaches

There are many challenges to address with the current techniques available to analyse epigenetic alterations in AD. There is a lack of cell type, brain region, or cortical layer specific quantitative analysis in immunohistochemical studies within the literature (Bradley-Whitman & Lovell, 2013; Chouliaras et al., 2013; Coppieters et al., 2013; D. Mastroeni et al., 2010). Meanwhile, there have been few true genome-wide studies of epigenetic alterations in AD (Sanchez-Mut et al., 2016; J. Zhao et al., 2017; Michael J Ziller et al., 2013; M. J. Ziller et al., 2013). Most DNA methylation studies have performed HumanMethylation 450K or similar arrays (Bakulski et al., 2012; Chibnik et al., 2015; P. L. De Jager et al., 2014; Gasparoni et al., 2018; Lunnon et al., 2014) that are not genome-wide but provide a reference of candidate loci across the genome and as a result do not assess many CpG sites and intergenic regions. WGBS addresses this by analyzing at base pair resolution throughout the entire genome, however, there have been few studies to date to incorporate WGBS into their experiments (Sanchez-Mut et al., 2016; J. Zhao et al., 2017; M. J. Ziller et al., 2013). While new research is incorporating a range of single-cell RNA-seq, ChIP-seq and WGBS technologies to show ever increasing complexity of the epigenetic landscape, as illustrated by DeJager and colleagues' (2018) landmark multi-omics map of the frontal cortex in the aging and AD brain (Philip L. De Jager et al., 2018). However, there are still many factors that need to be taken into consideration when performing these experiments including sequencing depth and analytical methods. Many genomic regions are still difficult to sequence with current technology producing artifacts in output and therefore, are excluded from many analyses (Consortium, 2012). There are few bioinformatics based pipelines for addressing biological replicates (A. T. L. Lun & Smyth, 2016; M. D. Robinson, McCarthy, & Smyth, 2010), and there are few standardized procedures that recognize inter-individual variation between samples (Landt et al., 2012). There are also impeding issues in cost for genome-wide next-generation sequencing in large experiments.

Advances in cell sorting, multiplexed ChIP-seq, and single-cell WGBS have provided new resolution at a cell-type specific and genome-wide level (Luo et al., 2017), and studies are now using such methodologies to characterize the aging and AD brain (Nativio et al., 2018). The vast majority of studies investigating epigenetic changes in AD have used whole brain homogenate (Bakulski et al., 2012; P. L. De Jager et al., 2014; Gjoneska et al., 2015; Koldamova et al., 2014; Lunnon et al., 2014; Marzi et al., 2018; Nativio et al., 2018; Sanchez-Mut et al., 2014; Sanchez-Mut et al., 2016; Siegmund et al., 2007; J. Zhao et al., 2017; M. J. Ziller et al., 2013), including a mixture of neuronal and glial cell types. Two studies have

performed next-generation sequencing in neurons and glia (Benito et al., 2015; Gasparoni et al., 2018), potentially masking neuron specific changes to the epigenome. Indeed, the isolation of neurons demonstrated differential methylation between neurons and glia with increasing Braak stage in the occipital cortex (Gasparoni et al., 2018), while neurons were selectively depleted for H4K12ac marking with increasing age and in AD (Benito et al., 2015). Histone deacetylase inhibitors were able to selectively reinstate H4K12ac marking in neurons. These two studies highlight the importance of generating cell type specific epigenetic data to understand how AD impacts vulnerable or disease resistant cell types.

Many questions remain unanswered in the burgeoning field of epigenetics and Alzheimer's disease. Studies have shown that the epigenome is both region and cell-type specific (Luo et al., 2017), however it is not known whether different cortical regions exhibit differential DNA methylation or histone modification patterns in AD. Although initial studies have shown that neurons and glia exhibit different epigenetic landscapes in AD (Benito et al., 2015; Gasparoni et al., 2018), there have been no studies of the epigenome in neuronal sub-types that are vulnerable or resistant to AD pathology. Finally, despite the correlations with Braak or neuritic plaque load, it is still unknown whether epigenetic alterations in AD are an early consequence or are causal for disease pathogenesis (review: (Lord & Cruchaga, 2014b)).

Aims & Hypothesis

Alzheimer's disease is a terminal condition and affects the lives of more than 26 million people globally and is estimated to impact more than 100 million people by 2050 (Brookmeyer, Johnson, Ziegler-Graham, & Arrighi, 2007). Despite current research, there is little understanding of the onset and progression of sporadic AD, which account for ~90% of all AD cases. Known familial gene loci, including *PS1, PS2, APOE,* and *APP,* are involved in familial AD onset and progression. In the absence of highly penetrant risk alleles, epigenetic alterations are well poised to contribute to the pathogenesis and progression of AD, but this role is yet to be fully explored. Despite the key role epigenetics has in the regulation of the genome, there have been relatively few studies that have characterised the epigenome of neurons, neither in the healthy aging brain nor in neurodegenerative diseases. With this in mind, there is a need to incorporate a range of techniques to characterise epigenetic alterations in AD including quantitative immunohistochemistry at a cell-type specific and layer specific level and genome-wide next-generation sequencing.

Hypothesis

The hypothesis for this PhD study is that the epigenome will be cell-type specific, and the neuronal epigenome will evolve with age and be dysregulated in AD.

The research in this thesis will characterise DNA methylation in post-mortem human AD brains in a cell type specific manner, and will characterise key histone modifications in neurons across a time-course of healthy aging, and in a model of AD with the following three aims:

Aim 1: Characterise DNA methylation of specific cell types in Alzheimer's disease

Assess global alterations in common DNA methylation marks in specific cell types in post-mortem human control, early-sporadic AD, and late-sporadic AD cases using immunohistochemistry. Studies have implicated DNA methylation alterations through the progression of AD, however few have performed quantitative analysis in a cell-type specific manner, or quantified changes in tandem with AD pathology. With this in mind, the aim of this study was to investigate global alterations in DNA methylation (5mC) and DNA hydroxymethylation (5hmC) in different neuronal and glial cell types including neurofilament-labelled pyramidal neurons, calretinin positive interneurons, microglia and astrocytes using immunohistochemistry in post-mortem human tissue in early-sporadic AD (Braak stages I-III) and late-sporadic AD (Braak stages IV-VI) cases compared to age matched controls. This study also investigated whether the cells adjacent to Aβ plaques or tangle-bearing neurons were more susceptible to global alterations in DNA methylation. Immunohistochemistry is the only technique available to date that can determine global DNA methylation changes in specific sub-types of neurons and glia in the human brain, including changes in cells relative to AD pathology.

Aim 2: Charting histone modifications in neurons across aging

Generate temporal maps of histone modifications in aging neurons using ChIP-seq. Aging is widely accepted as the greatest risk factor for AD, however, there have been few studies to characterise histone modifications in neurons in the aging brain. Hence, this study characterised histone modifications in neurons from 3- , 6- , 12- , and 24-month old C57/BL6 mice using chromatin immunoprecipitation and next generation sequencing (ChIP-seq). These timepoints corresponded to juvenile, young, adult and old mice and enabled the assessment of the alterations in neuronal histone modifications to occur as the result of healthy aging. Neuronal nuclei were purified by fluorescence activated cell sorting with NeuN from the forebrain of C57/BL6 mice. The histone modifications examined included those that commonly mark enhancers (H3K27Ac) and promoters (H3K4me3). The ChIP-seq technique allowed for the generation of temporal maps of active and repressive epigenetic marks and whether alterations exist at gene regulatory regions (gene promoters/enhancers) in early life and how histone modifications evolve throughout aging.

Aim 3: Identifying histone modification alterations in neurons in Alzheimer's disease mice

Generate temporal maps of histone modifications in neurons in a mouse model of AD using ChIP-seq. There have been four studies to date investigating histone modifications at base-pair resolution in AD, with most performing ChIP-seq on a single histone modification, and few have characterised histone modifications in specific cell-types. Hence, this study characterised histone modifications in neurons from 3- , 6- , and 12-month old APP/PS1 mice and age-matched wild-type control mice using Chromatin Immunoprecipitation and next generation sequencing (ChIP-seq). These timepoints corresponded to pre-pathology, pathology onset and dense-pathology time points in the APP/PS1 model and enabled the assessment of the earliest neuronal histone modification alterations to occur in this mouse model of amyloidosis. Neuronal nuclei were isolated by cell sorting with NeuN from the forebrain of APP/PS1 and wild type mice. This study generated temporal maps of histone modifications that commonly mark enhancers (H3K27ac) and promoters (H3K4me3) across a time-course of amyloidosis in neurons.

Chapter 2: Methods

2.1 Human brain tissue sources and processing

Human post-mortem tissue was sourced from the Victorian Brain Bank Network (Melbourne, Victoria, Australia), and the South Australian Brain Bank (Adelaide, South Australia, Australia). Informed consent for the collection of tissue was obtained prior to death and institutional approval for the use in research was granted by the University of Tasmania's Human Research Ethics Committee, consistent with the Declaration of Helsinki (Tracey C. Dickson et al., 1999). Permission for brain autopsy and use for research was obtained by the original tissue sources. Tissue blocks of the inferior temporal gyrus were immersion fixed in 10% formalin, or perfusion fixed in picric acid and 4% paraformaldehyde. Tissue was stored in 0.01 PBS with 0.01% sodium azide (Table 2.1).

Human cases included the inferior temporal gyrus (ITG) of 5 control (mean age, age range; mean PMI, PMI range: 74.2±4.0 years, 58-84 years; 44.4±6.0 hours, 27-57 hours), 5 early-AD (80.6±2.8 years, 74-91 years; 49.2±5.2 hours, 32-68 hour) and 6-8 late-AD cases (76.5±2.7 years, 60-91 years; 30.2±6.0 hours, 5-65 hours; Table 2.1). Late-AD cases conformed to CERAD criteria (Murayama & Saito, 2004), and exhibited Braak stage IV-VI pathology (Braak & Braak, 1991). Control cases exhibited no AD pathology. Early-AD cases did not conform to CERAD criteria and were representative of Braak stage III pathology (Braak & Braak, 1991). There was no significant difference in the age or PMI of control, early-AD and late-AD cases.

2.2 Tissue sectioning

Blocks of human ITG were incubated in an 18% sucrose solution overnight, followed by a 30% sucrose solution (Appendix 1) overnight. Tissue was then submerged and frozen in Tissue-Tek Optimum Cutting Temperature (O.C.T) compound (VWR, Radnor, Pennsylvania, USA), and sections were cut coronally at 40µm on the Leica CM 1850 cryostat (Leica Microsystems, Wetzlar, Germany). Tissue sections were stored in 0.1% 0.01 PBS-azide tissue storage solution (Appendix 1).

Table 2.1: Human brain cases used for immunohistochemistry and analysis

Type	Source	Fixative	Cause of Death	PMI (hrs)	Sex	Age	Plaque Load (% Area)	NFT Density (/mm^2)
AD	VBBN	Formalin	mesothelioma	64	F	91	4.83	52.0
AD	VBBN	Formalin	COAD	65	M	60	9.95	21.3
AD	VBBN	Formalin	Respiratory	31	M	67	10.48	35.1
AD	VBBN	Formalin	Respiratory	24	M	79	2.75	19.7
AD	VBBN	Formalin	Cardiac	24	M	81	4.50	20.2
AD	SABB	PFA & picric acid	AD	13	F	71	6.10	24.5
AD	SABB	PFA & picric acid	AD	26	F	76	9.40	44.2
AD	SAAB	PFA & picric acid	AD	5	F	83	4.05	56.7
AD	SABB	PFA & picric acid	Heart failure	17	F	84	7.58	32.0
AD	SABB	PFA & picric acid	Pneumonia	34	M	73	7.10	61.5
Early AD	VBBN	Formalin	Cardiac	32	M	74	0.35	-
Early AD	VBBN	Formalin	Cardiac	68	M	74	3.98	-
Early AD	VBBN	Formalin	Renal failure	48	M	91	0.05	-
Early AD	VBBN	Formalin	Cardiac	50	M	82	1.68	-
Early AD	VBBN	Formalin	MI	49	M	82	1.30	-
Control	VBBN	Formalin	Asthma	30	F	58	-	-
Control	VBBN	Formalin	PE, DVT	27	F	73	-	-
Control	VBBN	Formalin	Cardiac	54	M	77	-	-
Control	VBBN	Formalin	Respiratory	57	M	79	-	-
Control	VBBN	Formalin-	MI	55	M	84	-	-

SABB – South Australian Brain Bank; VBBN – Victorian Brain Bank Network; MI – myocardial infarction; PE - pulmonary embolism; DVT – deep vein thrombosis; COAD – chronic obstructive airways disease

2.3 Immunohistochemistry

Immunohistochemistry was performed to assess astrocytes, microglia, calretinin-positive interneurons, NF-positive pyramidal neurons, NFTs, Aβ plaques, 5mC and 5hmC marks (Table 2.2). Optimal concentrations were determined for each primary antibody, with positive control single-immunolabelling experiments performed for each antibody. Negative control experiments were performed, in which the primary antibody was omitted eliminating all immunosignal. The specificity of the rabbit polyclonal anti-5hmC antibody was verified with a mouse monoclonal 5hmC antibody (GTX629765, GenTex/Sapphire Bioscience, Michigan USA) which demonstrated analogous extranuclear immunofluorescence signal (Appendix 2: Supplementary Figure 1)

Tissue sections were incubated in 3% horse serum in 0.01M PBS for 60 minutes at room temperature, washed 3X in 0.01M PBS and incubated in primary antibodies (Table 2.2) diluted in 0.01M PBS-X (Appendix 1) for 24 hours at room temperature. Following 3X washes in 0.01M PBS, tissue sections were incubated with AlexaFluor488 and AlexaFluor594 (1:1000; Invitrogen/Life technologies, Carlsbad, CA) secondary antibodies diluted in 0.01M PBS-X for two hours at room temperature. Sections were washed 3X in 0.01M PBS and were mounted, dried, and coverslipped with DAKO fluorescent mounting medium (DAKO, USA). 90% formic acid was used as antigen retrieval for immunolabelling Aβ plaques (Tracey C. Dickson et al., 1999), while thioflavin-S staining (Sigma-Aldrich, Missouri, USA) was used to stain fibrillar plaques in conjunction with 5mC/5hmC and GFAP immunolabelling (T. C. Dickson & Vickers, 2001). The fluorescent signal was amplified *via* biotin/streptavidin immunofluorescence for the mouse anti-IBA1 antibody: immunolabelling was performed as detailed above, but following primary antibody incubation tissue sections were incubated in goat anti-mouse/rabbit biotinylated secondary antibodies (1:200, 5mg/mL; DAKO) in 0.01M PBS-X for two hours at room temperature, washed 3X in 0.01M PBS and incubated in Streptavidin AlexaFluor488 (1:500) diluted in 0.01M PBS for two hours at room temperature. Antibodies penetrated the entire depth of tissue sections, both with and without formic acid antigen retrieval; clear double immunolabelling with optimal intensity was present at a depth of 12.8-18.4µm in formic acid treated tissue sections and at a depth of 12.4-17.7µm in non-formic acid treated tissue sections.

Table 2.2: Antibodies

A summary of the primary antibodies utilised within this study:

Name	Epitope	Manufacturer	Catalogue number	Host species	Concentration
5hmC	5-hydroxy-methylcytosine	Active Motif (Carlsbad, CA, USA)	39769	Rabbit polyclonal	1:2000
5hmC	5-hydroxy-methylcytosine	GenTex/Sapphire Bioscience	GTX629765	Mouse monoclonal	1:2000
5mC	Modified base 5-methylcytidine	Active Motif (Carlsbad, CA, USA)	39649	Mouse monoclonal	1:500
Anti-human tau	Recombinant human tau C-terminal (AA243-AA441)	Dako (Glostrup, Denmark)	A 0024	Rabbit polyclonal	1:4000
AT8	PHF-tau (Ser202/Thr205)A	Thermo Scientific (Waltham, MA, USA)	MN1020	Mouse monoclonal	1:1000
Calretinin	Human calretinin-22k	Swant (Marley, Switzerland)	$6B_3$/010399	Mouse monoclonal	1:500
Calretinin	Recombinant rat calretinin	Millipore (Massachusetts, USA)	AB5054	Rabbit monoclonal	1:500
Ferritin	Ferritin 21kD/19kD (human spleen)	Abcam (Cambridge, MA, USA)	Ab7332	Rabbit polyclonal	1:1000
GFAP	GFAP isolated from cow spinal cord	Dako (Glostrup, Denmark)	Z 0334	Rabbit polyclonal	1:3000
GFAP	Clone 4A11	BD Bioscience	556327	Mouse IgG2b	1:500
IBA1	NP_001614, NP_116573	Abcam (Cambridge, MA, USA)	Ab5076	Goat polyclonal	1:250
NFL	Purified porcine NF-L	Millipore (Massachusetts, USA)	AB9568	Rabbit polyclonal	1:250
Pan-beta amyloid	Aβ 1-40 (aa15-30)	Invitrogen Molecular Probes (Carlsbad, CA)	44-136	Rabbit polyclonal	1:1000
6E10	Purified anti-β-amyloid, 1-16	Covance Antibody (Dedham, MA, USA)	SIG-39320	Mouse monoclonal	1:1000
SMI32	NFM and NFH-dephosphorylated	Covance Antibody (Dedham, MA, USA)	SMI-32R-500	Mouse monoclonal	1:500
NeuN (A60)	Anti Neuronal nuclei (A60)	Millipore (Massachusetts, USA)	MAB377	Mouse monoclonal	1:1000
H3K4me3	Histone 3 lysine 4 tri-methyl	Active Motif (Carlsbad, CA, USA)	39159	Rabbit polyclonal	2µg/ml (2µl per sample)
H3K27Ac	Histone 3 lysine 27 acetyl	Active Motif (Carlsbad, CA, USA)	39133	Rabbit polyclonal	2µg/ml (2µl per sample)
H3K27me3	Histone 3 lysine 27 tri-methyl	Millipore (Massachusetts, USA)	07-449	Rabbit polyclonal	2µg/ml (2µl per sample)

2.4 Autofluorescence quenching

Autofluorescence quenching was used to remove lipofuscin autofluorescence and lower background autofluorescence to enhance clarity for analysis. Free floating or mounted sections were incubated in potassium permanganate solution (Appendix 1) for 20 minutes at room temperature on an orbital shaker, before being washed twice in 0.01M PBS for two minutes at room temperature. Samples were then incubated in a solution containing potassium metabisulphite and oxalic acid (Appendix 1) for approximately two minutes to clear the potassium permanganate from the region of interest. Samples were then washed three times in 0.01M PBS for ten minutes at room temperature on the orbital shaker.

2.5 Microscopy

Cell counts were performed on a Leica DM LB2 fluorescent microscope (Leica microsystems, Wetzlar, Germany) for NF-positive pyramidal neurons and NFTs. For astrocytes, microglia and calretinin-labelled interneurons cell counts were performed on images of whole tissue sections collected on Perkin Elmer's Ultraview VoX spinning disk confocal microscope (Nikon Ti Eclipse microscope (Minato, Tokyo, Japan), Yokogawa Electric Corporation CSU-X1 spinning disk confocal scanner (Musashino, Tokyo, Japan) and Volocity software 6.3 (Perkin Elmer, Massachusetts, USA). All image acquisition and cell counts were performed blinded to case type.

2.6 Immunohistochemistry image analysis

Cell counts were performed systematically by starting at the edge of tissue section in the appropriate layer of the ITG at a Z plane (between 12.4-18.4µm depth) in the tissue corresponding to clear double-immunolabelling, and counting the first 50 cells encountered on that Z plane in the correct cortical layer. Cells were defined as having extranuclear labelling if any labelling for 5mC or 5hmC was observed in the cytoplasm of the cell outside of the nucleus.

Neurofilament positive pyramidal neurons: 50 NF-positive pyramidal neurons in layers 2/3 and layer 5 were counted with 5mC/5hmC co-localisation recorded, in each control (n=5), early-AD (n=5) and late-AD (n=8; n= 6, respectively) case.

Interneurons: Whole tissue sections were imaged. 50 calretinin-positive neurons were counted in layers 2/3; 25 calretinin-positive neurons were counted in layer 4 (due to the limited number of calretinin-positive cells in layer 4) with 5mC/5hmC labelling recorded in each control (n=5), early-AD (n=5) and late-AD (n=8) case.

Microglia: Whole tissue sections were imaged. 50 microglia were counted in layers 2/3 and in layer 4 with 5mC/5hmC co-localization noted in each control (n=5), early-AD (n=5) and late-AD (n=7) case.

Astrocytes: Whole tissue sections were imaged. 50 astrocytes were counted across cortical layers 2-6 with 5mC/5hmC co-localization noted in each control (n=5), early-AD (n=5) and late-AD (n=8) case.

NFTs: 50 NFTs in layers 2/3 and layer 5 were counted with 5mC/5hmC co-localisation recorded in early- and late-AD cases (n=7 and 6, respectively).

Aβ plaques and 5mC/5hmC nuclei: 10 plaques were imaged in layer 2/3 of late-AD cases (n=8) and 10 plaque-free zones were imaged in layer 2/3 of control (n=5) and late-AD cases (n=8). Images were obtained systematically, by starting at the edge of the tissue section and taking images of the first 10 isolated plaques or plaque free zones encountered in layer 2/3. 5mC and 5hmC labelled nuclei were counted in near-plaque donut shaped region of interest (ROI) that was 150% of the plaque diameter (Chapter 3 - Figure 6; (Mitew et al., 2013b). The average area of the near-plaque ROI was used to define equivalent plaque-free ROI ((Fernandez-Martos, King, Atkinson, Woodhouse, & Vickers; Mitew et al., 2013b).

Aβ plaque load: This analysis was performed as previously (Woodhouse et al., 2009); briefly four systematically selected 1200μm wide strips of the ITG from the pia to the white matter were imaged for each early-AD and late-AD case, and the percentage area occupied by Aβ plaques was then calculated (Image J, version 1.39p).

NFT density: This analysis was performed as previously (Woodhouse et al., 2009); briefly one systematically selected 1200μm wide strip of the ITG from the pia to the white matter was imaged for each late-AD case, the number of NFTs in the sampled area was counted and the NFT density calculated (Image J, version 1.39p). Representative images for figures were taken with a Perkin Elmer's Ultraview VoX spinning disk confocal microscope.

2.7 Immunohistochemistry Statistical Analysis

Image data was analysed in SigmaPlot (Version 12.0, Systat Software Inc.) with one-way ANOVAs; different post-hoc tests were performed depending on the distribution and normality of the data including: Kruskal-wallis one-way ANOVA on ranks and Holm-sidak one-way ANOVA. Statistical significance was defined as $p<0.05$. All data is presented as the mean with the standard error of the mean.

2.8 Mouse tissue source and processing

All animal procedures were undertaken with ethical approval from the Animal Ethics Committee of the University of Tasmania (A12780/A15120) and all experiments abided by the Australian Code of Practice for the Care and Use of Animals for Scientific Purposes (Council, 2013). The AD mouse model used for this study was the APP_{SWE}/PSENdE9 (APP/PS1) (B6.Cg-Tg(APPswe,PSEN1dE9)85Dbo/Mmjax; stock number: 34832-JAX). APP/PS1 mice and age matched wild-type control littermates were aged to 3 months (pre-pathology), 6 months (pathology onset), and 12 months (advanced pathology), with n = 5 biological replicates per genotype, per time-point. An additional cohort of 5 wild-type mice were aged to 24 months. Animals were housed in standard conditions (12hr day/night cycle, housing temperature of 20ºC, *ad-libatum* access to food). Mice were sacrificed with an intraperitoneal injection of Lethobarb (pentobarbitol) at 110mg/kg body weight. Animals were tested for pain response before undergoing cardiac perfusion with 0.01M PBS (Appendix 1). The forebrain was then rapidly dissected and snap frozen in liquid nitrogen after perfusion ready for downstream processing.

2.9 Genotyping

Genotyping was performed as previously described (Collins, King, Woodhouse, Kirkcaldie, & Vickers, 2015). Tail clippings were taken from mice at weaning for initial genotyping, and at perfusion for replicate genotyping of all animals. Tails were incubated in 45µL of extraction solution (95091-025, QUANTA Biosciences, Beverly, Massachusetts, USA) for 30 minutes at 95°C to extract genomic DNA. Genotypes were identified by PCR using MyTaq Red Mix (BIO-25044, Bioline, London, UK) and primers (GeneWorks, Thebarton, South Australia,

Australia) to amplify PS1 and an internal control gene (IL-2) as per the manufacturer's protocol. PCR products were electrophoresed against Hyperladder V 100bp ladder (BIO-33031, Bioline, London, UK) on a 2% agarose gel (BIO-41025, Bioline, London, UK) containing 0.0001% SYBR safe DNA gel stain (S33102, Invitrogen, Thermo Fisher Scientific, Waltham, Massachusetts, USA) at 110V for 4five minutes and imaged using the Amersham Imager 600 (GE Healthcare Life Sciences, South Logan, Utah, USA) image station.

2.10 Isolation of neuronal nuclei

Squares ($2cm^2$) of cheesecloth (9338918004577, Ogilvies Designs, Belmont, Western Australia, Australia) were pre-soaked in nuclei extraction buffer (NEB) (Appendix 1) and placed in 15ml falcon tubes (Thermo Fisher Scientific, Waltham, MA, USA) until required. Fresh-frozen mouse forebrains were sectioned along the midline, and half of the forebrain was immersed in 4.8mL of freshly prepared NEB, while the other half of the forebrain was frozen for future analysis. The forebrain was then homogenised on ice using a dounce tissue homogeniser (357544, Wheaton, Millville, New Jersey, USA) for one minute with a loose-fitting pestle with 0.114mm clearance. Homogenised tissue was then filtered through four layers of cheesecloth, followed by 70µm and 40µm Falcon cell strainers (Thermo Fisher Scientific, Waltham, MA, USA) on ice. Homogenate was then centrifuged at 500g for minutes at 4ºC and the supernatant was then discarded. The nuclei pellet was resuspended in 5mL of 0.22µm filtered 0.01M PBS, centrifuged at 500g for five minutes at 4ºC, and the pellet resuspended in 500µL 0.01M PBS for downstream processing. 10µL of each sample was diluted 1:5 in 0.01M PBS, then diluted 1:1 with trypan blue (15250061, Thermo Fisher Scientific, Waltham, MA, USA). Haemocytometer counts were performed to calculate the number of nuclei per sample and to ensure a consistent number of nuclei were being isolated between samples.

2.11 Neuronal nuclei immunolabelling

To provide secondary antibody only control solutions for downstream nuclei sorting, 50µL of each nuclei sample was incubated with Alexafluor 647 at 1:2000 (A31571, Invitrogen/Life technologies, Carlsbad, CA, USA), 10µL of blocking solution containing 0.5% BSA (B4287-25G, Sigma-Aldrich, St Louis, Missouri, USA), 10% normal goat serum (G9023-10, Sigma-

Aldrich, St Louis, Missouri, USA), and 35µL 0.01M PBS, for a total of 100µL on a slow rotator in the dark for 40 minutes at 4ºC. DAPI working stock (10µL; Appendix 1) was added to the secondary antibody solution for the last five minutes of the incubation. For primary samples, mouse anti-NeuN antibody (A60) (MAB377, Merk Millipore, Billerica, Massachusetts, USA) at 1:1000 (Table 2.2) was conjugated with donkey anti-mouse AlexaFluor 647 secondary antibody at 1:2000 (1:10 stock was prepared previously for accurate pipetting) (A31571, Invitrogen/Life technologies, Carlsbad, CA, USA), 100µL 0.5% BSA (B4287-25G, Sigma-Aldrich, St Louis, Missouri, USA) and 10% normal goat serum (G9023-10, Sigma-Aldrich, St Louis, Missouri, USA), and 394µL 0.01M PBS for a total of 500µL. Primary antibody solutions were incubated for five minutes at room temperature on an orbital shaker in the dark. 50µL 0.01M PBS was added to the remaining nuclei, then combined with the preconjugated block/NeuN/AlexaFluor 647 solution for a total volume of 1000uL and incubated for 40 minutes at 4ºC on a slow rotator in the dark. After 40 minutes, the nuclei solution was centrifuged at 500g for five minutes at 4ºC, the supernatant was discarded and the sample was then resuspended in 1000µL ice cold 0.01M PBS for further experimentation.

2.12 Fluorescence activated cell sorting

Fluorescence activated cell sorting (FACS) was performed on a BD Biosciences FACSAria III (Becton Dickinson Biosciences, Franklin Lakes, NJ, USA). Falcon tubes (15mL; Thermo Fisher Scientific, Waltham, MA, USA) were coated with a small amount of foetal calf serum (SH30084.02, Hyclone, GE Healthcare Life Sciences, South Logan, Utah, USA) prior to use. DAPI and secondary antibody only negative control samples were used to identify nuclei on fluorescence and forward/side scatter plots to eliminate cellular debris, and to set a threshold for background secondary antibody fluorescence for each sample (Figure 2.1a,c). Doublet discrimination was set (Figure 2.1b). NeuN labelled samples were then sorted with the established gates (Figure 2.1c-f). Sample purity was determined by re-running a small amount of sorted sample through the FACS. Sorted samples all exhibited >97% purity from their respective gates. NeuN+ and NeuN- samples were collected, fixed in 1% methanol-free formaldehyde (28906, Pierce, Thermo Fisher Scientific, Waltham, MA, USA) for 1five minutes at room temperature then quenched with 0.125M glycine (G8898, Sigma-Aldrich, Missouri, USA) for five minutes at room temperature, prior to freezing at -80ºC for downstream processing. Parameters for FACS were extensively optimised, including testing:

multiple nozzle sizes (70µM, 100µM, 130µM), sheath pressures, primary and secondary antibody concentrations, secondary fluorophores (AlexaFluor 488, 546, 594, 647), nuclei solution concentration, forward/side-scatter gating strategies, blocking solutions, and testing jet-in-air and cuvette-based flow cytometers. To assess whether NeuN expression alters across aging, the number of NeuN+ nuclei from the FACS results was analysed, showing that there was no significant difference in the number of neuronal nuclei collected between time-points for WT mice (3 months old: $2.75x10^6 \pm 0.15$ nuclei, 6 months old: $2.59x10^6 \pm 0.13$ nuclei, 12 months old mean: $2.51x10^6 \pm 0.04$ nuclei, 24 months old: $2.149x10^6 \pm 0.18$; all mean±SEM) (One way ANOVA, p=>0.05, Tukey's multiple comparisons test). To confirm the differences between whole forebrain homogenate samples (n=3 per genotype, 12 months of age) and NeuN+ nuclei purified from the forebrain (n = 2 per genotype, 12 months of age). ChIP-qPCR was performed for H3K4me3, H3K27me3 and H3K27ac at known enhancers for AD risk factor genes and compared in wildtype and APP/PS1 mice demonstrating distinct differences between whole forebrain homogenate and isolated neuronal nuclei (Figure 2.2).

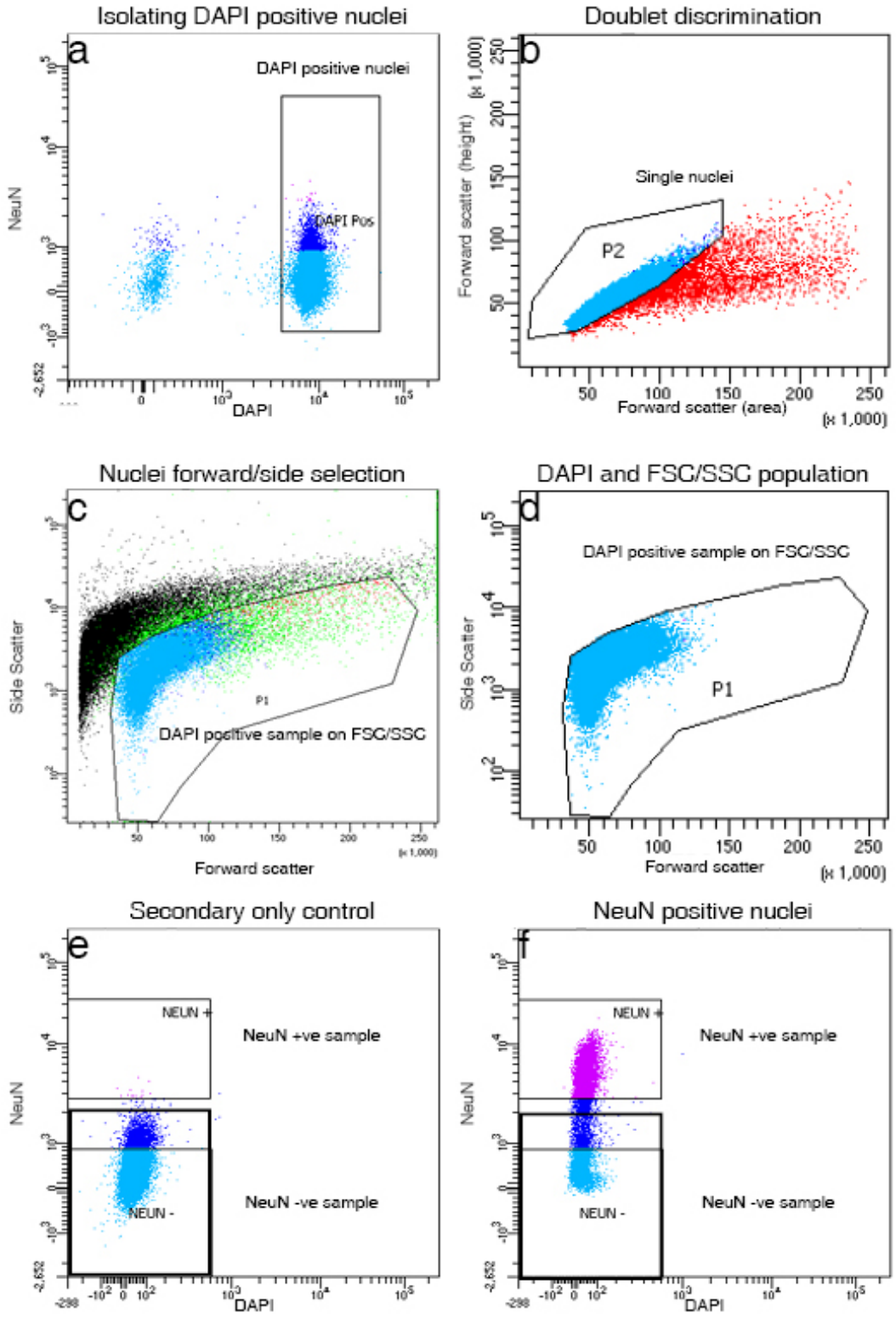
Isolating DAPI positive nuclei
a
DAPI positive nuclei
DAPI Pos
NeuN
DAPI
Doublet discrimination
b
Single nuclei
P2
Forward scatter (height)
(x 1,000)
Forward scatter (area)
(x 1,000)
Nuclei forward/side selection
c
P1
DAPI positive sample on FSC/SSC
Side Scatter
Forward scatter
(x 1,000)
DAPI and FSC/SSC population
d
DAPI positive sample on FSC/SSC
P1
Side Scatter
Forward scatter
(x 1,000)
Secondary only control
e
NEUN +
NeuN +ve sample
NEUN -
NeuN -ve sample
NeuN
DAPI
NeuN positive nuclei
f
NEUN +
NeuN +ve sample
NEUN -
NeuN -ve sample
NeuN
DAPI

Figure 2.1: Gating strategy for isolation of neuronal nuclei

(a) DAPI labelled nuclei and, (b) doublet discrimination used to determine pure, single nuclei sub-population on (c) forward scatter (linear) and side scatter (log). (d) Forward scatter and side scatter gate for DAPI + nuclei were used to gate out debris. (e, f) Gating strategy applied to NeuN labelled sample to reduce the amount of debris collected in sorted samples and NeuN fluorescence determined from secondary only gate. (f) The distance between NeuN negative and positive gates was placed to maintain purity of the sorted populations.

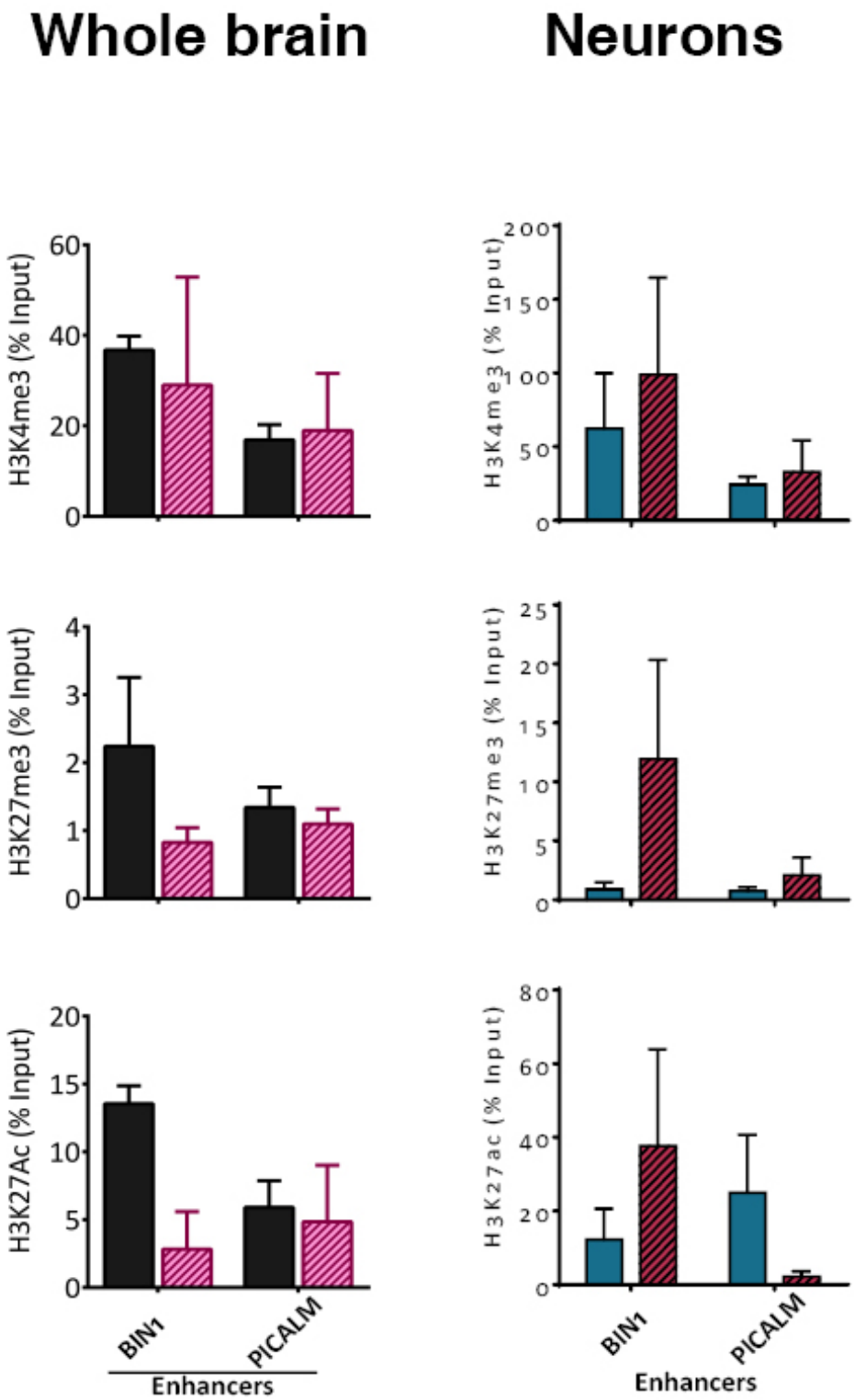
Whole brain
Neurons
H3K4me3 (% Input)
60
40
20
0
200
150
100
50
0
H3K27me3 (% Input)
4
3
2
1
0
25
20
15
10
5
0
H3K27Ac (% Input)
20
15
10
5
0
80
60
40
20
0
BIN1
PICALM
Enhancers
BIN1
PICALM
Enhancers

Figure 2.2: Difference in histone marking between whole brain homogenate and purified neuronal nuclei in wild-type mice and APP/PS1 mice.

Differential enrichment was detected for H3K4me3 (top), H3K27me3 (middle) and H3K27ac (bottom) between chromatin from whole forebrain (left) and neuronal nuclei purified from forebrain (right) in both wildtype (black/blue) and transgenic AD (pink/red) mice. Data = % total input. Bar, mean ± SEM, n=3 whole brain, n = 2 for neuronal nuclei purified from forebrain

2.13 Sonication

Sorted neuronal nuclei (NeuN+) were pelleted in at 52000g, 4ºC for 25 minutes using the Sorvall WX Ultra 90 ulracentrifuge and TH-641 swinging bucket rotor (54295, Thermo Fisher Scientific, Waltham, MA, USA). Nuclei pellets were resuspended in 300µL of SDS lysis buffer (Appendix 1) and transferred to 1.5ml Bioruptor+ TPX microtubes (C30010010-300, Diagenode, Seraing, Belgium) for sonication. Sonication was optimised to obtain DNA fragments between 200-500bp length. Sonication was performed on a Bioruptor Plus next-gen ultrasonicator (Diagenode, Seraing, Belgium) under the following conditions: 10 cycles of 30s on/30s off, repeated 5 times, replacing ice-water every 10 cycles. Fragment size was confirmed using a sample of purified DNA electrophoresed on a 2% agarose gel and additionally tested on a Agilent 4200 tape-station (Agilent Technologies, California, USA). After sonication, samples of 500,000 nuclei were aliquoted for chromatin immunoprecipitation (ChIP) experiments.

2.14 DNA purification

DNA samples were purified using the following protocol modified from (Sambrook & Russell, 2006). Samples (300µL in 0.01M PBS) were incubated with 1µL Proteinase K (50µg/mL (MPRK092, Epicentre, Middleton, Wisconsin, USA) per 200,000 nuclei at 65ºC overnight. Equal volume of phenol:chloroform solution (P0269-100M, Sigma-Aldrich, Missouri, USA) was added to each sample and vortexed for one minute until an emulsion formed. Samples were then centrifuged at 6,000g for five minutes at room temperature. The aqueous layer was collected and combined with 2.5 volumes of ethanol (E7023-1L, Sigma-Aldrich, Missouri, USA). Sodium chloride (NaCl) was added to 0.3M final concentration in the sample solution. Samples were precipitated overnight at -20ºC. Samples were then centrifuged at 16,000g for 30 minutes to pellet purified DNA. The supernatant was discarded, the pellet was washed in 70% ethanol and centrifuged at 16,000g for five minutes. The pellet was then dried at room temperature five minutes to remove residual ethanol. Samples were then resuspended in 20µL filtered TE buffer (Appendix 1) or sterile water.

2.15 Chromatin immunoprecipitation

Chromatin immunoprecipitation (ChIP) was performed as previously described (Oakford et al., 2010; P. C. Taberlay et al., 2011; Phillippa C. Taberlay et al., 2014) with minor modifications. Briefly, samples containing approximately 500,000 nuclei were adjusted to 1mL with IP dilution buffer (Appendix 1), mixed gently by pipetting and 1% of the total sample was removed for total input control samples (TI) and frozen at -20ºC. Antibodies utilised for ChIP-seq experiments included: anti-H3K4me3 (39160; Active Motif, Carlsbad, CA, USA), anti-H3K27me3 (07-449; Millipore Massachusetts, USA) and anti-H3K27ac (39134; Active Motif, Carlsbad, CA, USA). All antibodies have been previously validated for specificity and use in ChIP assays. All samples (n = 35) were processed in parallel for each ChIP antibody to eliminate batch effects. Samples were incubated with primary antibodies overnight at 4ºC with rotation with a concentration of 2µg or 2µL of antibody per sample. Samples were then incubated with 20µL ChIP grade magnetic A/G beads (26162, Pierce, Thermo Fisher Scientific, Waltham, Massachusetts, USA) for two hours at 4ºC with rotation. Samples were then placed on a MagnaRack (CS15000; Invitrogen/Life technologies, Carlsbad, CA, USA) for one minute and supernatant was removed. Samples were washed in 1mL low salt wash buffer (Appendix 1) for three minutes at room temperature. After incubation samples were placed on a magnetic rack for one minute, and supernatant was removed and discarded. This process was repeated for one high salt buffer wash, one LiCl buffer wash, and two TE buffer washes (Appendix 1). After the final TE buffer wash, samples were incubated for 1five minutes at room temperature in 50µL of freshly prepared ChIP elution buffer (Appendix 1). The supernatant was collected and the elution step was repeated with an additional 50µL ChIP elution buffer for a total volume of 100µL. Chromatin samples and TI control samples were then incubated with 4µL 5M NaCl and 1.5µL (50µg/mL) Proteinase K (MPRK092, Epicentre, Middleton, Wisconsin, USA) overnight at 65ºC to reverse crosslinks. RNase A (1µL of 10mg/mL; EN0531, Thermo Fisher Scientific, Waltham, Massachusetts, USA) was then added to each sample and incubated for 1 hour at 37ºC. ChIP samples and TI control samples were further purified using the Chromatin IP DNA Purification Kit (58002, Active Motif, Carlsbad, California, USA) according to the manufacturer's instructions, and eluted in 50µL of elution buffer. ChIP experiments were performed for 500,000 nuclei for H3K4me3, H3K27ac, and in technical duplicate for H3K27me3. H3K27me3 ChIPs were pooled prior to library preparation for a total of approximately 1000000 nuclei.

Next-generation sequencing

2.16 Library preparation

Libraries were prepared using the Nugen Ovation Ultralow V2 (0347 V2 1-96/0344 V2 1-16, Redwood City, CA, USA) library preparation kits as per the manufacturer's protocol with minor modification. Cycling conditions for PCR amplification were optimised using EvaGreen dye 20X (31000-T, Biotium, Fremont, CA, USA), with H3K27ac samples amplified for 17 cycles, H3K4me3, H3K27me3 and total input control samples amplified for 18 cycles.

2.17 Sequencing

Libraries were subjected to quality control and normalisation with the Agilent 4200 tape-station system and D1000 tapes (Agilent, Santa Clara, CA, USA), and qPCR analysis performed at Australian Genomics Research Facility. Illumina flow-cell adaptors were added prior to sequencing (Illumina, San Diego, CA, USA). An equal amount of DNA was added from each sample to normalise all samples across the flow lanes. Samples were sequenced on the Illumina Hi-Seq 2500 Next-Generation-Sequencer (Illumina, San Diego, CA, USA) using 50bp single-end sequencing parameters. Primary image analysis was performed in real time by HiSeq Control Software v2.2.68 and Real Time Analysis v 1.18.66.3. The Illumina bcf2fastq 2.20.0.422 pipeline was used to generate FASTQ files for downstream analysis. Prior to sequencing, all samples from H3K27ac and H3K4me3 were pooled to minimise batch effects and all sequenced equally across 7 lanes. Mean sequencing depth for these samples was 29,235,684 single-end reads with a range of 14,772,920 – 52,363,200 single-end reads (Table 2.3). H3K27me3 samples were similarly pooled to minimise lane effects, then sequenced over 7 lanes. Mean sequencing depth for H3K27me3 was 54,193,632 single-end reads with a range of 39,039,879 – 65,999,514 single-end reads (Table 2.3). An input control was sequenced from one sample of each time-point and genotype. The input control samples were and sequenced across one lane, with mean sequencing depth of 37,412,073 single-end reads and a range of 35,141,517 – 41,405,294 single-end reads.

Table 2.3: ChIP-seq sequencing depth

A summary table of the sequencing depth for each histone modification used in this study:

Samples	Minimum read depth	Maximum read depth	Mean read depth
H3K27ac	9,576,466	24,491,555	16,223,033
H3K27me3	26,531,221	45,023,509	34,992,581
H3K4me3	9,670,943	23,040,946	13,921,824

Bioinformatic analysis

The bioinformatic analysis included in the results chapter of this thesis required extensive optimisation. Included below is the final parameters used for each part of the analysis.

2.18 Sample pre-processing

FASTQ files generated from Illumina HiSeq 2500 were imported onto the Nectar research cloud for all processing running Ubuntu 16.0.4.3 LTS Xenial Server Edition. Raw reads were checked for quality control with FASTQC version 0.11.7 and MultiQC (Andrews, 2010; Ewels, Magnusson, Lundin, & Kaller, 2016). Illumina flow-cell adaptors were trimmed from all sequences using the Trim Galore wrapper version 0.4.3 for Cutadapt (version 1.15) (Martin, 2011). Nugen Ovation Ultralow v2 adaptors were trimmed from individual samples with Cutadapt (Martin, 2011) prior to sequence alignment. Any samples not meeting quality control standards were removed from further analysis.

2.19 Sequence alignment

Bowtie2 is a highly efficient hardware accelerated alignment tool frequently utilised in read mapping for ChIP-seq experiments (Langmead & Salzberg, 2012). ChIP-seq samples were aligned with Bowtie2 version 2.3.4 Linux distribution (accessed 30/1/2018). Samples were mapped to *Mus musculus* reference genome mm10 (accessed 08/12/2017 at UCSC http://hgdownload.cse.ucsc.edu/downloads.html#mouse) using default parameters (Waterston et al., 2002). The mean percentage of aligned reads was 95.63%, with a minimum of 87.41%. Samples containing more than 9.5 million uniquely aligned reads were utilised for downstream analysis. After mapping, samples were converted to BAM file format and indexed with SAMtools version 1.7, then visualised with Integrated Genomics Viewer (IGV) version 2.4.8 (H. Li et al., 2009). Further quality control was performed with deepTools multibamSummary and plotPCA version 3.0, and bigwig files were generated with bamCompare for visualisation on IGV (Diaz, Nellore, & Song, 2012; Ramírez et al., 2016). Total input control samples were merged using SAMtools merge, then sorted and indexed prior to peak calling.

2.20 Pseudoreplicate generation

Two pseudoreplicates were generated for each time-point and genotype (Gjoneska et al., 2015; Landt et al., 2012) prior to performing differential enrichment analysis. Biological replicates were merged into a single file using samtools merge, read with samtools view, shuffled and separated into files containing equivalent numbers of randomly distributed reads, then sorted with samtools sort utilising the following code (based off ENCODE IDR analysis):

```
samtools merge -u -@62
/NGS_Data/Andrew/Pseudoreplicate_BAM/H3K27me3_inter
mediate/H3K27me3_WT3_merged.bam *WT3*.bam

for file in *.bam ; do

echo ""$file" "is being processed...""

samtools view -H $(Akiyama et al.) >
${file}_header.sam

nlines=$(samtools view -@62 ${file} | wc -l)
#identify the number of reads in a bam file

echo "total number of reads:"

echo "$nlines"

nlines=$(( (nlines + 1) / 2 ))

samtools view -@62 ${file} | shuf - | split -d -l
${nlines} -
"/NGS_Data/Andrew/Pseudoreplicate_BAM/H3K27ac_inter
mediate/test/${file}_pseudo.sam"

done
```

2.21 Peak Calling

Peaks were called for H3K4me3 and H3K27ac against a merged input control utilising MACS2 with a Q value cut-off of 0.05 (Yong Zhang et al., 2008). H3K27me3 peaks were also called with MACS2, with –broad option enabled to composite broad genomic regions into wider peaks and analysed with both Q value cut off of 0.05, and also a relaxed Q value cut-off of 0.01 as described in (Gjoneska et al., 2015). ENCODE blacklisted regions for mm10 (downloaded: 24/2/2018) were noted and removed from downstream analysis.

2.22 Differential enrichment analysis with CSAW

Differential enrichment analysis was performed within R using the ChIP-seq Analysis with Windows (csaw) package (A. T. L. Lun & Smyth, 2016). Briefly, mapped reads from pseudoreplicate samples were imported into csaw as bam files, setting the fragment size to 250bp as identified from sonication and tape-station quality control. The ENCODE mm10 blacklist file was imported and reads were filtered from blacklisted regions (Consortium, 2012). Reads were then counted into bins of 2000bp, then log count-per-million reads were filtered by an average of $\log_2(3)$ for H3K4me3, $\log_2(4)$ for H3K27ac, and $\log_2(2)$ for H3K27me3 to remove low abundance regions of non-specific binding. The background filtering was optimised for each histone modification to ensure removal of the bulk of background reads, subsequently increasing detection power and reducing multiple testing bias. Filtered reads were then binned into 10kb bins, and used for removal of library composition bias, and trended biases based on the scaling normalisation strategy of trimmed mean of M values (TMM) from EdgeR (A. T. L. Lun & Smyth, 2016; M. D. Robinson et al., 2010; Mark D. Robinson & Oshlack, 2010). Differential enrichment analysis was then performed with a quasi-likelihood framework and negative binomial modelling from the EdgeR package (M. D. Robinson et al., 2010). Trends in read variance were estimated from the total read number with negative binomial dispersions from all 10kb binned reads. Read counts were then fitted to a generalised linear model that accounted for the negative binomial dispersions, quasi-likelihood dispersions, and effective (log) library size. The variance within samples was reduced to the previously determined dispersion test using an empirical Bayes strategy, and P-values were then assigned to each bin using a quasi-likelihood F-test (A. T. L. Lun & Smyth, 2016; M. D. Robinson et al., 2010; Mark D. Robinson & Oshlack, 2010). Binned reads were then clustered into 2000bp tolerance regions for H3K4me3 and H3K27ac, or 6000bp tolerance regions for H3K27me3, and false discovery rate error control was established with Benjamini Hochberg correction for multiple testing (Benjamini & Hochberg, 1995). Gene annotation was then established for each region based on intron/exon and promoter data from the TxDb.Mmusculus.UCSC.mm10.KownGene library, where promoters were defined as 3000bp upstream + 1000bp downstream of a transcriptional start site, and annotated regions within 5000bp the TSS were also reported. Differentially enriched sites were saved as .bed files with rtracklayer for downstream analysis (Lawrence, Gentleman, & Carey, 2009). Tables were generated for all data, also including logCPM and logFC as identified from 'getBestTest' for the top enriched window from each tolerance clustered region for descriptive plotting and

downstream analysis. For scripts on csaw see the following link: https://github.com/ajphipps/EpiAD/blob/master/csaw_example_script.rd

2.23 Gene ontology analysis

BED files of significantly differentially enriched sites generated from differential enrichment analyses were uploaded to the Genomic Regions Enrichment of Annotations Tool (GREAT), by Stanford University (C. Y. McLean et al., 2010). Samples were compared against 'whole genome background' using the UCSC mm10 genome assembly. Genomic regions were associated with 'basal+extension' (5000bp upstream and 1000bp downstream, with max extension of 1000kb), included curated regulatory domains, and samples that covered a large proportion of the genome were corrected with the 'significant by region-based binomial' option when prompted. All raw GO data, and the top 20 terms ranked by 'observed hypergeometric hits' from each GO analysis was downloaded from GREAT as .tsv files and imported into R studio for visualisation with ggplot2.

2.24 Putative enhancer track generation

H3K27ac pseudoreplicate files previously generated (Section 2.20) were subjected to peak calling with MACS2 as specified in (Section 2.21). All H3K27ac peak bed files (from both genotypes and time points) were concatenated to generate a single track with all potential HK27ac binding sites from neuronal nuclei. The track was sorted by chromosome and start position, and overlapping sites were merged with BEDTools 2.25 (Quinlan, 2014). The UCSC mm10 KnownGene track was downloaded from the UCSC table browser (downloaded 20/7/2018), and start locations for both strands were padded with ±2000bp from the TSS using the following script:

```
awk '($6 == "+") { print $0 }' input bed12file.bed |
awk 'BEGIN{ OFS="\t" }($2 > 2000){ print $1, ($2 -
2000), ($2 + 2000), $4, $5, $6, $7, $8, $9, $10, $11,
$12}' > UCSCKnowngene.tss.for.padded2kb.bed

awk '($6 == "-") { print $0 }'
mm10_knowngene_edited.bed | awk 'BEGIN{ OFS="\t" }($3 >
2000){ print $1, ($3 - 2000), ($3 + 2000), $4, $5, $6,
$7, $8, $9, $10, $11, $12}' >
UCSCKnowngene.tss.rev.padded2kb.bed
```

```
cat UCSCKnowngene.tss.for.padded.bed
UCSCKnowngene.tss.rev.padded.bed >
UCSCKnowngene_5kb_padded12.bed

bedtools sort -i UCSCKnowngene_5kb_padded12.bed >
UCSCKnowngene_5kb_padded.sorted12.bed

bedtools merge -i UCSCKnowngene_5kb_padded.sorted12.bed
> UCSCKnowngene_5kb_final_merged_sorted.bed

bedtools subtract -a
K27ac_allmerge_peaks_summits.sorted.merged.bed -b
UCSCKnowngene_5kb_final_merged_sorted.bed >
K27ac_knowngene_NeuN_putative_enhancer_track.bed
```

The forward and reverse padded KnownGene bed files were then concatenated, sorted by chromosome and start position, then merged with BEDTools 2.25. The resulting padded KnownGene bed file was used with BEDTools to subtract the TSS ±2000bp from the H3K27ac merged bam file, leaving only H3K27ac binding sites that were outside of the TSS ±2000bp window, resulting in 73,610 putative enhancer binding sites. These sites were saved as a bed file and used for mean signal plots and heatmap generation.

2.25 Percentage breadth of genomic coverage

The percentage genomic coverage at 5× sequencing depth was determined from the .bam files with Samtools mpileup, then converted to a percentage of the mm10 genomic coverage (calculated from bowtie2-inspect-s and counted with unix wc), which was then calculated in Microsoft Excel.

```
for file in *.bam
samtools mpileup ${file} | awk -v X="${5}" '$4>=5' | wc
-l > K27ac_breadth.txt
done

#total number of reads in reference genome

bowtie2-inspect-s /NGS_Data/Andrew/mm10/mm10btref | awk
'-F "\t" BEGIN{L=0}; {L=L+$2}; END{print L}'

#calculate total number of characters in the mm10 bt2
reference that are titles
```

```
bowtie2-inspect-s -n /NGS_Data/Andrew/mm10/mm10btref |
wc -m

#912 characters to subtract from reference genome
output - base 2776387315  subtract 912 = final size
2776386403
```

The genomic coverage was then plotted as histograms in GraphPad prism 6.

2.26 CpG island analysis

Tracks for CpG islands in mm10 were downloaded from the UCSC table browser. This data was subset against UCSC KnownGene TSS for mm10 with BEDTools 2.25 to be able to identify TSS that contained CpG islands. H3K4me3 and H3K27ac marking was then mapped against these tracks as heatmaps.

2.27 Plot generation

Heatmaps and mean profile data intersecting histone modifications with UCSC KnownGene TSS and putative enhancer tracks were generated with deepTools (version 3.0) computeMatrix, plotProfile, and plotHeatmap (Ramírez et al., 2016), or Seqplots v1.12.1 (Stempor & Ahringer, 2016). Combined profile plots for APP/PS1 and WT control mice samples were generated with Seqplots v1.12.1 (Stempor & Ahringer, 2016). Representative genomic regions of interest of pseudoreplicates were exported from IGV (H. Li et al., 2009) and with edited with Adobe Illustrator. Volcano plots were generated with ggplot2 utilising the logFC from 'getBestTest' generated in csaw (2.23).

2.28 Venn diagram analysis

To determine whether sites of differential H3K27ac and H3K4me3 enrichment were shared between time-points, venn diagrams were generated with BEDTools 2.25 multi-intersect and gplots in the R studio environment (Quinlan, 2014). BED files generated from pairwise differential enrichment analysis were analysed with bedtools:

```
bedtools multiinter -header -i H3K4me3_3FC_AD3_DBsites.bed H3K4me3_3FC_AD6_DBsites.bed H3K4me3_3FC_AD12_DBsites.bed -names K4me3_AD3 K4me3_AD6 K4me3_AD12 > K4me3_intersect.txt
```

The output of the mutli-intersect analysis was then imported into Rstudio and venn diagrams were generated as follows:

```
K27ac_intersect <-
read_delim("D:/Dropbox/Dropbox/Documents/2018/ChIP-seq/Intersect_bedfiles/K27ac_intersect.txt","\t",
escape_double = FALSE, trim_ws = TRUE)

View(K27ac_intersect)

K27ac_sub <- data.frame(K27ac_intersect$K27ac_AD3,
K27ac_intersect$K27ac_AD6, K27ac_intersect$K27ac_AD12)

colnames(K27ac_sub) <- c("3m APP/PS1 DB sites", "6m APP/PS1 DB sites", "12m APP/PS1 DB sites")

venn(K27ac_sub)
```

To identify whether H3K4me3 or H3K27ac marked sites that were shared across time-points were consistently enriched or depleted, differential enrichment data was subset into significantly enriched or significantly depleted, then analysed pairwise with bedtools BEDTools 2.25 intersect (Quinlan, 2014).

2.29 RNA-seq overlap analysis

RNA-seq data was obtained from (Mathys et al., 2019). All neuronal RNA-seq data (excitatory and inhibitory neurons) was compiled and filtered for unique genes to be comparable with the NeuN+ ChIP-seq enrichments. Human gene symbols were converted to mouse symbols with the MGI database. Genes enriched for H3K27ac and H3K4me3 were also filtered for unique sites. An overlap analysis was performed in R based on gene symbols as follows:

```
library(csaw)
library(TxDb.Mmusculus.UCSC.mm10.knowngene)
library(EdgeR)
```

```
library(splitstackshape)
library(dplyr)
library(tidyverse)
library(GenomicRanges)


#import dataset
library(readr)
H3K4me3_12m_AD12_allresults <-
read_csv("F:/Dropbox/Documents/2019/Projects/ChIP-
seq_2019/ANZ_masons_ChIP-
seq_data/H3K4me3/H3K4me3_AD/H3K4me3_12m_AD12_allresults_copy.csv")
View(H3K4me3_12m_AD12_allresults_copy)

#split the overlaps column
# find commas positioned after + or - and replace with a space
H3K4me3_12m_AD12_allresults$overlap <- gsub("([+-]),", "\\1 ",
H3K4me3_12m_AD12_allresults$overlap)
# count number of regions per observation
H3K4me3_12m_AD12_allresults$n_regions <-
ifelse(!is.na(H3K4me3_12m_AD12_allresults$overlap),
str_count(H3K4me3_12m_AD12_allresults$overlap,' ') + 1,NA)
#find the maximum amount of regions found in an observation
max_regions <- max(H3K4me3_12m_AD12_allresults$n_regions, na.rm = TRUE)
#partition into multiple coloumns
H3K4me3_12m_AD12_allresults <- H3K4me3_12m_AD12_allresults %>%
separate(col = overlap, into = paste0('overlap', 1:max_regions), sep = '
', remove = FALSE)
H3K4me3_12m_AD12_allresults$overlap1 <-
ifelse(H3K4me3_12m_AD12_allresults$overlap1=="", NA,
H3K4me3_12m_AD12_allresults$overlap1)

#load comparison gene data into R
library(readxl)
sig_Mathys_all_neuron_no_path_vs_path <-
read_excel("Mathys_data/no_path_vs_path/sig.Mathys_all_neuron_no.path_vs_p
ath_gene_names_MGI.xlsx")
View(sig_Mathys_all_neuron_no_path_vs_path)

#subset both datasets by significance
unique.mathys_nopath_path <-
unique(sig_Mathys_all_neuron_no_path_vs_path$Symbol)
H3K4me3_AD12_sig <- subset(H3K4me3_12m_AD12_allresults, FDR <=0.05)
d <- H3K4me3_AD12_sig

#isolate gene names without the pipes and tidy
d[, 14:38] <- apply(d[, 14:38], 2, function(x) stringr::str_extract(x,
"[^|]*"))

#convert long form columns into short form rows
k <- reshape2::melt(d[, c(1, 13:38)], id.vars = c("X1", "overlap")) %>%
  mutate(genes = value) %>%
  select(-c(variable, value)) %>%
  na.omit() %>%
```

```
  left_join(select(d, -starts_with("overlap")), by = "X1") %>%
  arrange(X1)

#make the mouse genes lowercase
mouse_genes <- (unique(k$genes))

#find the overlapping genes in mouse and human datasets
keep <- mouse_genes[mouse_genes %in% unique.mathys_nopath_path]

#join the human and mouse data together into a single datatable
j <- left_join(k, sig_Mathys_all_neuron_no_path_vs_path , by = c("genes" =
"Symbol"))

write.csv(j, file = "H3K4me3_AD12_overlap_nopath_vs_path.csv")
```

Example scripts utilised in this thesis can be viewed on github:

https://github.com/ajphipps/EpiAD

Chapter 3: Neurofilament-labelled pyramidal neurons and astrocytes are deficient in DNA methylation marks in Alzheimer's disease

3.1 Introduction

Despite increasing research efforts, the underlying cause of sporadic AD remains unknown. In the absence of genetic aberrations, it is possible that epigenetic alterations may contribute to the multiple pathological pathways implicated in the onset and progression of AD (Coppieters et al., 2013; Diego Mastroeni, McKee, Grover, Rogers, & Coleman, 2009; Siegmund et al., 2007). The epigenome encompasses a variety of components that act in concert, such as DNA methylation and post-translational histone modifications (Christensen et al., 2009; Narayan et al., 2015). The epigenetic machinery exerts exquisite control over gene regulation programs and allows for all cell types to be genetically homogenous, while structurally and functionally heterogeneous. Importantly, the epigenome also provides a link between environmental factors and sporadic AD risk (D. Mastroeni et al., 2010).

A number of studies have investigated changes in DNA methylation marks 5mC (usually associated with gene silencing) and 5hmC (associated with active de-methylation and increased gene expression) throughout the progression of AD at specific genes or genome-wide using whole brain homogenate (A. I. Bernstein et al., 2016; Chouliaras et al., 2013; P. L. De Jager et al., 2014; Lunnon et al., 2014). The location of 5mC/5hmC methylation marks on the genome has differential effects on transcription, and the outcome further depends on interplay with other epigenetic modifications such as the presence or absence of particular histone marks (Cedar & Bergman, 2009; Narayan et al., 2015). The majority of studies investigating DNA methylation in AD have shown that AD is associated with global DNA hypermethylation relative to control cases (Bradley-Whitman & Lovell, 2013; P. L. De Jager et al., 2014; Sanchez-Mut et al., 2013; Siegmund et al., 2007), while some studies have detected DNA hypomethylation (West et al., 1995). Other studies report that DNA hypo- and hyper-methylation can co-occur in AD brain but at different loci (Bakulski et al., 2012). Two independent studies recently reported similar sets of differentially methylated regions that changed in tandem with neuritic plaque load or Braak staging, clearly showing that epigenetic alterations occur early in AD (P. L. De Jager et al., 2014; Lunnon et al., 2014). However, the cell types in which these alterations occur remain to be determined.

There is increasing interest in cell type specific alterations in DNA methylation in AD. This is due to the cell-type specific vulnerability that exists in different subsets of neuronal cells. For example, neurons that contain the neurofilament (NF) 'triplet' proteins in layers 2/3 and 5 of the cortex are selectively vulnerable to NFT pathology (Patrick R. Hof & Morrison, 1990;

Thangavel et al., 2009; J. C. Vickers et al., 1994). Whereas, a subset of calretinin-positive interneurons are resistant to AD pathology (P. R. Hof et al., 1993; Mitew et al., 2013b). Seminal studies have characterized the epigenome of different neuronal populations, identifying different DNA methylation patterns between neurons and non-neuronal cells in the CNS (Coppieters et al., 2013; Ryan Lister et al., 2013; Mo et al., 2015). Cell type specific alterations in DNA methylation have also been implicated in the progression of AD (Coppieters et al., 2013; D. Mastroeni et al., 2010), however few studies have quantitated cell type specific changes in DNA methylation (Chouliaras et al., 2013; Gasparoni et al., 2018). Additionally, no study to date has determined whether the cells adjacent to Aβ plaques or tangle-bearing neurons are more susceptible to epigenetic alterations.

There is emerging evidence of a role for epigenetic aberrations in the pathophysiology of AD. There is, however, little information regarding cell type specific epigenetic alterations in the brain, or whether there is any direct association between epigenetic modifications and AD pathology. This study characterises 5mC and 5hmC methylation in subsets of cortical neurons with differential vulnerability to degeneration in AD, including NF-positive pyramidal neurons and calretinin-labelled interneurons, as well as in microglia and astrocytes. This study has also examined DNA methylation changes in close proximity to Aβ plaques, as well as in NFT-bearing neurons.

3.2 Results

3.2.1 Less extranuclear 5mC labelling in pyramidal neurons in cortical layer 5 of late-AD cases

Initially, 5mC and 5hmC was examined in NF-rich pyramidal neurons that are vulnerable to AD pathology. The majority of NF-positive pyramidal neurons co-localised with nuclear 5mC (Figure 3.1a-c) and 5hmC (Figure 3.1d-f) immunolabelling, and, in a subset of NF-rich pyramidal neurons, this labelling extended into the cell body and proximal processes. There was no significant difference in the percentage of NF-rich pyramidal neurons that co-localised with nuclear 5mC labelling in layers 2/3 or 5 across control (mean±SE; 98.4± 0.7%; 94.8± 2.1%), early-AD (99.6± 0.4%, 93.6± 1.4%) and late-AD cases (97.3± 0.9%, 98.5± 0.6%; Figure 3.1j,k). Similarly, there was no significant difference in the percentage of NF-labelled pyramidal neurons in layers 2/3 or 5 with nuclear 5hmC labelling between control (100.0 ± 0.0%, 98.0± 1.0%), early-AD (98.0± 0.8%, 98.0± 1.0%) and late-AD (96.8± 1.7%, 97.0± 1.2%) cases (Figure 1j,k). Interestingly, significantly less NF-positive pyramidal neurons contained extranuclear 5mC labelling in layer 5 in late-AD cases (14.8± 1.3%) compared to control and early-AD cases (28.8± 3.0%, 31.2± 4.1%, respectively; Kurskal-Wallis one way ANOVA on ranks; p=<0.05; Figure 3.1k). There was no significant difference in the proportion of NF-positive pyramidal neurons in layer 2/3 with extranuclear 5mC across control (33.6± 7.1%), early AD (36.8± 4.3%) and AD cases (26± 3.2%; Figure 3.1j). There was no significant difference in extranuclear labelling in layer 2/3 or layer 5 for 5hmC between control (78± 2.3%; 58.8± 8.3), preclinical (65.6± 7.5%; 55.6± 13.7%), and AD (57.2± 4.0%; 45.3± 11.4%; Figure 3.1j,k) case types.

The samples required to power this investigation could not be predicted *a priori*, thus, for the value of change detectable for each of the datasets within Chapter 3 refer to Table 3.1. To ensure that variations in PMIs and age had not impacted this study, linear regression analysis was performed on all datasets. There were no correlations between the data presented and PMI or age with the exception of: a negative correlation between the percentage of microglia with nuclear 5hmC and age in layer 2/3 (but not in layer 4), and a positive correlation between the proportion of pyramidal neurons with nuclear 5mC and extranuclear 5mC and PMI in layer 2/3 (see Appendix 2: Supplementary Figure 2). In addition, no gender effects were present in cell type specific datasets.

Table 3.1: Power Calculations

Dataset	**Change detected with 90% power***
% NF pyramidal neurons with 5hmC L2/3	6.8%
% NF pyramidal neurons with 5hmC L5	5.9%
% NF pyramidal neurons with 5mC L2/3	4.4%
% NF pyramidal neurons with 5mC L5	9.6%
% Calretinin interneurons with 5hmC L2/3	19.9%
% Calretinin interneurons with 5hmC L4	21.3%
% Calretinin interneurons with 5mC L2/3	28.6%
% Calretinin interneurons with 5mC L4	24.3%
% Microglia with 5hmC L2/3	31.7%
% Microglia with 5hmC L4	30.9%
% Microglia with 5mC L2/3	29.7%
% Microglia with 5mC L4	17.7%
% Astrocytes 5hmC	23.6%
% Astrocytes 5mC	25.5%
Density 5hmC nuclei (near plaque vs plaque free)	0.0019 nuclei/μm^2
Density 5mC nuclei (near plaque vs plaque free)	0.0015 nuclei/μm^2

* The maximum change detectable for each dataset with 90% power (Graphpad Statmate 2).

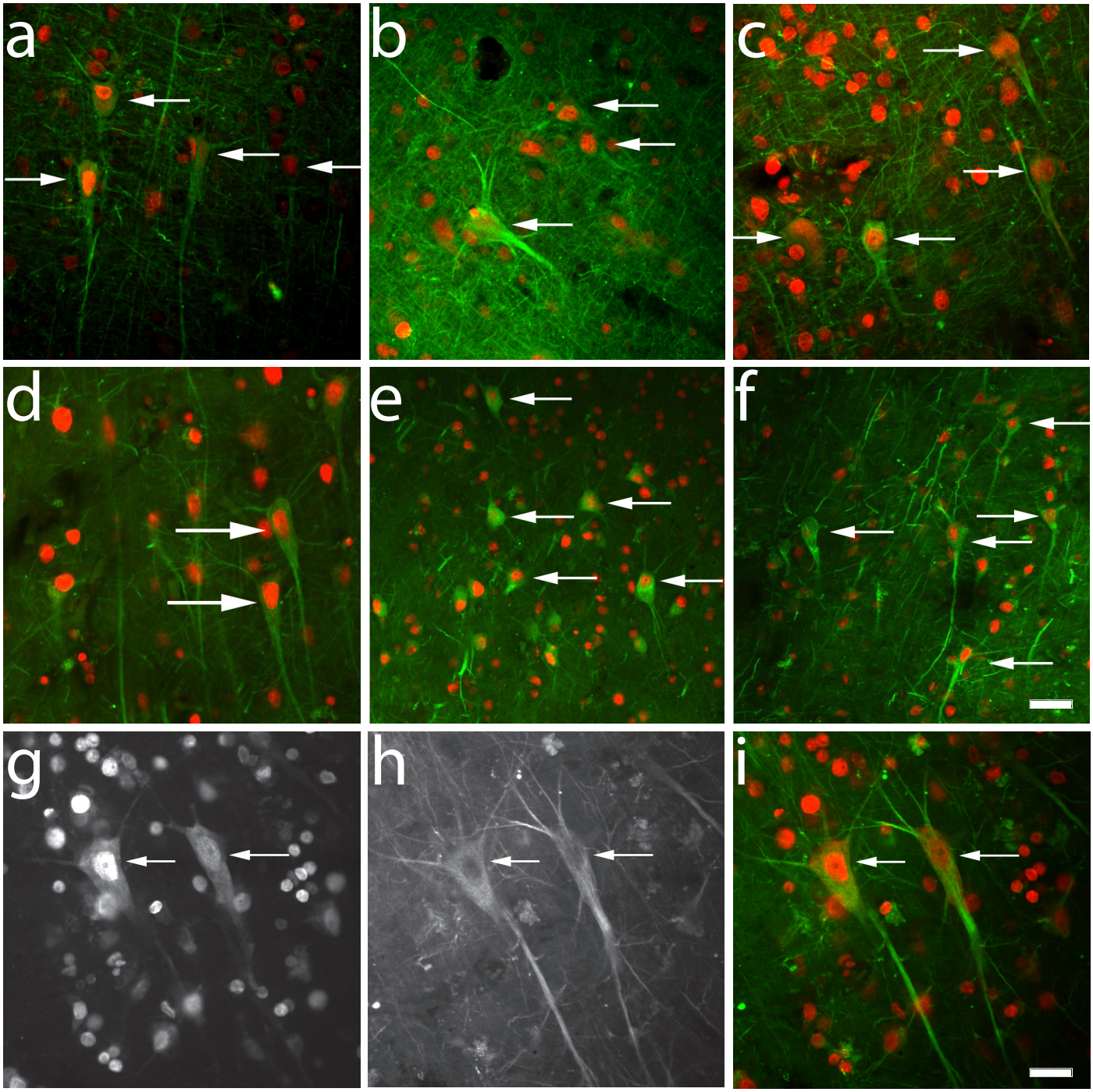
a
b
c
d
e
f
g
h
i

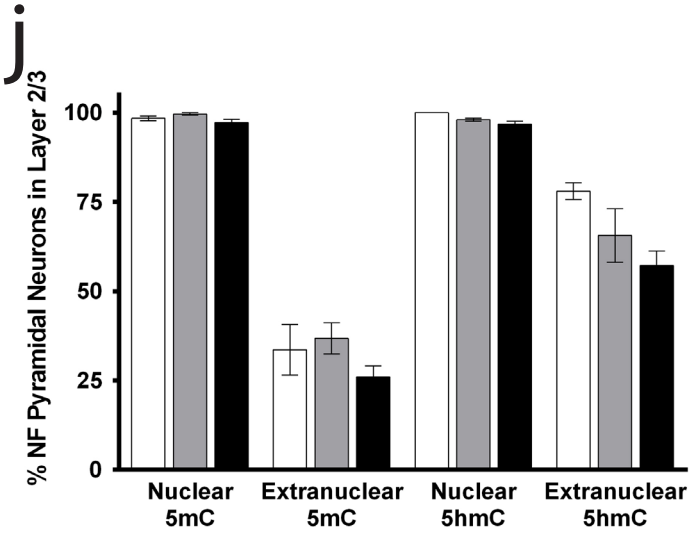
j
% NF Pyramidal Neurons in Layer 2/3
100
75
50
25
0
Nuclear 5mC
Extranuclear 5mC
Nuclear 5hmC
Extranuclear 5hmC

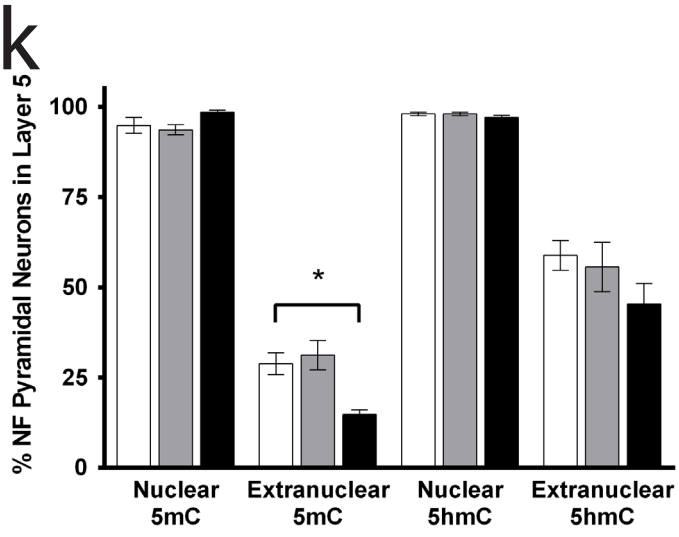
k
% NF Pyramidal Neurons in Layer 5
100
75
50
25
0
*
Nuclear 5mC
Extranuclear 5mC
Nuclear 5hmC
Extranuclear 5hmC

Figure 3.1: A significantly lower proportion of NF-rich pyramidal neurons co-localised with 5mC in cortical layer 5 of late-AD cases

(a-f, green) The majority of NF labelled pyramidal neurons in layer 2/3 of the ITG exhibited nuclear (a-c, red) 5mC and (d-f, red) 5hmC labelling (arrows) in (a,d) control, (b,e) early-AD and, (c,f) late-AD cases. (g-i) High magnification representative images show the co-localisation of (g) 5hmC, (h) NF positive pyramidal neurons and, (i) merge in a control case. (j) histogram showing the percentage of NF-positive pyramidal neurons in Layers 2/3 of the ITG that co-localised with nuclear/extranuclear 5mC or 5hmC in control (white), early AD (grey) and late AD (black) cases. (k) histogram of the percentage of NF-positive pyramidal neurons in Layers 5 of the ITG that co-localised with 5mC or 5hmC in (white) control, (grey) early AD and (black) AD cases. Bar graphs represent the mean value for each case type; error bars represent the SEM. Scale bars: (a-f) 34μm; (g-i) 20μm.

3.2.2 No difference in the percentage of calretinin-labelled interneurons co-localised with 5hmC/5mC between case types

Next, 5mC and 5hmC immunolabelling was assessed in calretinin-labelled interneurons that are resistant to AD pathology. There was no significant difference in the proportion of calretinin-positive interneurons co-localised with nuclear 5mC immunoreactivity within pathology-rich cortical layers 2/3 or in relatively pathology-poor layer 4 between control (mean±SE: layer 2/3: 76.0± 4.7%; layer 4: 70.4± 5.6%), early-AD (67.2± 3.4%; 72.8± 3.5%) and late-AD case types (70.0± 5.8%; 77.1± 2.1%; Figure 3.2j,k). There was also no significant difference in the percentage of calretinin-positive interneurons in layers 2/3 or 4 with nuclear 5hmC labelling between control (77.2 ± 1.9%; 70.4± 1.4%), early-AD (80.4± 5.0%; 77.6± 5.6%) and late-AD (85.3± 2.7%; 82.0± 3.4%, respectively) cases (Figure 3.2j,k). A small number of calretinin-labelled interneurons contained extranuclear 5mC labelling, with no significant difference in layer 2/3 or layer 4 between control (5.6± 1.5%; 10.4± 2.9%), early-AD (6.4± 1.0%; 13.6± 2.4%) or late-AD (4.6± 1.3%; 10.9± 1.9%) case types (Figure 3.2j,k). There was also no significant difference in extranuclear 5hmC labelling (Figure 3.2j,k) in cortical layers 2/3 and layer 4 across control (4.8± 1.7%; 8.8± 2.9%), early-AD (9.6± 1.9%; 7.2± 1.6%) and late-AD cases (7.3± 1.9%; 6.0± 2.3%; Figure 3.2j,k).

Comparison of calretinin-positive interneurons between pathology-rich layer 2/3 and pathology-poor layer 4 showed no significant difference in nuclear or extranuclear 5mC labelling between the layers. Interestingly, there was a significantly higher percentage of calretinin immunopositive interneurons with nuclear 5hmC in control, early AD and AD cases in layers 2/3 compared to layer 4 (one way ANOVA; all $p=<0.001$), but no significant difference in the percentage of calretinin positive neurons that had extranuclear 5hmC immunoreactivity in cortical layers 2/3 compared to layer 4 any of the case types. Comparative analysis identified inherent differences in 5mC and 5hmC marks between NF-positive neurons and calretinin-labelled interneurons. In layer 2/3 a significantly higher percentage of NF-positive pyramidal neurons exhibited nuclear 5mC in control cases compared to calretinin-positive interneurons in layer 2/3 (Mann-Whitney Rank Sum T-test; $p=<0.05$). Additionally, a significantly higher proportion of NF-positive pyramidal neurons contained nuclear 5hmC compared to calretinin-positive interneurons in layer 2/3 of control cases (T-test; $p = <0.001$).

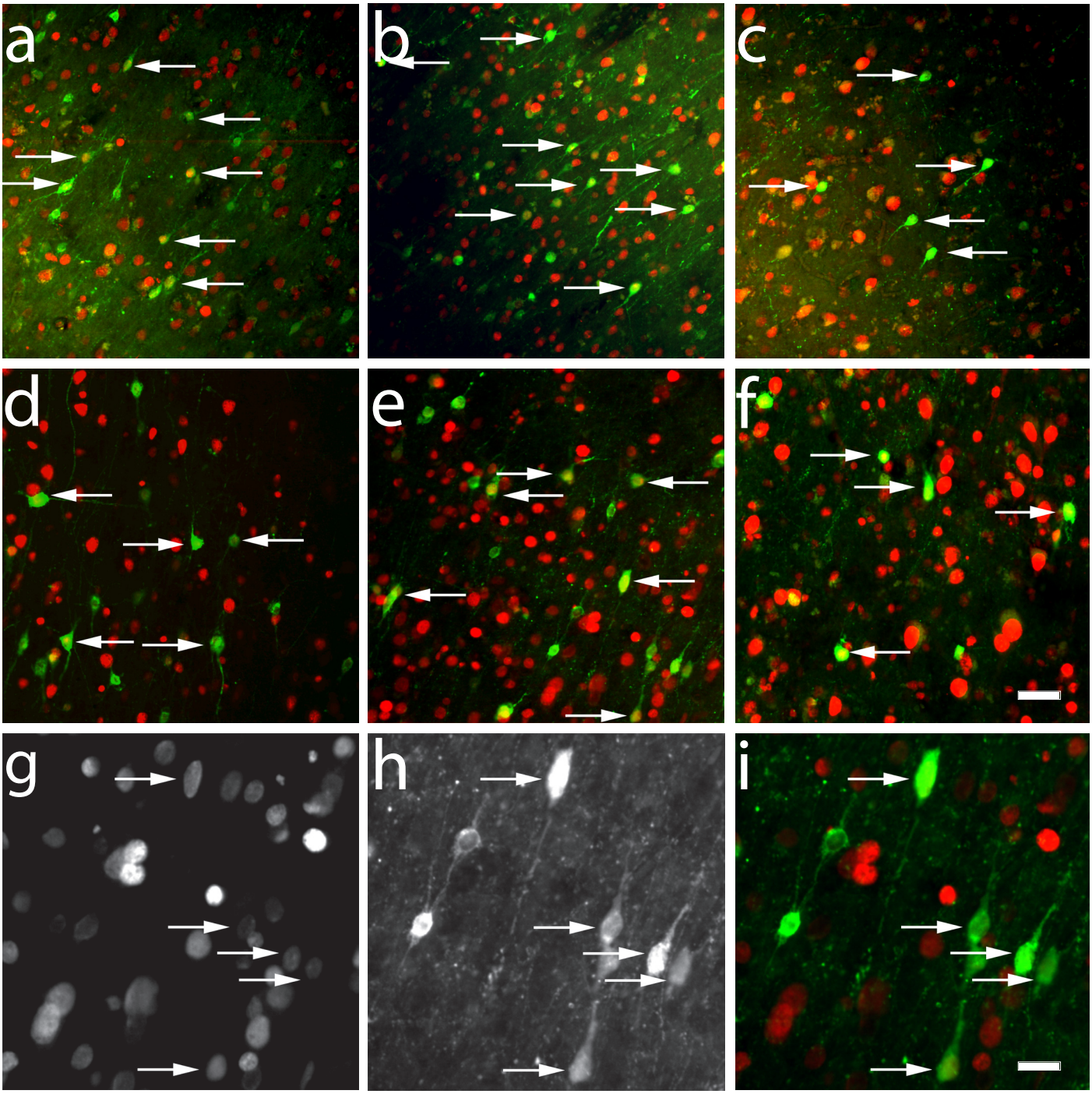
a
b
c
d
e
f
g
h
i

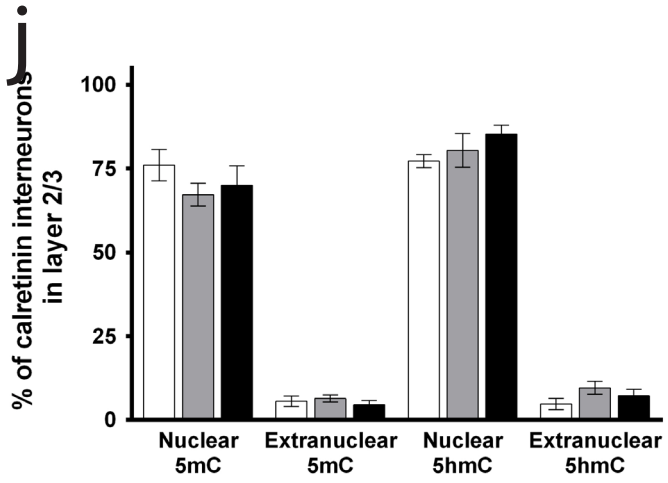
j
% of calretinin interneurons in layer 2/3
100
75
50
25
0
Nuclear 5mC
Extranuclear 5mC
Nuclear 5hmC
Extranuclear 5hmC

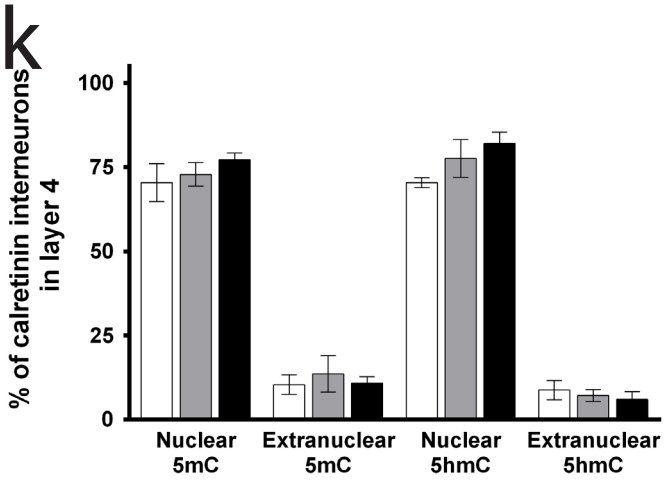
k
% of calretinin interneurons in layer 4
100
75
50
25
0
Nuclear 5mC
Extranuclear 5mC
Nuclear 5hmC
Extranuclear 5hmC

Figure 3.2: No significant difference in calretinin-labelled interneurons co-localised with 5mC or 5hmC through the progression of AD

(a-f, i, green) Calretinin labelled interneurons in layer 2/3 of the ITG exhibited nuclear (a-c, red) 5mC and (d-f, i, red) 5hmC labelling (arrows) in (a,d) control, (b,e) early AD and, (c,f) late AD cases. (g-i) High magnification representative images of (g) 5hmC, (h) calretinin and, (i) merge in an early-AD case. (j) Bar graph showing the percentage of calretinin-labelled interneurons in layers 2/3 of the ITG that co-localised with nuclear/extranuclear 5mC or 5hmC in (white) control, early AD (grey) and late AD (black) cases. (k) Bar graph of the percentage of calretinin-labelled interneurons in layers 4 of the ITG that co-localised with 5mC or 5hmC in (white) control, (grey) early AD and, (black) AD cases. Bar graphs represent the mean value for each case type; error bars represent the SEM. Scale bars: (a-f) 34μm; (g-i) 20μm.

The percentage of NF-rich pyramidal neurons with extranuclear 5mC in layer 2/3 was significantly greater than that of calretinin-positive interneurons in control cases (Mann-Whitney Rank Sum T-test; p=<0.05), while the proportion of NF-positive pyramidal neurons co-localised with extranuclear 5hmC in layer 2/3 was also significantly higher than that of calretinin-positive interneurons in control cases (Mann-Whitney Rank Sum T-test; p = <0.05).

3.2.3 No difference in the percentage of microglia that co-localised with 5mC and 5hmC between case types

There was no significant difference in the percentage of microglia that contained nuclear 5mC in layers 2/3 or layer 4 across control (layer2/3: 77.6± 2.9%; layer4: 75.2± 3.2%), early-AD (78.4± 5.2%; 72.8± 3.42%) and late-AD cases (74.6± 5.8%; 66.9± 3.2%, respectively, Figure 3.3j,k). There was also no significant difference in nuclear 5hmC in microglia in layer 2/3 or layer 4 in control (77.2± 6.8%; 76.4± 4.7%), early-AD (68.0± 5.2%; 65.6± 6.2%) and late-AD cases (72.0± 4.6%; 70.6± 6.8%; Figure 3.3j,k). There was limited extranuclear 5mC/5hmC labelling observed in microglia (Figure 3.3g-i). There was no significant difference in the proportion of microglia that contained extranuclear 5mC labelling across control (13.2± 2.6%; 9.2± 1.6%), early-AD (12.8 ± 2.5%;9.2± 0.9%), and late-AD (18.0± 2.3%;13.7± 2.1%; Figure 3.3j,k) case types, as well as extranuclear 5hmC in layer 2/3 or layer 4 across control (12.8± 3.1%; 11.6± 2.1%), early-AD (19.6± 3.6%; 15.6± 4.1%) and late-AD cases (17.4± 4.0%; 15.1± 3.0%, Figure 3.3j,k). A comparison of microglia between pathology-rich layers 2/3 and pathology-poor layer 4 showed that there was no significant difference in the percentage of microglia co-localised with nuclear or extranuclear 5mC or 5hmC between the layers in control, early-AD and late-AD case types.

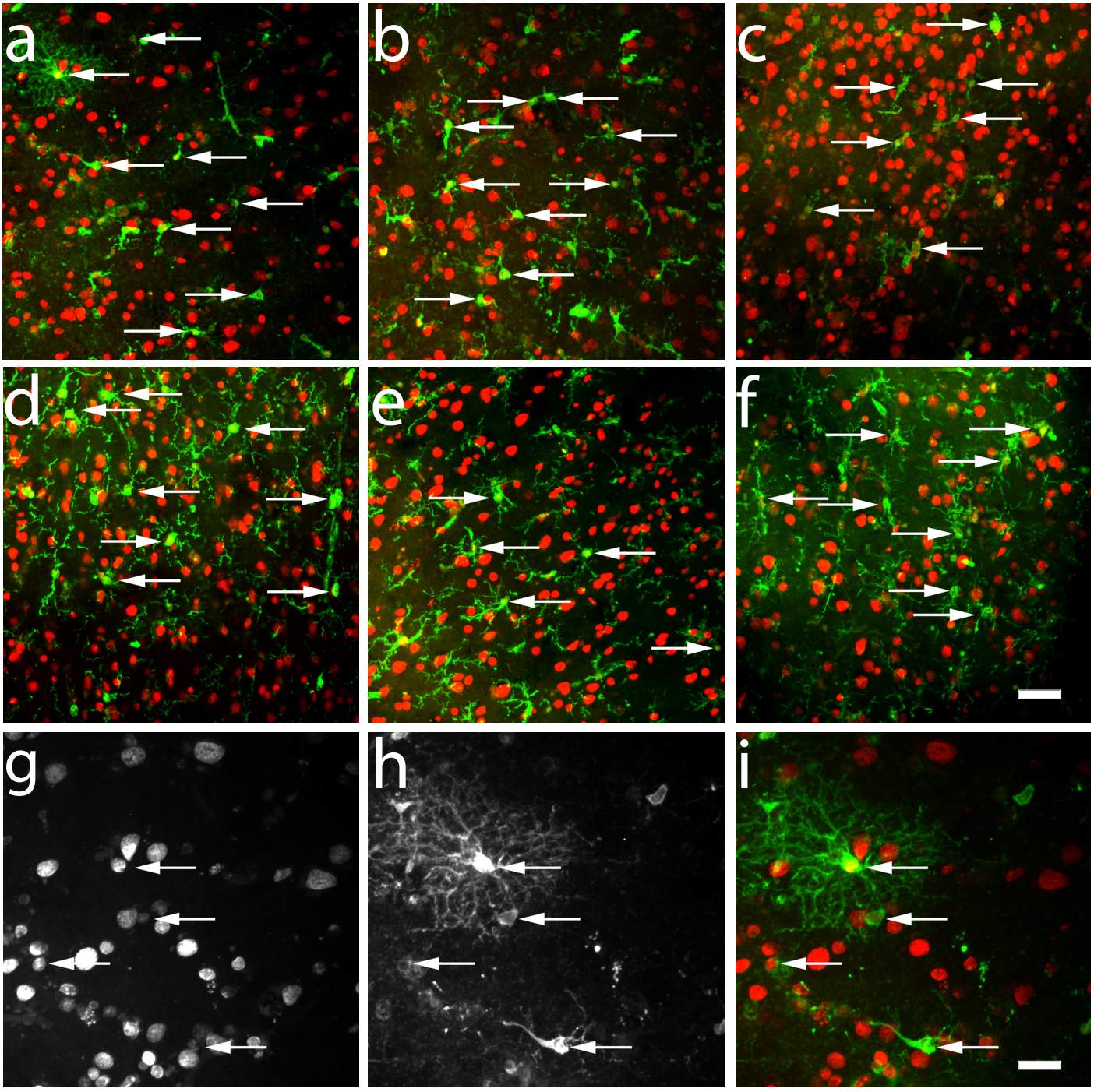
a
b
c
d
e
f
g
h
i

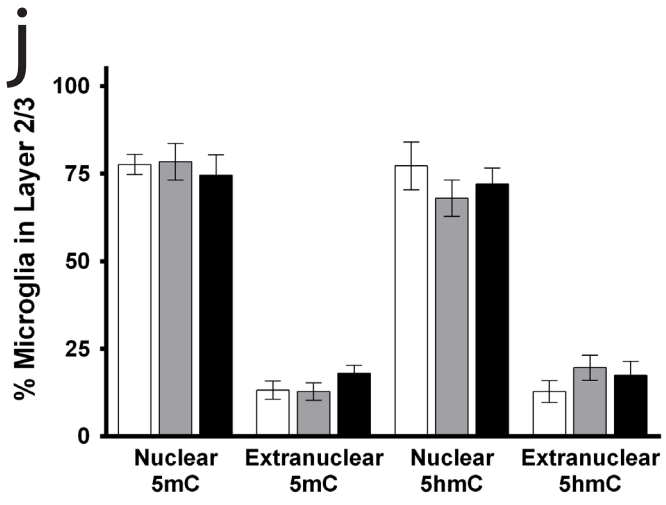
j
% Microglia in Layer 2/3
100
75
50
25
0
Nuclear 5mC
Extranuclear 5mC
Nuclear 5hmC
Extranuclear 5hmC

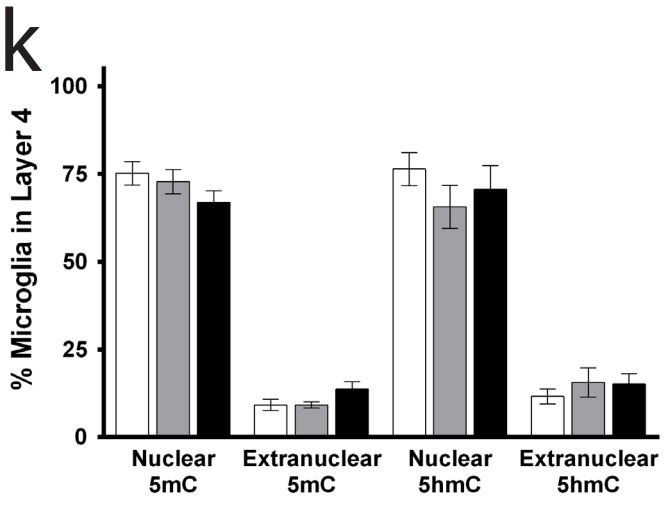
k
% Microglia in Layer 4
100
75
50
25
0
Nuclear 5mC
Extranuclear 5mC
Nuclear 5hmC
Extranuclear 5hmC

Figure 3.3: No significant difference in microglia co-localised with 5mC or 5hmC through the progression of AD

(a-f, i, green) Microglia in layer 2/3 of the ITG exhibited (a-c, i, red) nuclear 5mC and (d-f, red) 5hmC labelling (arrows) in (a, d) control, early (b, e) AD and, (c,f) late AD cases. (g) High magnification representative images of 5mC, (h) ferritin labelled microglia and (i) merge in a control case. (j) Bar graph showing the percentage of microglia in layers 2/3 of the ITG that co-localised with nuclear/extranuclear 5mC or 5hmC in (white) control, (grey) early AD and (black) late AD cases. (k) Bar graph of the percentage of microglia in layer 4 of the ITG that co-localised with 5mC or 5hmC in (white) control, (grey) early AD and, (black) AD cases. Bar graphs represent the mean value for each case type; error bars represent the SEM. Scale bars: (a-f) 35μm; (g-i) 20μm.

3.2.4 Less nuclear 5mC and 5hmC in astrocytes in late-AD cases compared to control and early-AD cases

A significantly lower percentage of astrocytes exhibited co-localisation with nuclear 5mC in late-AD cases (64.5± 3.9%) when compared to control cases (83.2± 5.4%, Holm Sidak one way ANOVA; p=<0.05; Figure 3.4), however there was no significant difference between the proportion of astrocytes with nuclear 5mC in early-AD cases (72.8± 4.3%) and late-AD or control case types. Similarly, a significantly lower proportion of astrocytes contained nuclear 5hmC in late-AD (67.5± 5.0%) cases compared to control cases (85.2± 0.9%; Kruskal-Wallis one way ANOVA on ranks; p=<0.05; Figure 3.4j,k), and again there was no difference in the proportion of astrocyte with nuclear 5hmC between early-AD (74.4± 1.8%) and the other case types. There was no significant difference in extranuclear 5mC or 5hmC labelling between control (14.8± 4.5%; 17.6± 2.2%), early-AD (14.0± 2.5%; 15.2± 3.8%) and late-AD (7.3± 1.2%; 22.0± 5.1%, respectively; Figure 3.4j,k) case types. Qualitative analysis of astrocytes showed no robust differences in 5mC or 5hmC labelling of astrocytes located in close proximity to Aβ plaques.

3.2.5 A high proportion of NFT's co-localised with 5mC and 5hmC

Analysis of NFTs with 5mC/5hmC in late-AD cases showed a high proportion of NFTs co-localised with 5mC and 5hmC in cortical layers 2/3 and layer 5 (Figure 3.5). There was no significant difference in the percentage of NFTs that contained nuclear 5mC between layers 2/3 and layer 5 (76.3± 7.6%; 66.9± 8.5%), and no difference in extranuclear 5mC labelling between layers 2/3 and layer 5 (8.9± 2.2%, 8.6± 1.96%; Figure 3.5). In comparison, a significantly higher proportion of NFTs co-localised with nuclear 5hmC in layer 2/3 compared to layer 5 (99.3% ± 0.38, 92.8% ± 1.37, respectively; one way ANOVA; p = <0.05), but there was no significant difference in NFTs with extranuclear 5hmC in layer 2/3 when compared to layer 5 (22.6% ± 7.68, 22.8% ± 9.82; Figure 3.5c). The NFT density was also determined for each late-AD case (Table 1). There were no correlations detected between the NFT density and the proportion of specific cell types (NF-labelled pyramidal neurons, calretinin-labelled interneurons, microglia or astrocytes) positive for nuclear or extranuclear 5mC or 5hmC.

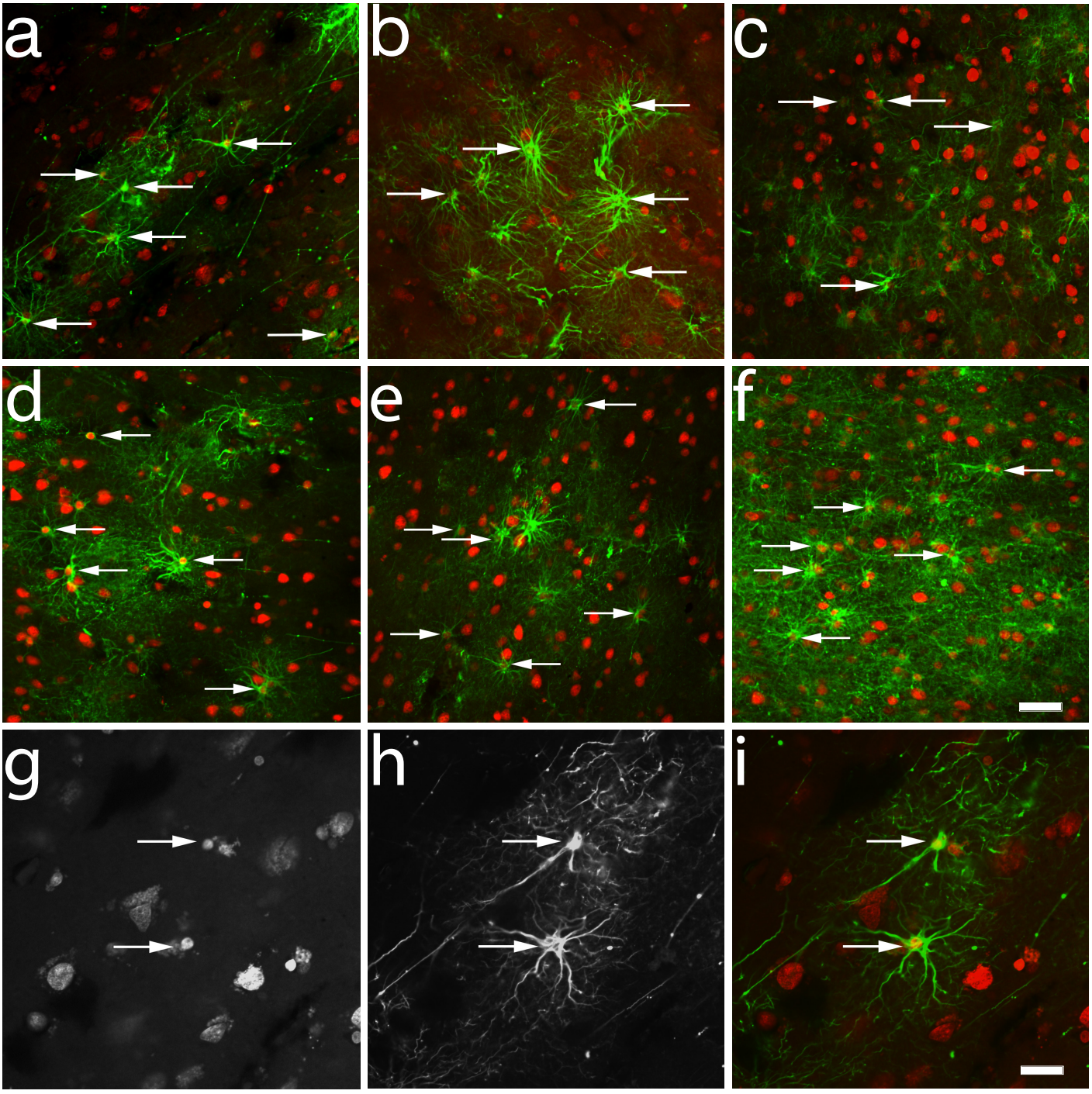
a
b
c
d
e
f
g
h
i

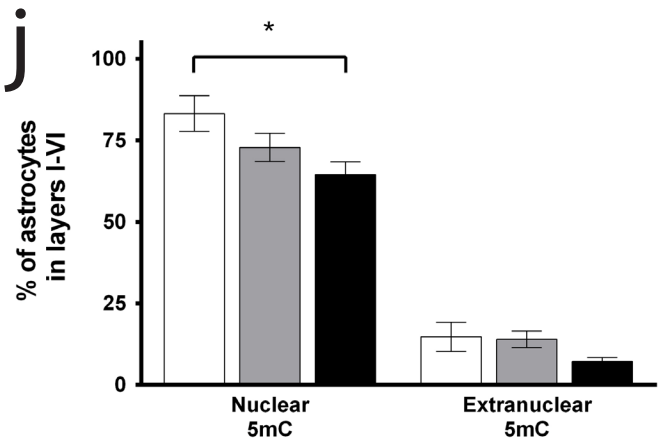
j
*
100
75
50
25
0
% of astrocytes in layers I-VI
Nuclear 5mC
Extranuclear 5mC

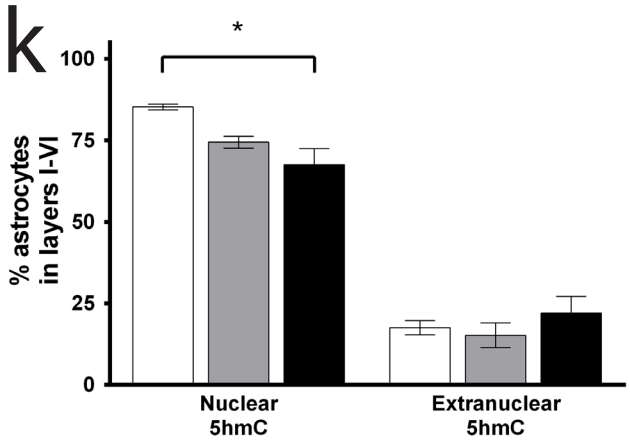
k
*
100
75
50
25
0
% astrocytes in layers I-VI
Nuclear 5hmC
Extranuclear 5hmC

Figure 3.4: A significantly lower proportion of astrocytes co-localised with 5mC and 5hmC in late-AD cases compared to control

(a-f, i, green) Astrocytes in layer 2/3 of the ITG exhibited nuclear (a-c, i, red) 5mC and (d-f, red) 5hmC labelling (arrows) in (a,d) control, (b,e) early AD and (c,f) late AD cases. High magnification representative images of (g) 5mC, (h) GFAP positive astrocytes and (i) merge in a control case. (j) Bar graph showing the percentage of astrocytes in layers 1-6 of the ITG that co-localised with nuclear/extranuclear 5mC in (white) control, (grey) early AD and, (black) late AD cases. (k) Bar graph of the percentage of astrocytes in layers 1-6 of the ITG that co-localised with 5hmC in (white) control, (grey) early AD and, (black) late-AD cases. Bar graphs represent the mean value for each case type; error bars represent the SEM. Scale bars: (a-f) 35μm; (g-i) 20μm.

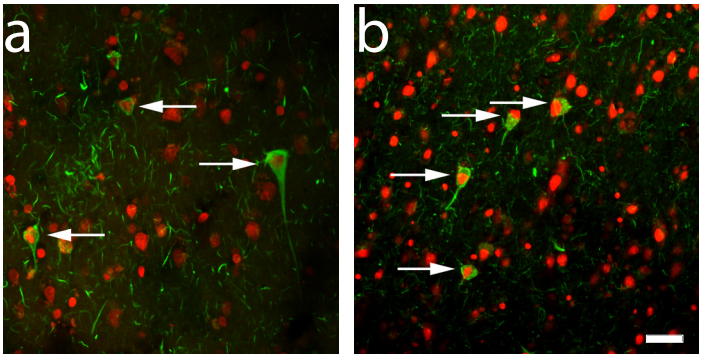
a
b

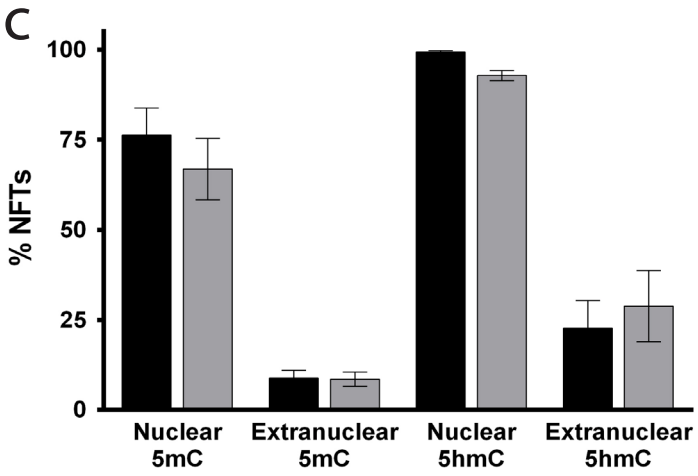
C
100
75
50
25
0
% NFTs
Nuclear 5mC
Extranuclear 5mC
Nuclear 5hmC
Extranuclear 5hmC

Figure 3.5: No significant difference in NFTs co-localised with 5mC or 5hmC through the progression of AD

A high proportion of NFTs co-localised with 5mC and 5hmC. (a,b, green) NFTs in layer 2/3 and layer 5 of the ITG exhibited nuclear/extranuclear (a) 5mC, and (b) 5hmC in late AD cases. Bar graph showing the percentage of NFTs with nuclear/extranuclear 5mC and 5hmC in (black) layer 2/3 and (grey) layer 5 in late AD cases. Bar graphs represent the mean value for each case type; error bars represent the SEM. Scale bars: (a,b) 35μm.

3.2.6 No difference in the density of 5mC and 5hmC positive nuclei in near-plaque and plaque-free regions of interest in late-AD cases

To determine if the density of 5mC and 5hmC labelled nuclei was altered near Aβ plaques in layer 2/3, the density 5mC and 5hmC labelled nuclei in near-plaque regions of interest (ROI) in late-AD cases, as well as in equivalent plaque-free ROI in late-AD and control cases was quantitated (Figure 3.6). There was no significant difference in the density of 5hmC positive nuclei in near-plaque ROI in late-AD cases (0.003555±0.000354 cells/μm^2) compared to plaque-free ROI in late-AD cases (0.003516±0.000390 cells/μm^2) and control cases (0.002405± 0.000195 cells/μm^2). Similarly, no significant difference was detected between the density of 5mC labelled nuclei in near-plaque ROI (0.003812±0.000267 cells/μm^2) and plaque-free ROI (0.003769±0.000314 cells/μm^2) in late-AD cases. However, plaque-free ROI in control cases exhibited a lower density of 5mC positive nuclei (0.002305±0.000166 cells/μm^2) compared to near-plaque and plaque-free ROI in late-AD cases (One way ANOVA;Holm-Sidak method, p= 0.007). The Aβ plaque load was determined for each AD case (Table 3.1). There were no correlations between the Aβ plaque load and the proportion of specific cell types (NF-labelled pyramidal neurons, calretinin-labelled interneurons, microglia or astrocytes) positive for nuclear or extranuclear 5mC or 5hmC.

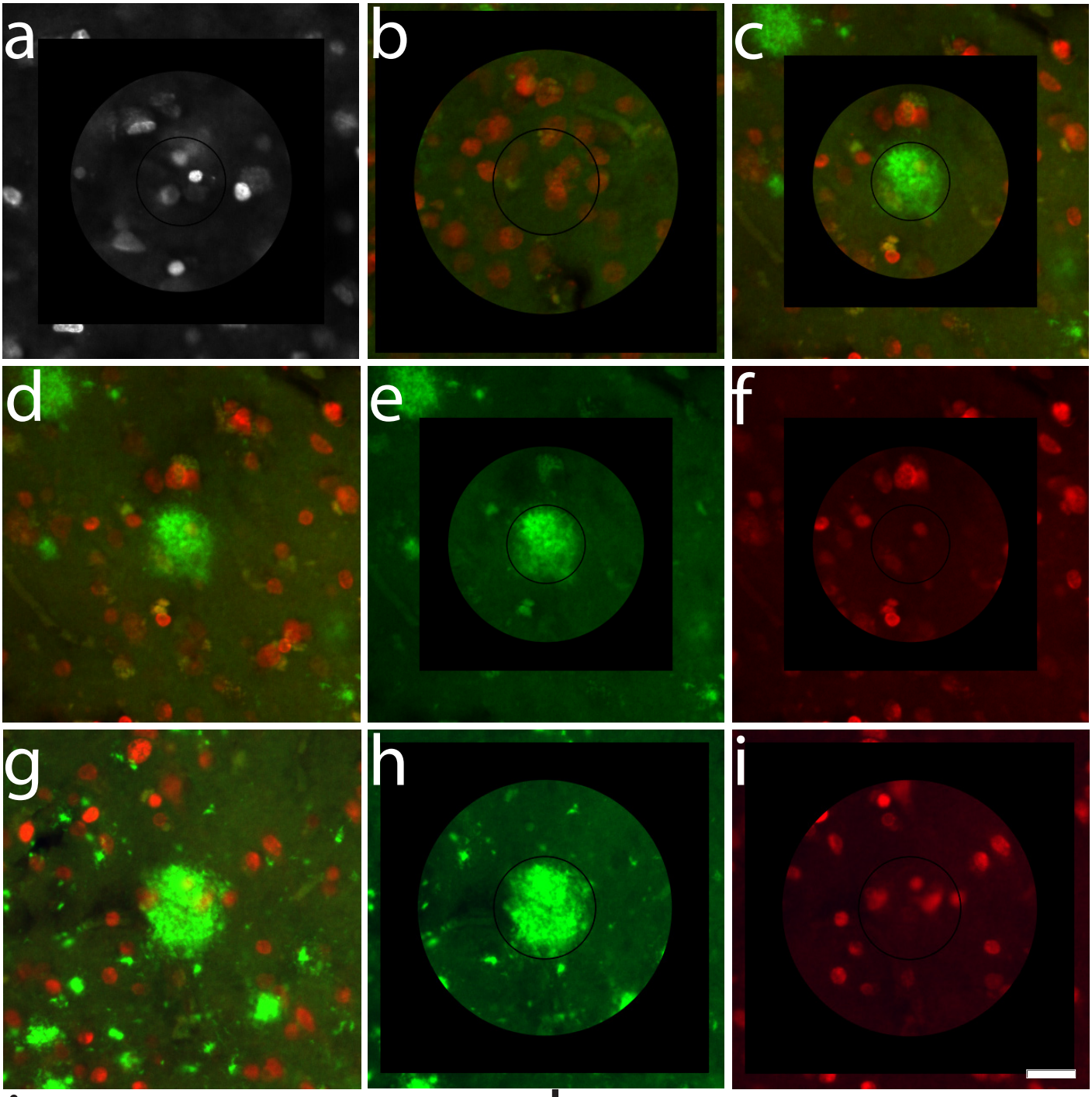
a
b
c
d
e
f
g
h
i

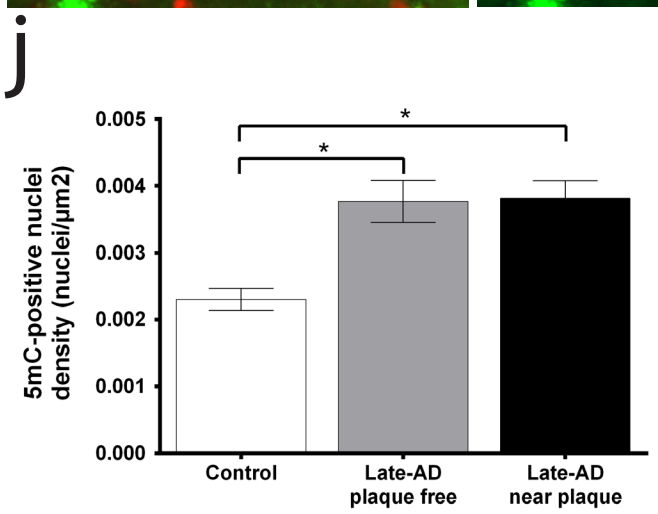
j
5mC-positive nuclei density (nuclei/µm2)
0.005
0.004
0.003
0.002
0.001
0.000
*
*
Control
Late-AD plaque free
Late-AD near plaque

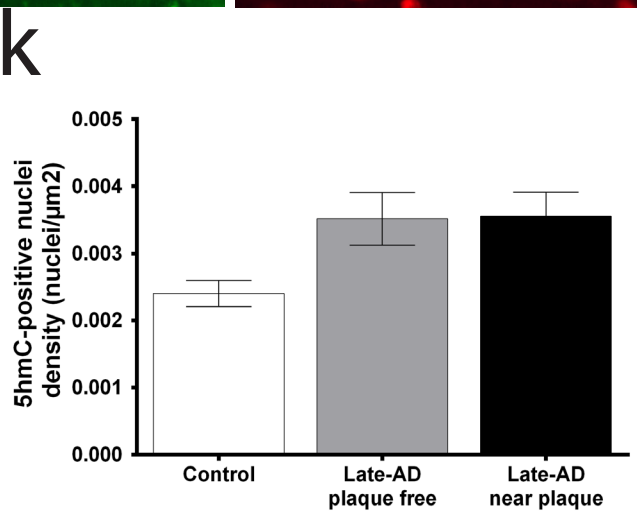
k
5hmC-positive nuclei density (nuclei/µm2)
0.005
0.004
0.003
0.002
0.001
0.000
Control
Late-AD plaque free
Late-AD near plaque

Figure 3.6: No difference in the density of 5mC and 5hmC positive nuclei in near-plaque and plaque-free regions of interest in late-AD cases

Example images of (red) 5mC labelled nuclei in layer 2/3 of a plaque-free (a) control ROI, (b) plaque-free ROI in a late-AD case and (c, green) a near-plaque ROI in a late-AD case. Representative images showing (a-f, red) 5mC and (g-i, red) 5hmC labelled nuclei in (e-f, h-i) near-plaque (green) ROI in (d-i) late-AD cases. (j) Bar graph of the density of 5mC labelled nuclei in plaque-free ROI in control cases compared to plaque-free ROI and near-plaque ROI in late-AD cases. (k) Bar graph of the density of 5hmC labelled nuclei in plaque-free ROI in control cases compared to plaque-free ROI and near-plaque ROI in late-AD cases. Bar graphs represent the mean value for each ROI type; error bars represent the SEM. Scale bar: 20μm.

3.3 Discussion

Given the small proportion of sporadic AD cases that have identifiable genetic risk factors, the pathogenesis of sporadic AD remains unknown. Epigenetics provides a potential link between environmental and pathological exposures and gene expression; thus, understanding epigenetic alterations in AD may help to elucidate mechanisms of pathogenesis and disease progression. Previous studies have detected correlations between AD pathology and DNA methylation in all cell types/whole brain homogenate, however the nature of the change in DNA methylation from many of these investigations is inconsistent (Bradley-Whitman & Lovell, 2013; Chouliaras et al., 2013; Coppieters et al., 2013; P. L. De Jager et al., 2014; Lunnon et al., 2014; D. Mastroeni et al., 2010; Sanchez-Mut et al., 2013; Siegmund et al., 2007).

This study investigated global levels of 5mC and 5hmC methylation in NF-positive pyramidal neurons, calretinin-labelled interneurons, microglia, astrocytes and methylation marks associated with disease pathology. There was no significant difference in the global levels of nuclear 5mC or 5hmC in NF-positive pyramidal neurons, calretinin-positive interneurons and microglia across disease progression, and no significant differences in extranuclear 5mC or 5hmC in calretinin-positive interneurons, microglia (Table 3.2). A significantly lower percentage of astrocytes exhibited nuclear 5mC or 5hmC in late-AD cases compared to controls. Interestingly, there were significantly less NF-pyramidal neurons with extranuclear 5mC in layer 5 of late-AD cases compared to control and early-AD cases. Finally, a high proportion of NFTs contained nuclear 5mC and 5hmC, while no specific association was observed between 5mC- and 5hmC-positive nuclei and Aβ plaques.

Table 3.2: Change in labelling of late-AD cases compared to controls

	Nuclear Labelling		Extranuclear Labelling	
Cell type	**5mC**	**5hmC**	**5mC**	**5hmC**
NF-positive pyramidal neurons	✖	✖	↓	✖
Calretinin-positive interneurons	✖	✖	✖	✖
Microglia	✖	✖	✖	✖
Astrocytes	↓	↓	✖	✖

Legend: ✖ - no change between control and late-AD case types, ↓ - significant decreased

This study was conducted using all cases available that were of sufficient quality and quantity (12 tissue sections spanning 1.0-1.5cm of the ITG). A common caveat of working with post-mortem human tissue is its limited availability due to its precious nature, thus, the number of cases of each case type examined is one of the limitations of the current study. The value of change detectable for each of the datasets presented in this study has been reported in Table 3.1. The current study was able to detect a change of 4.4% for NF pyramidal neurons co-localised with nuclear 5mC in layers 2/3, and of 31.7% of microglia containing nuclear 5hmC in layers 2/3 with 90% power. The number of cases analysed in this study is consistent with the current literature (Ahmadian et al., 2015; J. Liu & Jia, 2014; D. Mastroeni et al., 2015).

A number of epigenome-wide association studies have identified changes at a gene specific level, however, they have not taken into account artefacts caused by cell type specific differences in DNA methylation and as a result have reported wide variation in DNA methylation profiles (Bakulski et al., 2012; Bradley-Whitman & Lovell, 2013; Sanchez-Mut et al., 2013; Siegmund et al., 2007). More recently, two studies reported that DNA methylation alterations correlated with pathology load in AD, and differential CpG methylation occurred early in AD progression (P. L. De Jager et al., 2014; Lunnon et al., 2014), however both studies used whole brain homogenate, thus identifying the cell types in which these DNA methylation changes occur is crucial for understanding the pathological processes in AD (Lord & Cruchaga, 2014a). Cell type specific resolution for DNA methylation alterations is critical as cell type specific differences in DNA methylation between NF-, calretinin- and parvalbumin-positive neuronal populations were observed in mouse brain (Mo et al., 2015). Gasparoni and colleagues (2018) have also identified differences in DNA methylation between neurons and glia in the occipital lobe of AD cases after isolation with FACS. Although the study demonstrated that both neurons and glia were hypomethylated in AD, they had different methylation profiles that dynamically progressed with increasing Braak stage of AD cases (Gasparoni et al., 2018).

A number of studies have investigated changes in DNA methylation in neurons using immunohistochemistry. Coppieters et al. (2013) identified increased 5mC and 5hmC immunoreactivity in nuclei from the human medial frontal gyrus (MFG) and the medial temporal gyrus (MTG) with intensity based analysis (Coppieters et al., 2013). Chouliaras et al. (2013) also observed a global decrease in 5mC and 5hmC in neurons and glia in the hippocampus of AD cases compared to age matched controls (Chouliaras et al., 2013). Sub-region analysis of the hippocampus showed decreased 5mC in neurons of CA1, but not CA3

or dentate gyrus, and also a decrease in 5hmC in neurons in the dentate gyrus, but not in CA1 or CA3 (Chouliaras et al., 2013). In contrast this study did not detect a difference in nuclear 5mC or 5hmC localization in either NF-positive pyramidal neurons or in calretinin labelled interneurons in the ITG across disease progression. Similar to the current study, no significant difference in 5mC and 5hmC in neuronal nuclei of the entorhinal cortex was detected in AD cases compared to controls (Lashley et al., 2014). The differences between studies may be due to different methods of analysis (cell counts, immunofluorescence intensity analysis), different regions studied, and different cell populations being analysed. Differential DNA methylation patterns exist in different brain regions in the normal and disease brain (Sanchez-Mut et al., 2013), while distinct DNA methylation profiles also characterise different neuronal subpopulations (Mo et al., 2015). The data presented in this study also show inherent differences in DNA methylation patterns between distinct neuronal subtypes in the ITG. For example, >95% of NF-rich pyramidal neurons in control cases exhibit nuclear 5mC/5hmC labelling, while significantly less (~76%) calretinin-positive interneurons co-localised with 5mC/5hmC nuclei. However, it is important to note that although global measurements of DNA methylation can provide an indication of overall changes occurring in the AD brain, DNA methylation can finely control gene expression at a gene specific level. Recently, studies have demonstrated cell-type specific DNA methylation profiles in mouse and human cortex using genome wide approaches (Luo et al., 2017). Luo and colleagues (2017) characterised methylation profiles using single-cell DNA methylation sequencing, identifying 21 different excitatory and inhibitory neuronal sub-populations based on methylation status in the human frontal cortex (Luo et al., 2017). In contrast to the current study, Luo et al.,(2017) showed that interneuron populations were generally enriched to a greater level than NF+ excitatory neurons. Immunohistochemistry has a detection limit and can not detect gene or base specific differences in methylation status. It is also important to note that bisulphite sequencing cannot differentiate between 5mC and 5hmC, which may explain some of the differences between the two studies (Luo et al., 2017). Interestingly, both Luo, et al., (2017) and the current study showed layer specific differences in DNA methylation in excitatory and inhibitory neurons, however it should be noted that there were many gene specific differences in DNA methylation based on cortical layer and neuronal cell-type in Luo's study. Despite the differences in studies, the use of single cell sequencing can allow for visualization and analysis of methylation states at a gene specific level, which should be expanded upon in future studies. This PhD study also detected significant differences in the same neuronal subtype between cortical layers, with a significantly higher percentage of calretinin-positive interneurons co-localised with nuclear

5hmC in layers 2/3 compared to layer 4 in control cases. These inherent differences in DNA methylation marks between neuronal cell types is likely related to the diverse functions of different neuronal populations. Pyramidal neurons and interneurons play different roles in learning and memory (A. J. Murray et al., 2011), which cause DNA methylation changes in neurons (Day et al., 2013; Feng et al., 2010a; Levenson et al., 2006), thus it is likely that differential levels of epigenetic plasticity exist in neuronal sub-populations (Mo et al., 2015). Interestingly, a similar percentage of calretinin-labelled interneurons, astrocytes and microglia had nuclear 5mC and 5hmC (70%-80% of the population). In contrast, extranuclear 5mC and 5hmC were also observed in all cell types at varying levels. A higher proportion of NF-positive neurons contained extranuclear 5mC and 5hmC than calretinin-positive interneurons in the control cases in layer 2/3. Coppieters et al. (2013) also described extranuclear 5mC and 5hmC labelling in the processes of cells in the MFG and MTG of control and late AD cases (Coppieters et al., 2013). 5mC and 5hmC labelling has been detected in RNA and mitochondrial DNA and studies have characterised methylation of RNA as a novel mechanism of translational modification (Bradley-Whitman & Lovell, 2013; J. Liu & Jia, 2014; Squires et al., 2012). This study has shown a significant reduction in the percentage of NF-rich pyramidal neurons with extranuclear 5mC in layer 5 in late-AD cases compared to early-AD and control cases (Table 2), which may indicate altered RNA methylation in this vulnerable subset of neurons in AD.

This study detected a significantly lower percentage of astrocytes with nuclear 5mC and 5hmC in late-AD cases compared to controls, but no significant differences in 5mC or 5hmC labelling in microglia across case types (Table 2). Previous studies reported that astrocytes and microglia had weak 5mC and 5hmC labelling compared to neurons in the MTG and MFG (Coppieters et al., 2013), and that 5mC and 5hmC were decreased in glial cells in hippocampal subregions of AD cases compared to controls (Chouliaras et al., 2013). Astrocytes become activated and respond to the presence of Aβ plaques in AD (Itagaki et al., 1989), thus, it is perhaps not surprising that the epigenetic profile of astrocytes differs between control and AD cases. Studies have identified a core set of genes to be up-regulated in reactive astrocytes, however there are a range of different genes that are up-regulated depending on disease state (Zamanian et al., 2012). There were no robust differences in 5mC or 5hmC labelling of astrocytes located in close proximity to Aβ plaques in the current study, suggesting an alteration in the state of the epigenome of astrocytes throughout the cortex. The differences in astrocyte 5mC and 5hmC labelling was interesting to detect in this PhD study. However, immunohistochemistry has an inherent detection limit which is a caveat of the technique. The findings of the current study

could be further characterized and expanded upon with genome-wide approaches such as single cell sequencing. Such approaches would allow for analysis of redistribution of DNA methylation at a base specific level in control, early AD, and late stage AD cases rather than global presence or absence as found in the current study.

Several studies have reported significant positive correlations between 5mC and 5hmC levels and AD pathology load globally (Coppieters et al., 2013; P. L. De Jager et al., 2014; Lunnon et al., 2014), while other studies have reported negative or no correlations between 5mC and 5hmC levels and pathology load (Bradley-Whitman & Lovell, 2013; Chouliaras et al., 2013). There were no correlations between plaque load or NFT density and the proportion of specific cell types (NF-labelled pyramidal neurons, calretinin-labelled interneurons, microglia or astrocytes) that were positive for nuclear or extranuclear5mC or 5hmC. In addition, there was no alteration in the density of 5mC or 5hmC labelled nuclei in near-plaque versus plaque-free ROI in late-AD cases. This study has also observed a high proportion (>97%) of NF-positive pyramidal neurons with 5mC compared to the proportion of NFTs with nuclear 5mC (~75%) in AD cases. NFTs form in NF-rich pyramidal neurons, however, the NFT population measured in our study contained both intracellular NFTs and extracellular 'ghost' tangles that correspond to the death of some neurons. As extracellular NFTs in the ITG accounted for 27% of all NFTs, (James C. Vickers, Tan, & Dickson, 2003), this suggests that there is little or no loss of nuclear 5mC or 5hmC in tangle bearing neurons.

This study clearly demonstrates that there are cell type specific differences in DNA methylation, and highlights the importance of cell type specific analysis to better understand the DNA methylation profiles of neural and glial cell types in both the healthy brain and disease states. The data presented in this study indicate that epigenetic alterations occur in NF-positive pyramidal neurons and astrocytes in late-AD cases, and such epigenetic changes may play a role in AD progression. To develop a complete picture of the epigenetic changes and their role in AD both DNA methylation and histone modifications will need to be examined in different cell types across disease progression, including time-points prior to and during disease onset.

Chapter 4: Alteration of the neuronal epigenome in the aging brain

4.1 Introduction

Aging is the leading risk factor for development of AD, however there have been few studies to characterise histone modifications within the healthy aging brain (Chapter 1.12). This is particularly important as epigenetic regulation is a dynamic process in the brain, with roles in neuronal development, maintenance, memory formation and consolidation, synaptic maintenance, and long-term potentiation, many of which are disrupted in AD (Feng et al., 2010b; Levenson et al., 2006; Lubin et al., 2008).

There have been few studies to characterise global levels of histone modifications within the aging brain (Peleg et al., 2010; Rodrigues et al., 2014; Walker et al., 2013). The most widely studied histone modification has been H3K9 methylation and acetylation. Of the few studies to measure global histone modifications, the data suggest that different cell-types and cortical regions exhibit different global levels for histone modifications such as H3K9ac and H3K9 methylation (Rodrigues et al., 2014; Walker et al., 2013). Rodrigues and colleagues (2014) showed enrichment of H3K9ac marking in the aged mouse cortex, but depletion of H3K9me3, indicative of increased chromatin accessibility and transcriptional activity when measured with Western blot and immunocytochemistry (Rodrigues et al., 2014). While an *in vitro* study identified no change in total H3 acetylation, but depletion of H4 acetylation and H3K9 methylation in aging hippocampal and cortical neurons across a time-course from 2-21 months of age (Walker et al., 2013). Interestingly, depletion of H3K9ac marking correlated with decreased expression of BDNF in cultured neurons (Walker et al., 2013). However, another study demonstrated that there was no global change in H3K9ac, H3K14ac, H4K5ac, H4K8ac, H4K12ac and H4K16ac in 16 month old hippocampal neurons from the C57/BL6 mice, compared to 3 month controls when measured with immunoblot (Peleg et al., 2010).

Although global measurements of histone modifications can provide an indication of overall changes occurring within the aging brain, epigenetic regulation of the genome is finely controlled at specific promoters and enhancers to regulate gene expression. To date, there have been 4 studies that have characterised histone modifications in the aging brain at a genome-wide level (Benito et al., 2015; Cheung et al., 2010; Nativio et al., 2018; Shulha et al., 2013). These studies have identified a redistribution of histone acetylation with increasing age. For example, Nativio, et al., (2018) performed ChIP-seq for H4K16ac in post-mortem human lateral temporal lobe from cases in the 'young' (mean age 52) and 'old' (mean age 68) cohorts. Nativio and colleagues identified an enrichment of H4K16ac genome-wide, with 127000 peaks

unique to old cases compared to 50000 peaks unique to young cases, and ~156000 peaks shared by young and old cases (Nativio et al., 2018). Gene ontology analysis further elucidated that the top aging associated genes were annotated to pathways involving respiration processing, insulin stimulus and inflammatory response (Nativio et al., 2018). Interestingly, the study also identified a linear correlation between aging and neurodegenerative disease, implicating a component of normal aging in disease (Nativio et al., 2018).

To date, only 3 studies have utilised FACS to isolate neuronal nuclei from the cortex to identify neuron specific changes to histone modifications in the aging brain (Benito et al., 2015; Cheung et al., 2010; Shulha et al., 2013). A ChIP-seq study of neurons in the post-mortem human prefrontal cortex from 0.5-69 years demonstrated an age associated depletion of H3K4me3 (Cheung et al., 2010). Analysis of developmental (<1 year old) and aged (>60 years of age) neuronal samples showed 589 significant H3K4me3 peaks enriched in the developmental neurons, but not aged neurons, while 101 peaks were enriched in the aged neurons (Cheung et al., 2010). The study demonstrated that enrichment of H3K4me3 in all samples was specific to key neuronal pathways involving neurogenesis, neurite development, and synaptic transmission, however there were no significant gene ontology terms identified from the 101 peaks specific to aged neurons (Cheung et al., 2010). In accordance with Cheung, another genome-wide study in neurons from the prefrontal cortex has identified rapidly occurring developmental changes to H3K4me3 at 1157 loci in neurons at sites pertaining to neuronal development, synaptogenesis, and intracellular signalling, but few changes to H3K4me3 marking in adult or aging neurons (Shulha et al., 2013). Finally, Benito and colleagues (2015) identified genome-wide depletion of H4K12ac in neurons from the hippocampus of C57/BL6 mice at 20 months of age compared to 3 months of age, at sites involved in RNA modifications, metabolic processes, apoptosis, and RNA localisation (Benito et al., 2015). Interestingly, H4K12ac depletion with age was specific to neuronal cells, and reversed by administration of a HDACi (Benito et al., 2015). The studies to date have demonstrated both enrichment and depletion of histone modifications associated with transcription in the aging brain.

The current study sought to characterise the histone landscape of neurons within healthy aging brain in a time-course by utilising chromatin immunoprecipitation and next-generation sequencing (ChIP-seq) of H3K27ac and H3K4me3 from the forebrain of C57/BL6 mice at 3, 6, 12, and 24 months of age. These data present the first comprehensive genome-wide characterisation of both H3K27ac and H3K4me3 in neurons of the aging brain.

4.2 Results

4.2.1 Histone acetylation changes in neurons during development and aging

The epigenome is regulated through a wide range of epigenetic modifiers. Here, H3K27ac; a key marker of active promoters and active enhancers, was characterised in forebrain neurons from C57/BL6 animals at 3 months of age, 6 months of age, 12 months of age, and 24 months of age.

An assessment of the total genomic coverage can provide an indication of the changes to H3K27ac marking in aging neurons at a global level. Here, an analysis of the total genomic coverage was performed of neurons from mice at 3, 6, 12, and 24 months of age by determining the percentage of the genome that contained greater than 5× depth for H3K27ac. At 3 months of age, H3K27ac marking was present in approximately 2.23% of the neuronal genome, similarly 6 month old neurons exhibited approximately 2.46% genome coverage for H3K27ac (Figure 4.1a). By 12 months of age, neurons were depleted for H3K27ac compared to the previous time-points (12 months: 1.86% genome coverage; Figure 4.1a). Strikingly, 24 month old neurons sustained a ~50% increase in H3K27ac marking compared to the earlier time-points (24 months: 3.70%; Figure 4.1a).

Next, a pairwise analysis of differential enrichment for H3K27ac was performed genome-wide across 3, 6, 12, and 24 month old neurons. This analysis demonstrated an evolution of H3K27ac marking in aging neurons (Figure 4.1b-d). Initially, there were 11901 sites significantly enriched for H3K27ac in 3 month old neurons compared to 6 months old neurons, and 122 sites that were depleted in 3 month old neurons compared to 6 month old neurons (Benjamini Hochberg FDR adjusted p-value <0.05; Figure 4.1b). There were 1230 differentially enriched and 103 depleted H3K27ac marked sites in neurons at 12 months of age compared to those at 6 months of age (Benjamini Hochberg FDR adjusted p-value <0.05; Figure 4.1c). Interestingly, 11823 sites were enriched for H3K27ac in 24 month old neurons compared to those at 12 months of age, and 155 sites were depleted for H3K27ac marking in 24 month old neurons compared to 12 months of age (BH FDR adjusted p-value <0.05; Figure 4.1d). Differential enrichment for H3K27ac peaked in 3 month, and 24 month old neurons (Figure 4.1b-d). The top ranked differentially enriched sites from the neuronal aging time-course were visualised with IGV, showing multiple genomic regions that were differentially enriched for H3K27ac.

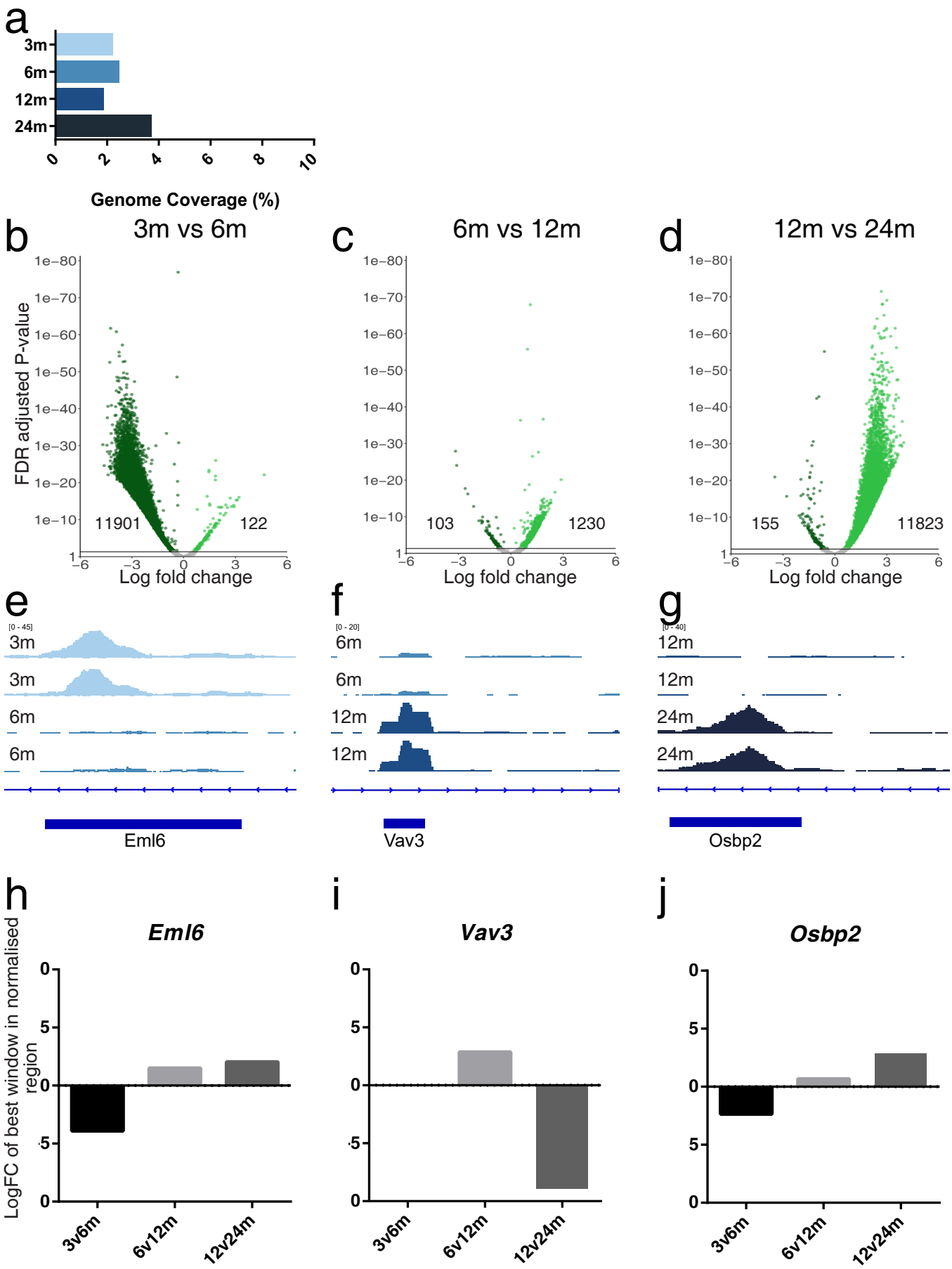
a
3m
6m
12m
24m
0
2
4
6
8
10
Genome Coverage (%)
b
3m vs 6m
c
6m vs 12m
d
12m vs 24m
FDR adjusted P-value
1e−80
1e−70
1e−60
1e−50
1e−40
1e−30
1e−20
1e−10
1
11901
122
103
1230
155
11823
−6
−3
0
3
6
Log fold change
e
f
g
[0 - 45]
[0 - 20]
[0 - 40]
3m
3m
6m
6m
6m
12m
12m
12m
24m
24m
Eml6
Vav3
Osbp2
h
i
j
Eml6
Vav3
Osbp2
LogFC of best window in normalised region
5
0
-5
3v6m
6v12m
12v24m

Figure 4.1: H3K27ac is enriched during development and in aging neurons

(a) Percentage 5× genomic coverage of H3K27ac in 3 month (light blue), 6 month (blue), 12 month (dark blue), and 24 month old (dark grey) neurons from C57/BL6 mice. (b-d) Volcano plots show the logFC and FDR adjusted P-value of H3K27ac marking through a time-course of aging in neurons. (b) LogFC and FDR adjusted P-value of 3 month versus 6 month old neurons, (c) 6 month versus 12 month old neurons and, (d) 12 month versus 24 month old neurons; positive logFC (light green) represents enrichment in the older time-point of pairwise comparison, and negative logFC (dark green) depletion from the older time-point of the pairwise comparison (i.e. enrichment in the younger time-point). (e-g) Representative tracks visualised in IGV showing the top-ranked sites of enrichment in pseudoreplicates between (e) 3 (light blue) and 6 (blue) month old neurons at an enhancer across the *Eml6* gene; (f) 6 (blue) and 12 (dark blue) month old neurons at the *Vav3* enhancer and; (g) 12 (dark blue) versus 24 (dark grey) month old neurons at the *Osbp2* enhancer. (h-j) Histograms showing the logFC of the best window within the normalised region of H3K27ac marking in neurons from the pairwise differential enrichment analysis at (h) *Eml6*, (i) *Vav3* and, (j) *Osbp2* enhancers.

For example, an enhancer for *Eml6* encoding Echinoderm Microtubule Associated Protein Like 6, was enriched in 3 month old neurons compared to neurons in 6 month old mice. *Eml6* is a member of a protein family reported to stabilise microtubules in the mammalian brain (Houtman, Rutteman, De Zeeuw, & French, 2007). Interestingly, *Vav3*; Vav Guanine Nucleotide Exchange Factor 3, a protein involved in actin cytoskeletal rearrangements and axon guidance, (Sauzeau et al., 2010) was depleted in 6 month old neurons compared to those at 12 months of age. *Vav3* has also been implicated in neurological disorders such as schizophrenia (Aleksic et al., 2013). Similarly, H3K27ac was enriched at a putative enhancer for *Osbp2*; Oxysterol Binding Protein 2 in 24 month old neurons compared neurons at 12 months of age. Oxysterol binding proteins are known to regulate lipid and cholesterol metabolism and are thought to interact with intermediate filaments (C. Wang, JeBailey, & Ridgway, 2002),. To further illustrate the dynamic nature of H3K27ac marking in aging neurons, the LogFC of *Eml6*, *Vav3*, and *Osbp2* were plotted as histograms across the aging time-course, demonstrating the dynamic nature of H3K27ac marking over time (Figure 4.1e-j).

Taken together, these data demonstrate a global enrichment of H3K27ac marking in aging neurons, and differential enrichment of H3K27ac marking in 3 and 24 month old neurons, while there was little change in neuronal H3K27ac marking between 6 and 12 months of age.

4.2.2 H3K27ac is enriched at TSS in neurons during development and late aging

H3K27ac marking is generally present at active enhancers, and to a lesser degree at the TSS of active genes (Creyghton et al., 2010b; Rada-Iglesias et al., 2011). Initially, the average distribution of H3K27ac marking was plotted around a 2kb region upstream and downstream of TSS. Here it was identified that H3K27ac marking was enriched in neurons around the TSS particularly during development and late aging (Figure 4.2a). The marking exhibited a bimodal distribution, with the greatest signal identified at the +1 nucleosome sitting immediately 3'- to the TSS (Figure 4.2a). The average H3K27ac marking was approximately 2-fold greater in 3 month old neurons compared to 6 month old neurons (3 month max: 2.04, 6 month max: 1.13, respectively; Figure 4.2a). At 12 months of age, H3K27ac marking was slightly enriched in neurons at the TSS compared to 6 month old neurons (12 month max: 1.34; Figure 4.2a).

Interestingly, in 24 month old neurons, H3K27ac marking was approximately 2-fold greater than 12 month old neurons (24 month max: 2.90; Figure 4.2a).

Next, heatmaps of H3K27ac marking were plotted against UCSC KnownGene TSS. This analysis showed that approximately 33% of TSS contained H3K27ac marking in neurons at 3 months of age. The magnitude and distribution of H3K27ac marking was depleted in neurons by 6 months of age, then increased at 12 months of age. By 24 months of age, the proportion of TSS and magnitude of H3K27ac marking in neurons was enriched to a greater level than in 3 month old neurons (Figure 4.2b).

CpG islands are key regulatory regions of the genome, predominantly found at the TSS, and are key sites for DNA methylation to regulate transcription (review: (Deaton & Bird, 2011)). To further elucidate the distribution of H3K27ac marking at TSS and to identify if the changes seen at the TSS were predominantly found at CpG islands, the data was subset into CpG islands containing TSS and non-CpG island TSS. Interestingly, approximately 40% of all TSS contained CpG islands. At 3 months of age H3K27ac marking covered approximately 2/3 of all CpG islands containing TSS in neurons (Figure 4.2c). By 6 months of age, the proportion of H3K27ac marked CpG island TSS and the magnitude of H3K27ac marking were depleted in neurons (Figure 4.2c). While at 12 months of age, the proportion of CpG islands containing TSS marked with H3K27ac in neurons increased to a similar number as observed in 3 month old neurons, however the magnitude of H3K27ac marking was still lower than in 3 month old neurons (Figure 4.2c). Interestingly, 24 month old neurons were enriched in both the proportion of CpG island containing TSS marked and the magnitude of H3K27ac marking to a level greater than in 3 month old neurons. Moreover, the distribution of H3K27ac marking shifted slightly downstream of the TSS in 24 month old neurons compared to neurons at all the other ages examined (Figure 4.2c). In contrast to CpG island containing TSS, non-CpG island containing TSS exhibited a lower proportion and magnitude of H3K27ac enrichment in neurons (Figure 4.2d). At 3 months of age, approximately 1/5 of non-CpG island TSS contained H3K27ac marking in neurons (Figure 4.2d). However, by 6 months of age, the proportion of non-CpG island TSS enriched for H3K27ac and the magnitude of enrichment were depleted in neurons (Figure 4.2d). At 12 months of age, there was a slight increase in the proportion and magnitude of H3K27ac marking at non-CpG island TSS compared to 6 months of age, which was then further increased in 24 month old neurons, back to the levels seen in 3 month old neurons (Figure 4.2d).

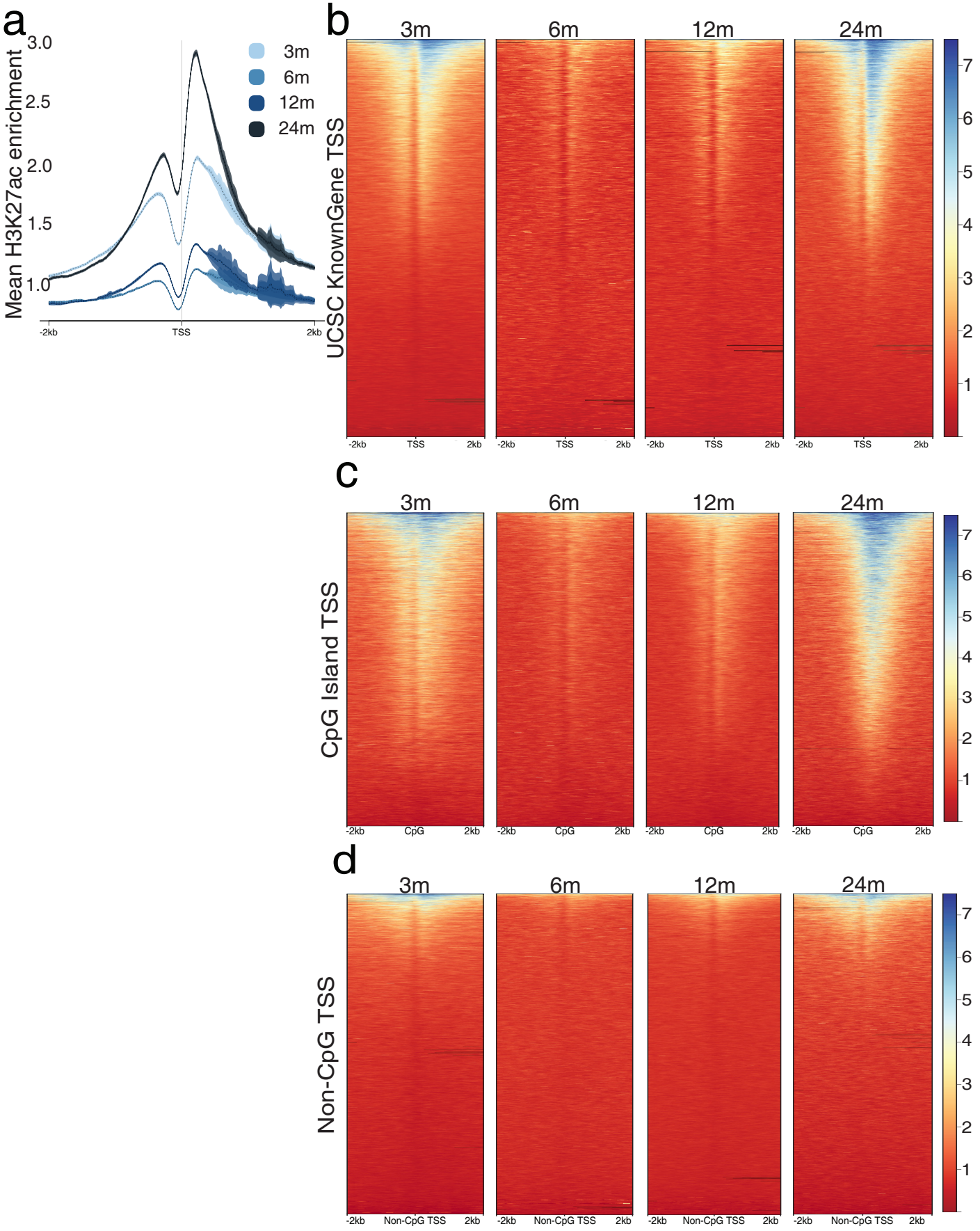
a
Mean H3K27ac enrichment
3.0
2.5
2.0
1.5
1.0
3m
6m
12m
24m
-2kb
TSS
2kb
b
3m
6m
12m
24m
UCSC KnownGene TSS
-2kb
TSS
2kb
7
6
5
4
3
2
1
c
CpG Island TSS
-2kb
CpG
2kb
d
Non-CpG TSS
-2kb
Non-CpG TSS
2kb

Figure 4.2: H3K27ac is enriched at the TSS in neurons during development and late aging (a) Average enrichment plots for H3K27ac within a 2kb window of TSS for the UCSC KnownGene track in neurons at 3 (light blue), 6 (blue), 12 (dark blue) and 24 months of age (dark grey). (b) Heatmaps of H3K27ac marking at TSS for UCSC KnownGene sorted by strongest (blue) to weakest (red) signal in neurons from 3, 6, 12 and 24 months of age. (c) Heatmaps of H3K27ac marking at CpG island containing TSS from the UCSC mm10 CpG island track sorted by strongest (blue) to weakest (red) signal in neurons from 3, 6, 12 and 24 month old C57/BL6 mice. (d) Heatmaps of H3K27ac marking at non-CpG containing TSS from the UCSC mm10 KnownGene track sorted by strongest (blue) to weakest (red) signal in neurons from 3, 6, 12 and 24 month old C57/BL6 mice.

Taken together, these data demonstrate that H3K27ac marking is enriched at TSS in 3 and 24 month old neurons and H3K27ac marking is depleted from adult neurons at 6 and 12 months of age. TSS are enriched for H3K27ac marking in 24 month old neurons, to levels similar to those observed at 3 months of age. The majority of differential H3K27ac marking in neurons across aging is occurring at CpG island containing TSS.

4.2.3 H3K27ac marking is enriched at putative enhancers and cortical super enhancers in development and late aging

There are a range of transcriptional elements that are responsible for appropriate cellular identity and function. Enhancers are key distal regulatory elements that allow for appropriate cellular identity and function. To identify epigenetic modifications occurring at enhancers specifically, a track of all H3K27ac marking outside of a 2kb window of UCSC KnownGene TSS was generated and used to map 'putative enhancers'. Herein, 'putative enhancers' as defined above will be referred to as enhancers.

The average distribution of H3K27ac at enhancers was measured by visualising the mean abundance of reads around a 2kb window of the enhancer mid-point. Initially, H3K27ac marking at enhancers were collated and mapped. 3 month old neurons were highly enriched for H3K27ac marking (3 month max: 37.98; Figure 4.3a), which was similar at 6 months of age (6 month max: 31.32; Figure 4.3a). Interestingly, at 12 months of age, the magnitude of marking for H3K27ac at enhancers was increased in neurons (12 month max: 45.60; Figure 4.3a). Interestingly, the magnitude of enhancer H3K27ac marking was depleted in 24 month old neurons (24 month max: 30.56; Figure 4.3a). The average enrichment of enhancers was highly dynamic throughout the aging time-course.

Next, H3K27ac marking was mapped against enhancers by visualising the data with heatmaps. Enhancers were highly enriched in neurons at 3 months of age, with the vast majority of enhancers containing H3K27ac marking at the mid-point of the 2kb window (Figure 4.3b). By 6 months of age, only a small proportion of enhancers in neurons were highly enriched for H3K27ac marking, however the mid-point of all enhancers showed weak marking for H3K27ac (Figure 4.3b). Enhancers were slightly enriched in the magnitude of H3K27ac marking in neurons at 12 months of age compared to 6 months of age (Figure 4.3b), and by 24 months of age, the proportion and magnitude of H3K27ac marking at enhancers were further enriched.

Interestingly, at 24 months of age, H3K27ac marking was widely distributed across the 2kb window in a small subset of enriched enhancers in neurons (Figure 4.3b).

Super-enhancers are recently discovered regulatory regions responsible for cell-type specific gene expression that aid in the determination of cellular identity ((Hnisz et al., 2013; Whyte et al., 2013); Chapter 1.10). A cortical super-enhancer track was obtained from dbSUPER; a database of known super-enhancers, to map changes in H3K27ac enrichment around known cortical super-enhancers (Khan & Zhang, 2016). The majority of known cortical super-enhancers were enriched for H3K27ac marking, with approximately 25% of all super enhancers highly enriched for H3K27ac marking in neurons at 3 months of age (Figure 4.3c). However, in 6 month old neurons, the magnitude and proportion H3K27ac marking at super enhancers was lower than in 3 month old neurons (Figure 4.3c). At 12 months of age, neurons showed slight enrichment for H3K27ac at super-enhancers compared to the 6 month time-point (Figure 4.3c). Interestingly, the magnitude and proportion of H3K27ac enrichment at super-enhancers increased in 24 month old neurons to levels seen at 3 months of age (Figure 4.3c). This was further illustrated with example tracks of H3K27ac marking at the top ranked sites enriched for H3K27ac overlapping cortical super-enhancers.

Next, an overlap analysis for differentially enriched H3K27ac sites (from Figure 4.1a) was performed with the cortical super-enhancer track. There were 1165 differentially marked H3K27ac sites that were enriched in 3 month versus 6 month old neurons that overlapped cortical super-enhancers. However, there were only 5 differentially marked H3K27ac sites that intersected cortical super-enhancers that were enriched in 6 month old versus 3 month old neurons. The top ranked H3K27ac marked site from 3 month old versus 6 month old neurons was at the super-enhancer overlapping the *Bsn* gene (Figure 4.3d). While 277 differentially enriched H3K27ac sites were overlapping super-enhancers in 12 month old neurons, with the top ranked H3K27ac site was at the super-enhancer at the *Celf2* gene (Figure 4.3e). There were 9 H3K27ac marked sites that were overlapping super-enhancers in 6 month old neurons compared to 12 months of age. Interestingly, there were 1028 H3K27ac differentially marked sites enriched in 24 month old neurons compared to 12 month old neurons that were also sites for known cortical super-enhancers, as well as 16 sites of H3K27ac enrichment in 12 month old versus 24 month old neurons. The top ranked H3K27ac marked site was overlapping a super-enhancer at the *Tbr1* gene (Figure 4.3f).

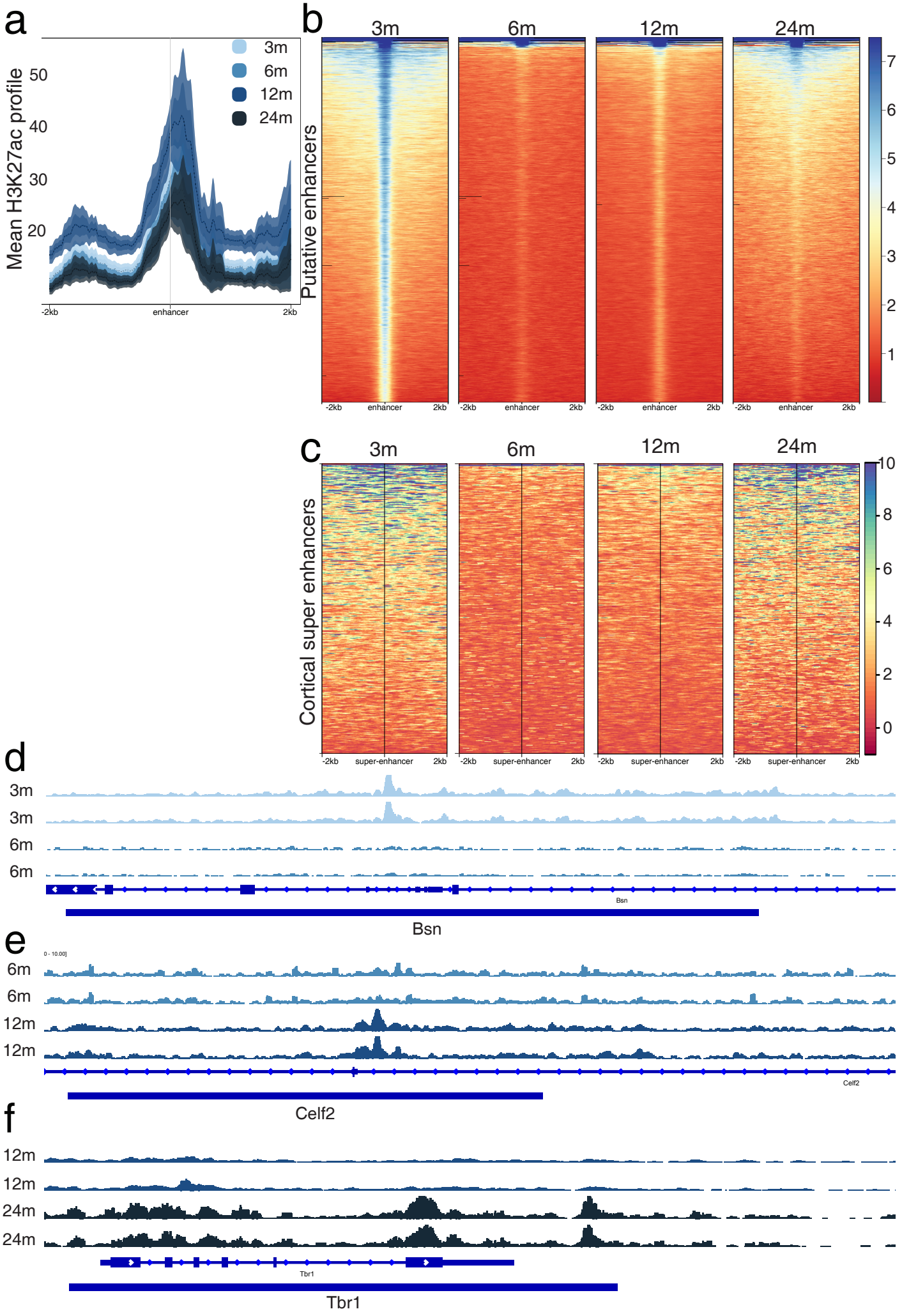
a
Mean H3K27ac profile
50
40
30
20
3m
6m
12m
24m
-2kb
enhancer
2kb
b
3m
6m
12m
24m
Putative enhancers
7
6
5
4
3
2
1
-2kb
enhancer
2kb
c
3m
6m
12m
24m
Cortical super enhancers
10
8
6
4
2
0
-2kb
super-enhancer
2kb
d
3m
3m
6m
6m
Bsn
Bsn
e
0 - 10.00]
6m
6m
12m
12m
Celf2
Celf2
f
12m
12m
24m
24m
Tbr1
Tbr1

Figure 4.3: H3K27ac is enriched at enhancers and super-enhancers in neurons in development and aging

(a) Average enrichment plots for H3K27ac within a 2kb window of putative enhancers in neurons at 3 (light blue), 6 (blue), 12 (dark blue) and 24 (dark grey) months of age. (b) Heatmaps for H3K27ac marking at putative enhancers sorted by strongest (blue) to weakest (red) signal in 3, 6, 12 and 24 month old neurons from the forebrain of C57/BL6 animals. (c) Heatmaps for H3K27ac marking against the Super-Enhancer Database (dbSUPER) track were sorted by strongest (blue) to weakest (red) signal in neurons at 3, 6, 12 and 24 months of age. (d-f) Representative tracks visualised using the IGV browser are shown. H3K27ac signal overlap was evident in neurons at super-enhancers overlapping the top ranked differentially enriched sites including between pseudoreplicates at; (d) 3 and 6 months of age at the *Bsn* loci, (e) 6 and 12 months of age at the *Celf2* loci and (f) 12 and 24 months of age at the *Tbr1* loci.

Taken together, these data demonstrate that H3K27ac marking is dynamically regulating enhancers and super-enhancers throughout the genome in aging neurons. There is enrichment of H3K27ac at both enhancers and super enhancers in neurons at 3 months of age, which is then depleted at 6 and 12 months of age, before becoming enriched in 24 month old neurons.

4.2.4 H3K27ac marking of the epigenome annotates to synaptic pathways in aging

Next, the underlying molecular and biological pathways associated with the differential enrichment of H3K27ac in neurons was assessed with gene ontology using the Genomic Regions Enrichment of Annotations Tool (GREAT) (C. Y. McLean et al., 2010). H3K27ac marking was dynamically enriched in a range of molecular and biological processes. For example, H3K27ac marked sites that were differentially enriched in neurons between 3 and 6 months of age were annotated to 'GO molecular functions' such as 'calmodulin binding', 'divalent inorganic cation transmembrane transporter activity', 'calcium channel activity' and 'actin filament binding', while annotation to 'GO biological process' identified pathways such as 'regulation of synaptic transmission', 'metal ion transport', 'calcium ion transport' and 'learning' (Figure 4.4a,d). H3K27ac marked sites that were differentially enriched between 6 and 12 month old neurons were annotated to 'GO molecular functions' including 'protein N-terminus binding', 'ankyrin binding' and 'voltage-gated sodium channel activity'. H3K27ac marked sites were also annotated to 'GO biological processes' of 'synapse organisation', 'regulation of synaptic plasticity', and 'protein localisation to membrane' (Figure 4.4b,e). Between 12 and 24 months of age, H3K27ac marking in neurons was annotated to 'GO molecular functions' including 'actin filament binding', 'unfolded protein binding', 'SNARE binding' and 'polyubiquitin binding', and annotations to 'GO biological processes' included 'regulation of RNA splicing', 'maintenance of protein location in cell', 'regulation of receptor activity' and 'execution phase of apoptosis' (Figure 4.4c,f).

Together these data identified a transition from synaptic and ion transport pathways in juvenile neurons, while cortical aging led to enrichment in pathways for the maintenance of cellular function and cellular senescence such as RNA splicing, protein localisation and apoptosis.

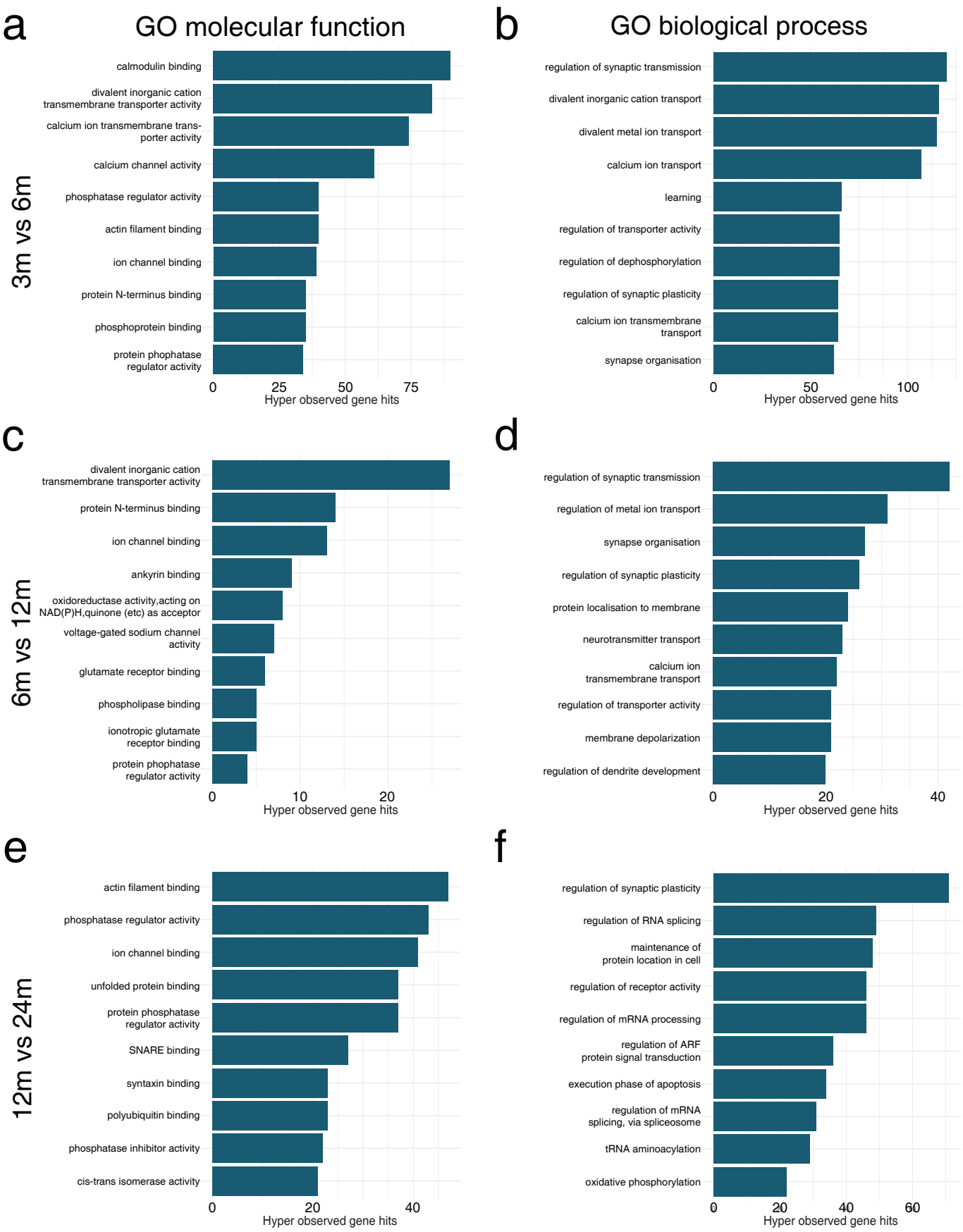
a
GO molecular function
3m vs 6m
calmodulin binding
divalent inorganic cation transmembrane transporter activity
calcium ion transmembrane trans-porter activity
calcium channel activity
phosphatase regulator activity
actin filament binding
ion channel binding
protein N-terminus binding
phosphoprotein binding
protein phophatase regulator activity
0
25
50
75
Hyper observed gene hits
b
GO biological process
regulation of synaptic transmission
divalent inorganic cation transport
divalent metal ion transport
calcium ion transport
learning
regulation of transporter activity
regulation of dephosphorylation
regulation of synaptic plasticity
calcium ion transmembrane transport
synapse organisation
0
50
100
Hyper observed gene hits
c
6m vs 12m
divalent inorganic cation transmembrane transporter activity
protein N-terminus binding
ion channel binding
ankyrin binding
oxidoreductase activity,acting on NAD(P)H,quinone (etc) as acceptor
voltage-gated sodium channel activity
glutamate receptor binding
phospholipase binding
ionotropic glutamate receptor binding
protein phophatase regulator activity
0
10
20
Hyper observed gene hits
d
regulation of synaptic transmission
regulation of metal ion transport
synapse organisation
regulation of synaptic plasticity
protein localisation to membrane
neurotransmitter transport
calcium ion transmembrane transport
regulation of transporter activity
membrane depolarization
regulation of dendrite development
0
20
40
Hyper observed gene hits
e
12m vs 24m
actin filament binding
phosphatase regulator activity
ion channel binding
unfolded protein binding
protein phosphatase regulator activity
SNARE binding
syntaxin binding
polyubiquitin binding
phosphatase inhibitor activity
cis-trans isomerase activity
0
20
40
Hyper observed gene hits
f
regulation of synaptic plasticity
regulation of RNA splicing
maintenance of protein location in cell
regulation of receptor activity
regulation of mRNA processing
regulation of ARF protein signal transduction
execution phase of apoptosis
regulation of mRNA splicing, via spliceosome
tRNA aminoacylation
oxidative phosphorylation
0
20
40
60
Hyper observed gene hits

Figure 4.4: H3K27ac alterations in neurons annotate to pathways involving synaptic plasticity and RNA modifications in the aging brain

(a-f) The top 10 gene ontology annotations, ranked by hypergeometric observed gene hits for sites of significant (FDR adjusted P value <0.05) H3K27ac differential enrichment in neurons at (a,d) 3 versus 6 months of age (b,e), 6 versus 12 months of age and (c,f) 12 versus 24 months of age. Gene ontology analysis predicts annotated pathways in (a, b, c) molecular function and, (d, e, f) biological processes. All GO terms reported = FDR adjusted P value <0.05

4.2.5 H3K27ac marking is evolving in neurons, and demonstrate a partial recapitulation of development in neurons from the aging brain

To determine whether enrichment of H3K27ac occurred at similar or different loci in aging neurons an intersection analysis of bed files containing all sites of significant differential enrichment at each time-point was performed.

Initially, there were 10209 differentially enriched H3K27ac sites specific to the 3 month old versus 6 month old neuron comparison, with only 112 sites were shared with the analysis performed on 6 versus 12 month old neurons (Figure 4.5a). Strikingly, there were 7203 sites (>33% of the sites) of H3K27ac differential binding that were shared between young (3 versus 6 months) and old (12 versus 24 months) neurons (Figure 4.5a). There was also a group of 1225 differentially enriched H3K27ac sites in neurons that were present in all pairwise timepoint comparisons (Figure 4.5a). The majority of H3K27ac differentially marked sites between the 6 versus 12 month old neurons were shared with the other time-points, with only 75 sites of differential H3K27ac marking specific to this pairwise comparison. The majority (12747) of H3K27ac differentially marked sites in neurons from the 12 versus 24 month old comparison were specific to that time-point (Figure 4.5a).

Next, gene ontology analysis was performed for the sites identified in the intersection analysis to assess the biological pathways in neurons that were common across time-points or specific to certain ages. Sites of differential H3K27ac marking specific to 3 versus 6 month old neurons were annotated to ‘GO biological processes’ including ‘ion transmembrane transport’, ‘regulation of neurological system process’, ‘regulation of transmission of nerve impulse’ and ‘divalent metal ion transport’ (Figure 4.5c). Interestingly, differentially H3K27ac marked sites shared between the 3 versus 6 month old neurons and 12 versus 24 month old neurons were annotated to ‘GO biological processes’ including the ‘regulation of synaptic plasticity’, ‘regulation of transporter activity’, ‘regulation of phosphatase activity’, and ‘regulation of dendrite development’ (Figure 4.5d). Sites that were unique to the 12 versus 24 month time-point were annotated to pathways involving the ‘regulation of mRNA processing’, ‘regulation of ARF protein signal transduction’, ‘execution phase of apoptosis’, ‘vacuolar transport’, and ‘oxidative phosphorylation’ among others (Figure 4.5e).

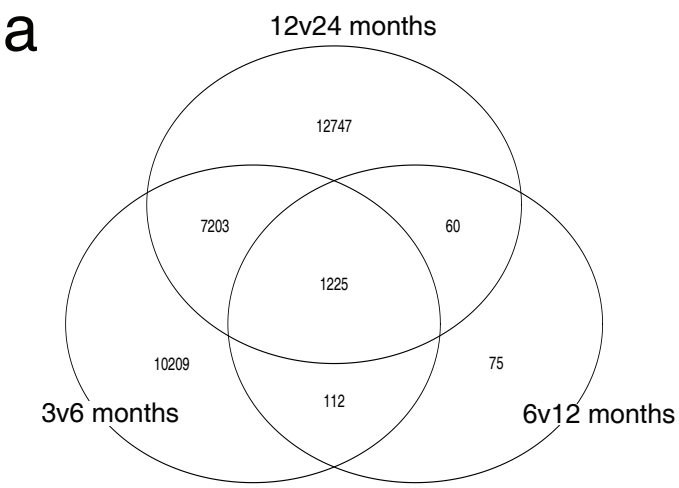
a
12v24 months
12747
7203
60
1225
10209
75
112
3v6 months
6v12 months

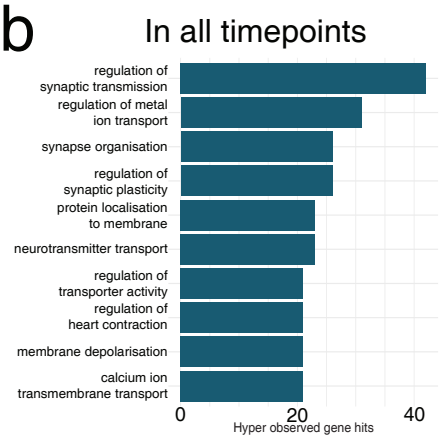
b
In all timepoints
regulation of synaptic transmission
regulation of metal ion transport
synapse organisation
regulation of synaptic plasticity
protein localisation to membrane
neurotransmitter transport
regulation of transporter activity
regulation of heart contraction
membrane depolarisation
calcium ion transmembrane transport
0
20
40
Hyper observed gene hits

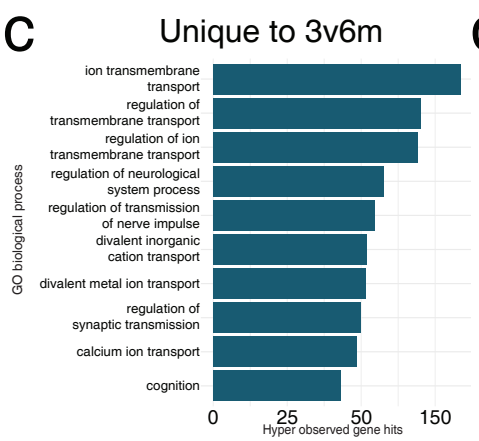
c
Unique to 3v6m
GO biological process
ion transmembrane transport
regulation of transmembrane transport
regulation of ion transmembrane transport
regulation of neurological system process
regulation of transmission of nerve impulse
divalent inorganic cation transport
divalent metal ion transport
regulation of synaptic transmission
calcium ion transport
cognition
0
25
50
150
Hyper observed gene hits

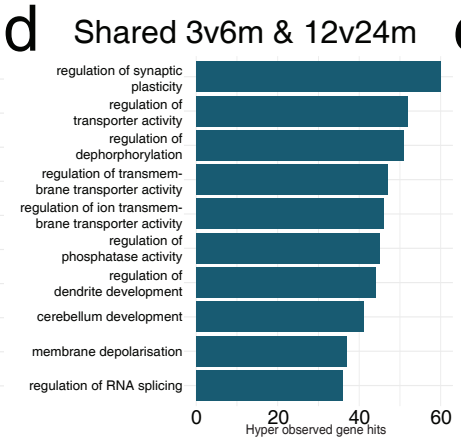
d
Shared 3v6m & 12v24m
regulation of synaptic plasticity
regulation of transporter activity
regulation of dephorphorylation
regulation of transmembrane transporter activity
regulation of ion transmembrane transporter activity
regulation of phosphatase activity
regulation of dendrite development
cerebellum development
membrane depolarisation
regulation of RNA splicing
0
20
40
60
Hyper observed gene hits

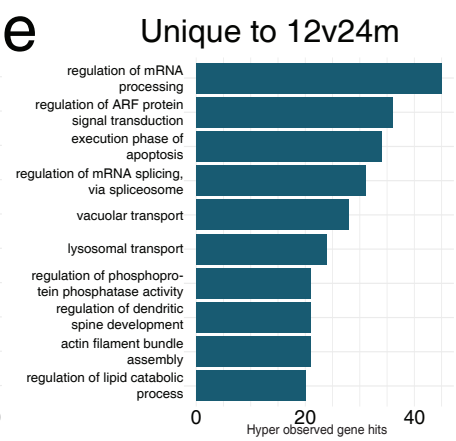
e
Unique to 12v24m
regulation of mRNA processing
regulation of ARF protein signal transduction
execution phase of apoptosis
regulation of mRNA splicing, via spliceosome
vacuolar transport
lysosomal transport
regulation of phosphoprotein phosphatase activity
regulation of dendritic spine development
actin filament bundle assembly
regulation of lipid catabolic process
0
20
40
Hyper observed gene hits

Figure 4.5: Evolution of differential H3K27ac marking and partial recapitulation of a juvenile-like epigenetic state in aging neurons

(a) Venn diagram plotting the overlap in sites that were differentially enriched in neurons from the 3 months versus 6 months, 6 months versus 12 months and 12 months versus 24 months old pairwise comparisons. (b) Functional annotations for 'GO biological process' for the 1225 sites that were differentially enriched in neurons at all time points, (c) the 10209 H3K27ac sites unique to the 3 versus 6 months of age differential enrichment analysis, (d) the 7203 sites shared between the 3 versus 6 months of age and 12 versus 24 months of age pairwise comparison and, (e) the 12747 H3K27ac marked sites unique to 12 versus 24 month old comparison. There were no pathways enriched for H3K27ac marking between 3 versus 6 month old neurons and 6 versus 12 month old neurons, unique to 6 versus 12 month old neurons, or shared between 6 versus 12 month old neurons and 12 versus 24 month old neurons.

While the differentially H3K27ac marked sites that were common across all ages were annotated to pathways such as 'regulation of synaptic transmission', 'regulation of metal ion transport', 'synapse organisation', 'regulation of synaptic plasticity', 'protein localisation to membrane', and 'neurotransmitter transport' (Figure 4.5b). There were no pathways that were annotated for H3K27ac marking between 3 versus 6 month old and 6 versus 12 month old, unique to 6 versus 12 month old, or shared between 6 versus 12 month old and 12 versus 24 month old pairwise comparisons, which all had less than 200 differentially marked sites.

To determine whether sites of differential H3K27ac enrichment that were shared across time-points in neurons exhibited a consistent pattern of depletion or enrichment over time; differential enrichment data from csaw was separated into enriched or depleted at each time-point and the data was analysed with BEDTools intersect to determine the number and direction of H3K27ac marked sites over time. When the enrichment or depletion of H3K27ac marking at sites was analysed for neurons across 3, 6 and 12 months of age the vast majority (92%) of sites were enriched for H3K27ac at 3 and 12 months of age compared the 6 month time-point. Furthermore, when the enrichment or depletion of H3K27ac was assessed in neurons across 6, 12 and 24 months of age most (87%) sites exhibited a progressive increase in the enrichment of H3K27ac across 6-24 months of age. Interestingly, there was a small proportion of H3K27ac marked sites (7.5%) that demonstrated enrichment in neurons at 12 months of age compared to at 6 and 24 months of age.

Taken together these analyses indicate that the majority of sites that are dynamically marked for H3K27ac in neurons across aging exhibit enrichment of H3K27ac at 3 months of age, depletion of H3K27ac at 6 months of age followed by a progressive enrichment of H3K27ac between 6 and 24 months of age.

4.2.6 H3K4me3 marking is enriched in neurons in the developing and aged brain of C57/BL6 mice

One key histone modification that increases transcription factors accessibility to chromatin and subsequent gene expression is H3K4me3. H3K4me3 marking predominantly located at the promoter elements of active genes (B. E. Bernstein et al., 2005; Nathaniel D. Heintzman et al., 2007; Rada-Iglesias et al., 2011). H3K4me3 was sequenced genome wide in neurons from C57/BL6 mice to identify differential enrichment across a time-course of brain aging

incorporating 4 time-points: 3 months of age,6 months of age, 12 months of age, and 24 months of age.

Initially, the total genomic coverage of H3K4me3 marking was measured by quantitating the percentage of the genome that contained more than 5× reads. This analysis gave an indication of gross changes occurring in the aging brain. Initially, in 3 month old neurons H3K4me3 marking was present in approximately 2.94% of the genome (Figure 4.6a). While in 6 month old neurons H3K4me3 marking was depleted covering only 1.85% of the genome (Figure 4.6a). H3K4me3 marking then remained relatively stable in 12 month old and 24 month old neurons with a total genomic coverage of 1.92% and1.77%, respectively (Figure 4.6a). Neurons initially had enrichment for H3K4me3, which then depleted in young adult neurons and was stable through aging (Figure 4.6a).

Next, differential enrichment analysis of H3K4me3 was performed genome-wide. There was an evolution of H3K4me3 marking over time in aging neurons (Figure 4.6b-d). Initially, there were 23258 sites that were enriched in 3 month old neurons compared to 6 month old neurons, while only 623 H34me3 marked sites were enriched in 6 month neurons (Figure 4.6b). There were 16018 H3K4me3 marked sites that were enriched in 12 month old neurons compared to those at 6 months of age, with 406 sites were enriched in 6 month old neurons compared to 12 month old neurons (Figure 4.6c). When comparing 12 and 24 month old neurons, there were 15271 H3K4me3 marked sites significantly enriched in 24 month old neurons compared to 12 months of age, while 1341 sites were enriched in 12 month old neurons compared to 24 months of age (Figure 4.6d). To further elucidate the change in H3K4me3 marking, the top ranked differentially enriched H3K4me3 marked sites were visualised with IGV (Figure 4.6e-g). For example, the promoter of the *Grin1* gene was enriched in 3 month old neurons compared to neurons that were 6 months of age. *Grin1* encodes the Glutamate Ionotropic Receptor NMDA Type 1 Subunit, which is an essential subunit of N-methyl-D-aspartate receptors, and important for normal brain function ((W. Chen et al., 2017) Figure 4.6e). The top differentially enriched site between 6 and 12 months old neurons was at the promoter for the *Brsk1*gene, which encodes the Brain-Specific Serine/Threonine Kinase 1 protein, which regulates the polarisation of neurons ((Sample, Ramamurthy, Gorshkov, Ronnett, & Zhang, 2015); Figure 4.6f).

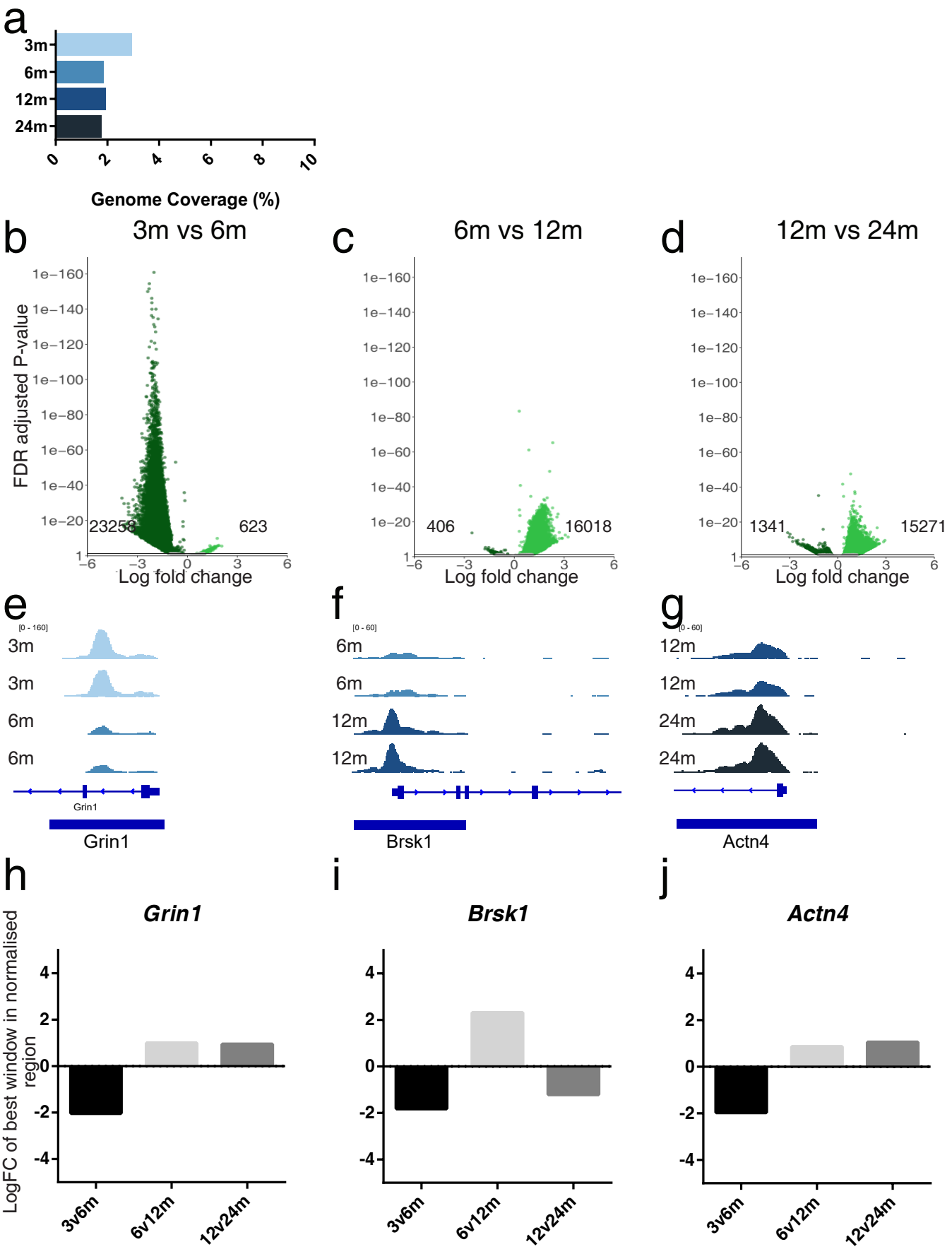
a
3m
6m
12m
24m
0
2
4
6
8
10
Genome Coverage (%)
b
3m vs 6m
c
6m vs 12m
d
12m vs 24m
FDR adjusted P-value
1e−160
1e−140
1e−120
1e−100
1e−80
1e−60
1e−40
1e−20
1
23258
623
406
16018
1341
15271
−6
−3
0
3
6
Log fold change
e
f
g
[0 - 160]
[0 - 60]
3m
3m
6m
6m
6m
12m
12m
12m
24m
24m
Grin1
Grin1
Brsk1
Actn4
h
i
j
Grin1
Brsk1
Actn4
LogFC of best window in normalised region
4
2
0
-2
-4
3v6m
6v12m
12v24m

Figure 4.6: H3K4me3 is enriched in neurons of the developing and aging brain

(a) Percentage 5× genomic coverage of H3K4me3 in neurons of 3 (light blue), 6 (blue), 12 (dark blue) and 24 (dark grey) months of age from C57/BL6 mice. (b-d) Volcano plots show the logFC and FDR adjusted P-value of H3K4me3 marking through a time-course of aging in neurons. (b) LogFC and FDR adjusted P-value of 3 month versus 6 month old neurons, (c) 6 month versus 12 month old neurons and (d) 12 month versus 24 month old neurons. Positive logFC (light green) represents enrichment in the older time-point of pairwise comparison, and negative logFC (dark green) depletion from the older time-point of the pairwise comparison (enrichment in the younger time-point). (e-g) Representative tracks visualised in IGV showing the top-ranked sites of enrichment in neuronal pseudoreplicates between: (e) 3 (light blue) and 6 (blue) months of age at the promoter of the *Grin1* gene; (f) 6 (blue) and 12 (dark blue) months of age at the *Brsk1* promoter and (g) 12 (dark blue) versus 24 (dark grey) months of age at the *Actn4* promoter. (h-j) Histograms showing the logFC of the best window within the normalised region of H3K4me3 marking in neurons from the pairwise differential enrichment analysis at (h) *Grin1*, (i) *Brsk1* and, (j) *Actn4* promoters.

Similarly, the top differentially enriched site between 12 and 24 month old neurons was at the promoter for *Actn4*, which encodes the Actinin Alpha 4 protein, a member of the spectrin family of cytoskeletal proteins, which has been shown to influence spine morphology ((Kalinowska et al., 2015) Figure 4.6g). To illustrate the dynamic nature of H3K4me3 marking at specific loci in neurons over time, the logFC from the differentially enriched sites was plotted as a histogram across the aging time-course (Figure 4.6h-j).

4.2.7 H3K4me3 marking at promoters in neurons is enriched at 3 months, depleted at 6 months, and re-established with age

H3K4me3 marking is predominantly found at the TSS and promoter of active genes in mammalian species (B. E. Bernstein et al., 2005; Nathaniel D. Heintzman et al., 2007; Rada-Iglesias et al., 2011). To identify if the differential enrichment of H3K4me3 marking was occurring at promoters, H3K4me3 was plotted against tracks for UCSC KnownGene TSS and then further subset into CpG island containing TSS and non-CpG island containing TSS. The mean abundance of reads was mapped within a 2kb window either side of TSS (Figure 4.7a). H3K4me3 marking was enriched at the +1 and -1 nucleosomes proximal and distal to the TSS in neurons. Quantitation of the mean enrichment plots showed that H3K4me3 marking was strongest at the TSS in 3 months old neurons (3 month max: 7.12; Figure 4.7a), while at 6 months of age neurons the TSS were depleted for H3K4me3 marking (6 month max: 3.24; Figure 4.7a). At 12 months of age the mean abundance of H3K4me3 marking at the TSS in neurons increased (12 month max: 5.17; Figure 4.7a), before plateauing at the TSS of 24 month old neurons (24 month max: 5.17; Figure 4.7a). To further assess the change in H3K4me3 over time, heatmaps were generated against UCSC KnownGene TSS. At 3 months of age, H3K4me3 marking was present at approximately 50% of TSS in neurons (Figure 4.7b), however by 6 months of age the proportion of TSS marked by H3K4me3 slightly decreased, and the magnitude of H3K4me3 marking was depleted from the TSS of neurons (Figure 4.7b). At 12 months of age, the proportion of H3K4me3 marked TSS remained constant in neurons, however, there was an increase in the magnitude of H3K4me3 marking.

The proportion of TSS enriched for H3K4me3 and the magnitude of the H3K4me3 marking remained consistent in 24 month old neurons (Figure 4.7b). Further analysis indicated that the majority of H3K4me3 marking was present at CpG island containing TSS (Figure 4c,d). Approximately 4/5 of CpG island containing TSS were enriched for H3K4me3 marking in 3

month old neurons (Figure 4.7c). At 6 months of age, the proportion of CpG island containing TSS marked with H3K4me3 in neurons was slightly lower than at 3 months of age, hand the magnitude of marking H3K4me3 was also depleted (Figure 4.7c). In 12 and 24 month old neurons, the proportion (~80%) of CpG island containing TSS enriched for H3K4me3 remained relatively stable, with a sustained increase in the magnitude of H3K4me3 marking compared to 6 month old neurons. Interestingly, at 24 months of age, the distribution of H3K4me3 marking around CpG island containing TSS changed, with a loss of marking upstream of the TSS (Figure 4.7c). In comparison, H3K4me3 marking at non-CpG containing TSS in neurons was more stable. At 3 months of age, approximately 20% of non-CpG containing TSS in neurons were enriched for H3K4me3 marking. However, in 6 month old neurons the magnitude of H3K4me3 marking at non-CpG TSS was depleted, and the proportion of non-CpG island containing TSS marked with H3K4me3 was slightly reduced (Figure 4.7d). H3K4me3 marking remained relatively constant in non-CpG TSS in 12 month old neurons compared to 6 month old neurons (Figure 4.7d). Finally, at 24 months of age, the magnitude of H3K4me3 marking at non-CpG TSS in neurons increased (Figure 4.7d).

H3K4me3 is highly enriched at TSS in 3 month old neurons, while 6 month old neurons exhibit a lower magnitude of H3K4me3 marking at a similar proportion TSS. H3K4me3 enrichment at TSS in neurons was then partially re-established at the 12 and 24 month old time-points, however the magnitude of H3K4me3 enrichment did not reach the levels observed in 3 month old neurons. Taken together, these data demonstrate that H3K4me3 marking at TSS is dynamic in the aging brain, and primarily occurring at CpG island containing TSS.

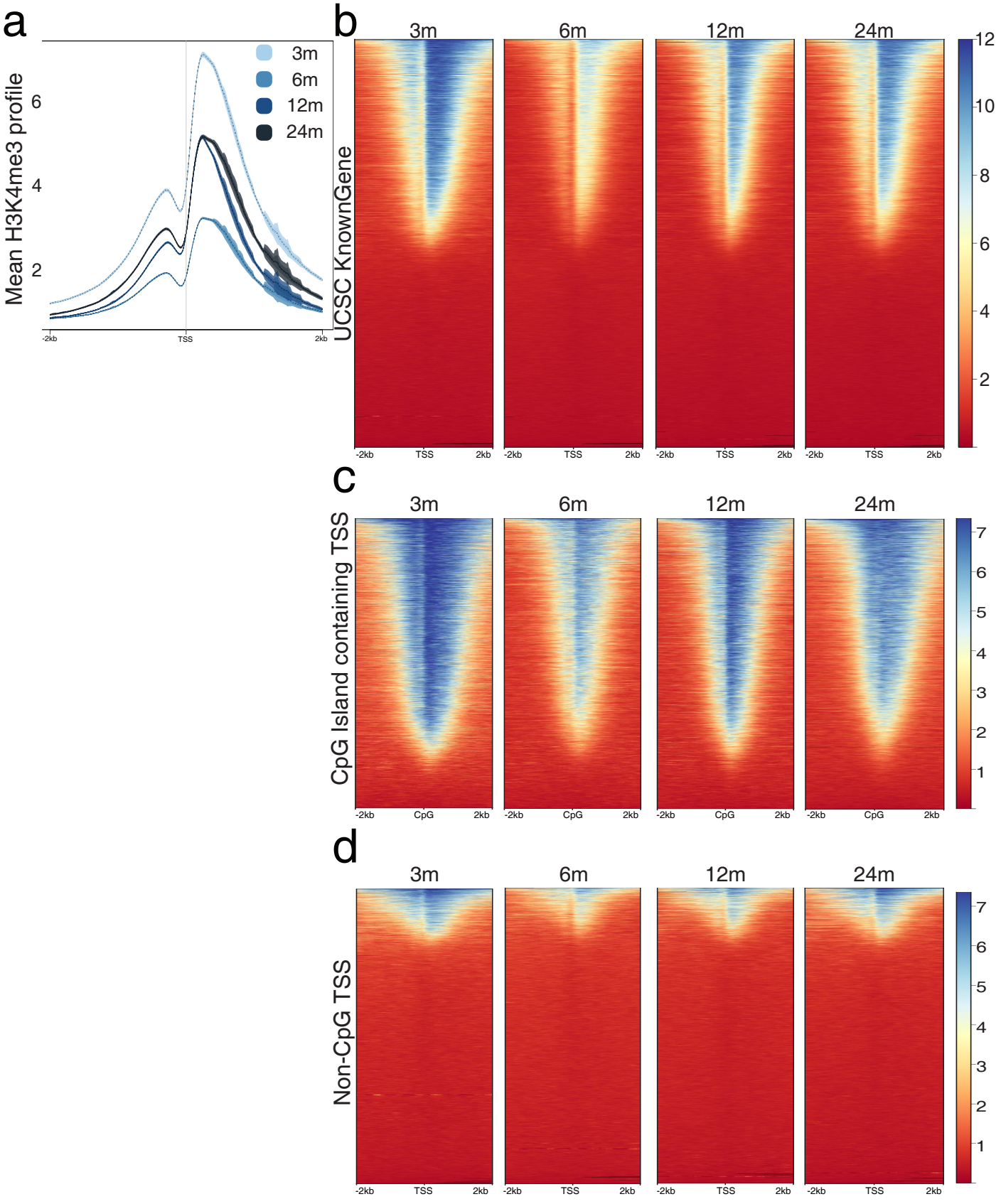
a
Mean H3K4me3 profile
6
4
2
3m
6m
12m
24m
-2kb
TSS
2kb
b
3m
6m
12m
24m
UCSC KnownGene
12
10
8
6
4
2
-2kb
TSS
2kb
c
3m
6m
12m
24m
CpG Island containing TSS
7
6
5
4
3
2
1
-2kb
CpG
2kb
d
3m
6m
12m
24m
Non-CpG TSS
7
6
5
4
3
2
1
-2kb
TSS
2kb

Figure 4.7: H3K4me3 is enriched in promoters in neurons during development and aging (a) Average enrichment plots for H3K4me3 within a 2kb window of TSS for the UCSC KnownGene track in neurons of 3 (light blue), 6 (blue), 12 (dark blue) and 24 (dark grey) months of age. (b) Heatmaps of H3K4me3 marking at TSS for UCSC KnownGene sorted by strongest (blue) to weakest (red) signal in neurons from 3, 6, 12 and 24 months old mice. (c) Heatmaps of H3K4me3 marking at CpG island containing TSS from the UCSC mm10 CpG island track sorted by strongest (blue) to weakest (red) signal in neurons from 3, 6, 12 and 24 month old C57/BL6 mice. (d) Heatmaps of H3K4me3 marking at non-CpG containing TSS from the UCSC mm10 KnownGene track sorted by strongest (blue) to weakest (red) signal in neurons from 3, 6, 12 and 24 month old mice.

4.2.8 Enhancers exhibit minimal H3K4me3 enrichment in neurons across ages

In the normal mammalian genome H3K4me3 is generally not found at active enhancer elements (Local et al., 2018; Outchkourov et al., 2013; Rada-Iglesias et al., 2011). To determine if there was any alteration in the distribution of H3K4me3 marking at enhancers in aging neurons, average H3K4me3 marking was mapped at a 2kb region around the mid-point of enhancer elements marked by H3K27ac.

First, the mean abundance of H3K4me3 marking was visualised at enhancers in neurons. There was some H3K4me3 enrichment at putative enhancers in neurons, which did not alter dramatically in 3, 6, 12 or 24 month old neurons (max: 56.33, 54.42, 63.43, 72.40, respectively; Figure 4.8a). Next, H3K4me3 marking was mapped against the enhancer track and visualised with heatmaps around a 2kb window of the mid-point of enhancers. H3K4me3 marking was highly enriched at a small proportion of putative enhancers in neurons. In neurons at all ages, the majority of enhancers displayed slight enrichment for H3K4me3 marking at the mid-point of enhancers, while in the small proportion of enhancers that were highly enriched for H3K4me3 marking, H3K4me3 was distributed across the 2kb window upstream and downstream of the mid-point of enhancers (Figure 4.8b). In 6 month old neurons, there was a slight decrease to the proportion of enhancers that were highly enriched for H3K4me3 marking (Figure 4.8b).

Together these data show that the majority of enhancers have minimal H3K4me3 marking, however, a small subset of putative enhancers are highly enriched for H3K4me3 marking in the aging brain.

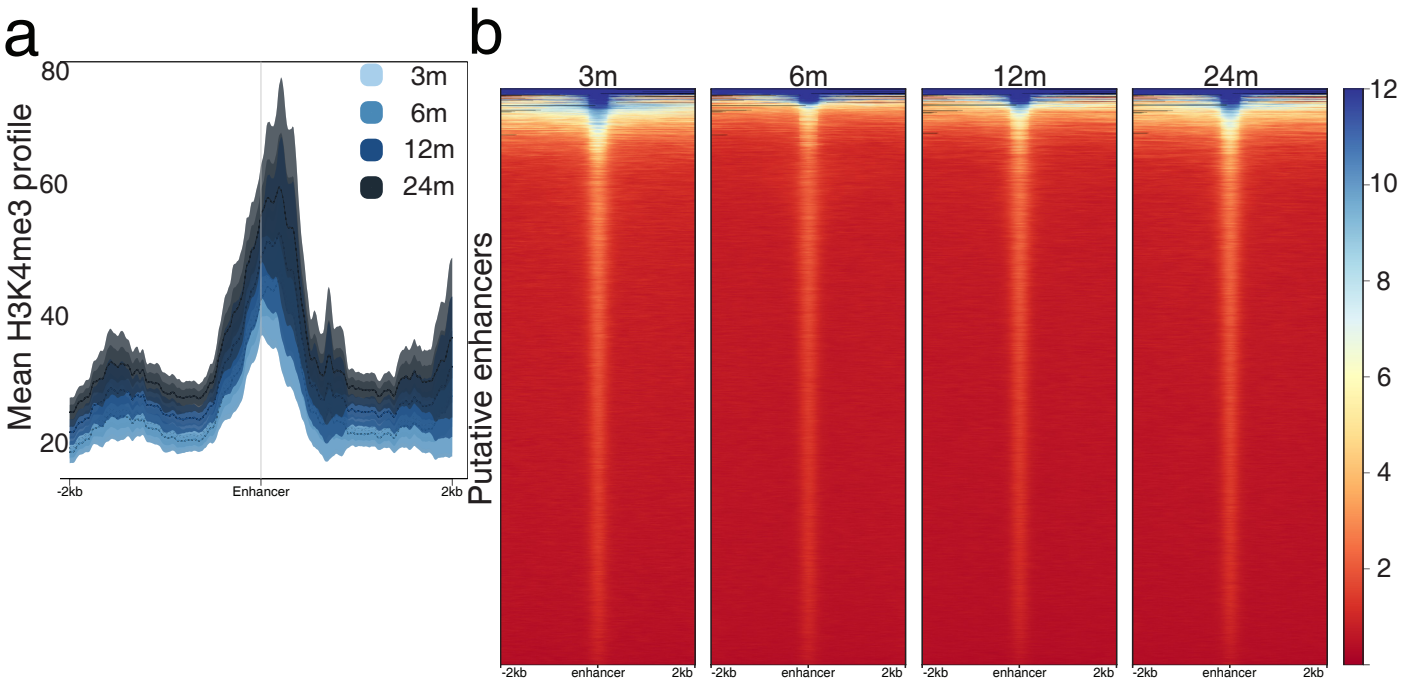
a
b
Mean H3K4me3 profile
80
60
40
20
3m
6m
12m
24m
-2kb
Enhancer
2kb
Putative enhancers
3m
6m
12m
24m
12
10
8
6
4
2
-2kb
enhancer
2kb

Figure 4.8 Enhancers in neurons exhibit minimal H3K4me3 marking across aging
(a) Average enrichment plots for H3K4me3 within a 2kb window of putative enhancers at 3 months (light blue), 6 months (blue), 12 months (dark blue) and 24 months (dark grey) of age. (b) Heatmaps for H3K27ac marking at putative enhancers sorted by strongest (blue) to weakest (red) signal in 3, 6, 12 and 24 month old neurons from the forebrain of C57/BL6 animals.

4.2.9 H3K4me3 is annotated to pathways involving cellular function, maintenance, and post-translational modifications in aging neurons

To identify the underlying pathways of differential H3K4me3 marking, gene ontology analysis of bed files containing all sites of significant differential enrichment from each pairwise comparison was performed.

Initially, H3K4me3 marking analysis was performed against 'GO molecular function'. Between 3 and 6 month old neurons, H3K4me3 marking was annotated to pathways including 'unfolded protein binding', 'rRNA binding', 'endonuclease activity with RNA or DNA producing 5'- posphomonoesters', and 'translation regulator activity' (Figure 4.9a). While between 6 and 12 month old neurons, differential sites of H3K4me3 enrichment were annotated to terms including 'ribonucleoprotein complex binding', 'tRNA, rRNA and snRNA binding', and 'translation elongation factor and translation regulator activity' (Figure 4.9c). Between 12 and 24 month old neurons, annotations to 'GO molecular function' were similar to the previous ages, with pathways including 'unfolded protein binding', 'rRNA and snRNA binding', 'intramolecular transferase activity' and 'gamma-tubulin binding' (Figure 4.9e). Next, H3K4me3 marking from neurons of the aging brain were annotated to 'GO biological process'. Between 3 and 6 month old neuronsH3K4me3 marking was annotated to terms including 'spindle assembly', 'GPI anchor metabolic process', 'antigen processing & presentation of peptide antigen via MHC class I' and 'tRNA modification' (Figure 4.9b). While in neurons between 6 and 12 months of age, H3K4me3 marking was annotated to pathways including the 'GPI anchor metabolic process', 'regulation of gene silencing', 'tRNA modification', 'oxidative phosphorylation' and 'chaperone-mediated protein folding' (Figure 4.9d). Between 12 and 24 months of age, H3K4me3 marking in neurons was annotated to 'GO biological processes' including 'macroautophagy', 'glutathione metabolic process', 'tRNA modification', and 'autophagic vacuole assembly' and gene silencing pathways (Figure 4.9f).

Together these data demonstrate that H3K4me3 marking is altered over time in pathways that are involved in the maintenance of core molecular functions and post-transcriptional modifications.

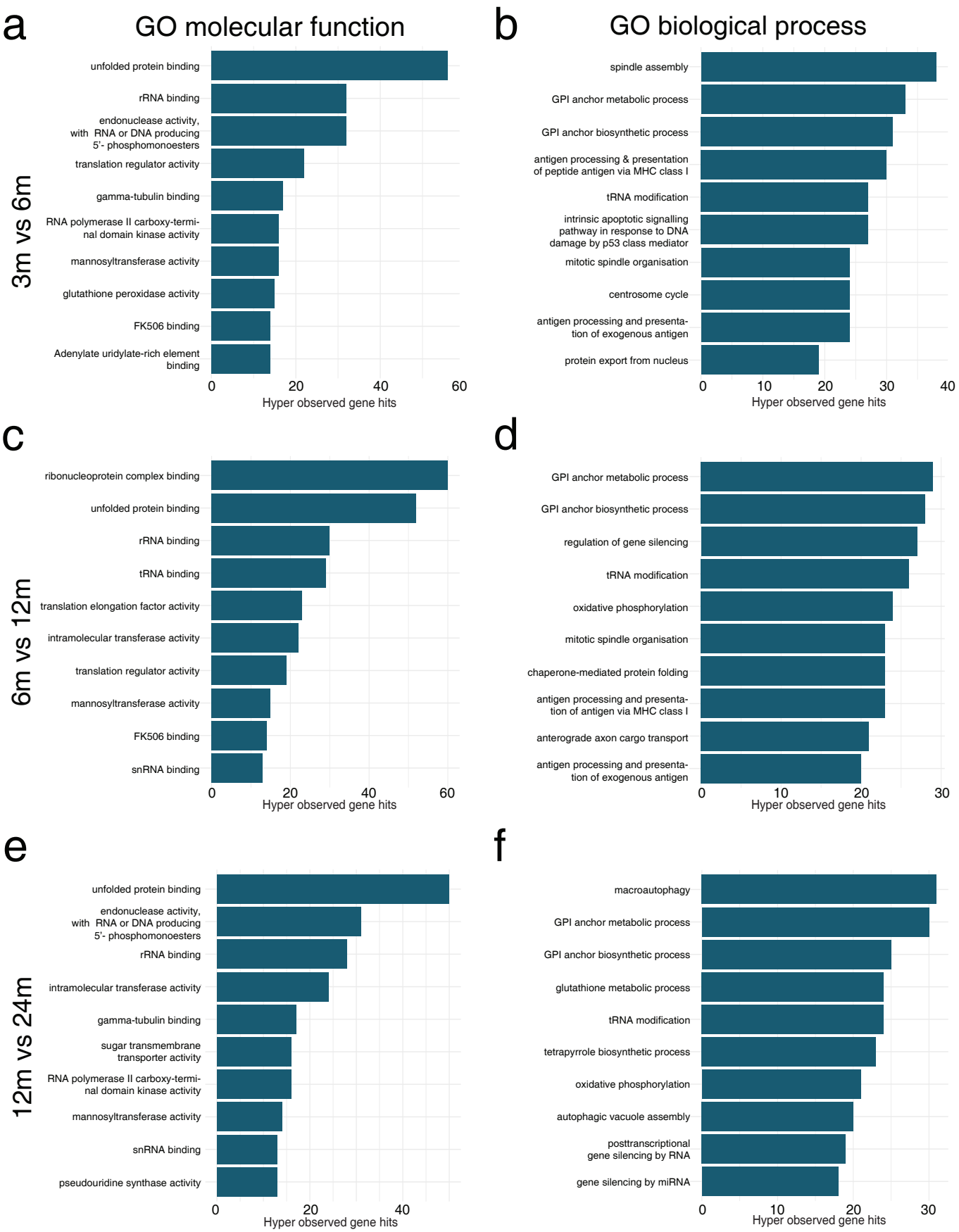
a
GO molecular function
3m vs 6m
unfolded protein binding
rRNA binding
endonuclease activity, with RNA or DNA producing 5'- phosphomonoesters
translation regulator activity
gamma-tubulin binding
RNA polymerase II carboxy-terminal domain kinase activity
mannosyltransferase activity
glutathione peroxidase activity
FK506 binding
Adenylate uridylate-rich element binding
0
20
40
60
Hyper observed gene hits
b
GO biological process
spindle assembly
GPI anchor metabolic process
GPI anchor biosynthetic process
antigen processing & presentation of peptide antigen via MHC class I
tRNA modification
intrinsic apoptotic signalling pathway in response to DNA damage by p53 class mediator
mitotic spindle organisation
centrosome cycle
antigen processing and presentation of exogenous antigen
protein export from nucleus
0
10
20
30
40
Hyper observed gene hits
c
6m vs 12m
ribonucleoprotein complex binding
unfolded protein binding
rRNA binding
tRNA binding
translation elongation factor activity
intramolecular transferase activity
translation regulator activity
mannosyltransferase activity
FK506 binding
snRNA binding
0
20
40
60
Hyper observed gene hits
d
GPI anchor metabolic process
GPI anchor biosynthetic process
regulation of gene silencing
tRNA modification
oxidative phosphorylation
mitotic spindle organisation
chaperone-mediated protein folding
antigen processing and presentation of antigen via MHC class I
anterograde axon cargo transport
antigen processing and presentation of exogenous antigen
0
10
20
30
Hyper observed gene hits
e
12m vs 24m
unfolded protein binding
endonuclease activity, with RNA or DNA producing 5'- phosphomonoesters
rRNA binding
intramolecular transferase activity
gamma-tubulin binding
sugar transmembrane transporter activity
RNA polymerase II carboxy-terminal domain kinase activity
mannosyltransferase activity
snRNA binding
pseudouridine synthase activity
0
20
40
Hyper observed gene hits
f
macroautophagy
GPI anchor metabolic process
GPI anchor biosynthetic process
glutathione metabolic process
tRNA modification
tetrapyrrole biosynthetic process
oxidative phosphorylation
autophagic vacuole assembly
posttranscriptional gene silencing by RNA
gene silencing by miRNA
0
10
20
30
Hyper observed gene hits

Figure 4.9 In neurons differential H3K4me3 marking across aging occurs at promoters responsible for core molecular and post-transcriptional functions

(a-f) The top 10 gene ontology annotations, ranked by hypergeometric observed gene hits for sites of significant H3K27ac differential enrichment at (a,b) 3 versus 6 months, (c,d) 6 versus 12 months and, (e,f) 12 versus 24 months of age. Gene ontology analysis predicts annotated pathways in (a, c, e) molecular function and, (b, d, f) biological processes.

4.2.10 Sites of H3K4me3 enrichment are shared between the developing and aging brain

An intersection analysis of bed files containing all sites of significant differential enrichment across the time-course of differential H3K4me3 marking was performed to determine whether enrichment of H3K4me3 occurred at similar or different loci over time.

Initially, 24739 H3K4me3 marked sites were differentially enriched specifically in the 3 month versus 6 month old neuron comparison, while there were only 2683 H3K4me3 differentially marked sites specific to the comparison between 6 month and 12 month old neurons (Figure 4.10a). Moreover, 11273 differentially H3K4me3 marked sites were enriched in neurons only between 12 and 24 months of age. Strikingly, there were 20370 H3K4me3 marked sites that were differentially enriched in neurons in both the 3 versus 6 month old comparison and the 12 versus 24 month old comparison (Figure 4.10a). In contrast, only 3492 differentially enriched H3K4me3 sites shared between neurons in the pairwise analyses of 3 versus 6 months of age, and the 6 versus 12 month time-points (Figure 4.10a). Likewise, only 1037 of the H3K4me3 differentially enriched sites in neurons between 6 and 12 months of age were shared with those detected between 12 and 24 months of age (Figure 4.10a). Finally, there were 10777 sites of differential H3K4me3 enrichment detected across all time-points examine (Figure 4.10a).

Next, gene ontology analysis was performed for differential H3K4me3 marking that were shared between developing and aging neurons. H3K4me3 marked sites were annotated to 'GO biological process'. Sites that were differentially enriched for H3K4me3 specifically in neurons between 3 month and 6 months of age were annotated to 'protein folding', 'spindle organisation', 'nuclear export', 'spindle assembly', and 'protein peptidyl-prolyl isomerisation' (Figure 4.10c). Differentially enriched H3K4me3 sites in neurons specific to the 6 versus 12 months of age comparison but were annotated to pathways such as 'cardiac cell development', 'regulation of myotube differentiation', and 'nephron morphogenesis' (Figure 4.10d). Sites that were differentially enriched for H3K4me3 in neurons specifically between 12 and 24 months of age were annotated to pathways including 'actin filament bundle assembly', 'GPI anchor metabolic process', 'release of cytochrome c from mitochondria', and 'posttranscriptional gene silencing by RNA' (Figure 4.10e). Interestingly, sites of differential H3K4me3 marking in neurons that were shared between 3 versus 6 months of age, and the 12 versus 24 month time-points were annotated to biological processes including 'protein folding', 'tRNA processing',

‘maintenance of protein location in cell’ and ‘nuclear export’. H3K4me3 differentially marked sites in neurons that were shared by all time-points were also annotated to biological processes including ‘protein folding’, ‘tRNA processing’, ‘nuclear export’, and ‘nucleotide-excision repair’ (Figure 4.10f). There was no annotation of any ontologies of ‘GO biological processes’ when the differentially marked H3K4me3 sites in neurons were compared between the 3 versus 6 month of age and the 6 versus 12 months of age data, nor for the comparison of the 6 versus 12 month of age and the 12 versus 24 months of age data.

When the enrichment or depletion of H3K4me3 marking at sites was assessed for neurons across 3, 6 and 12 months of age almost all (99%) of the sites were enriched for H3K4me3 at 3 and 12 months of age compared the 6 month time-point. Moreover, when the enrichment or depletion of H3K4me3 was assessed in neurons across 6, 12 and 24 months of age the vast majority (87%) of sites demonstrated a progressive increase in the enrichment of H3K4me3 across 6-24 months of age. It should be noted that there was as small subset of sites (7.7%) that showed enrichment in neurons at 12 months of age compared to the 6 and 24 month time-points. Overall, these data reveal that the majority of sites that exhibit alterations in H3K4me3 marking in neurons across the aging time course follow a similar pattern of H3K4me3 enrichment: enrichment of H3K4me3 at 3 months of age, depletion of H3K4me3 at 6 months of age followed by a progressive enrichment in H3K4me3 between 6 and 24 months of age. This is strikingly similar to the overall pattern of H3K37ac dynamic enrichment observed at sites across neuronal aging.

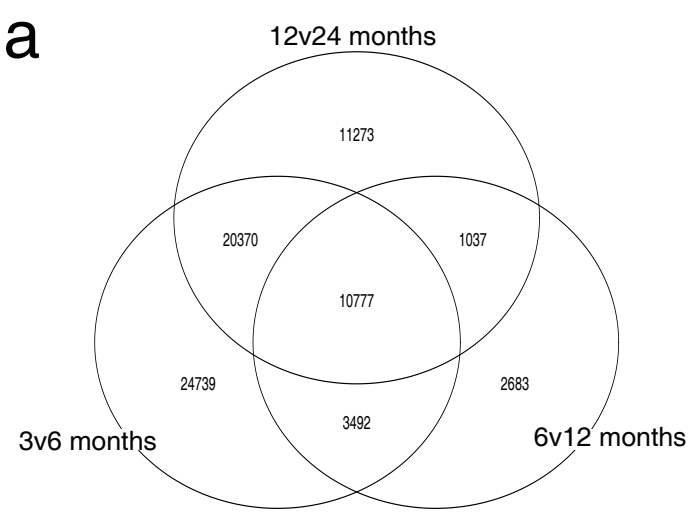
a
12v24 months
11273
20370
1037
10777
24739
2683
3492
3v6 months
6v12 months

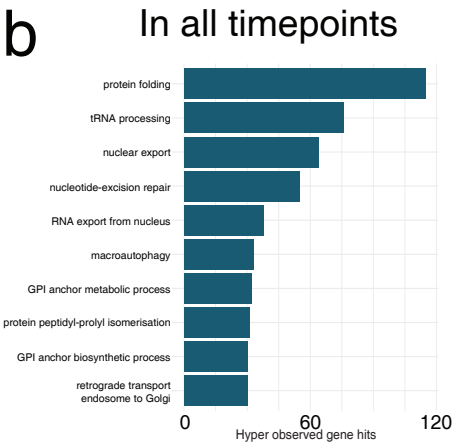
b
In all timepoints
protein folding
tRNA processing
nuclear export
nucleotide-excision repair
RNA export from nucleus
macroautophagy
GPI anchor metabolic process
protein peptidyl-prolyl isomerisation
GPI anchor biosynthetic process
retrograde transport endosome to Golgi
0
60
120
Hyper observed gene hits

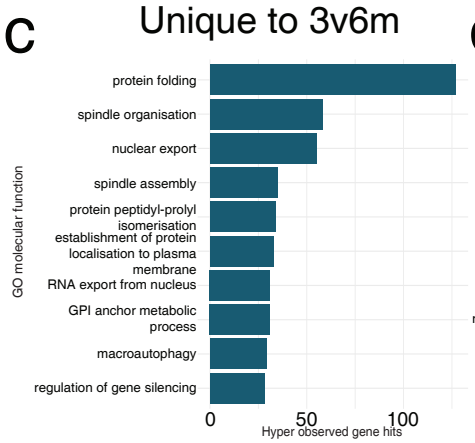
c
Unique to 3v6m
GO molecular function
protein folding
spindle organisation
nuclear export
spindle assembly
protein peptidyl-prolyl isomerisation
establishment of protein localisation to plasma membrane
RNA export from nucleus
GPI anchor metabolic process
macroautophagy
regulation of gene silencing
0
50
100
Hyper observed gene hits

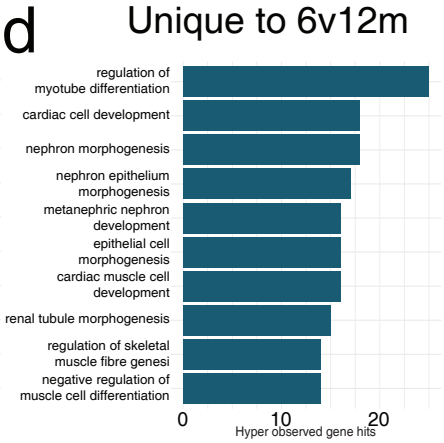
d
Unique to 6v12m
regulation of myotube differentiation
cardiac cell development
nephron morphogenesis
nephron epithelium morphogenesis
metanephric nephron development
epithelial cell morphogenesis
cardiac muscle cell development
renal tubule morphogenesis
regulation of skeletal muscle fibre genesi
negative regulation of muscle cell differentiation
0
10
20
Hyper observed gene hits

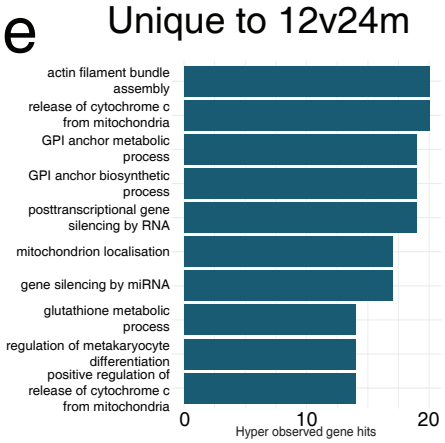
e
Unique to 12v24m
actin filament bundle assembly
release of cytochrome c from mitochondria
GPI anchor metabolic process
GPI anchor biosynthetic process
posttranscriptional gene silencing by RNA
mitochondrion localisation
gene silencing by miRNA
glutathione metabolic process
regulation of metakaryocyte differentiation
positive regulation of release of cytochrome c from mitochondria
0
10
20
Hyper observed gene hits

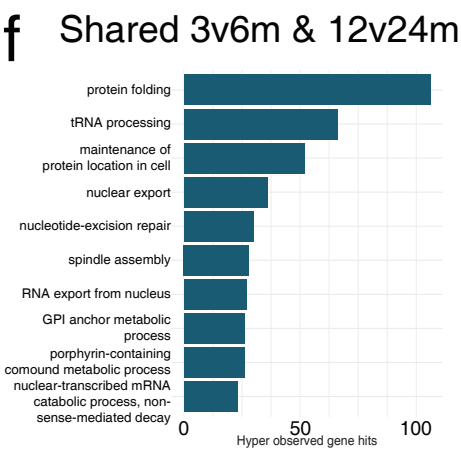
f
Shared 3v6m & 12v24m
protein folding
tRNA processing
maintenance of protein location in cell
nuclear export
nucleotide-excision repair
spindle assembly
RNA export from nucleus
GPI anchor metabolic process
porphyrin-containing comound metabolic process
nuclear-transcribed mRNA catabolic process, non-sense-mediated decay
0
50
100
Hyper observed gene hits

Figure 4.10 Sites of H3K4me3 enrichment are shared between the developing and aging neurons

(a) Venn diagram plotting the overlap in sites that were differentially enriched for H3K4me3 in neurons from the 3, 6, 12 and 24 month old pairwise comparisons. (b) Functional annotations for 'GO biological process' for the 10777 sites that were differentially enriched for H3K4me3 in neurons at all time points, (c) the 24739 sites unique to the 3 versus 6 months of age H3K4me3 differential enrichment analysis, (d) the 2683 sites unique to neurons in the 6 versus 12 month old comparison, (e) the 11273 H3K4me3 differentially marked sites unique to 12 versus 24 month comparison and, (f) the 20370 sites of differential H3K4me3 enrichment shared in neurons between the 3 versus 6 month and the 12 versus 24 month time-points.

4.3 Discussion

The epigenome is integral to the regulation of transcription in the developing and aging brain. Studies have demonstrated the epigenome is vital for learning and memory, executive function, synaptic plasticity, and motor function (Feng et al., 2010b; Leighton et al., 2018; Levenson et al., 2006; X. Li et al., 2014; Swank & Sweatt, 2001; Widagdo et al., 2016). However, there have been few studies to characterise the histone landscape in the aging brain.

This study has characterised both H3K27ac and H3K4me3 marking in neurons from the forebrain of C57/BL6 mice at 3, 6, 12, and 24 months of age. Interestingly, H3K27ac and H3K4me3 marking was enriched at promoters and enhancers in neurons from juvenile and aging mice. Furthermore, H3K4me3 and H3K27ac marking was predominantly enriched in neurons at TSS that contained CpG islands in the juvenile and aging brain. H3K4me3 marking was enriched in aging neurons for pathways involving lipid transport, RNA modifications, apoptotic signalling, centrosome cycling, oxidative phosphorylation and protein export. While H3K27ac marking was enriched in pathways pertaining to synaptic plasticity, ion transport, dephosphorylation, protein localisation, membrane depolarisation, dendrite development, apoptosis and oxidative phosphorylation in aging neurons. Strikingly, this study observed a partial recapitulation of a juvenile-like epigenetic state in aged neurons. These data demonstrate a complex and dynamic pattern of H3K27ac and H3K4me3 marking in neurons throughout life.

H3K4me3 and H3K27ac are enriched in juvenile neurons in a critical period of neuronal plasticity as the nervous system is established

Neurons between 3 and 6 months of age represent the transition from juvenile to young adult mice (Fu, Rusznak, Herculano-Houzel, Watson, & Paxinos, 2013) (review: (Semple, Blomgren, Gimlin, Ferriero, & Noble-Haeusslein, 2013)). Strikingly, the epigenome was highly dynamic in neurons between 3 and 6 months of age. H3K27ac and H3K4me3 marking was enriched at the TSS, and H3K27ac marking was enriched at enhancers in neurons at 3 months of age but were depleted from neurons by 6 months of age. H3K27ac and H3K4me3 markings are generally indicative of increased transcriptional activity (Creyghton et al., 2010b; Santos-Rosa et al., 2002; Z. Wang et al., 2008; Wysocka et al., 2006), and enrichment of these marks may reflect a critical time of neuronal plasticity during the transition from juvenile to

young adult mice (Handley et al., 2017).The current dogma of cortical aging suggests that neuronal connections are established in mice by 3 months of age (review: (Semple et al., 2013)). Although epigenetic modifications such as DNA methylation are highly dynamic during development, such marks have previously been shown to stabilise in mice by 3 months of age (Ryan Lister et al., 2013). However, emerging evidence shows the cortex to still be undergoing developmental changes at 3 months of age. Widespread synaptic pruning has been reported in layer V pyramidal neurons in the cortex of Thy1-YFP (C57/BL6) mice at 3 months of age (Handley et al., 2017). Studies have also shown adult levels of neurotransmitters and synaptic density stabilise after 3 months of age in mice (Fu et al., 2013). Myelination and total brain volume also dramatically increase in mice up to 3 months of age (Fu et al., 2013). Moreover, the emergence of adult behavioural tendencies such as reduced risk taking and increased parental tendencies occurs after 3 months of age (Fu et al., 2013) (review: (Semple et al., 2013)). Enrichment for H3K27ac and H3K4me3 marking in neurons between 3 and 6 months of age may also reflect the developmental plasticity critical to establishing stable gene expression profiles in neurons for later life (reviews: (Hochberg et al., 2011; Murgatroyd & Spengler, 2011)). (Fu et al., 2013; Hochberg et al., 2011).

Gene ontology analysis further illustrated that developmental and neuronal specific pathways were differentially enriched in neurons between 3 and 6 months of age. For example, H3K27ac marking was enriched in pathways for synaptic transmission, ion transport, learning, and dephosphorylation in neurons between 3 and 6 months of age. While H3K4me3 marking was annotated to pathways involved in spindle assembly, lipid transport, RNA modifications, apoptotic signalling, and protein trafficking in neurons between 3 and 6 months of age. Synaptic plasticity is critical for learning, memory and the establishment of executive function in the adolescent brain (review: (Selemon, 2013)). Synaptic pruning events have been observed in studies of non-human primate, where enrichment of cortical synapses occurs until 2 years of age and then declines from adolescence until adulthood (Bourgeois, Goldman-Rakic, & Rakic, 1994; Zecevic, Bourgeois, & Rakic, 1989). Alongside synaptic pruning, apoptotic signalling may be activated in the juvenile nervous system for neuronal remodelling and die-back as functional pathways are established in neurons (review: (Yaron & Schuldiner, 2016)). Neuronal die-back may be triggered through NMDA receptor hypersensitivity (Ikonomidou et al., 1999) (review: (Kuan, Roth, Flavell, & Rakic, 2000)). NMDA receptors are critical to activity dependent synaptic plasticity and have been shown to activate pathways leading to the reduction of plasticity during neuronal maturation *in-vitro* (Sala, Rudolph-Correia, & Sheng,

2000). Indeed, previous evidence also suggests that H3K4me3 marking is developmentally enriched at promoters in neurons from post-mortem human prefrontal cortex and the frontal pole at many developmental pathways, but is stabilised as the nervous system matures (Cheung et al., 2010; Shulha et al., 2013). Previous literature has also demonstrated widespread transcriptional activity during development that stabilised later in life in the human prefrontal cortex (Colantuoni et al., 2011). Therefore, enrichment of H3K27ac and H3K4me3 marking at promoters and enhancers may reflect the activation of pathways essential to shaping gene transcription for the establishment of the neuronal network at 3 months of age, while loss of H3K27ac and H3K4me3 marking in neurons at 6 months of age could reflect the stabilisation of neuronal networks in young adult mice.

The neuronal epigenome dynamically regulates core molecular functions and is enriched for H3K4me3 and H3K27ac in pathways to combat oxidative stress and promote experience dependent plasticity in the adult brain

The mammalian cortex undergoes prolonged maturation throughout life, which is associated with underlying transcriptional change (Colantuoni et al., 2011). The data presented in this study indicate that H3K4me3 marking was enriched in 12 month old neurons compared to 6 months of age, however there was little difference in H3K27ac marking between neurons from 6 and 12 months of age. H3K4me3 marking was enriched at the TSS in 12 month old versus 6 month old neurons; predominantly at TSS that contained CpG islands. However, there were only 1333 differentially enriched sites in neurons for H3K27ac marking between 6 and 12 months of age. Gene ontology analysis further illustrated the pathways changing in aging neurons between 6 and 12 months of age. Differential enrichment for H3K4me3 was annotated to pathways that centred around core molecular processes for cell survival including regulation of oxidative phosphorylation, gene silencing, anterograde transport and chaperone-mediated protein folding. Many of these pathways have been previously identified to alter with brain aging. For example, research has demonstrated an age associated impairment of oxidative phosphorylation in synaptic mitochondrial fractions from ~3 month and 18 month old mice (Ferrándiz et al., 1994). Post-mitotic neuronal cells are particularly vulnerable to the effects of oxidative stress, and express anti-oxidant genes to compensate for oxidative stress (Miquel, Economos, Fleming, & Johnson, 1980; X. Wang et al., 2005). It has also been suggested that different neuronal sub-types are selectively vulnerable to the effects of oxidative stress, and

that the vulnerability may be due to damage or loss of mitochondria from reactive oxygen species (Mattiasson, Friberg, Hansson, Elmer, & Wieloch, 2003; X. Wang et al., 2005) (review: (Xinkun Wang & Michaelis, 2010)). Axonal transport also declines in the aging brain (Milde, Adalbert, Elaman, & Coleman, 2015; Takihara et al., 2015). Research has shown the duration and distance of mitochondrial transport to decrease in retinal ganglion cells in 12-13 month old mice, and again in 23-25 month old mice compared to 2 months of age (Takihara et al., 2015). Studies have also shown a decline in heat shock protein activity in response to misfolded proteins in the aging brain (Hsu, Murphy, & Kenyon, 2003). Heat shock proteins act as molecular chaperones to repair or remove dysfunctional proteins by refolding or degrading them (review: (Calderwood, Murshid, & Prince, 2009)). H3K4me3 marking may be enriched in these pathways to compensate for molecular degradation occurring in neurons from the aging brain.

Although H3K27ac marking was differentially enriched at a small number of sites, differential marking was annotated to pathways for the regulation of synaptic transmission and plasticity, ion and neurotransmitter transport, membrane depolarisation and dendrite development. These pathways may be activated to support experience-dependent plasticity and adaptive remodelling in the adult brain (Trachtenberg et al., 2002). The pathways identified in the current study could also be linked to the homeostasis of intrinsic excitability, necessary to ensure network stability as mice learn and accumulate memories over time (review: (Turrigiano, 2011)). Indeed, multiple studies have shown that structural plasticity is ongoing in the adult brain of mammals (Bergami et al., 2015; T. Xu et al., 2009) (review: (Holtmaat & Svoboda, 2009)). For example, motor-based learning tasks cause rapid growth of dendritic spines of the motor cortex and repeat training caused stabilisation of spines in adult mice (T. Xu et al., 2009). Mice also exhibit a range of behavioural changes between 6 and 12 months of age as they mature, including decreased motor function, startle response and spatial/fear contextual memory, and enrichment of H3K27ac marking in neuronal specific pathways may reflect such behavioural changes in the adult brain (Shoji, Takao, Hattori, & Miyakawa, 2016).

In the current study H3K4me3 marking was annotated to core molecular pathways necessary for the function of all cell types, whereas H3K27ac marking was mostly annotated to neuron specific pathways. The widespread enrichment for H3K4me3, but not H3K27ac marking in 12 month old neurons compared to those 6 months of age was unexpected, and likely reflects the activation of transcriptional pathways for cellular maintenance in aging neurons, however further research is required to confirm this hypothesis. Strikingly, pathways related to oxidative

stress and DNA damage were enriched for H3K4me3 in 12 month old neurons. The subtle enrichment of H3K27ac marking in 12 month old neurons compared to 6 month old neurons may reflect ongoing experience-dependent plasticity and the accumulation of memories in the adult brain.

H3K27ac and H3K4me3 marking is enriched in aged neurons in response to the accumulation of reactive oxygen species and age associated cognitive decline

Aging is commonly associated with cognitive decline, cortical atrophy, and a loss of motor functions (Kalpouzos, Persson, & Nyberg, 2012; Marchand et al., 2011). In the current study, H3K27ac and H3K4me3 marking were compared between 12 and 24 month old neurons from C57/BL6 mice; characterising the differences in the neuronal epigenome between adult and aged neurons. Differential enrichment analysis demonstrated that both H3K27ac and H3K4me3 marking were enriched in neurons from 24 month compared to 12 month old mice. Interestingly, H3K27ac marking was enriched at the TSS in 24 month old neurons, particularly at TSS that contained CpG islands. H3K27ac marking was also enriched at enhancers in neurons from 24 months of age compared to 12 months of age. While H3K4me3 marking was relatively stable at TSS, there was a small redistribution of H3K4me3 marking downstream of the TSS in 24 month old neurons compared to 12 months of age. Enrichment for H3K27ac and H3K4me3 marking in 24 month old neurons may reflect transcriptional changes occurring as a result of age associated cognitive decline. Interestingly, differential H3K27ac marking was annotated to pathways involved in the maintenance of protein location, regulation of apoptosis, oxidative phosphorylation, RNA processing, and synaptic plasticity. While differential H3K4me3 marking was enriched in pathways for autophagy, RNA modification and RNA mediated gene silencing, and oxidative phosphorylation. Many of the differentially enriched pathways between 12 and 24 month old neurons have been previously implicated in aging research. For example, oxidative stress has been implicated as a central cause for cognitive decline in the aging brain by multiple mechanisms including: causing synaptic function decline (Serrano & Klann, 2004), selectively damaging the promoters of genes associated with synaptic function and vesicular transport (T. Lu et al., 2004), and causing epigenetic dysfunction and gene silencing (Gu, Sun, Li, Wu, & Li, 2013) (review: (Bishop, Lu, & Yankner, 2010)). RNA processing, modification and RNA mediated gene silencing have all been implicated in the aging brain. Age associated changes to aspects of RNA processing such as RNA splicing occurs

in healthy aging, and is dysregulated in some neurodegenerative diseases (T. Raj et al., 2018) (review: (Tollervey et al., 2011)). MicroRNA based gene silencing is critical to many cell regulatory functions including cognition, inflammation, lipid metabolism, mitochondrial function, and are differentially expressed in the cortex and hippocampus of the aging brain (Danka Mohammed, Park, Nam, & Kim, 2017). There is a range of literature suggesting that apoptotic pathways are dysfunctional in neurodegenerative disease (review: (Moh et al., 2011)), and apoptosis may also have a role in cellular senescence in the aging brain (Anglade, Vyas, Hirsch, & Agid, 1997) (review: (Caballero & Coto-Montes, 2012)). Previous research has demonstrated that genes associated with synaptic function, vesicular transport and mitochondrial activity decline in the human frontal cortex after 40 years of age (T. Lu et al., 2004). Moreover, as previously discussed, genes involved in oxidative stress are highly enriched in the aging non-human primate and human prefrontal cortex (Fraser, Khaitovich, Plotkin, Pääbo, & Eisen, 2005; T. Lu et al., 2004). Autophagy was also differentially marked by H3K4me3 in 12 versus 24 month old neurons. Autophagic pathways, encompassing the recognition, transport and processing of lysosomes for degeneration are generally considered to be neuroprotective in the aging brain (Decressac et al., 2013). However, functional decline of autophagic pathways has been observed in the aging brain (Lipinski et al., 2010) (review: (Martinez-Lopez, Athonvarangkul, & Singh, 2015)). Indeed, studies have observed an age associated decline in transcription for key regulators of autophagy, including type III phosphoinositide 3-kinase in human cortex (Lipinski et al., 2010; Loerch et al., 2008).

A wide range of mechanisms associated with synaptic plasticity have been shown to decline in the aging brain, including: long-term potentiation, long-term depression and alteration of neurotransmitter receptor expression and trafficking (Henley & Wilkinson, 2013) (reviews: (Bergado & Almaguer, 2002; Burke & Barnes, 2006)). These age-related changes at the cellular level are thought to underlie age-associated cognitive decline (review: (Bergado & Almaguer, 2002; Burke & Barnes, 2006)). For example, previous literature suggests that aging is associated with a reduction in executive function and localised neuronal activity in the aging human prefrontal cortex (Cabeza, 2002), and key proteins for structural remodelling, including debrin, GAP-43, β3-tubulin and synaptophysin decline in the axons and dendrites of aging neurons (Hatanpää, Rapoport, Brady, Isaacs, & Shirao, 1999). Enrichment of H3K27ac and H3K4me3 marking in aging neurons may be to assist in the maintenance of synaptic connections, but also to ensure appropriate signalling for cellular senescence (Chinta et al., 2015), autophagic and apoptotic pathways (review: (Caballero & Coto-Montes, 2012)). Indeed,

studies have also hypothesised a link between autophagic pathways aiding in the regulation of synaptic remodelling (Liang, 2019).

Together these data indicate that H3K27ac and H3K4me3 are enriched in neurons late in aging as a compensatory mechanism for the neuronal changes that underlie age associated cognitive decline, and likely also to try to maintain core metabolic cellular function in the presence of factors such as oxidative stress and protein misfolding that increase with age.

A partial recapitulation of a juvenile-like epigenetic state occurs in aged neurons

A comparison of differential enrichment of H3K27ac and H3K4me3 marking across an aging time-course of 3, 6, 12 and 24 months old neurons demonstrated a large number of sites to be shared between juvenile and aged neurons. Surprisingly, the majority of differentially enriched H3K4me3 sites (20370) marked sites and a large proportion of H3K27ac marked sites (7203) were shared in neurons between juvenile and aged mice. This posed the question of whether the majority of the differentially enriched H3K27ac and H3K4me3 marked sites shared between juvenile and aged neurons were consistently enriched in aged and juvenile neurons, representing a recapitulation of a juvenile-like epigenetic state in aged neurons, or whether there was age associated depletion of sites that were previously enriched in juvenile neurons. Almost all (99%) H3K4me3 differentially marked sites shared between juvenile and aged neurons were consistently enriched in juvenile and aged neurons, similarly 92% of shared H3K27ac differentially marked sites were consistently enriched in aged and juvenile neurons. These data suggest that there is a partial recapitulation of a juvenile-like histone landscape in the aging brain, possibly as a compensatory mechanism to the effects of oxidative stress and age associated cognitive decline. The concept of aging associated recapitulation of a juvenile-like epigenetic state has been proposed in previous literature (Douaud et al., 2014; Oh et al., 2016). Studies have shown that the epigenome is divergent throughout life (Cheung et al., 2010), but cortical aging leads to a convergence of inter-individual DNA methylation states, suggesting cell de-differentiation in the aging human frontal cortex (Oh et al., 2016). While a recent structural magnetic resonance imaging study has suggested that the grey matter structure of the aging brain mirrors a developmental state (Douaud et al., 2014).

H3K27ac marking between juvenile and aged neurons was annotated to similar pathways when compared to the time-point specific analysis (3 versus 6 month old neurons and 12 versus 24 month old neurons); however, specific pathways including the regulation of dendrite

development, cerebellum development and phosphatase activity were among the top 10 pathways shared between juvenile and aged neurons. Genes that were identified from the gene ontology analysis for dendrite development and cerebellum development included *Cdk5, Camk1/2, Ache, Shank1/3, Grin1, Efna1/3,* and *Ngef*. For example, the *Ngef* gene encodes a guanine nucleotide exchange factor that is highly expressed in the developing mouse brain and is thought to contribute to dendritic spine development (Yoshizawa et al., 2003) (review: (Tolias, Duman, & Um, 2011)). While *Efna1* and *Efna3* encode ephrin tyrosine kinase genes which are crucial for cell migration, axon guidance signalling and cellular adhesion in development (review: (Palmer & Klein, 2003)). Early literature suggested that neuronal aging encompasses a combination of both neuronal loss and dendritic growth of the surviving neurons to maintain neuronal networks (S. Buell & Coleman, 1979; S. J. Buell & Coleman, 1981). More recently, studies have shown that neurite outgrowth increases in some aged neurons from *C. elegans*, often associated with a decrease in synaptic vesicle density (Toth et al., 2012). Interestingly, H3K4me3 marked sites that were shared between juvenile and aged neurons were annotated to pathways including protein folding, maintenance of protein location, nucleotide excision repair, and RNA export from nucleus, all of which are necessary for appropriate cellular function across life. Brain development and aging require large amounts of energy, to establish the nervous system during development, and maintain the nervous system during cellular senescence and cognitive decline. As previously discussed, oxidative stress contributes to age related cognitive decline. Oxidative stress is also responsible for some aspects of DNA damage in aging neurons (review: (Cooke, Evans, Dizdaroglu, & Lunec, 2003)). Both development and aging lead to accumulation of reactive oxygen species and activation of pathways of compensation (Driver, Kodavanti, & Mundy, 2000). Some studies have suggested that age related decline in DNA repair pathways may be influenced by changes to the epigenome (Langie et al., 2017). Alongside DNA damage, oxidative stress can also damage proteins and inhibit normal protein folding, leading to activation of protein refolding and chaperone pathways to repair or degrade misfolded proteins (review: (Kikis, Gidalevitz, & Morimoto, 2010)). Neuronal development and aging require high levels of energy for neuronal activity; in juvenile mice for synaptic development, neurite extension and synaptic pruning (Handley et al., 2017) (review: (Selemon, 2013)), and for appropriate regulation of dendritic regression and dendrite spine loss in aging (review: (Dickstein, Weaver, Luebke, & Hof, 2013)), which may account for some of the similarity juvenile and aged neurons. It is also possible that developmental pathways are reactivated in aged neurons to combat dendritic loss in aging (Toth et al., 2012). The recapitulation of a juvenile-like epigenetic state in aging

neurons may be to promote developmental pathways to combat the cellular mechanisms of age associated cognitive decline.

Histone modifications are enriched in development and aging neurons and regulate diverse pathways for synaptic and core molecular functions throughout life

This study characterised both H3K27ac and H3K4me3 in neurons across a time-course of the aging brain. H3K4me3 and H3K27ac marking are generally associated with active promoters and enhancers respectively, both of which are key regulatory regions for cellular identity and transcription (Creyghton et al., 2010b; Santos-Rosa et al., 2002; Z. Wang et al., 2008; Wysocka et al., 2006). Histone modifications have previously been characterised in post-mortem human aging brain and rodent brain (Benito et al., 2015; Cheung et al., 2010; Shulha et al., 2013). Although there were differences in methodology, sample source and bioinformatic analysis, there are points of agreeance between the current study and others in the literature.

Nativio and colleagues (2018) previously identified an evolution of H4K16ac marking in the post-mortem lateral temporal lobe of the aging brain. H4K16ac marking was enriched at promoters and enhancers of actively transcribed genes and presented with a bimodal distribution at promoters. The study demonstrated age associated enrichment of H4K16ac marking between adult (~52 years old) and old (~68 years old) human lateral temporal lobe (Nativio et al., 2018). There were ~50000 peaks unique to the adult time-point, compared to 127000 peaks that were unique to the aged brain (~68 years old), and ~156000 peaks shared between the two age groups (Nativio et al., 2018). The current study also observed age associated enrichment in H3K27ac and H3K4me3 marking in 24 month old neurons compared to 12 month old neurons. Nativio, et al., (2018) observed that H4K16ac marking was enriched predominantly around TSS in old cases, however there was little change in H4K16ac marking distal to the TSS (Nativio et al., 2018). Similarly, the current study observed less H3K4me3 (associated with active promoters) marking at the TSS of young adult neurons at 6 months of age than in neurons at 12 and 24 months of age. However, the current study also observed H3K27ac marking (also associated with transcriptionally active promoters and enhancers) enriched at TSS, enhancers and super enhancers in aged 24 month old neurons compared to adult neurons at 6 and 12 months of age. Many of the pathways that were annotated for H4K16ac marking in the previous literature were also annotated for H3K27ac or H3K4me3 marking in the current study. For example, both studies identified several similar pathways to

be enriched for histone marking including synaptic, cytoskeletal, autophagic and apoptosis related pathways (Nativio et al., 2018). Pathways that were inconsistent for histone marking between the two studies included many pathways for molecular function such as RNA signalling, oxidative phosphorylation, and gene silencing, in comparison with leukocyte, hydrolase, hypoxia and RAS signal transduction pathways (Nativio et al., 2018). Overall, both studies demonstrated enrichment of histone modifications associated with active transcription in the aging brain, however variances in gene ontology annotations may be due to the inherent differences between post-mortem human lateral temporal lobe in comparison to the mouse forebrain, or indeed the use of brain homogenate in comparison with isolated neuronal nuclei for ChIP-seq. It is also possible that H3K27ac, H3K4me3 and H4K16ac are marking diverse subsets of TSS and enhancers, resulting in different pathways being enriched between the two studies.

To date there have been three studies that have utilised FACS to isolate neuronal nuclei for ChIP-seq in the aging brain (Benito et al., 2015; Cheung et al., 2010; Shulha et al., 2013). Isolation of neuronal nuclei has allowed for an accurate characterisation of the neuronal epigenome and further insight to the dynamic histone landscape in the aging brain. Benito, et al., (2015) performed ChIP-seq for H4K12ac marking from neurons of the CA1 hippocampus of C57/BL6 mice at 3 and 20 months of age. H4K12ac marking was present at the TSS of transcriptionally active genes and correlated with gene transcription (Benito et al., 2015; Lopez-Atalaya, Ito, Valor, Benito, & Barco, 2013). The study demonstrated an age associated depletion in H4K12ac marking at the TSS in neurons, which was not observed in glial populations (Benito et al., 2015). In contrast, the current study identified enrichment of H3K27ac and H3K4me3 marking in the aging brain. The current study observed enrichment of H3K27ac marking at TSS and enhancers and H3K4me3 marking at TSS in 3 month old neurons, that was depleted throughout adulthood at 6 and 12 months of age, then re-established in 24 month old neurons. It may be possible that the enrichment for H3K27ac and H3K4me3 marking between 12 and 24 month old neurons in the current study occurs after 20 months of age and is missed in Benito and colleagues (2015) dataset, however it may also be possible that H3K27ac, H3K4me3 and H4K12ac are marking different subsets of TSS. Benito, et al., (2015) performed RNA-seq of the CA1 hippocampus alongside their ChIP-seq analysis and identified age associated enrichment in pathways relating to inflammatory responses, but depletion in pathways linked to core metabolic processes such as gene expression, RNA splicing and apoptosis. Similar to Benito, et al., (2015), the current study identified RNA splicing, and

apoptosis to be differentially enriched in aging neurons. However, the current study also identified synaptic pathways, lipid transport, oxidative phosphorylation and gene silencing to be enriched for H3K27ac or H3K4me3 marking in the aging brain.

Two studies have isolated neurons and performed ChIP-seq for H3K4me3 in human prefrontal cortex identifying developmental enrichment and age associated decline in H3K4me3 marking (Cheung et al., 2010; Shulha et al., 2013). Cheung, et al., (2010) demonstrated enrichment of H3K4me3 marking in the cortex of young brains (0-1 year old, n=3), but depletion of H3K4me3 marking in neurons from aged cases (65-69 years of age, n=3). Shulha, et al., (2013) also performed ChIP-seq for H3K4me3 in young (prenatal, n=3) and aged (1-81 years old, n=25) in neurons from the human rostral prefrontal cortex. The study showed a mix of enrichment and depletion in prenatal development and early childhood that stabilised in neurons in later life (Shulha et al., 2013). In contrast, the current study showed H3K4me3 and H3K27ac marking was enriched in neurons at 3 months of age, but also enriched in neurons from the aging brain. The mice utilised in the current study between 3-6 month old are generally considered to be equivalent to humans between 18-30 years of age, while 18-24 month old mice are more similar to humans between 50-70 years of age (Fox et al., 2006; Semple et al., 2013). In contrast to the data from Cheung (2010) and Shulha (2013), the current study identified H3K4me3 and H3K27ac marking to be enriched in juvenile mice, and interestingly also enriched in 12 and 24 month old mice for H3K4me3 marking, and 24 month old mice for H3K27ac marking. Due to the young age of cases from Cheung (2010) and Shulha (2013), much of the gene ontology and pathways identified in the study were annotated to sites for neurogenesis, neurite development, neuron development, synaptic plasticity and the regulation of cell differentiation (Cheung et al., 2010; Shulha et al., 2013). The youngest time-point measured in the current study did not capture the early developmental epigenome, however H3K4me3 and H3K27ac marking was annotated to similar pathways for synaptic plasticity and transmission, but also pathways for molecular function such as lipid and ion transport, RNA processing, and oxidative phosphorylation. Differences between the current study and previous literature may also be due to inherent differences that may exist in H3K4me3 marking between aging rodent and human neurons, brain area sampled, sample size or bioinformatic methods for analysis (peak calling versus differential enrichment analysis with csaw). It is also possible that the differences may due to the wide inter-individual variation in the epigenome that can be seen in post-mortem human tissue (Cheung et al., 2010), where it is necessary to identify confounding factors due to physical health, cognitive reserve, and age.

Despite the strengths of the current study, there are a few caveats to consider when interpreting the results. The NeuN antibody, first discovered in 1992, labels neuronal nuclei expressing the transcription factor FOX-3, which is present in the vast majority of neuronal nuclei in vertebrates (K. K. Kim, R. S. Adelstein, & S. Kawamoto, 2009; Richard J Mullen, Charles R Buck, & Alan M Smith, 1992). Current research into the NeuN/FOX-3 antibody shows that it labels the vast majority of neuronal nuclei from adult mammalian brain, first detectable during development after neurons withdraw from the cell-cycle (Richard J Mullen et al., 1992). However, there has not been extensive research into differential expression of NeuN during aging. Although the FACS data from the current study showed no significant differences in the number of NeuN+ nuclei between 3, 6, 12 and 24 months of age, it is possible that the distribution of NeuN changes throughout aging in the mammalian brain and this is an important avenue for future characterisation. Independent techniques such as immunohistochemistry and single-cell sequencing could be utilised for verification of the findings from the current study. Indeed, recent research into H3K4me3 and H3K27ac marking in the aging brain suggest that there are global changes in the distribution of H3K4me3 and H3K27me3 marking in NF-positive pyramidal neurons and calretinin-positive interneurons throughout aging (Dyer, Phipps, Mitew, Taberlay, & Woodhouse, 2019). Dyer et al., (2019) demonstrated an age associated loss in H3K27ac marking in NF+ pyramidal neurons between 3 and 6 months of age when measured with immunohistochemistry, and an age associated enrichment in H3K27ac between 6 and 12 months of age. The study also identified H3K27me3 marking to significantly increase in calretinin labelled interneurons between 3 and 12 months of age (Dyer et al., 2019). This PhD study also identified enrichment for H3K27ac marking at 3 months of age compared to 6 months, however little change between 6 and 12 months for H3K27ac marking. However, this study showed that the genomic coverage of H3K27ac to remain relatively constant until 24 months of age. Another caveat to consider in the current study is the use of pseudo-replicates for bioinformatic analysis. Despite many different bioinformatics pipelines being tested and optimised for the analysis in this study, current pipelines are not well suited for the heterogenous samples seen in the mammalian brain. Although the current study performed the analysis similarly to previously published studies (Benito et al., 2015; Gjoneska et al., 2015; Nativio et al., 2018), future research could develop despoke bioinformatic pipelines to analyse the biological replicates and inter-individual differences to determine whether histone enrichment across the genome becomes more or less divergent with aging. Despite the use of pseudoreplicates, it is still possible that technical differences may have influenced the data, including potential inefficiencies between ChIPs at different time-points. Inefficiencies in ChIP

experiments may have influenced the results, and explain some of the differences between the ages identified in the current study, however all ChIP experiments and library preparation was performed in a single batch to minimise any technical differences. These imitations should also be minimized due to the use of 5 biological replicates for each genotype and timepoint to generate the pseudoreplicates in the current study.

Conclusion

In summary, this study identified enrichment of H3K27ac and H3K4me3 marking in juvenile and aged neurons compared to adult neurons. This data provides the first comprehensive characterisation of H3K27ac and H3K4me3 at promoters, enhancers and super-enhancers across a time-course of aging in neurons. Strikingly, H3K27ac and H3K4me3 dynamically regulate neuronal processes including synaptic plasticity, ion channel binding, transporter activity, calcium channel activity and cellular metabolic processes across life. These data also point towards a partial recapitulation of a juvenile-like epigenetic state in aging neurons, which may be necessary for the maintenance of neuronal structure and function in healthy aging.

Chapter 5: Alteration of the neuronal epigenome occurs prior to pathology onset and is altered throughout Alzheimer's disease progression

5.1 Introduction

The epigenome is dysregulated in AD, correlating with increasing Braak stage and neuritic plaque load (Chapter 1.13-1.14;(P. L. De Jager et al., 2014; Lunnon et al., 2014)). Despite increasing research effort in this space, there have been few studies that have investigated histone modifications in AD (Benito et al., 2015; Gjoneska et al., 2015; Klein et al., 2019; Marzi et al., 2018; D. Mastroeni et al., 2013; Nativio et al., 2018), and importantly, there has been no investigation of the core ENCODE histone modifications in neurons in AD.

The limited literature that is available regarding histone modifications in AD points towards depletion of certain histone modifications at putative enhancers and promoters associated with synaptic plasticity along with enrichment at immune response genes (Gjoneska et al., 2015), and genome-wide depletion of histone 4 lysine 16 acetylation (H4K16ac) and histone 4 lysine 12 acetylation (H4K12ac) at transcriptional start sites (TSS) (Benito et al., 2015; Nativio et al., 2018). There have only been five studies that performed ChIP-seq in post-mortem human or mouse brain, and one study that examined histone modifications with immunohistochemistry (Benito et al., 2015; Gjoneska et al., 2015; Klein et al., 2019; Marzi et al., 2018; D. Mastroeni et al., 2013; Nativio et al., 2018). An earlier study by Gjoneska and colleagues (2015) was a significant advance in the field at the time, in that they performed genome-wide RNA-seq and ChIP-seq for H3K4me1, H3K4me3, H3K27ac, H3K27me3, H3K36me3, and H4K20me1 attempting to dissect coordinate changes in the transcriptome and histone modification landscape in the CK-p25 inducible neurodegeneration mouse model. This study compared wildtype and transgenic animals at a single 3 month old time point, after either two weeks or six weeks induction of *Cdk5* (Gjoneska et al., 2015). The results from this study demonstrated a depletion of histone modifications associated with promoter and enhancer activity with genes involved in synaptic plasticity and the immune response and increased immune-cell-specific signalling pathways. ChromHMM identified enhancers were found to be upregulated at known AD-associated loci including *Picalm, Bin1, Inpp5d, Celf1* and *Ptk2b* in the CK-p25 mouse model (Gjoneska et al., 2015). However, the use of whole brain homogenate and the CK-p25 model, which is associated with a range of neurodegenerative diseases, means that it is difficult to establish the histone modification alterations that are directly related to AD pathology, or identify changes that are occurring in specific cell types (Cruz, Tseng, Goldman, Shih, & Tsai, 2003). Histone modification changes may also be due to metabolic load or the rapid pathology accumulation in this model. More recently, a study by Nativio et al. (2018) showed that

H4K16ac was enriched and accumulates with increasing age in the healthy brain, however interestingly, H4K16ac was depleted in the lateral-temporal-lobe in post-mortem human AD cases compared to controls (Nativio et al., 2018). Gene ontology analysis demonstrated that H4K16ac depletion occurred in pathways relating to myeloid differentiation, cell death, and Wnt/Ras signalling (Nativio et al., 2018). Correlating these finding with accumulating AD pathology led to the identification of three separate classes of change in H4K16ac marking; age-regulated, age-dysregulated and age-independent changes (Nativio et al., 2018). This study also found H4K16ac dysregulation at AD-associated quantitative trait loci curated from previous genome-wide association studies, finding 143 age-regulated, 231 age-dysregulated and 220 disease specific overlaps (Nativio et al., 2018). Another recent genome-wide study of H3K27ac identified 4162 sites of differential enrichment between post-mortem entorhinal cortex from AD cases and matched control cases (Marzi et al., 2018). This study identified differentially enriched sites associated with Aβ and tau pathology (APP, PS1, PS2, MAPT), and ontology analysis showed lipoprotein-particle binding, apolipoprotein binding, response to hypoxia and Aβ metabolic process to be differentially enriched for H3K27ac (Marzi et al., 2018). In accordance with other recent literature, genome-wide analysis of H3K9ac using ChIP-seq in the prefrontal cortex of post-mortem AD cases has shown that tau, but not Aβ correlates with altered H3K9ac profile (affecting 5990 H3K9ac marked sites) at promoters and enhancers, leading to transcriptional changes in AD as measured by RNA-seq (Klein et al., 2019). These data also complement an analysis of global histone modifications in post-mortem human brain; immunohistochemistry and Western blot demonstrate global loss of nuclear H3K4me3, and cytoplasmic accumulation of H3K4me3 in neurons of the hippocampus and middle-temporal gyrus that correlated with early markers of tau pathology and Braak staging in AD (D. Mastroeni et al., 2015).

The studies reported above utilised whole brain homogenate containing a mixture of cells. The inherent definition of the epigenome means that it is regulated in a cell type specific manner; however, there has been only one study that has performed ChIP-seq in neurons in AD (Benito et al., 2015) and no comprehensive studies across a time-course of pathology accumulation in an AD model. Benito, et al., (2015) performed RNA-seq, and ChIP-seq for H4K12ac in neurons from the CA1 hippocampal subregion and dentate gyrus in 3 month and 20 month old APP/PS1-21 mice (Benito et al., 2015). These data revealed a genome-wide loss of H4K12ac in neurons, with dysregulation of H4K12ac leading to altered epigenetic signatures at regulatory elements of genes associated with synaptic plasticity and subsequent changes in

gene expression in neurons. These alterations occurred concomitant with enrichment of H4K12ac in pathways associated with an immune response in non-neuronal cells (Benito et al., 2015). Interestingly, administration of HDACi (SAHA) restored cognitive performance, stabilised H4K12ac and reduced the inflammatory response in the model (Benito et al., 2015).

This PhD study is the first to perform a time-course experiment examining H3K4me3 and H3K27ac alterations in neurons from APP/PS1 transgenic AD mice compared to WT control mice at 3, 6, and 12 months of age, representing pre-pathology, pathology onset, and pathology rich time-points in this AD model.

5.2 Results

5.2.1 Histone acetylation is enriched in neurons early in the APP/PS1 mouse model of AD

Histone modifications contribute to the compaction of DNA into chromatin and the access of transcriptional machinery to chromatin. These sites of regulation can be at promoters near TSS, or at distal regulatory elements. Currently, it is accepted that H3K27ac marks active enhancers (>2kB distal to TSS) and promoters (Rada-Iglesias et al., 2011). Core ENCODE histone modifications have not been characterised in neurons in AD. Here, H3K27ac was analysed in neurons genome-wide with ChIP-seq in the APP/PS1 mouse model of AD at 3 months of age representing pre-pathology, 6 months of age representing pathology onset, and 12 months of age, which is a pathology rich time-point in APP/PS1 mice.

An assessment of total genomic coverage can provide an indication of histone modification changes occurring in neurons in APP/PS1 neurons and WT control neurons on a global scale. At 3 months of age, APP/PS1 neurons exhibited greater total genomic coverage for H3K27ac marking than WT control neurons (APP/PS1 5.94% versus WT 2.23%; Figure 5.1a); however, by 6 months of age, H3K27ac covered a smaller percentage of the genome in APP/PS1 neurons compared to WT control neurons (APP/PS1 1.38% versus WT 2.46%; Figure 5.1b). At 12 months of age, H3K27ac exhibited greater genomic coverage in APP/PS1 neurons compared to WT control neurons (APP/PS1 2.72% versus WT 1.86%; Figure 5.1c). Over time, WT control neurons sustained a relatively consistent level of H3K27ac. By contrast, APP/PS1 neurons were dynamic across time (Figure 5.1a-c).

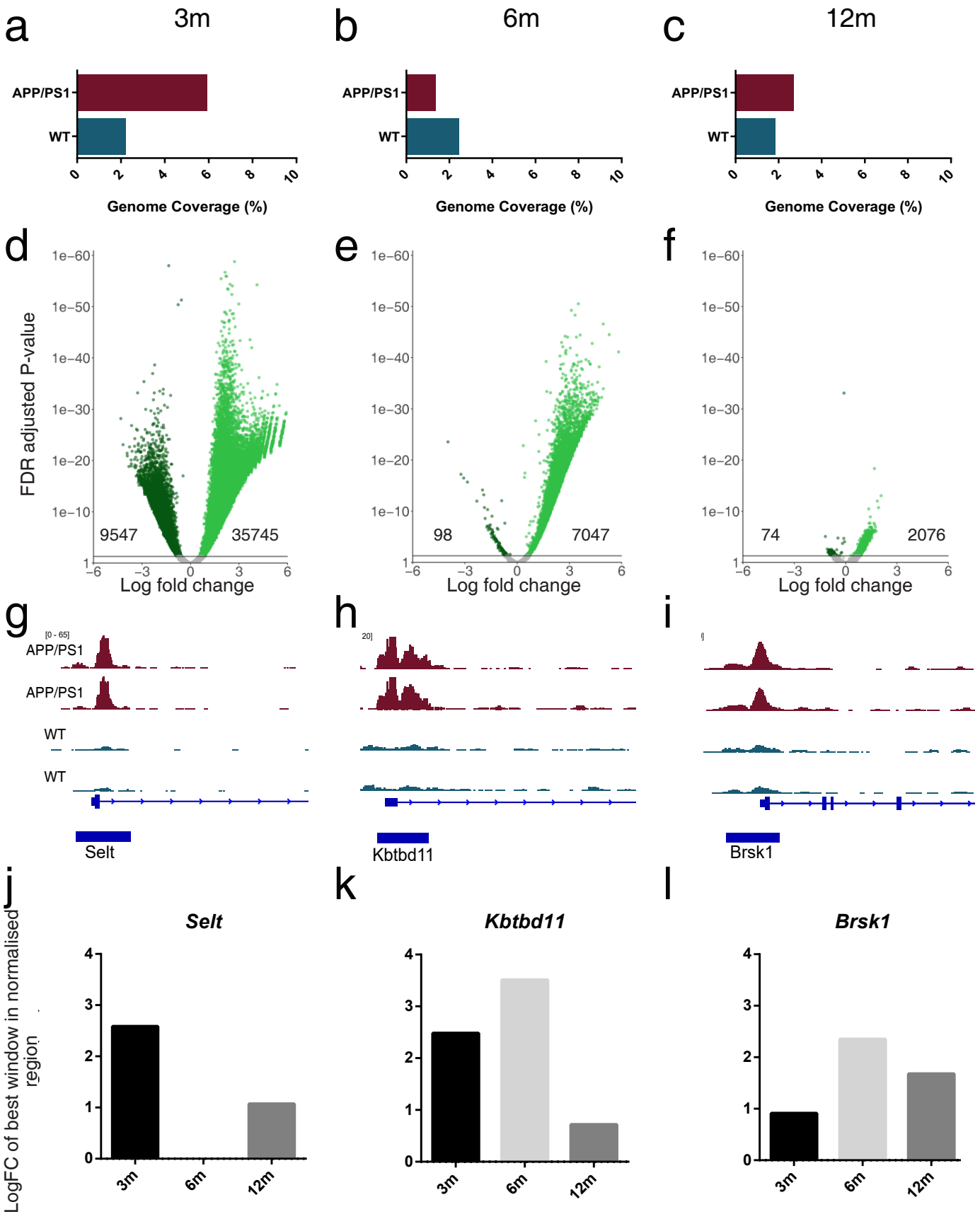
a
3m
b
6m
c
12m
APP/PS1
WT
0
2
4
6
8
10
Genome Coverage (%)
d
e
f
FDR adjusted P-value
1e−60
1e−50
1e−40
1e−30
1e−20
1e−10
1
9547
35745
98
7047
74
2076
−6
−3
0
3
6
Log fold change
g
h
i
[0 - 65]
20]
APP/PS1
APP/PS1
WT
WT
Selt
Kbtbd11
Brsk1
j
k
l
Selt
Kbtbd11
Brsk1
LogFC of best window in normalised region
4
3
2
1
0
3m
6m
12m

Figure 5.1: Global dysregulation of H3K27ac in neurons prior to pathology onset in APP/PS1 mice

ChIP-seq was performed for 5 biological replicates for H3K27ac per genotype, then merged into pseudoreplicate tracks for analysis. (a-c) Percentage of 5× genomic coverage of H3K27ac in neurons from APP/PS1 (red) and WT control (blue) mice at (a) 3 months, (b) 6 months and (c), and 12 months of age. (d-f) Volcano plots show the logFC and FDR adjusted P-value of APP/PS1 compared to WT control neurons; positive logFC (light green) and negative logFC (dark green) for all differentially enriched windows of H3K27ac marking at (d) 3 months, (e) 6 months and (f) 12 months of age. (g-i) Representative tracks of pseudoreplicates visualised in IGV showing the top-ranked sites of enrichment between APP/PS1 (red) and WT control mice (blue). (g) The *Selt* promoter at 3 months of age, (h) the *Kbtbd11* promoter 6 months of age and (i) the *Brsk1* promoter at 12 months of age. (j-l) Histograms showing the logFC of the best window within the normalised region of H3K27ac marking in APP/PS1 neurons compared to WT control mice at 3 months (black), 6 months (light grey) and 12 months (dark grey) of age for (j) the *Selt* promoter, (k), the *Brsk1* promoter and (l) the *Kbtbd11* promoter.

Next, differential enrichment of H3K27ac was assessed genome-wide in neurons from APP/PS1 and WT control mice. There was an evolution of H3K27ac marking in neurons between WT and APP/PS1 mice across disease progression (Figure 5.1d-f). There were 35745, 7049, and 2076 H3K27ac marked sites significantly enriched in 3, 6, and 12 month old APP/PS1 neurons compared to WT control neurons, respectively (Figure 5.1d-f; Benjamini Hochberg FDR adjusted p-value <0.05). Whereas, there were 9547, 98, and 74 differentially enriched H3K27ac sites depleted in APP/PS1 neurons at 3, 6, and 12 months of age, respectively (Figure 5.1d-f; Benjamini Hochberg FDR adjusted p-value <0.05). There was a progressive decline in the total number of H3K27ac differentially enriched sites across disease progression in APP/PS1 neurons (Figure 5.1d-f). Visualisation of H3K27ac marked sites in IGV showed multiple regions of differential enrichment in APP/PS1 neurons compared to WT control neurons. For example, the promoter of the *Selt* gene on chromosome 3 was differentially enriched for H3K27ac at 3 months of age; this gene encodes selenoprotein T, which is known to protect against oxidative stress in dopaminergic neurons in neurodegenerative disease (Figure 5.1g; (Boukhzar et al., 2016)). Similarly, in 6 month old neurons, the *Kbtbd11* promoter on chromosome 8, encoding the Kelch Repeat and BTB domain containing 11 protein, was enriched for H3K27ac in neurons from APP/PS1 neurons compared to WT control neurons (Figure 5.1h), and at 12 months of age, *Brsk1,* encoding the Serine/theonine-protein kinase 1 transmembrane protein was enriched for H3K27ac in APP/PS1 neurons compared to WT control neurons (Figure 5.1i). Histograms of H3K27ac enrichment at the promoters of *Selt, Kbtbd11,* and *Brsk1* at 3, 6 and 12 months demonstrated dynamic enrichment at these sites through pathology accumulation in APP/PS1 neurons compared to WT control neurons (Figure 5.1j-l).

5.2.2 H3K27ac is enriched at TSS in neurons prior to pathology onset in the APP/PS1 mice

H3K27ac can be present at both promoters and enhancers and is indicative of gene regulatory element activity (Creyghton et al., 2010b; Rada-Iglesias et al., 2011). First, the average distribution of H3K27ac was examined by visualising the mean abundance of reads around a 2kb region upstream and downstream of the TSS. Here, H3K27ac marking displayed a bimodal distribution and the mean enrichment was higher in APP/PS1 neurons compared to WT control neurons at 3, 6, and 12 months of age.

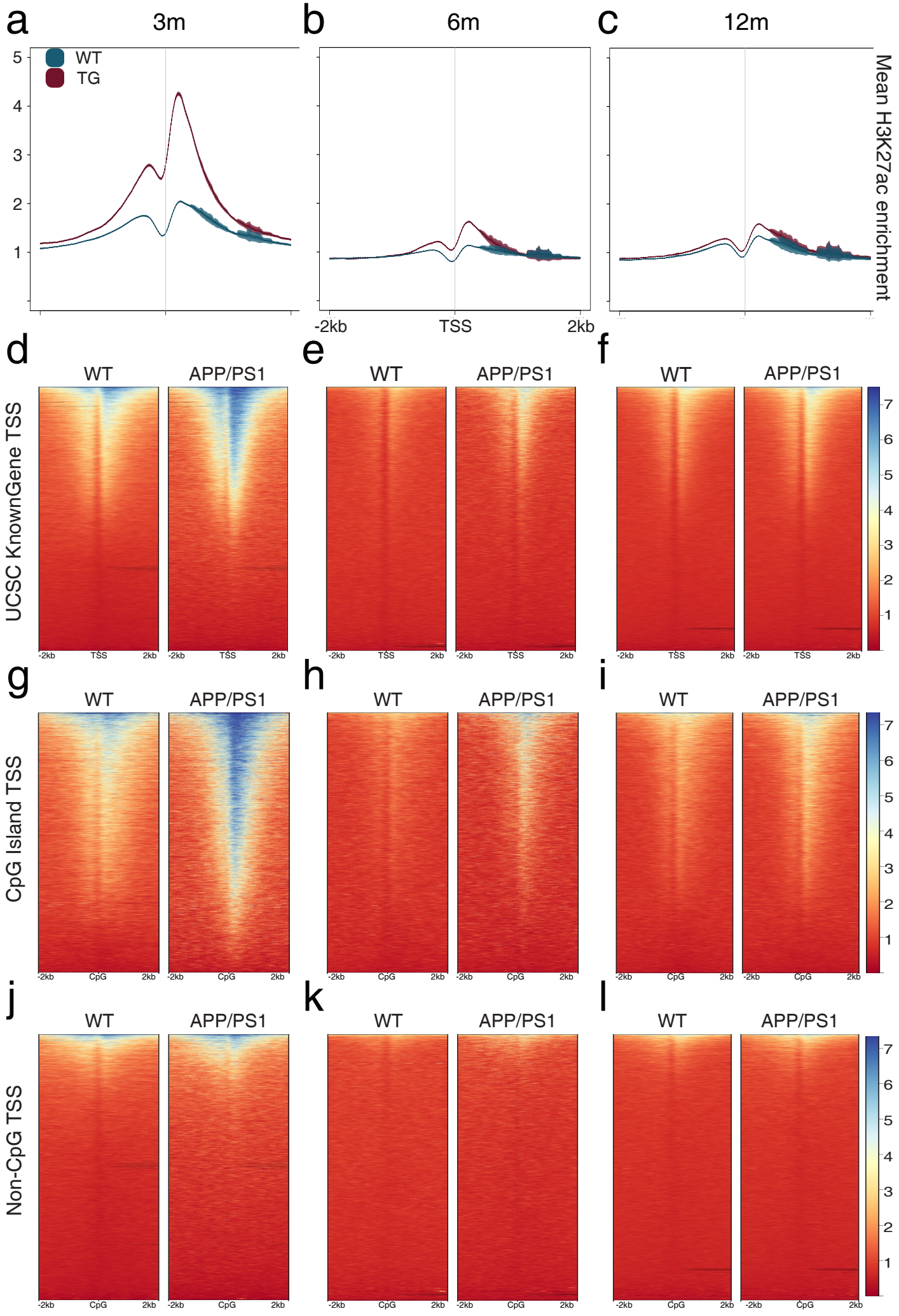
a
3m
b
6m
c
12m
WT
TG
5
4
3
2
1
Mean H3K27ac enrichment
-2kb
TSS
2kb
d
e
f
WT
APP/PS1
UCSC KnownGene TSS
7
6
5
4
3
2
1
g
h
i
CpG Island TSS
CpG
j
k
l
Non-CpG TSS

Figure 5.2: H3K27ac enrichment occurs at transcriptional start sites in neurons from APP/PS1 mice prior to pathology onset

(a-c) Average enrichment plots for H3K27ac within a 2kb window of TSS of the UCSC KnownGene track in APP/PS1 (red) and WT control neurons (blue) at (a) 3 months of age, (b) 6 months of age and (c) 12 months of age. (d-f) Heatmaps of H3K27ac marking for UCSC KnownGene sorted by strongest (blue) to weakest (red) signal in WT (left) and APP/PS1 neurons (right) at (d) 3 months, (e) 6 months and (f) 12 months of age. (g-i) Heatmaps of H3K27ac marking at CpG islands from the UCSC mm10 CpG island track sorted by strongest (blue) to weakest (red) signal in WT (left) and APP/PS1 neurons (right) at (g) 3 months of age, (h) 6 months of age, and (i) 12 months of age. (j-l) Heatmaps of H3K27ac marking at non-CpG containing TSS from the UCSC mm10 KnownGene track sorted by strongest (blue) to weakest (red) signal in WT (left) and APP/PS1 (right) at (j) 3 months of age, (k) 6 months of age, and (i) 12 months of age.

The difference in signal between genotypes was greatest over the highly positioned -1 nucleosome that sits immediately 5'- to the TSS in mammalian cells (Figure 5.2a-f). Quantitation of the mean enrichment plots (Figure 5.2a-c) showed that H3K27ac enrichment at the TSS in APP/PS1 neurons was highest at 3 months, approximately 2-fold increase compared to WT neurons (APP/PS1 max: 4.25; WT max: 2.04; Figure 5.2a). Whereas the mean H3K27ac signal at the TSS was increased approximately 0.5-fold in APP/PS1 neurons compared to WT control neurons at 6 months of age (APP/PS1 max: 1.62; WT max: 1.13; Figure 5.2b), and normalised by 12 months of age (APP/PS1 max: 1.59; WT max: 1.34, respectively; Figure 5.2c).

Next, H3K27ac marking was visualised with heatmaps against the UCSC KnownGene track, to determine the distribution of H3K27ac at a 2kb window around TSS. At 3 months of age H3K27ac was enriched at a greater magnitude at TSS and in a larger proportion of TSS in APP/PS1 neurons (approximately 50% of TSS were enriched for H3K27ac) compared to WT control neurons (approximately 30% of TSS were enriched for H3K27ac; Figure 5.2d). At 6 months of age, there was a dramatic loss of enrichment and altered distribution of H3K27ac from both APP/PS1 and WT neurons compared to 3 months of age. However, 6 month old APP/PS1 neurons were marginally enriched for H3K27ac, and marking was present at a greater number of TSS compared to WT control neurons (Figure 5.2e). Interestingly, at 12 months of age there was little change in the proportion of TSS or magnitude of H3K27ac marking in APP/PS1 neurons compared to WT control neurons.

CpG islands are predominantly found at TSS and are key sites for the regulation of DNA methylation and transcription (review: (Deaton & Bird, 2011)). To identify whether the enrichment seen at all TSS was predominantly at TSS containing CpG islands, H3K27ac marking was generated against heatmaps for TSS that contained CpG islands, and TSS that did not contain CpG islands (Figure 5.2g-l). At 3 months of age, the proportion of TSS and magnitude of H3K27ac marking at TSS that contained CpG islands were enriched in APP/PS1 neurons compared to WT control neurons, with marking present at approximately 80% of all CpG island TSS (Figure 5.2g). At 6 months of age, the magnitude and proportion of TSS that contained CpG islands were also enriched for H3K27ac in APP/PS1 neurons, however the overall magnitude of enrichment was reduced when compared to 3 months of age (Figure 5.2h). At 12 months of age, H3K27ac marking at TSS that contained CpG islands was similar between APP/PS1 neurons and WT neurons (Figure 5.2i). In comparison to CpG islands, non-CpG island TSS exhibited less H3K27ac marking (Figure 5.2j-l). At 3 months of age, there was a

minor enrichment in the proportion of TSS and magnitude of H3K27ac at non-CpG island TSS in APP/PS1 neurons compared to WT control neurons (Figure 5.2j), however at 6 and 12 months of age, non-CpG island TSS exhibited minimal H3K27ac enrichment in both WT and APP/PS1 neurons (Figure 5.2k,l).

Together, these results show that H3K27ac marking is enriched at TSS, and is present at a greater number of TSS in APP/PS1 neurons compared to WT control neurons prior to pathology onset at 3 months of age. The enrichment of H3K27ac at TSS in APP/PS1 neurons is then depleted at pathology onset at 6 months of age, and there is minimal difference between APP/PS1 neurons and WT control neurons in pathology rich animals at 12 months of age. TSS that contain CpG islands are enriched for H3K27ac in APP/PS1 neurons prior to pathology onset, and at pathology onset, however by 12 months of age there is minimal difference in H3K27ac marking at TSS that contain CpG islands when comparing APP/PS1 neurons and WT control neurons.

5.2.3 H3K27ac is reduced at enhancers genome-wide, but enriched at the majority of cortical super-enhancers in neurons prior to pathology onset in APP/PS1 mice

Similar to Chapter 4, to identify epigenetic modifications occurring at enhancers specifically, a track of all H3K27ac marking outside of a 2kb window of UCSC KnownGene TSS was generated and used to map ‘putative enhancers’. Herein, ‘putative enhancers’ as defined above will be referred to as enhancers.

Initially the average proportion of enhancers that contained H3K27ac marking was measured with by visualising the mean abundance of reads around a 2kb region upstream and downstream of enhancer elements. At 3 months of age, average H3K27ac marking was depleted at enhancers in neurons from APP/PS1 animals (max: 26.96) compared to WT control neurons (max: 37.98) (Figure 5.3a). The mean enrichment for H3K27ac marking at enhancers increased in APP/PS1 neurons compared to WT control neurons at 6 months (APP/PS1 max: 38.17; WT max: 31.32; Figure 5.3b) but was less at 12 months of age compared to WT control neurons (APP/PS1 max: 43.86; WT max: 45.60; Figure 5.3c). Interestingly, the average H3K27ac enrichment at enhancers gradually increased across the time-course in neurons from APP/PS1 animals up to 12 months of age; however, neurons from WT animals exhibited stable

H3K27ac marking at enhancers at 3 and 6 months of age, followed by enrichment at 12 months of age compared to 3 and 6 month time-points.

Next, H3K27ac was visualised with heatmaps within a 2kb window of enhancers to determine the magnitude and proportion of enhancers containing H3K27ac marking. At 3 months of age H3K27ac marking and magnitude was depleted at enhancers in APP/PS1 neurons compared to WT control neurons, while the proportion of enhancers containing H3K27ac marking remained constant with the vast majority of enhancers showing H3K27ac marking in APP/PS1 and WT neurons (Figure 5.3d). At 6 months of age, both the magnitude and proportion of enhancers containing H3K27ac marking was depleted from enhancers in both APP/PS1 and WT neurons compared to 3 months of age. Interestingly, H3K27ac was enriched to a greater magnitude in APP/PS1 neurons at 6 months of age compared to WT control neurons, however the distribution of H3K27ac marking remained the same between APP/PS1 neurons and WT control neurons. Whereas at 12 months of age, there was a slight increase in the magnitude and no difference in the distribution of H3K27ac marking between APP/PS1 neurons and WT neurons (Figure 5.3f). Visualisation of differential enrichment of H3K27ac marking at enhancers demonstrated multiple regions of enrichment in APP/PS1 neurons compared to WT control neurons (Figure 5.3g-i).

Super-enhancers are genomic regions responsible for the majority of cell-type specific gene expression and allow for appropriate cellular identity ((Hnisz et al., 2013; Whyte et al., 2013);chapter 1.10). A cortical super-enhancer track was obtained from dbSUPER, a database of known super-enhancers to map changes in H3K27ac enrichment around known cortical super-enhancers (Khan & Zhang, 2016). Interestingly, H3K27ac enrichment was identified at the majority of cortical super-enhancers in neurons from 3, 6, and 12 month old APP/PS1 neurons in comparison to WT controls (Figure 5.4a-f). Heatmaps for known cortical super-enhancers showed enrichment in the magnitude and proportion of enhancers containing H3K27ac marking in APP/PS1 compared to WT neurons at 3 months of age (Figure 5.4a). Enrichment for H3K27ac at cortical super-enhancers was also present in 6 month old APP/PS1 neurons compared to WT control neurons (Figure 5.4b). Interestingly, there was an overall depletion of H3K27ac marking at super-enhancers at 6 months of age compared to the 3 month time-point (Figure 5.4a,b). At 12 months of age, there was slight enrichment of the proportion and magnitude of H3K27ac marking at cortical super-enhancers in APP/PS1 neurons compared to WT control neurons (Figure 5.4c). At 3 months of age there were 1389 sites of differential H3K27ac enrichment that overlapped cortical super-enhancers; 871 sites were enriched, and

488 super-enhancers were depleted for H3K27ac in APP/PS1 compared to WT control neurons. For example, at 3 months of age, H3K27ac was enriched in APP/PS1 neurons at the super-enhancer overlapping the *Cpeb2* gene (2.23 logFC versus WT control neurons; Figure 5.4d). At 6 months of age, there were 697 super-enhancers enriched and 7 super-enhancer sites depleted of H3K27ac in APP/PS1 neurons versus WT control neurons, with the highest enrichment of H3K27ac in APP/PS1 neurons observed at the super-enhancer overlapping the *Arhgef10* and *Kbtbd11* genes (3.51 logFC; Figure 5.4e). Whereas at 12 months, there were only 276 super-enhancer sites enriched for H3K27ac, and 10 sites depleted, in APP/PS1 neurons compared to WT neurons, with the top site of enrichment overlapping the *Sept8* gene (1.91 logFC; Figure 5.4f).

Taken together, the proportion of enhancers and super-enhancers containing H3K27ac marking illustrates an inverse pattern in APP/PS1 neurons compared to WT control neurons. Prior to pathology onset there is an overall loss of H3K27ac marking at enhancers, but interestingly, enrichment of H3K27ac in cortical super-enhancers in APP/PS1 compared to WT neurons. However, by 12 months of age there was minimal change in H3K27ac at both enhancers and cortical super-enhancers between APP/PS1 and WT neurons.

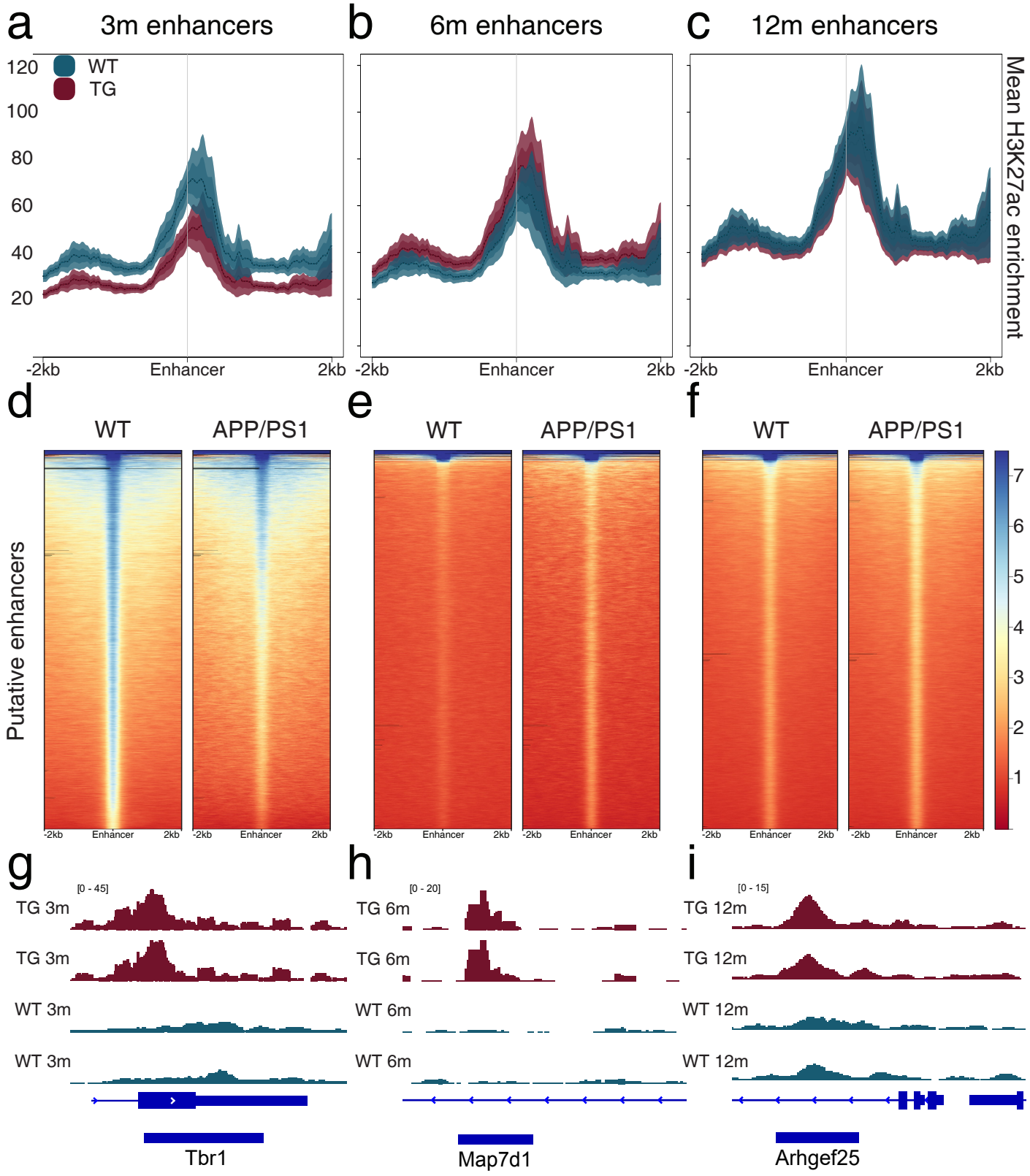
a
3m enhancers
b
6m enhancers
c
12m enhancers
WT
TG
120
100
80
60
40
20
-2kb
Enhancer
2kb
Mean H3K27ac enrichment
d
e
f
WT
APP/PS1
Putative enhancers
7
6
5
4
3
2
1
g
h
i
[0 - 45]
[0 - 20]
[0 - 15]
TG 3m
TG 6m
TG 12m
WT 3m
WT 6m
WT 12m
Tbr1
Map7d1
Arhgef25

Figure 5.3: H3K27ac is depleted from putative enhancers in APP/PS1 neurons prior to pathology onset

(a-c) Average enrichment plots for H3K27ac within a 2kb window of putative enhancers in APP/PS1 (red) or WT control neurons (blue) at (a) 3 months, (b) 6 months and (c) 12 months. (d-f) Heatmaps for H3K27ac signal at enhancers sorted by strongest (blue) to weakest (red) signal in WT (left) and APP/PS1 (right) at (d) 3 months, (e) 6 months and (f) 12 months of age. (g-i) Representative tracks of pseudoreplicates visualised in IGV showing example enhancer sites of enrichment between APP/PS1 (red) and WT control mice (blue). (g) The *Tbr1* enhancer at 3 months of age, (h) the *Map7d1* enhancer at 6 months of age and (i) the *Arhgef25* enhancer at 12 months of age.

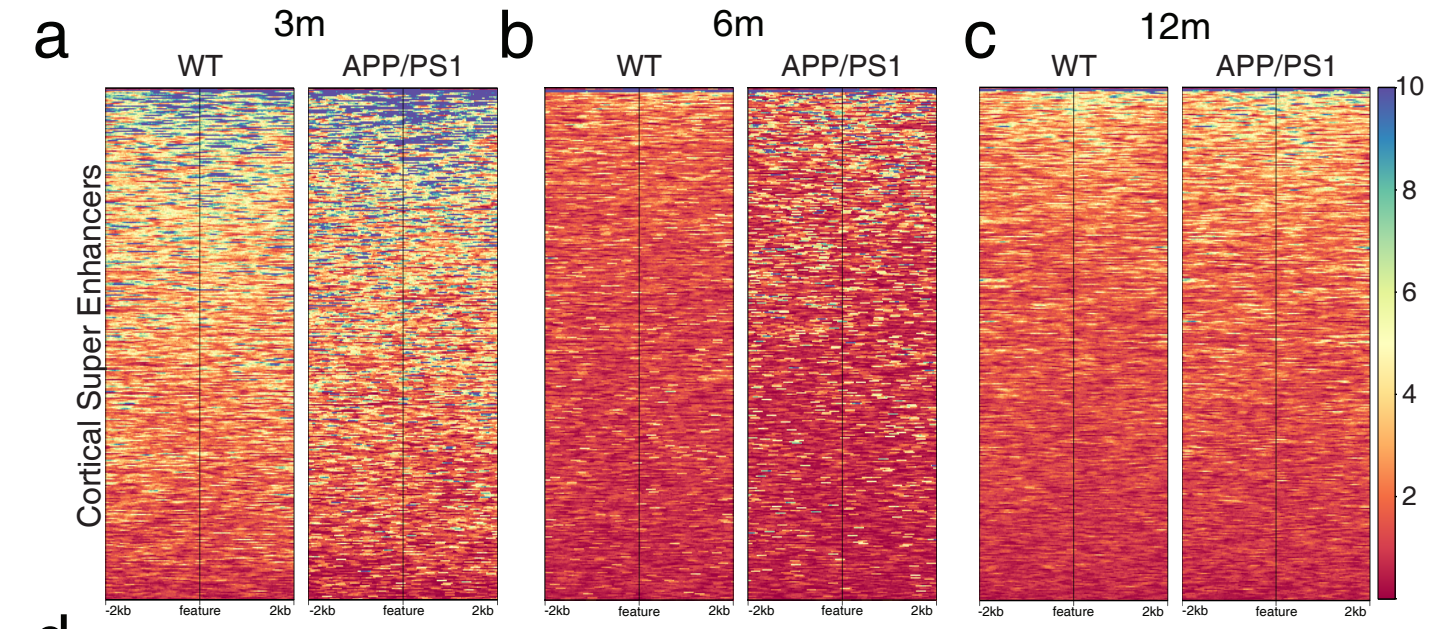
a
3m
WT
APP/PS1
b
6m
WT
APP/PS1
c
12m
WT
APP/PS1
Cortical Super Enhancers
10
8
6
4
2
-2kb
feature
2kb

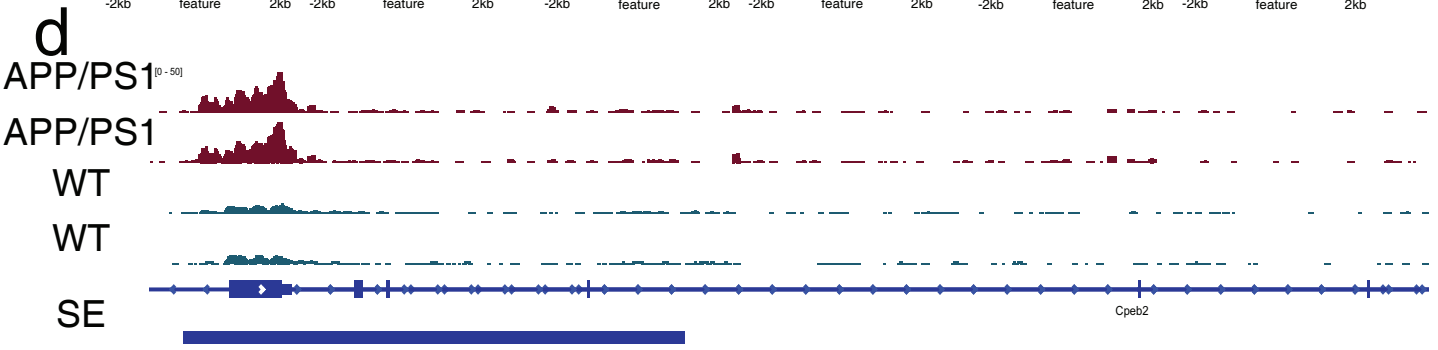
d
APP/PS1
[0 - 50]
APP/PS1
WT
WT
SE
Cpeb2

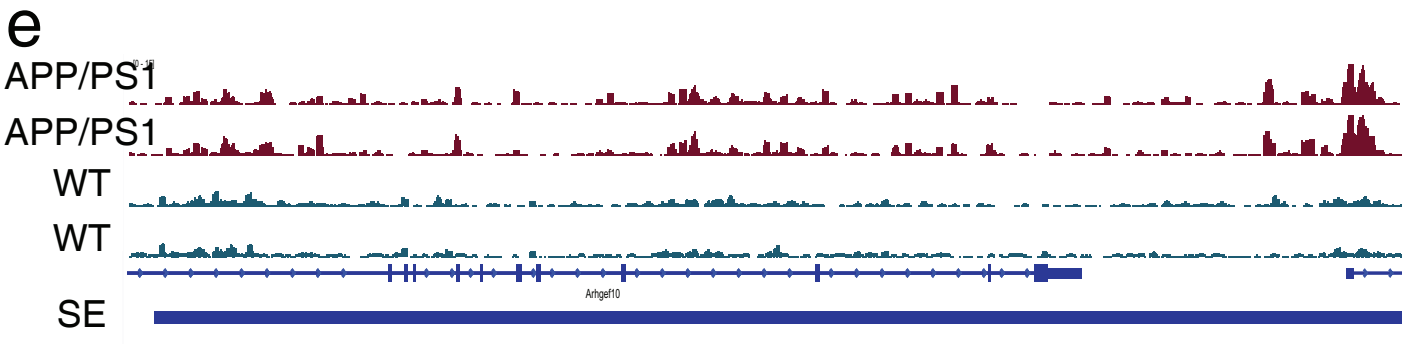
e
APP/PS1
APP/PS1
WT
WT
SE
Arhgef10

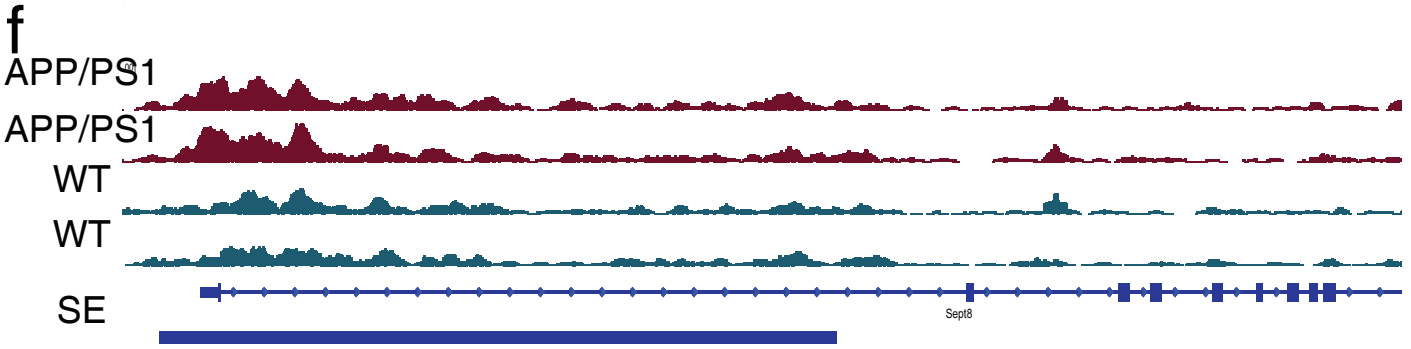
f
APP/PS1
APP/PS1
WT
WT
SE
Sept8

Figure 5.4: A subset of cortical super-enhancers are enriched for H3K27ac in APP/PS1 neurons at 3 months

Heatmaps for the Super-Enhancer Database (dbSUPER) track were sorted by strongest (blue) to weakest (red) signal in WT (left) and APP/PS1 (right) mice at (a) 3 months, (b) 6 months and (c) 12 months of age. Representative tracks visualised using the IGV browser are shown. H3K27ac signal overlap was evident between APP/PS1 neurons (red) and WT control mice (blue) at super enhancers overlapping the top ranked differentially enriched sites including (d) *Cpeb2*, (e), *Arhgef10* and (f) *Sept8* loci.

5.2.4 H3K27ac marking of the epigenome changes in neurons at sites associated with synaptic plasticity and post-translational modification pathways

Next, the molecular pathways and biological processes associated with differential enrichment of H3K27ac in neurons from APP/PS1 and WT mice was assessed using the Genomic Regions Enrichment of Annotations Tool (GREAT) (C. Y. McLean et al., 2010).

This analysis revealed that several key cellular networks were disrupted in APP/PS1 neurons compared to WT neurons. At 3 months of age, this encompassed annotations of differential H3K27ac enrichment to 'GO molecular functions' such as 'SNARE binding', 'syntaxin binding', 'polyubiquitin binding', and 'cholesterol binding' (Figure 5.5a), and annotations to 'GO biological processes' including 'regulation of synaptic plasticity', 'regulation of mRNA processing' and 'learning' (Figure 5.5d). These terms were mostly associated with neuronal specific functions and core cellular processes. At 6 months of age, differential H3K27ac marking in APP/PS1 neurons were annotated to 'GO molecular function' pathways for 'ion channel binding', 'glutamate receptor binding', and 'death domain protein binding' (Figure 5.5b). While H3K27ac marking for 'GO biological processes' was annotated to 'regulation of synaptic plasticity', 'regulation of protein complex disassembly', 'regulation of mRNA processing' and 'regulation of RNA splicing' (Figure 5.5e). At 12 months of age, 'GO molecular function' terms from differential H3K27ac enrichment in APP/PS1 neurons included terms such as 'glutamate receptor binding', 'clathrin binding', 'spectrin binding' and 'ion channel binding', while differential H3K27ac annotations for 'GO biological processes' encompassed the 'maintenance of protein location' as well as developmental pathways such as the 'regulation of dendrite development'. As an interesting proof of principal, gene ontology analysis was able to predict mouse phenotypes from differential H3K27ac enrichment that included well known characteristics of the APP/PS1 mouse model such as abnormal object recognition memory, abnormal dendritic spine and cell morphology, axonal transport, abnormal NMDA and AMPA mediated synaptic currents and synaptic plasticity (Figure 5.5g).

Taken together, these analyses illustrated changes in H3K27ac marking at gene loci involved in synaptic plasticity, core cellular processes and post-translational modifications, while pathology burden led to altered H3K27ac marking in pathways involved in protein location and axonal development, possibly as a result of diminished synaptic plasticity seen in the APP/PS1 mouse model (Figure 5.5a-f).

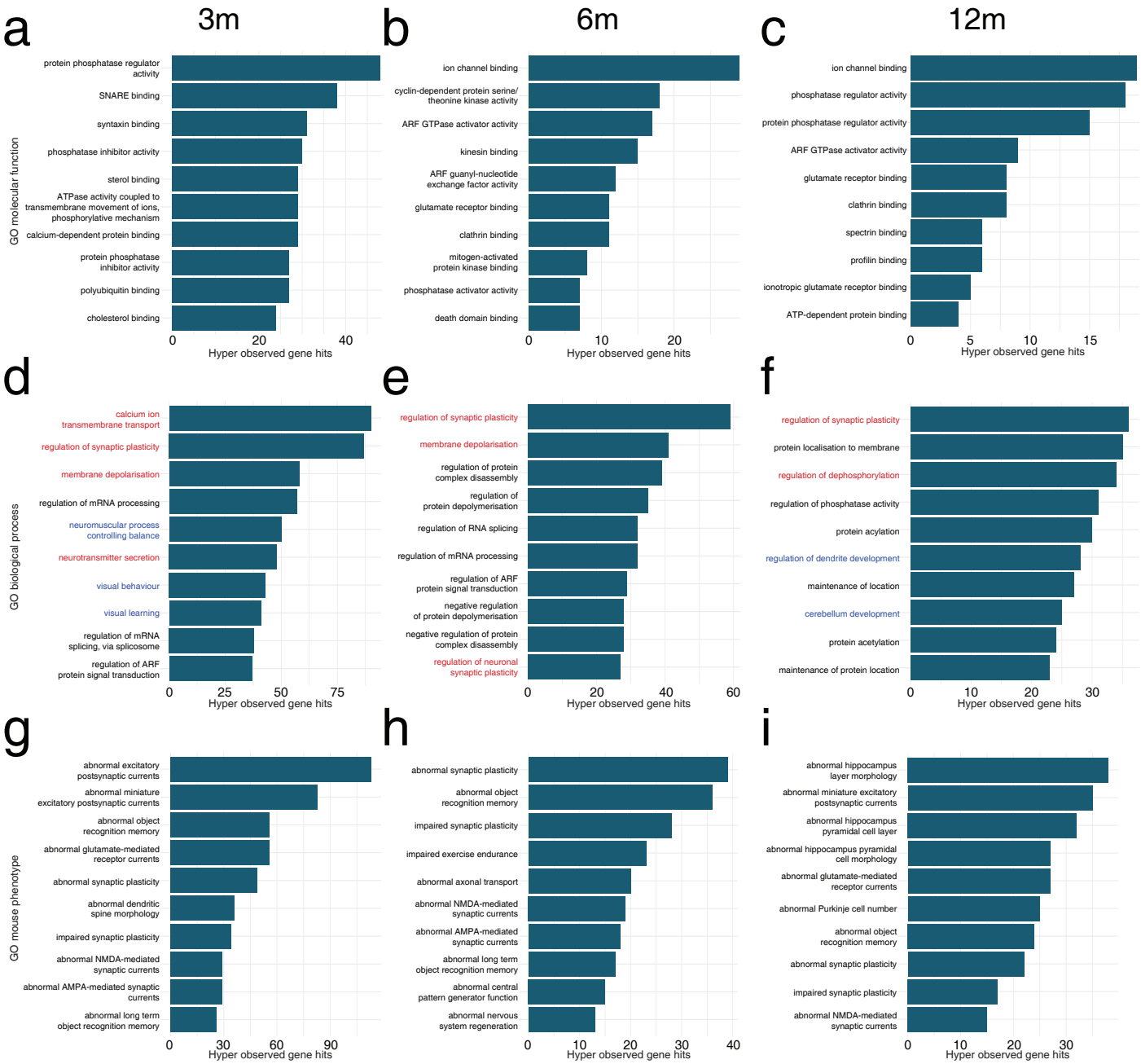
a
3m
GO molecular function
protein phosphatase regulator activity
SNARE binding
syntaxin binding
phosphatase inhibitor activity
sterol binding
ATPase activity coupled to transmembrane movement of ions, phosphorylative mechanism
calcium-dependent protein binding
protein phosphatase inhibitor activity
polyubiquitin binding
cholesterol binding
0 20 40
Hyper observed gene hits
b
6m
ion channel binding
cyclin-dependent protein serine/ theonine kinase activity
ARF GTPase activator activity
kinesin binding
ARF guanyl-nucleotide exchange factor activity
glutamate receptor binding
clathrin binding
mitogen-activated protein kinase binding
phosphatase activator activity
death domain binding
0 10 20
Hyper observed gene hits
c
12m
ion channel binding
phosphatase regulator activity
protein phosphatase regulator activity
ARF GTPase activator activity
glutamate receptor binding
clathrin binding
spectrin binding
profilin binding
ionotropic glutamate receptor binding
ATP-dependent protein binding
0 5 10 15
Hyper observed gene hits
d
GO biological process
calcium ion transmembrane transport
regulation of synaptic plasticity
membrane depolarisation
regulation of mRNA processing
neuromuscular process controlling balance
neurotransmitter secretion
visual behaviour
visual learning
regulation of mRNA splicing, via spliceosome
regulation of ARF protein signal transduction
0 25 50 75
Hyper observed gene hits
e
regulation of synaptic plasticity
membrane depolarisation
regulation of protein complex disassembly
regulation of protein depolymerisation
regulation of RNA splicing
regulation of mRNA processing
regulation of ARF protein signal transduction
negative regulation of protein depolymerisation
negative regulation of protein complex disassembly
regulation of neuronal synaptic plasticity
0 20 40 60
Hyper observed gene hits
f
regulation of synaptic plasticity
protein localisation to membrane
regulation of dephosphorylation
regulation of phosphatase activity
protein acylation
regulation of dendrite development
maintenance of location
cerebellum development
protein acetylation
maintenance of protein location
0 10 20 30
Hyper observed gene hits
g
GO mouse phenotype
abnormal excitatory postsynaptic currents
abnormal miniature excitatory postsynaptic currents
abnormal object recognition memory
abnormal glutamate-mediated receptor currents
abnormal synaptic plasticity
abnormal dendritic spine morphology
impaired synaptic plasticity
abnormal NMDA-mediated synaptic currents
abnormal AMPA-mediated synaptic currents
abnormal long term object recognition memory
0 30 60 90
Hyper observed gene hits
h
abnormal synaptic plasticity
abnormal object recognition memory
impaired synaptic plasticity
impaired exercise endurance
abnormal axonal transport
abnormal NMDA-mediated synaptic currents
abnormal AMPA-mediated synaptic currents
abnormal long term object recognition memory
abnormal central pattern generator function
abnormal nervous system regeneration
0 10 20 30 40
Hyper observed gene hits
i
abnormal hippocampus layer morphology
abnormal miniature excitatory postsynaptic currents
abnormal hippocampus pyramidal cell layer
abnormal hippocampus pyramidal cell morphology
abnormal glutamate-mediated receptor currents
abnormal Purkinje cell number
abnormal object recognition memory
abnormal synaptic plasticity
impaired synaptic plasticity
abnormal NMDA-mediated synaptic currents
0 10 20 30
Hyper observed gene hits

Figure 5.5: H3K27ac alterations affects synaptic plasticity and post-translational modification regulatory pathways in neurons in APP/PS1 neurons

(a-i) The top 10 gene ontology annotations, ranked by hypergeometric observed gene hits for sites of significant H3K27ac differential enrichment in neurons from APP/PS1 and WT control neurons at (a, d, g) 3 months (pre-pathology), (b, e, h) 6 months (pathology onset), and (c, f, i) 12 month (pathology rich) time-points. Gene ontology analysis predicts dysregulated pathways in (a, b, c) molecular function, (d, e, f) biological processes and, (g, h, i) mouse phenotype. Pathways involved in synaptic function are highlighted in red, developmental GO terms are highlighted in blue.

5.2.5 H3K27ac reprogramming occurs early and changes over time in APP/PS1 neurons

To determine whether the sites of differential H3K27ac enrichment between APP/PS1 and WT neurons occurred at similar or different loci at each time-point, an intersection analysis of bed files containing all sites of significant differential enrichment at each time-point was performed.

By identifying overlaps between differentially enriched sites in APP/PS1 versus WT neurons from the 3, 6 and 12 month time-points (5.2.1), a change of H3K27ac marking in neurons was observed across pathology accumulation in APP/PS1 mice (Figure 5.6). There were 50440 H3K27ac sites of differential enrichment specific to 3 month old APP/PS1 neurons, while 2404 sites were unique to 6 month old, and 39 sites unique to 12 month old APP/PS1 neurons (Figure 5.6a). Interestingly, the majority of H3K27ac differentially enriched sites at the 6 and 12 month old time-points overlapped with those found in 3 month old neurons (5852 and 3530 sites, respectively; Figure 5.6a). These overlaps also included 1176 H3K27ac sites that were consistently differentially enriched across all timepoints examined (Figure 5.6a).

To determine the functional pathways that shared differential H3K27ac marking over time in APP/PS1 neurons, functional annotation with GREAT 'GO biological process' was performed (Figure 5.6b-f). Sites of differential enrichment that were consistently altered across all time-points were annotated to pathways including 'regulation of dephosphorylation', 'protein acetylation', 'regulation of phosphatase activity' and 'regulation of RNA splicing' (Figure 5.6b). Differentially enriched sites unique to 3 month old APP/PS1 neurons were annotated to 'GO biological process' pathways involved in 'calcium ion transmembrane transport', 'regulation of synaptic plasticity', 'membrane depolarisation', 'regulation of mRNA processing' and 'regulation of receptor activity' (Figure 5.6c), while sites that were shared between 3 month and 6 month old neurons included 'regulation of protein complex disassembly', 'regulation of ARF signal transduction', 'protein stabilisation' and 'regulation of RNA splicing' (Figure 5.6d). Interestingly, differentially enriched sites in APP/PS1 and WT neurons that were common to both 3 and 12 month old timepoints included functional annotations for 'protein localisation to membrane', 'regulation of synaptic plasticity', 'regulation of dephosphorylation', 'calcium ion transmembrane transport', and 'regulation of dendrite development' (Figure 5.6e). Functional annotation of sites unique to 6 month old APP/PS1 neurons revealed terms including the 'negative regulation of cell projection

organisation', and 'protein deubiquitination' (Figure 5.6f). There were no annotations for comparisons between 6 and 12 month old neurons, or specific to 12 month old neurons. Differentially enriched pathways unique to 3 and 12 month old neurons were mostly shared with their relative time-point specific analysis, however pathways unique to 6 months of age were novel compared to the time-point specific analysis.

Next, analysis was performed to determine whether sites of differential H3K27ac marking shared enrichment or depletion between timepoints. Differential enrichment data from csaw was separated into subsets of H3K27ac sites that were enriched or depleted in APP/PS1 compared to WT neurons, then analysed with BEDTools intersect to determine the number and direction of overlapping differentially H3K27ac marked sites. Comparisons between 3 and 6 months of age showed that 75% of shared differentially marked H3K27ac sites were enriched in APP/PS1 neurons compared to wild-type neurons at both time-points, while less than 1% of differentially marked H3K27ac sites were depleted in APP/PS1 neurons at both time-points. 24% of differentially marked H3K27ac sites were depleted in neurons at 3 months of age, but enriched at 6 months of age; and less than 1% differentially marked H3K27ac sites were enriched at 3 months of age and depleted at 6 months of age in APP/PS1 neurons. Comparisons between 6 months of age and 12 months of age showed that 95% of differentially marked H3K27ac sites were enriched in neurons at both time-points, while only less than 1% of differentially marked H3K27ac sites were depleted at both time-points, or depleted in 6 month old neurons and enriched in 12 month old neurons, but 3.7% of differentially marked H3K27ac sites were enriched in 6 month old neurons and depleted in 12 month old neurons. Interestingly when comparing 3 months of age with 12 months of age, 70% of shared H3K27ac marked sites were consistently enriched in neurons at both time-points, while 2% of differentially marked H3K27ac sites were consistently depleted in neurons at both time-points. 27% differentially marked H3K27ac sites were depleted in neurons at 3 months of age, but enriched at 12 months of age in APP/PS1 neurons, and 2% of differentially marked H3K27ac sites were enriched in 3 month old neurons, but depleted in 12 month old neurons (Table 5.1).

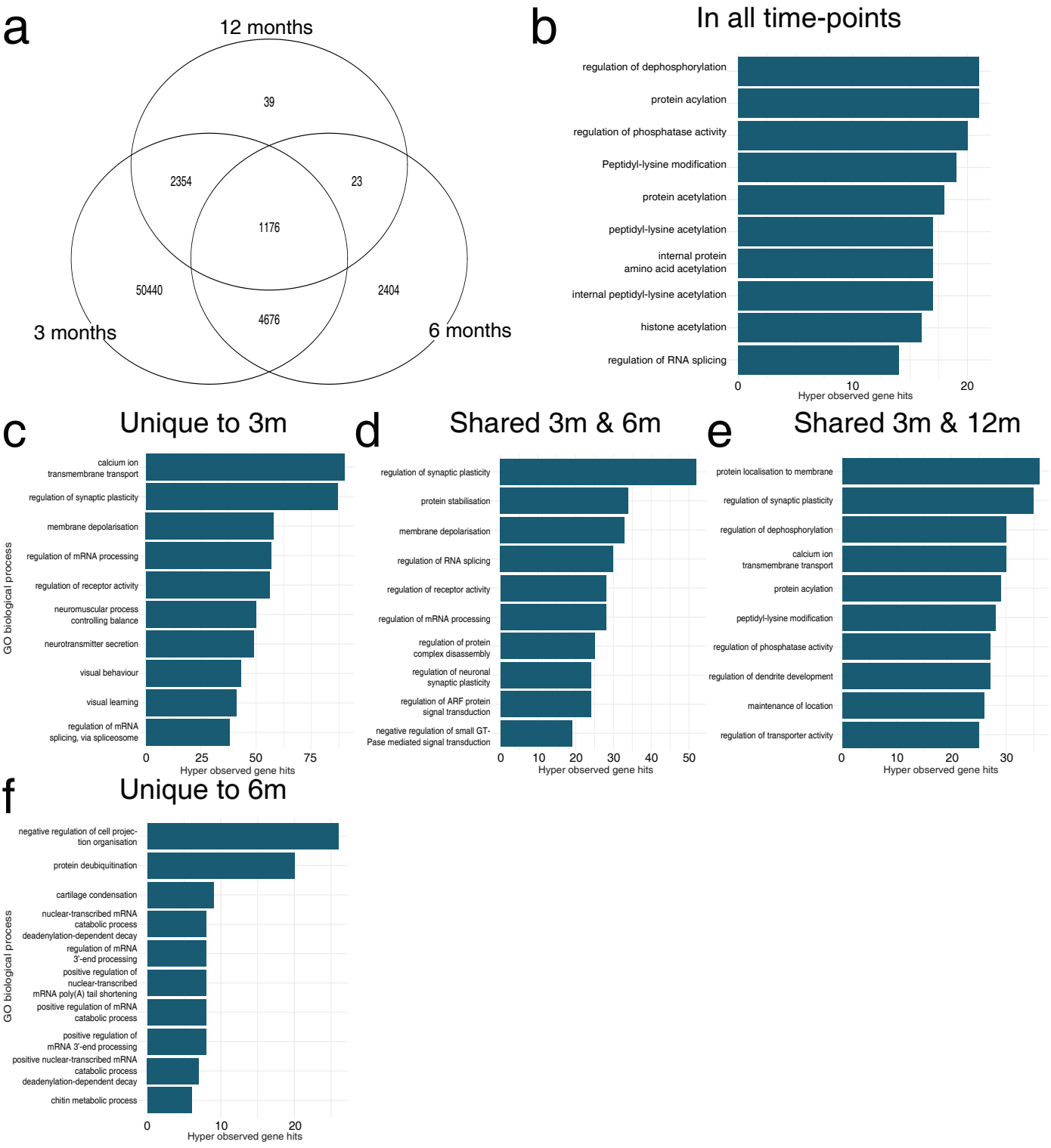
a
12 months
39
2354
23
1176
50440
2404
4676
3 months
6 months
b
In all time-points
regulation of dephosphorylation
protein acylation
regulation of phosphatase activity
Peptidyl-lysine modification
protein acetylation
peptidyl-lysine acetylation
internal protein amino acid acetylation
internal peptidyl-lysine acetylation
histone acetylation
regulation of RNA splicing
0
10
20
Hyper observed gene hits
c
Unique to 3m
GO biological process
calcium ion transmembrane transport
regulation of synaptic plasticity
membrane depolarisation
regulation of mRNA processing
regulation of receptor activity
neuromuscular process controlling balance
neurotransmitter secretion
visual behaviour
visual learning
regulation of mRNA splicing, via spliceosome
0
25
50
75
Hyper observed gene hits
d
Shared 3m & 6m
regulation of synaptic plasticity
protein stabilisation
membrane depolarisation
regulation of RNA splicing
regulation of receptor activity
regulation of mRNA processing
regulation of protein complex disassembly
regulation of neuronal synaptic plasticity
regulation of ARF protein signal transduction
negative regulation of small GTPase mediated signal transduction
0
10
20
30
40
50
Hyper observed gene hits
e
Shared 3m & 12m
protein localisation to membrane
regulation of synaptic plasticity
regulation of dephosphorylation
calcium ion transmembrane transport
protein acylation
peptidyl-lysine modification
regulation of phosphatase activity
regulation of dendrite development
maintenance of location
regulation of transporter activity
0
10
20
30
Hyper observed gene hits
f
Unique to 6m
GO biological process
negative regulation of cell projection organisation
protein deubiquitination
cartilage condensation
nuclear-transcribed mRNA catabolic process deadenylation-dependent decay
regulation of mRNA 3'-end processing
positive regulation of nuclear-transcribed mRNA poly(A) tail shortening
positive regulation of mRNA catabolic process
positive regulation of mRNA 3'-end processing
positive nuclear-transcribed mRNA catabolic process deadenylation-dependent decay
chitin metabolic process
0
10
20
Hyper observed gene hits

Figure 5.6: Alteration of H3K27ac marking in neurons across pathology accumulation in APP/PS1 neurons

(a) Venn diagram plotting the overlap in sites that were differentially enriched in APP/PS1 versus WT neurons from 3 month, 6 month, and 12 month old pairwise comparisons. (b) Functional annotations for biological process for the 1176 sites that were differentially enriched at all time-points, (c) the 50440 sites unique to the 3 month differential enrichment analysis, (d) sites shared between 3 and 6 month time-points and (e) 3 and 12 months of age. (f) Functional annotation of biological processes from the 2404 sites unique to 6 months of age.

Table 5.1: H3K27ac marking is consistently enriched in pre-pathology and pathology rich neurons

	Consistently Enriched	Consistently Depleted	Enriched depleted	Depleted enriched
3 vs 6 month	3826 (75%)	20 (<1%)	31 (<1%)	1238 (24%)
6 vs 12 month	1129 (94.9%)	9 (<1%)	45 (3.7%)	7 (<1%)
3 vs 12 month	1501 (69.6%)	35 (1.6%)	37 (1.7%)	582 (27%)

Taken together, these data demonstrate a complex pattern of H3K27ac marking across the time-course of pathology accumulation. H3K27ac marking was highly specific at individual time-points with over 50000 sites unique to neurons from 3 month old APP/PS1 mice. Interestingly, over 75% of differentially enriched H3K27ac sites were consistently enriched throughout pathology accumulation. These data demonstrate a partial recapitulation of a juvenile histone landscape in 12 month old APP/PS1 neurons.

5.2.6 Differential enrichment of H3K4me3 marking prior to pathology onset, and with increasing age in APP/PS1 neurons

Histone modifications contribute to the compaction of DNA into chromatin and the access of transcriptional machinery to chromatin. These sites of regulation can be at promoters near TSS, or at distal regulatory elements. Currently, it is accepted that H3K27ac marks active enhancers (>2kB distal to TSS) and promoters, and H3K4me3 is consistently indicative of active promoters (Rada-Iglesias et al., 2011). Here, H3K4me3 was analysed genome-wide with ChIP-seq in neurons from APP/PS1 and WT mice at 3 months of age (pre-pathology), 6 months of age (pathology onset), and 12 months of age (pathology rich).

Total genomic coverage assessments were performed to provide an indication of H3K4me3 changes in APP/PS1 and WT neurons at a global scale. At 3 months of age, APP/PS1 neurons exhibited reduced genomic coverage of H3K4me3 compared to WT control neurons (APP/PS1 mean: 1.98% versus WT mean: 2.94%; Figure 5.7a). However, by 6 months of age, H3K4me3 marking increased in APP/PS1 neurons compared to WT control neurons (APP/PS1 mean: 2.51% versus WT mean: 1.85%; Figure 5.7b), and by 12 months of age, the difference in total genomic coverage between APP/PS1 and WT control neurons further increased (APP/PS1 mean: 2.71% versus WT mean: 1.91%; Figure 5.7c). WT control neurons were initially

enriched for H3K4me3 at 3 months of age, but marking was depleted at 6 months of age which was sustained until 12 months of age. Whereas APP/PS1 neurons gradually gained H3K4me3 marking over time (Figure 5.7a-c).

Next, differential enrichment of H3K4me3 was assessed genome-wide in neurons from APP/PS1 and WT control mice. There was a change in H3K4me3 marking in APP/PS1 neurons compared to WT control neurons across disease progression (Figure 5.7d-f). A total of 20368 H3K4me3 sites were enriched and 3198 sites depleted in APP/PS1 neurons compared to WT control neurons at 3 months of age (Benjamini Hochberg FDR adjusted p-value <0.05; Figure 5.7d). However, by 6 months of age, there were 1,171 sites enriched for H3K4me3, and 1323 sites that were H3K4me3 depleted in APP/PS1 compared to WT neurons (Benjamini Hochberg FDR adjusted p-value <0.05; Figure 5.7e). Interestingly at 12 months of age, there were 26,616 H3K4me3 marked sites differentially enriched, and 6545 sites depleted in APP/PS1 versus WT neurons at 12 months of age (Benjamini Hochberg FDR adjusted p-value <0.05; Figure 5.7f). There was widespread enrichment of H3K4me3 marking prior to pathology onset in neurons from APP/PS1 mice. While there was a decline in the total number of H3K4me3 marked sites at pathology onset, that was reversed by 12 months of age, where plaque pathology is widespread in the APP/PS1 mouse model. This contrasted with the reported genomic coverage of H3K4me3 in APP/PS1 neurons between 3 and 6 months of age (Figure 5.7a-f).

Visualisation of H3K4me3 marked sites in IGV showed that the majority of H3K4me3 signal was located around the transcriptional start sites (Figure 5.7g-i). For example, the top differentially enriched site for H3K4me3 in 3 month old neurons was at the promoter for the *Ncdn* gene encoding Neurochondrin; this protein has known roles in neurite outgrowth and CaMKII phosphorylation ((Dateki et al., 2005); Figure 5.7g). At 6 months of age *Csgalnact2* was depleted in APP/PS1 neurons compared to WT control neurons. *Csgalnact2a* encodes the Chondroitin Sulfate N-Acetylgalactosaminyltransferase 2 protein, which is involved in chondroitin sulfate synthesis, which in turn is a component of brain extracellular matrix ((Kwok, Warren, & Fawcett, 2012);Figure 5.7h). Interestingly, the *Mark4* gene promoter was enriched in 12 month old APP/PS1 neurons compared to WT control neurons. *Mark4* encodes the Microtubule Affinity Regulating Kinase 4 protein, which is known to phosphorylate Microtubule-Associated Protein Tau (MAPT), and is associated with early MAPT phosphorylation in AD ((G. J. Gu et al., 2013; Lund et al., 2014);Figure 5.7i).

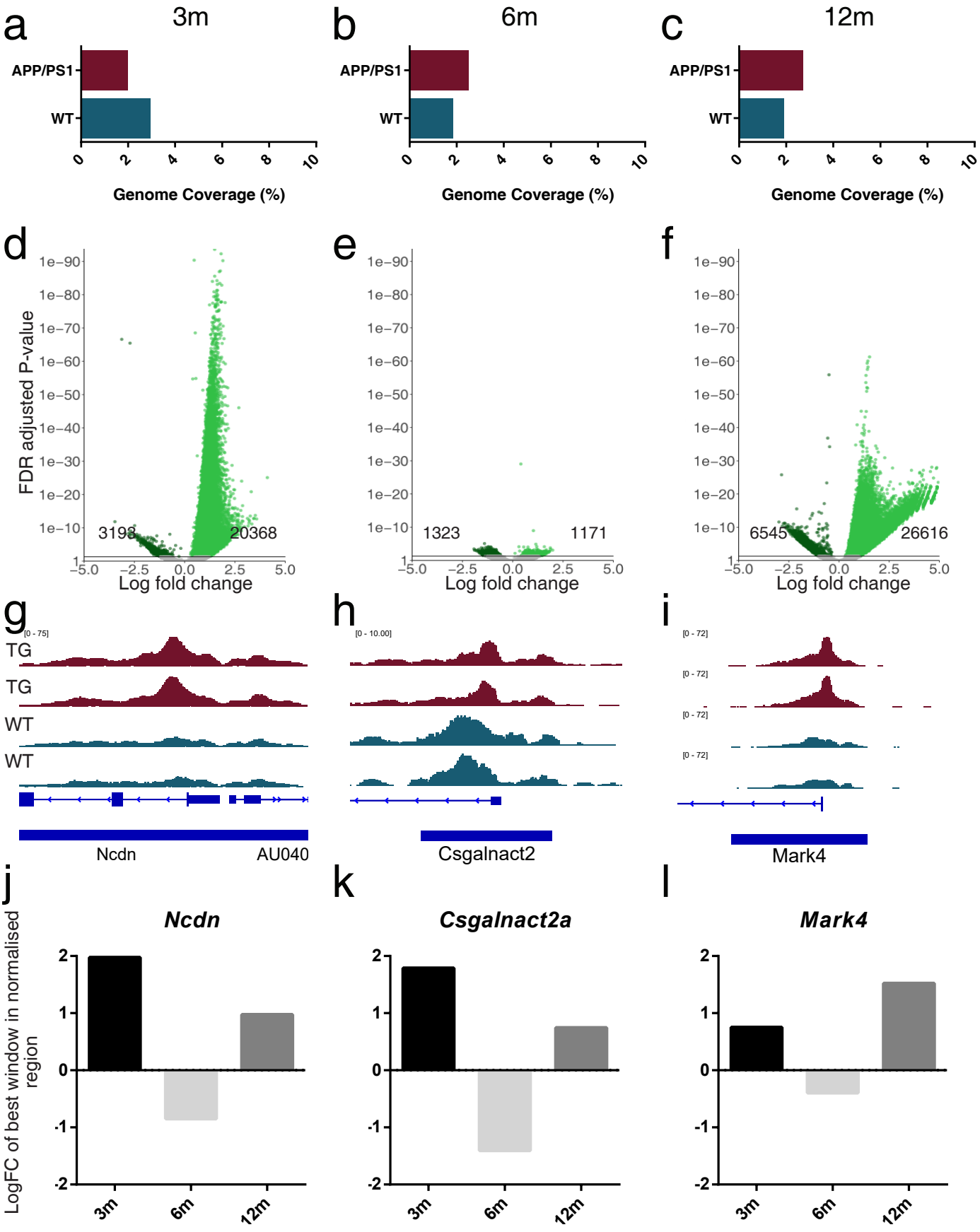
a
3m
APP/PS1
WT
0
2
4
6
8
10
Genome Coverage (%)
b
6m
APP/PS1
WT
0
2
4
6
8
10
Genome Coverage (%)
c
12m
APP/PS1
WT
0
2
4
6
8
10
Genome Coverage (%)
d
FDR adjusted P-value
1e−90
1e−80
1e−70
1e−60
1e−50
1e−40
1e−30
1e−20
1e−10
1
3198
20368
−5.0
−2.5
0.0
2.5
5.0
Log fold change
e
1e−90
1e−80
1e−70
1e−60
1e−50
1e−40
1e−30
1e−20
1e−10
1
1323
1171
−5.0
−2.5
0.0
2.5
5.0
Log fold change
f
1e−90
1e−80
1e−70
1e−60
1e−50
1e−40
1e−30
1e−20
1e−10
1
6545
26616
−5.0
−2.5
0.0
2.5
5.0
Log fold change
g
[0 - 75]
TG
TG
WT
WT
Ncdn
AU040
h
[0 - 10.00]
Csgalnact2
i
[0 - 72]
[0 - 72]
[0 - 72]
[0 - 72]
Mark4
j
Ncdn
LogFC of best window in normalised region
2
1
0
-1
-2
3m
6m
12m
k
Csgalnact2a
2
1
0
-1
-2
3m
6m
12m
l
Mark4
2
1
0
-1
-2
3m
6m
12m

Figure 5.7: H3K4me3 is dysregulated prior to pathology onset, and with increasing age in APP/PS1 neurons

(a-c) Percentage 5× genomic coverage of H3K4me3 in neurons from APP/PS1 (red) and WT control mice (blue) at (a) 3 months, (b) 6 months and, (c) 12 months of age. (d-f) Volcano plots show the logFC and FDR adjusted P-value of APP/PS1 neurons compared to WT control neurons; positive logFC (light green), and negative logFC (dark green) for all differentially enriched windows of H3K4me3 marking at (d) 3 months, (e) 6 months and (f) 12 months of age. (g-i) Representative tracks visualised in IGV showing the top-ranked sites of enrichment between pseudoreplicates of APP/PS1 (red) and WT control neurons (blue). (g) The *Ncdn* promoter at 3 months of age, (h) the *Csgalnact2a* promoter at 6 months of age and, (i) the *Mark4* promoter at 12 months of age. Histograms showing the logFC of the best window within the normalised region of H3K4me3 marking in APP/PS1 neurons compared to WT controls at 3 months (black), 6 months (light grey) and 12 months (dark grey) for (j) the *Ncdn* promoter, (k) the *Csgalnact2a* promoter and (l), the *Mark4* promoter.

Histograms of H3K4me3 enrichment at the promoters of *Ncdn*, *Csgalnact2a*, and *Mark4* demonstrated dynamic enrichment at these sites throughout pathology accumulation in APP/PS1 neurons compared to WT control neurons (Figure 5.7j-l)

Taken together, these data demonstrate a dynamic pattern of differential enrichment in APP/PS1 compared to WT neurons across a time-course of Aβ pathology accumulation (Figure 5.7j-l).

5.2.7 H3K4me3 is enriched at TSS at pre-pathology and pathology-rich time-points in APP/PS1 neurons

H3K4me3 is present at promoter elements of active genes (B. E. Bernstein et al., 2005; Nathaniel D. Heintzman et al., 2007; Rada-Iglesias et al., 2011). Initially, the mean distribution of H3K4me3 was examined by visualising the mean abundance of reads around a 2kb region upstream and downstream of the TSS. Here, similar to H3K27ac, H3K4me3 presented with a bimodal distribution around the TSS of UCSC KnownGenes (Figure 5.8a-f). The average enrichment for H3K4me3 was greatest over the -1 nucleosome 5'- to the TSS, and H3K4me3 marking extended 1kb into gene bodies (Figure 5.8a-c). Quantitation of the average enrichment plots showed that H3K4me3 enrichment was highest at 3 months in APP/PS1 neurons with an approximately 1.6-fold increase in signal compared to WT controls (APP/PS1 max: 11.02, WT max: 7.12; Figure 5.8a). Whereas at 6 months of age, H3K4me3 marking was depleted compared to 3 month old neurons, and H3K4me3 marking was lower in APP/PS1 neurons compared to WT neurons (APP/PS1 max: 2.97, WT max: 3.24; Figure 5.8b). Interestingly, by 12 months of age, APP/PS1 neurons were enriched ~1.6-fold for H3K4me3 at the TSS compared to WT neurons (APP/PS1 max: 8.11, WT max: 5.17; Figure 5.8c).

Next, H3K4me3 marking was visualised with heatmaps around a 2kb region from TSS of the UCSC KnownGene track. H3K4me3 marking was prominent around the TSS of approximately half of all sites identified by the UCSC KnownGene track. H3K4me3 marking was present up to 1kb upstream of the TSS and to 2kb downstream (Figure 5.8d-f). At 3 months of age H3K4me3 marking exhibited an increase in magnitude with similar proportion of TSS in APP/PS1 compared to WT neurons (Figure 5.8d). However, at 6 months of age, H3K4me3 marking covered a similar proportion of TSS, but the magnitude was depleted in APP/PS1 compared to WT neurons (Figure 5.8e). By 12 months of age, the magnitude and distribution

of H3K4me3 marking was increased in APP/PS1 neurons compared to WT control neurons, similar to the 3 month time-point (Figure 5.8f).

Similar to the analysis performed for H3K27ac enrichment at TSS, H3K4me3 was mapped to CpG island containing TSS, and non-CpG island containing TSS to identify if there was a difference in H3K4me3 marking at these two types of TSS in the APP/PS1 mouse model of AD (Figure 5.8g-l). At 3 months of age, the distribution and magnitude H3K4me3 marking were enriched to a small degree in APP/PS1 neurons compared to WT controls, with marking present at approximately 75% of all CpG islands (Figure 5.8g). At 6 months of age, the magnitude and distribution H3K4me3 marking was similar between APP/PS1 and WT neurons, but interestingly, the overall magnitude of H3K4me3 marking was lower than in 3 month old neurons (Figure 5.8h). At 12 months of age, the magnitude of H3K4me3 marking at CpG islands was enriched in APP/PS1 neurons compared to WT neurons (Figure 5.8i). In comparison, H3K4me3 marking at non-CpG island TSS covered approximately 20% of non-CpG island TSS (Figure 5.8j-l). At 3 months of age, there was no difference in the distribution and magnitude of H3K4me3 at non-CpG island TSS in APP/PS1versus control neurons (Figure 5.8j), which was maintained at 6 months of age (Figure 5.8k). At 12 months of age both the magnitude and distribution of H3K4me3 marking was slightly enriched in APP/PS1 compared to WT neurons (Figure 5.8l).

Together, these results show that although there is little difference in the proportion of TSS containing H3K4me3 over time in APP/PS1 neurons, the marking is present in neurons at a greater magnitude in APP/PS1 neurons prior to pathology onset and in pathology rich neurons compared to WT control neurons. The majority of the differences in H3K4me3 marking are driven by differential enrichment found at TSS containing CpG islands. These data demonstrate the dynamic nature of H3K4me3 marking around TSS in APP/PS1 neurons through pathology onset and accumulation.

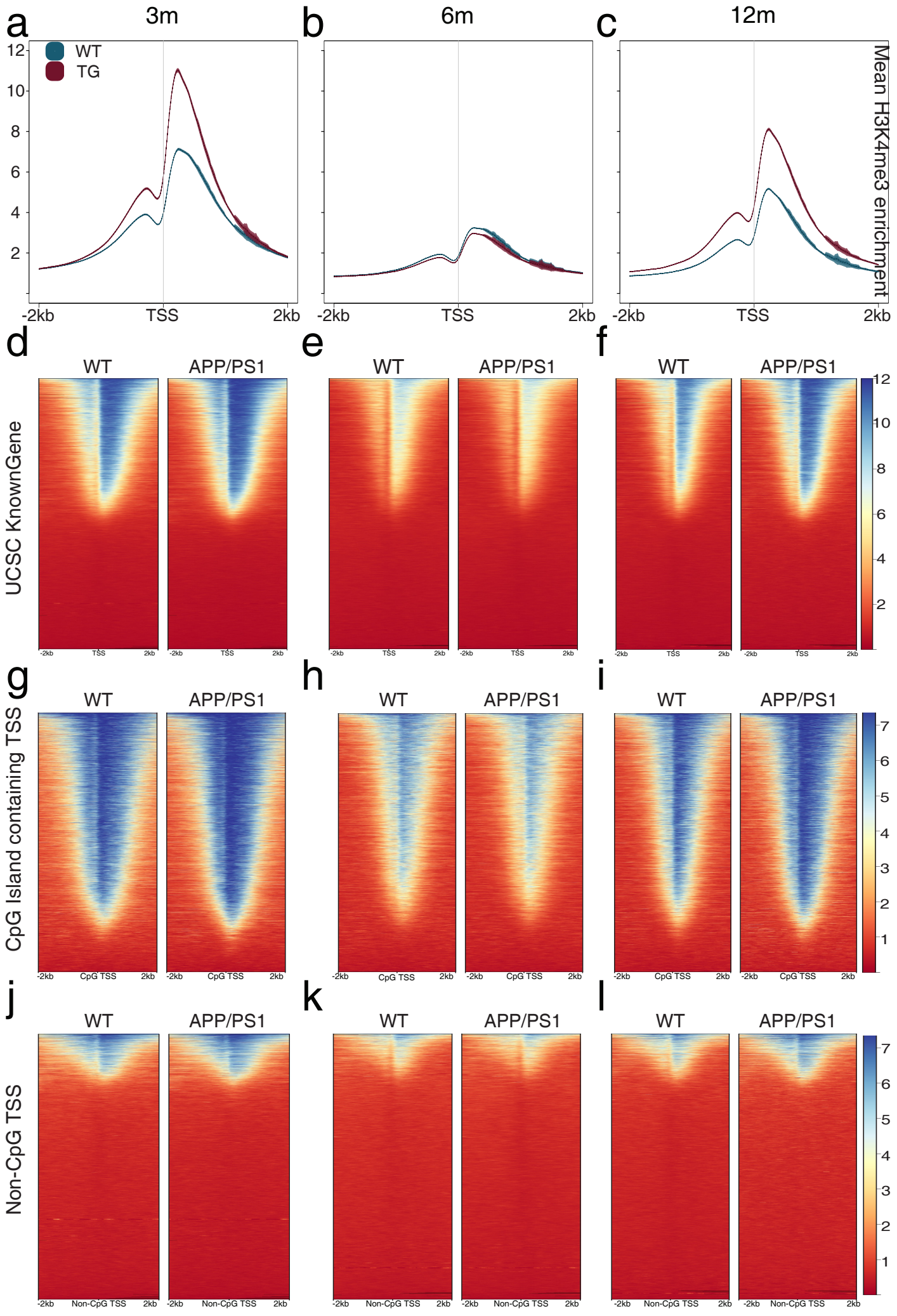
a
3m
b
6m
c
12m
WT
TG
Mean H3K4me3 enrichment
-2kb
TSS
2kb
d
e
f
WT
APP/PS1
UCSC KnownGene
g
h
i
CpG Island containing TSS
CpG TSS
j
k
l
Non-CpG TSS
Non-CpG TSS

Figure 5.8: H3K4me3 is enriched at TSS at pre-pathology and pathology-rich timepoints in APP/PS1 neurons

(a-c) Average enrichment plots for H3K4me3 within a 2kb window of TSS for the UCSC KnownGene track in APP/PS1 neurons (red) compared to WT control neurons (blue) at (a) 3 months, (b) 6 months and (c), 12 months of age. Heatmaps of H3K4me3 marking at TSS for UCSC KnownGene sorted by strongest (blue) to weakest (red) signal in WT control neurons (left) and APP/PS1 neurons (right) at (d) 3 months, (e) 6 months and, (f) 12 months of age. Heatmaps of H3K4me3 marking at CpG islands from the UCSC mm10 CpG island track sorted by strongest (blue) to weakest (red) signal in WT (left) and APP/PS1 neurons (right) at (g) 3 months of age, (h) 6 months of age, and (i) 12 months of age. (j-l) Heatmaps of H3K4me3 marking at non-CpG containing TSS from the UCSC mm10 KnownGene track sorted by strongest (blue) to weakest (red) signal in WT (left) and APP/PS1 (right) at (j) 3 months of age, (k) 6 months of age, and (i) 12 months of age.

5.2.8 H3K4me3 is not dysregulated at enhancers in APP/PS1 neurons

In the normal mammalian genome, H3K4me3 is generally not found at active enhancer elements (Local et al., 2018; Outchkourov et al., 2013; Rada-Iglesias et al., 2011). To determine if there was an aberrant change in the distribution of H3K4me3 marking from promoters to enhancers in APP/PS1 neurons, average H3K4me3 marking was mapped at a 2kb region around all enhancer elements marked by H3K27ac.

Initially, the average signal for H3K4me3 showed a single peak of enrichment just downstream of the mid-point of enhancers that was consistent between APP/PS1 and wild type neurons (Figure 5.9a-c). At 3 months, there was ~0.84-fold enrichment of H3K4me3 at enhancers in APP/PS1 neurons compared to WT controls (APP/PS1 max: 67.05, WT max: 56.33; Figure 5.9a). While at 6 months of age, APP/PS1 and WT neurons had similar levels of H3K4me3 marking at enhancers (APP/PS1 max: 55.46, WT max: 54.42; Figure 5.9c). At 12 months of age, APP/PS1 neurons were ~0.81-fold depleted for H3K4me3 at enhancers compared to WT neurons (APP/PS1 max: 51.27, WT max: 63.43; Figure 5.9c).

Next, H3K4me3 was mapped against enhancers and visualised with heatmaps within a 2kb window of the mid-point of enhancers. The magnitude of H3K4me3 marking was highly enriched at a small proportion of enhancers in both APP/PS1 neurons and WT neurons at all time-points (Figure 5.9d-f). The magnitude of H3K4me3 enrichment at enhancers was also similar between APP/PS1 and WT neurons at 3, 6 and 12 months of age (Figure 5.9d-f).

Taken together, these data demonstrate that H3K4me3 marking is not dysregulated at enhancers in APP/PS1 neurons, and there is a small subset of enhancers highly enriched for H3K4me3 in both APP/PS1 and WT control neurons across all time-points.

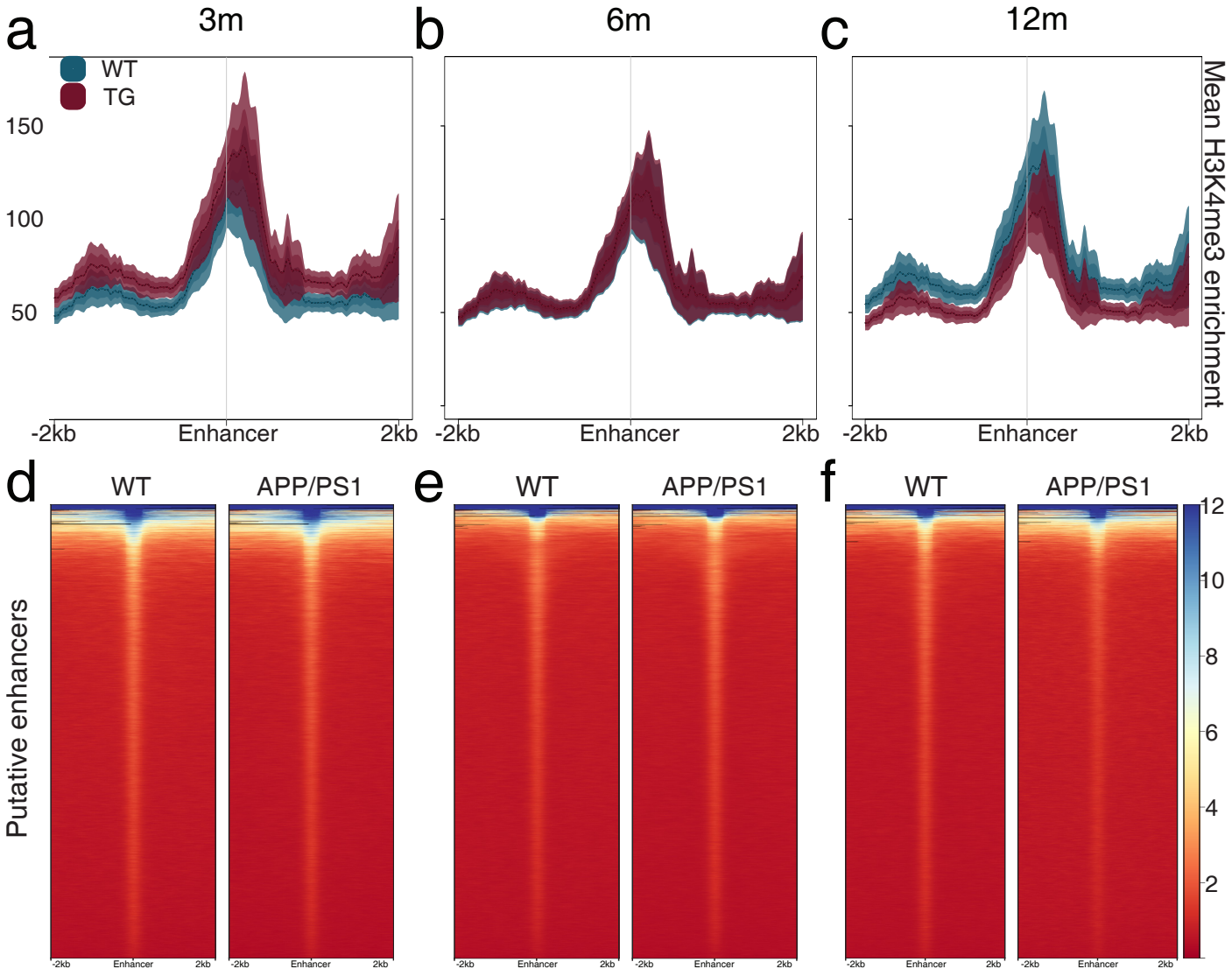
a
3m
b
6m
c
12m
WT
TG
150
100
50
-2kb
Enhancer
2kb
Mean H3K4me3 enrichment
d
e
f
WT
APP/PS1
Putative enhancers
12
10
8
6
4
2

Figure 5.9: H3K4me3 marking is not dysregulated at enhancers in APP/PS1 neurons
(a-c) Average enrichment plots for H3K4me3 within a 2kb window of putative enhancers in APP/PS1 (red) or WT (blue) at (a) 3 months, (b) 6 months and (c), 12 months of age. Heatmaps for H3K4me3 signal in putative enhancers sorted by strongest to weakest signal in WT control neurons (left) and APP/PS1 neurons (right) at (d) 3 months, (e) 6 months and, (f) 12 months of age.

5.2.9 H3K4me3 marking is enriched at sites associated with core molecular processes in APP/PS1 neurons

Gene ontology allows for the prediction of molecular pathways changing as a result of altered transcriptional regulation. Here, the 'GO molecular function' and the 'GO biological process' were assessed for the sites of differential H3K4me3 enrichment in APP/PS1 neurons and WT control neurons at 3, 6, and 12 months of age using GREAT as previously described (Chapter 2.23).

Gene ontology analysis demonstrated that differential enrichment of H3K4me3 in APP/PS1 neurons was annotated to pathways pertaining to core metabolic processes such as RNA modifications and post-translational modifications (Figure 5.10a-e). For example, at 3 months of age, 'GO molecular function' annotation of H3K4me3 differential enrichment was annotated to molecular pathways for 'unfolded protein binding', 'rRNA binding' and 'RNA polymerase II carboy-terminal domain kinase activity' among others, and interestingly, 'histone methyltransferase activity (H3K4 specific)' was also annotated (Figure 5.10a). Whereas at 12 months of age, the top pathways identified by 'GO molecular function' also included 'RNA polymerase II carboxy-terminal domain kinase activity', 'mannosyltransferase activity' and 'glutathione peroxidase activity', but also included 'TBP-class protein binding', and 'protein transmembrane transporter activity' (Figure 5.10b). Analysis of 'GO biological process' for differentially enriched H3K4me3 sites in 3 month old APP/PS1 neurons identified processes including 'GPI anchor metabolic process', 'regulation of gene silencing', 'tRNA modification' and interestingly, 'mRNA stabilisation' and 'regulation of protein dephosphorylation' (Figure 5.10c). Meanwhile at 12 months of age, pathways identified by 'GO biological process' included 'antigen processing and presentation of exogenous peptide antigen', 'de novo post-translational protein folding' and 'protein refolding' (Figure 5.10d). At 6 months of age, gene ontology analysis could not be performed due to the small number of differentially enriched sites, however a summary of the top sites of differential enrichment demonstrated overlap with genes involved in protein modification, ion channel maintenance, and core cell regulatory pathways (Figure 5.10e).

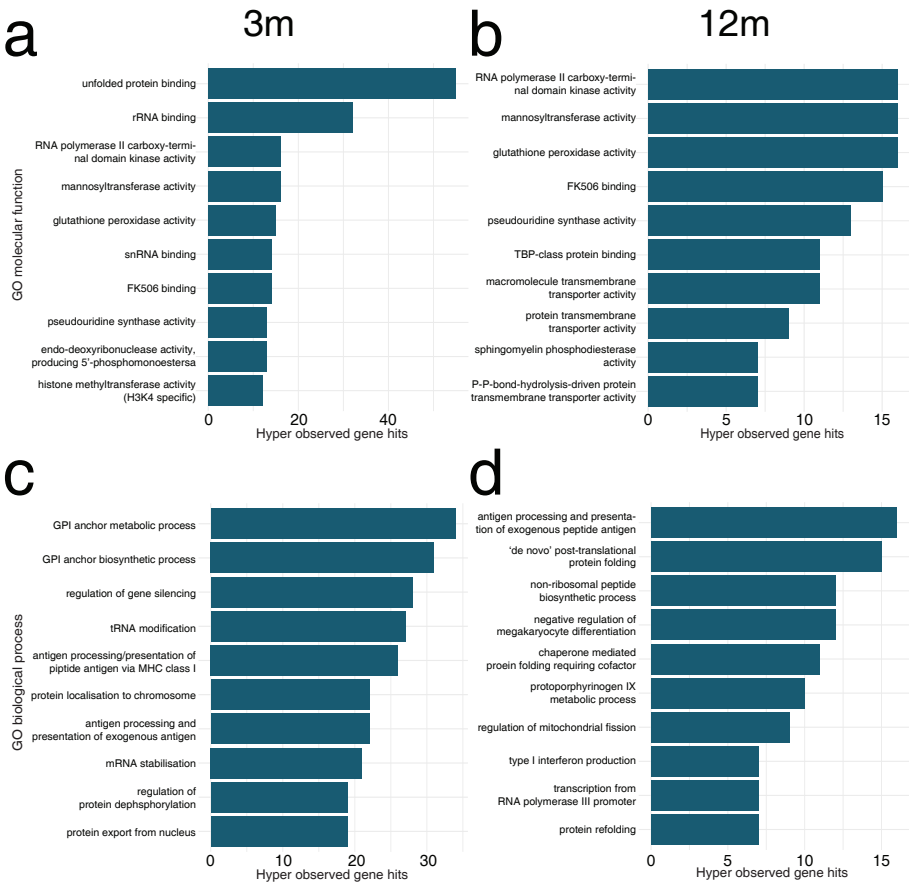

e

Chr	Start position	End position	FDR	Direction	Gene	Function (Entrez)
chr6	118138101	118139800	8.12E-6	down	*Csgalnact2*	Involved in elongation during chondroitin sulfate synthesis.
chr13	113614751	113618700	1.28E-5	up	*Snx18*	Member of sorting nexin family. Phosphoinositide binding domain, involved in intracellular trafficking.
chr9	27790201	27794850	6.89E-5	up	*Opcml*	Products include opioid binding-cell adhesion molecule. Member of immunoglobulin protein superfamily.
chr11	29718401	29720800	7.28E-5	up	*Rtn4*	Associated with endoplasmic retiuculum, invoved in neuroendocrine secretion and membrane trafficiking. May block neurite outgrowth
chr10	107271251	107273550	7.28E-5	down	*Lin7a*	Generation and maintenance of channels and receptors in the membrane. Protein products assist with channel localisation and synaptic vesicle exocytosis.
chr9	106477201	106478400	8.79E-5	down	*Parp3*	Poly-ADP-ribosylation producing gene. Products required for DNA repair and regulation of apoptosis.
chr15	95524951	95529200	8.79E-5	down	*Nell2*	Encodes for a glycoprotein. Homotrimer found in the cytoplasm. May regulate neural cell growth and differentiation.
chr2	25316201	25319250	8.79E-5	up	*Grin1*	Encodes a critical subunit for NMDA receptors and complexes to form ligand-gated ion channels. Assists in the regulation of synaptic plasticity.
chr19	10895101	10897000	9.23E-5	down	*Prpf19*	Gene products are essential for cell survival and DNA repair.
chr3	84951501	84958300	9.26E-5	up	*Fbxw7*	F-box protein - subunit for ubiquitin protein ligase complex.

Figure 5.10: H3K4me3 marking occurs at promoters responsible for core molecular and post-transcriptional modification pathways

(a-e) The top 10 gene ontology predictions ranked by hypergeometric observed gene hits for sites of significant H3K4me3 differential enrichment in neurons from APP/PS1 and WT control neurons at (a,c) 3 months (pre-pathology) and, (b,d) 12 month (pathology rich) time-points. Gene ontology annotates differentially enriched H3K4me3 sites in APP/PS1 neurons compared to WT control neurons to (a,b) molecular function and, (c,d) biological processes. (e) The top 10 differentially enriched sites between APP/PS1 and WT neurons at 6 months of age and Entrez gene summary ranked by FDR.

5.2.10 H3K4me3 differential enrichment peaks at pre-pathology and pathology rich time-points in APP/PS1 neurons

A comparison of sites that were differentially enriched for H3K4me3 between APP/PS1 and WT neurons at 3, 6, and 12 months of age was performed to determine if there are sites that overlap. This analysis demonstrated altered H3K4me3 binding through pathology onset and progression in APP/PS1 neurons. Initially, there were 35864 sites of H3K4me3 differential enrichment specific to 3 month old APP/PS1 neurons, while 572 sites were unique to 6 month old, and 19207 sites unique to 12 month old APP/PS1 neurons (Figure 5.11a). Interestingly, the majority of H3K4me3 differentially marked sites at 12 months of age overlapped with those at 3 months of age (16890 sites; Figure 5.11a), while there were 1833 sites that were differentially enriched at all time-points in APP/PS1 neurons compared to WT neurons (Figure 5.11a).

Gene ontology analysis was performed for all overlapping H3K4me3 marked sites. Gene ontology analysis for 'GO biological process' identified H3K4me3 marked sites unique to 3 months of age were annotated to pathways such as 'unfolded protein binding', 'nuclear export' and 'spindle assembly' (Figure 5.11b). Whereas H3K4me3 marked sites unique to 12 months of age were annotated to pathways involved in 'chemosensory behaviour', 'regulation of B cell receptor signalling pathway' and 'mitochondrial calcium ion homeostasis'. H3K4me3 marked sites shared between 3 and 12 months of age were annotated to biological processes including 'protein folding', 'porphyrin-containing compound metabolic process', 'macroautophagy', and interestingly 'tRNA modification' and the 'regulation of gene silencing' (Figure 5.11c). There were no pathways annotated for H3K4me3 marking from the remaining overlap comparisons between 3 and 6 months, 6 and 12 months, and shared between all time-points. Next, an assessment of the overlapping H3K4me3 differentially enriched sites was performed to determine whether the shared sites were indicating a recapitulation of the juvenile epigenome or dysregulation at sites from the juvenile epigenome. H3K4me3 differential enrichment data was subset into enrichment or depletion and an overlap analysis was performed with BEDTools. At 3 months of age, 35% of H3K4me3 differentially marked sites that were also enriched in 6 month old APP/PS1 neurons compared to wild-type neurons, and less than 1% of shared sites were depleted in both 3 month and 6 month old APP/PS1 neurons.

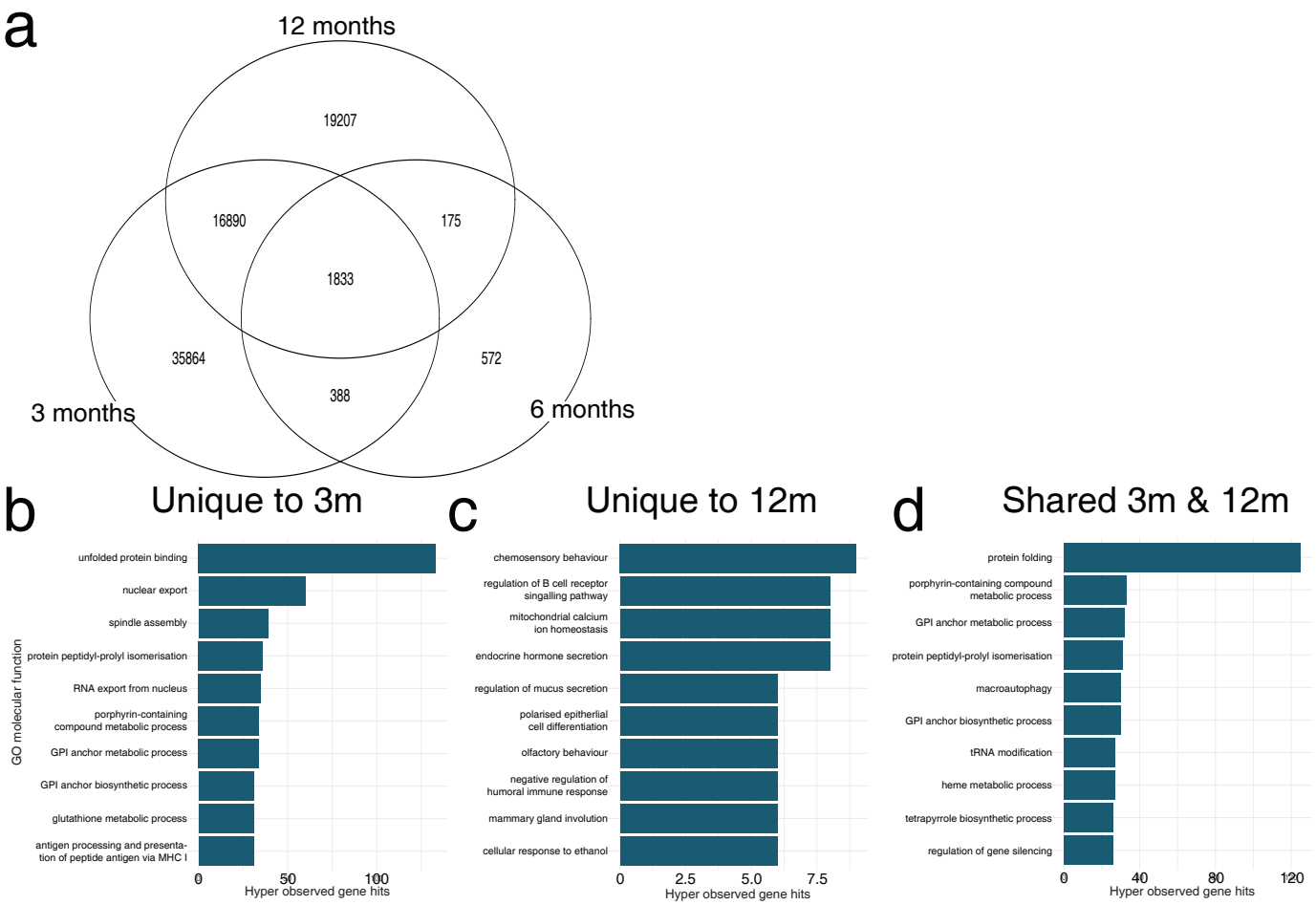
a
12 months
19207
16890
175
1833
35864
572
388
3 months
6 months
b
Unique to 3m
unfolded protein binding
nuclear export
spindle assembly
protein peptidyl-prolyl isomerisation
RNA export from nucleus
porphyrin-containing compound metabolic process
GPI anchor metabolic process
GPI anchor biosynthetic process
glutathione metabolic process
antigen processing and presentation of peptide antigen via MHC I
GO molecular function
0
50
100
Hyper observed gene hits
c
Unique to 12m
chemosensory behaviour
regulation of B cell receptor singalling pathway
mitochondrial calcium ion homeostasis
endocrine hormone secretion
regulation of mucus secretion
polarised epitherlial cell differentiation
olfactory behaviour
negative regulation of humoral immune response
mammary gland involution
cellular response to ethanol
0
2.5
5.0
7.5
Hyper observed gene hits
d
Shared 3m & 12m
protein folding
porphyrin-containing compound metabolic process
GPI anchor metabolic process
protein peptidyl-prolyl isomerisation
macroautophagy
GPI anchor biosynthetic process
tRNA modification
heme metabolic process
tetrapyrrole biosynthetic process
regulation of gene silencing
0
40
80
120
Hyper observed gene hits

Figure 5.11: H3K4me3 differential enrichment peaks at pre-pathology and pathology-rich time-points in APP/PS1 neurons

(a) Venn diagram plotting the overlap for differentially enriched H3K4me3 sites in APP/PS1 versus WT neurons from 3, 6, and 12 months of age. (b) Functional annotations for 'GO biological process' for the 35864 sites unique to 3 months differential enrichment analysis, (c) the 19207 sites unique to 12 month differential binding analysis and, (d) sites shared between 3 and 12 month months of age.

Approximately 62% of differentially marked H3K4me3 sites shared between 3 and 6 months of age were enriched in 3 month old APP/PS1 neurons compared to wild-type neurons, but depleted in 6 month old APP/PS1 neurons. 28% of H3K4me3 differentially marked sites were enriched in both 6 month, and 12 month old APP/PS1 neurons. While ~10% of H3K4me3 differentially marked sites were enriched at 6 months of age but depleted at 12 months of age, and 60% of H3K4me3 differentially marked sites were depleted at 6 months of age but enriched at 12 months of age in APP/PS1 neurons. There were far more sites overlapping between 3 months of age and 12 months of age: ~90% H3K4me3 differentially marked sites were enriched in both 3 month and 12 months old APP/PS1 neurons (including sites identified to be shared between all time-points), while only 1.4% of sites were depleted at both time-points in APP/PS1 neurons.

Table 5.2: H3K4me3 marking is consistently enriched in pre-pathology and pathology rich neurons

	Consistently		Enriched depleted	Depleted enriched
	Enriched	**Depleted**		
3 vs 6 month	693 (35.4%)	7 (<1%)	1220 (62.4%)	36 (1.8%)
6 vs 12 month	567 (28.6%)	15 (<1%)	206 (10.4%)	1195 (60.3%)
3 vs 12 month	14104 (89.5%)	222 (1.4%)	1220 (7.7%)	205 (1.3%)

Taken together, these data demonstrate that H3K4me3 enrichment peaked in neurons prior to pathology onset and in pathology rich neurons. H3K4me3 marking was highly specific at 3 and 12 months of age, although more than 15000 sites were shared between 3 and 12 month old neurons, of which the vast majority were consistently enriched in both time points. These data demonstrate a partial recapitulation of a juvenile histone landscape in 12 month old APP/PS1 neurons.

5.2.11 H3K27ac and H3K4me3 are enriched in known AD risk variants

Previous studies have shown that histone modifications are dysregulated at known AD risk loci in mouse models and post-mortem human entorhinal cortex from AD cases (Gjoneska et al., 2015; Marzi et al., 2018). To determine whether H3K27ac or H3K4me3 marking was dysregulated at sites of known AD risk variants, differentially enriched H3K27ac and H3K4me3 marked sites from APP/PS1 neurons were annotated to known AD risk variants (Giri, Zhang, & Lü, 2016). H3K4me3 and H3K27ac marking were enriched at 22 AD risk variant loci in neurons from APP/PS1 mice, including well-established loci from previous genome-wide association studies; *Bin1, Clu* and *Picalm* (Table 5.3) (Harold et al., 2009; Seshadri et al., 2010). Risk loci including *Clu, Cr1, Bin1, Cd2ap, Picalm, Mef2c, Cass4, Zcwpw1, Celf1, Fermt2, Slc24a4, Pld3, Unc5c, Akap9, Adam10* were enriched for H3K27ac marking in APP/PS1 neurons at 3 months of age (Table 5.3). While *Clu, Sorl1, Cr1, Bin1, Cd2ap, Picalm, Epha1, Inpp5d, Ptk2b, Zcwpw1, Celf1, Fermt2, Slc24a4, Pld3, Unc5c, Akap9* and *Adam10* were enriched for H3K4me3 marking in 3 month old APP/PS1 neurons. Interestingly *Clu, Sorl1, Bin1, Cd2ap, Mef2c, Ptk2b, Celf1, Fermt2, Scl24a4,* and *Unc5c* were enriched for H3K27ac marking in 6 month old APP/PS1 neurons, while *Sorl1* was the only risk loci that was enriched for H3K4me3 marking in APP/PS1 neurons at 6 months of age. At 12 months of age, H3K27ac marking was enriched in neurons at *Bin1, Cd2ap, Picalm, Ptk2b, Celf1,* and *Unc5c* loci. While *Bin1, Cd2ap, Picalm, Mef2c, Ptk2b, Zcwpw1, Celf1, Fermt2, Slc24a4, Pld3* and *Unc5c* were enriched for H3K4me3 marking in 12 month old APP/PS1 neurons. 7 of the 22 annotated AD risk alleles were depleted for H3K4me3 or H3K27ac marking in APP/PS1 neurons. At 3 months of age, *Mef2c* was depleted for H3K4me3 marking, while *Sorl1*, *Inpp5d*, and *Ptk2b* were depleted for H3K27ac marking in APP/PS1 neurons. At 6 months of age, H3K4me3 marking was depleted from *Picalm, Celf1,* and *Pld3* risk loci in APP/PS1 neurons, and no risk loci were depleted for H3K27ac marking, similar to 12 months of age, where no AD risk loci were depleted for H3K4me3 or H3K27ac marking in APP/PS1 neurons.

In summary, known AD risk loci are dysregulated in neurons from APP/PS1 mice, including well established risk loci from genome-wide association studies such as *Clu*, *Picalm* and *Bin1*. The majority of AD risk loci were significantly enriched for H3K27ac and H3K4me3 marking in APP/PS1 neurons, while few risk loci were depleted for H3K27ac and H3K4me3 marking in APP/PS1 neurons. Surprisingly, AD risk loci were enriched for H3K27ac and H3K4me3 prior to pathology onset.

Table 5.3: H3K4me3 and H3K27ac are differentially enriched at AD risk loci

Gene	Function	H3K4me3 3 month	H3K4me3 6 month	H3K4me3 12 month	H3K27ac 3 month	H3K27ac 6 month	H3K27ac 12 month
Clu	Synapse turnover, chaperone protein	Enriched	-	Enriched	Enriched	Enriched	-
Abca7	Phagocytosis, lipid homeostasis	-	-	Enriched	-	-	-
Sorl1	Endocytosis, receptor for APOE, processing of APP	Enriched	Enriched	Enriched	Depleted	Enriched	-
Cr1	Amyloid β clearance, complement activation	Enriched	-	Enriched	Enriched	-	-
Ms4a	Signal transduction, immune function	-	-	Enriched	-	-	-
Bin1	Synaptic vesicle, APP trafficking, cytoskeletal dynamics	Enriched	-	Enriched	Enriched	Enriched	Enriched
Cd2ap	Receptor-mediated endocytosis,cytoskeletal dynamics	Enriched	-	Enriched	Enriched	Enriched	Enriched
Picalm	Clathrin-mediated endocytosis	Enriched	Depleted	Enriched	Enriched	-	Enriched
Epha1	Synaptic development, immune function, neural development	Enriched	-	-	-	-	-
Inpp5d	Cytokine signaling, immune function	Enriched	-	-	Depleted	-	-
Mef2c	Myogenesis, synapse formation	Depleted	-	Enriched	Enriched	Enriched	-
Cass4	Cell migration, cell adhesion	-	-	-	Enriched	-	-
Ptk2b	Calcium homeostasis, MAP kinase signalling	Enriched	-	Enriched	Depleted	Enriched	Enriched
Zcwpw1	Epigenetic regulation, neural development	Enriched	-	Enriched	Enriched	-	-
Celf1	mRNA editing, pre-mRNA splicing	Enriched	Depleted	Enriched	Enriched	Enriched	Enriched
Fermt2	Cell–cell adhesion, angiogenesis	Enriched	-	Enriched	Enriched	Enriched	-
Slc24a4	Cell signalling, neural development	Enriched	-	Enriched	Enriched	Enriched	-
Pld3	Signal transduction, epigenetic modification	Enriched	Depleted	Enriched	Enriched	-	-
Unc5c	Neural development	Enriched	-	Enriched	Enriched	Enriched	Enriched
Akap9	Signal transduction	Enriched	-	Enriched	Enriched	-	-
Adam10	Hippocampal neurogenesis, cell adhesion	Enriched	-	Enriched	Enriched	-	-

5.2.12 H3K27ac and H3K4me3 enriched sites are transcribed in human AD cases

Recently, studies have utilised single cell sequencing techniques to show differential expression of RNA transcripts in numerous cell-types between age matched controls and AD cases, demonstrating cell-type specific transcriptional dysregulation in AD (Mathys et al., 2019). To validate the data in the current study, a comparison between the neuronal transcriptomic data from Mathys, et al., (2019) and the genes that were differentially enriched for H3K27ac and H3K4me3 marking in 12 month APP/PS1 neurons was performed. 5802 of the 6550 genes that were differentially expressed (88%) in human neurons between control and AD cases identified by Mathys, et al., (2019) were identified as having differential enrichment of H3K4me3 between wild-type and APP/PS1 neurons (Figure 5.12a). Furthermore 5793 of the 6557 (88.3%) genes that were differentially expressed in neurons between human control and early AD cases (Mathys et al., 2019) were differentially enriched for H3K4me3 marking between wild-type and APP/PS1 neurons (Figure 5.12b). However, 872 of 6550 genes (13.3%) that were differentially expressed between neurons from control versus AD cases were identified as having differential enrichment for H3K27ac marking in APP/PS1 neurons versus wild-type neurons (Figure 5.12c). Finally, 876 of 6557 genes (13.3%) that were differentially expressed between neurons from human control versus early AD cases also exhibited differential enrichment for H3K27ac marking in wild-type neurons versus APP/PS1 neurons (Figure 5.12d). Of note, as the number of genes that were differentially enriched for H3K4me3 and H3K27ac marking between wild-type and APP/PS1 neurons in this study were 15228 and 1854, respectively, this represents ~38% and ~47% overlap of the mouse data with differentially expressed genes between human control and AD neurons.

Taken together, these data validate the differential enrichment from H3K4me3 and H3K27ac ChIP-seq experiments and demonstrate that H3K4me3 and H3K27ac marking from APP/PS1 neurons can somewhat predict changes in gene expression in human neurons in AD. Furthermore, these data suggest that the changes in chromatin structure identified in the current study do not always lead to a change in transcription and warrant further investigation.

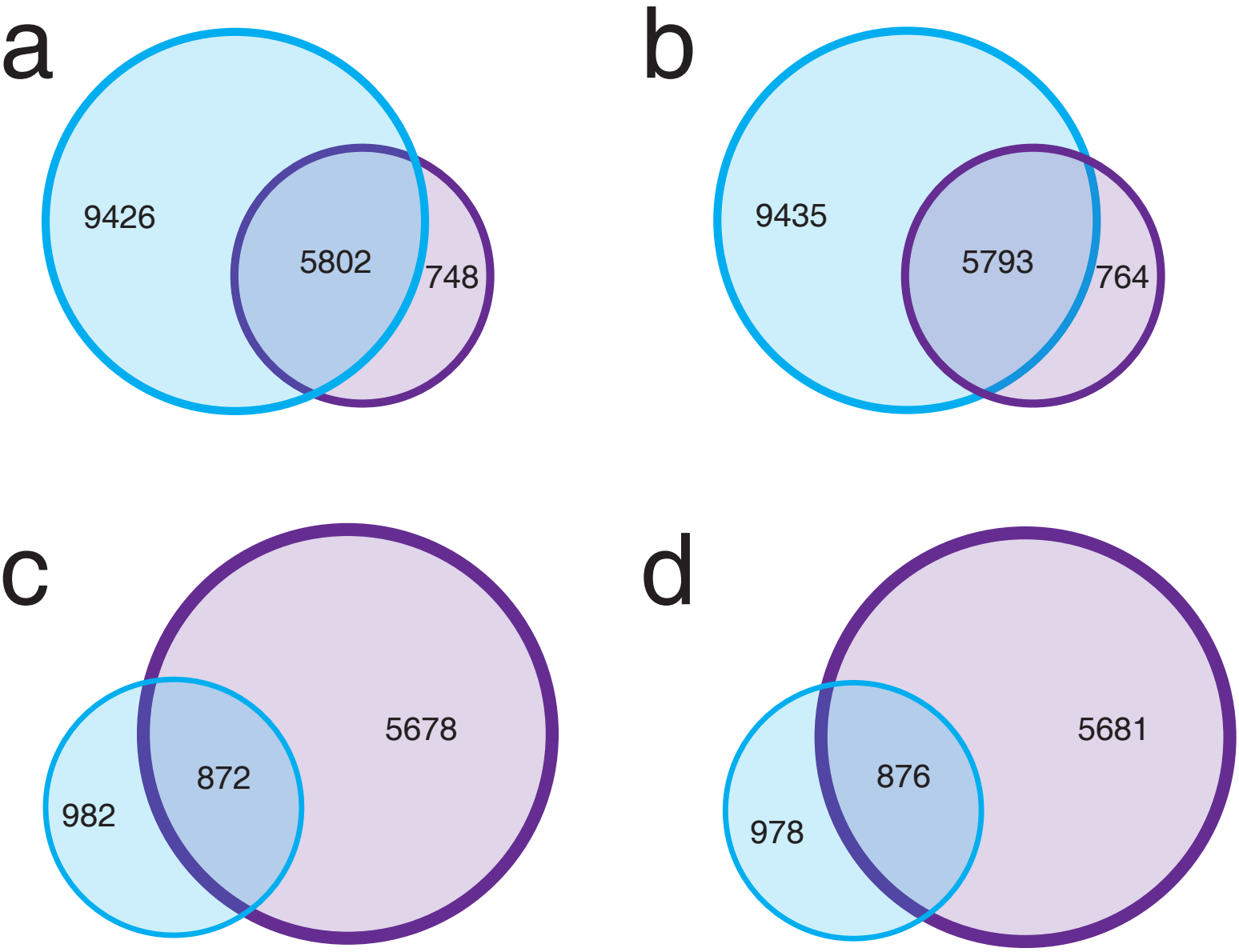
a
9426
5802
748
b
9435
5793
764
c
982
872
5678
d
978
876
5681

Figure 5.12: Genes differentially enriched for H3K27ac and H3K4me3 marking are also differentially expressed in human AD

(a) Venn diagram plotting the overlap of genes differentially enriched for H3K4me3 marking in 12 month old wild-type versus APP/PS1 neurons (blue) compared to differentially expressed genes in neurons from human control versus AD cases (purple). (b) Venn diagram plotting the overlap for genes with differential H3K4me3 marking in 12 month old wild-type versus APP/PS1 neurons (blue) compared to differentially expressed genes from human control neurons versus those in early-AD cases (purple). (c) Venn diagram plotting the overlap of genes differentially enriched for H3K27ac marking in neurons from 12 month old wild-type versus APP/PS1 mice (blue) compared to differentially expressed genes in human neurons in aged controls versus AD cases (purple). (d) Venn diagram plotting the overlap for genes differentially enriched for H3K27ac in 12 month old wild-type neurons versus APP/PS1 neurons (blue) compared to differentially expressed genes from human neurons in controls versus early-AD cases (purple).

5.3 Discussion

This study was the first to characterise both H3K27ac and H3K4me3 marking in neurons from APP/PS1 transgenic AD mice and WT control mice at 3, 6, and 12 months of age, representing pre-pathology, pathology onset, and pathology rich time-points in this amyloidosis model (Garcia-Alloza et al., 2006; Jankowsky et al., 2004). These data demonstrated widespread enrichment for H3K4me3 marking prior to pathology onset and in pathology rich cases in APP/PS1 neurons, while the majority of differential H3K27ac marking in APP/PS1 neurons occurred prior to or at pathology onset with few changes in pathology rich cases compared to WT control neurons. Furthermore, gene ontology analysis showed epigenetic dysregulation to be occurring at the promoters for key neuronal pathways implicated in the regulation of synaptic plasticity, as well as core molecular pathways for post-transcriptional modifications in APP/PS1 neurons compared to WT control neurons. Strikingly, a partial recapitulation of the juvenile epigenome was observed in APP/PS1 neurons in pathology rich cases.

Soluble Aβ may contribute to dysregulation of the neuronal epigenetic landscape pre-pathology in APP/PS1 mice

APP/PS1 mice at 3 months of age represents a pre-pathology time-point (Garcia-Alloza et al., 2006; Jankowsky et al., 2004). Surprisingly, the epigenome was highly dynamic in neurons from 3 month old APP/PS1 mice compared to WT control mice. Widespread enrichment of H3K27ac and H3K4me3 marking was observed across the genome in APP/PS1 neurons compared to WT control neurons. The enrichment of H3K27ac and H3K4me3 marking is generally associated with increased transcriptional activity (Creyghton et al., 2010b; Santos-Rosa et al., 2002; Z. Wang et al., 2008; Wysocka et al., 2006). Differential H3K4me3 marking was concentrated at the TSS of 3 month old APP/PS1 neurons, and specifically at CpG island containing TSS, and was not abnormally located at enhancer elements. Alongside enrichment at promoters at 3 months of age, H3K27ac marking was also depleted from enhancers, and interestingly, enriched at known cortical super enhancers in neurons from APP/PS1 mice. Super enhancers are large clusters of transcriptional enhancers that drive expression of genes that regulate cellular identity, maintain pluripotent state, and control differentiation from pluripotent stem-cells to terminally differentiated cell-types (Hnisz et al., 2013; Whyte et al., 2013). There have been 389 cortical super enhancers identified to date that regulate cell-type specific gene expression in the cortex (Khan & Zhang, 2016). The redistribution of neuronal

H3K27ac marking in APP/PS1 mice from enhancers to super-enhancers in the current study may indicate a loss of normal neuronal gene function. This was further illustrated by differential H3K27ac marking in neurons from APP/PS1 mice being annotated to pathways for the regulation of synaptic plasticity, membrane depolarisation, neurotransmitter secretion and calcium ion transmembrane transport at 3 months of age. Dysregulation of super-enhancers has also been previously identified in Huntington's disease, altering genes involved in neuronal identity (Achour et al., 2015; Le Gras et al., 2017), and a single study has identified a range of AD associated single nucleotide polymorphisms to overlap known super-enhancers, including super enhancers for *BIN1,* which was identified to be differentially enriched for histone marking in the current study and has been previously implicated in AD (Chapuis et al., 2013; Hnisz et al., 2013). However, as super-enhancers have only recently been discovered this is the first study of the epigenetic regulation around super-enhancers in AD to date.

Strikingly, there was widespread disruption of histone marking in neurons from APP/PS1 mice at 3 months of age. APP/PS1 mice harbour familial AD transgenes that are over-expressed from birth (Garcia-Alloza et al., 2006). Although Aβ plaque accumulation does not occur until approximately 6 months of age in APP/PS1 mice, soluble oligomeric Aβ can be detected as early as 1-2 months of age (Garcia-Alloza et al., 2006; Trinchese et al., 2004). Previous literature has demonstrated soluble oligomeric Aβ to be neurotoxic in mouse brain slice cultures at nanomolar doses, disrupt cognitive function and learned behaviour, and disrupt long-term potentiation in mice and rat hippocampal slices (James P. Cleary et al., 2004; Koffie et al., 2009a; Mota, Ferreira, Pereira, Oliveira, & Rego, 2012; Walsh et al., 2002; H. W. Wang et al., 2002) (review:(John Hardy & Selkoe, 2002)). Thus, the altered distribution of H3K27ac and H3K4me3 in APP/PS1 neurons at 3 months of age is likely due, at least in part, to the accumulation of soluble Aβ. This current study (including data in Chapter 4 and Chapter 5) has demonstrated that the epigenome is highly dynamic in neurons at 3 months of age. Thus, an alternate, but not mutually exclusive hypothesis is that the accumulation of soluble Aβ may have disrupted the maturation of the neuronal epigenome at 3 months of age. This is also supported by emerging literature that has shown that pyramidal neurons in the cortex are still undergoing synaptic pruning at 3 months of age (Handley et al., 2017). It is likely that some of the differences between 3 and 6 month old neurons represent an age of transition between juvenile and young adult mice. Total brain volume dramatically increases up to 3 months of age, though myelination is still occurring between 3 and 6 months of age (Fu et al., 2013). Adult levels of neurotransmitters and synaptic density stabilise after 3 months of age in mice,

which is associated with the emergence of adult behavioural tendencies such as reduced risk taking and increased parental tendencies (Fu et al., 2013) (review: (Semple et al., 2013).

Differential enrichment of H3K27ac in 3 month old APP/PS1 neurons was annotated to pathways involved in synaptic plasticity, calcium ion transport, membrane depolarisation, and mRNA processing. These findings are supported by previous AD literature. Alterations to synaptic transmission have been observed in APP/PS1 mice prior to pathology onset (Trinchese et al., 2004; Unger et al., 2016). Interestingly, exposure of soluble oligomeric Aβ also impaired long-term potentiation in hippocampal slices of 2-3 month old C57/BL6 mice (Puzzo et al., 2005; Shankar et al., 2008). Intracellular calcium homeostasis and calcium signalling have also been implicated in AD (reviews: (Demuro, Parker, & Stutzmann, 2010; Magi et al., 2016)). In line with the gene ontology data presented in the current study, it has been previously suggested that Aβ oligomers can form calcium-permeable channels in membranes that reduce synaptic plasticity and cause cytotoxicity in APPswe, and 3xTg mouse models of AD (Arispe, Pollard, & Rojas, 1993; Lopez et al., 2008). However, previous literature has also reported that 3 month old APP/PS1 mice do not show elevated calcium levels (Kuchibhotla et al., 2008). Taken together, these data indicate that soluble Aβ may be causing disruption to the neuronal epigenome prior to pathology onset in neurons from APP/PS1 mice.

Interestingly, gene ontology analysis of differential H3K4me3 marking indicated that pathways associated with RNA modification and stabilisation, gene silencing, protein localisation, and dephosphorylation were disrupted in 3 month old APP/PS1 neurons. Many of these pathways identified in the current study have been implicated in the AD literature. Indeed, some aspects of RNA processing, such as RNA splicing are dysregulated in AD, with accumulation of unspliced RNA products accumulating in the post-mortem human frontal cortex (Bing Bai et al., 2013). Hyperphosphorylation is widely implicated in AD literature. For example, paired helical filaments of hyperphosphorylated tau is a pathological hallmark of AD, resulting in disruption to microtubules and altered cytoskeletal integrity (Arriagada et al., 1992; Berg et al., 1998; M. E. Murray et al., 2015). While NFTs are not observed in APP/PS1 mice, neuritic processes containing hyperphosphorylated tau have been reported in 8 month old APP/PS1 mice (Maia et al., 2013; Radde et al., 2006). It is possible that soluble Aβ dysregulates common phosphorylation pathways, resulting in altered histone phosphorylation and epigenetic regulation of the transcriptome, or alternatively acetylation and aceylation of proteins is disrupted in AD (reviews: (Banerjee & Chakravarti, 2011; Rossetto, Avvakumov, & Côté, 2012)). Gene ontology data for differential H3K4me3 marking in 3 month old APP/PS1

neurons also identified gene silencing pathways as disrupted in AD. The genes associated with this term included *Tet1, Sirt1, Cdk2, Apobec1, Sin3a, Phf2/8, Tnrc6c* and the *Hist1h* family, many of which are involved in epigenetic regulation of transcription. Interestingly, epigenetic silencing of pathways involved in Aβ production have been implicated as an intervention to slow amyloid deposition (Scarpa, Fuso, D'Anselmi, & Cavallaro, 2003). It is possible that gene silencing pathways are altered in 3 month old APP/PS1 neurons, potentially to compensate for the overexpression of familial AD transgenes from birth in APP/PS1 mice. Alternatively, it is also possible that the change in histone marking that was observed in 3 month old neurons is a consequence of other epigenetic and chromatin changes that were not examined in the current study.

Pathology onset is associated with enrichment of H3K27ac marking in APP/PS1 neurons at enhancers and neuronal super-enhancers, potentially to promote neuronal function

6 month old APP/PS1 mice exhibit the appearance of Aβ plaque pathology, and represent pathology onset in this amyloidosis model (Garcia-Alloza et al., 2006; Jankowsky et al., 2004). Differential enrichment analysis showed that H3K27ac marked sites were enriched in APP/PS1 neurons compared to WT control neurons at 6 months of age, however there was minimal change in H3K4me3 marking in 6 month old APP/PS1 neurons. At 6 months of age H3K27ac marking was slightly enriched at TSS in APP/PS1 neurons compared to WT controls, while there was no change in H3K4me3 enrichment at TSS in APP/PS1 neurons. Interestingly, at 6 months of age H3K27ac marking was enriched at enhancers and super-enhancers in APP/PS1 neurons compared to WT control neurons. Enrichment of H3K27ac at TSS, enhancers, and super enhancers in APP/PS1 neurons at 6 months of age may be due to the activation of neuronal specific functions, potentially as a compensatory mechanism to Aβ plaque accumulation (Hnisz et al., 2013; Whyte et al., 2013). The enrichment of H3K27ac marking in pathways from neuronal specific functions at 6 months of age could be associated with Aβ plaque deposition and the associated disruption to the neuropil, including plaque-associated synapse loss and dystrophic neurites (Garcia-Alloza et al., 2006; Jankowsky et al., 2004; Mitew et al., 2013a, 2013b). Furthermore, soluble Aβ would still be present in the brain at 6 months of age leading to disruption to neuronal connections. For instance, dendritic spine loss is known to begin in the presence of soluble Aβ prior to plaque formation, and dendritic spines loss persists in pathology rich APP/PS1 brains (Bittner et al., 2012).

Differential H3K27ac marking in 6 month old APP/PS1 neurons was enriched at sites pertaining to synaptic plasticity, protein depolymerisation, RNA processing and the regulation of protein complex disassembly. As previously discussed, deficits in synaptic plasticity have been identified in APP/PS1 mice as early as 3 months of age, and have been shown to increase with Aβ plaque deposition (Trinchese et al., 2004; Unger et al., 2016). While studies of synaptic deficits in human AD have also observed cholinergic dysfunction to occur in early-AD and be proportional to Aβ plaque load (Potter et al., 2011). Furthermore, Aβ induced protein depolymerisation has been previously shown to occur in hippocampal cultures, causing DNA fragmentation and microtubule deregulation, possibly due to disruption of NMDA receptor function (Mota et al., 2012). It may also be possible that hyperphosphorylation of tau leads to depolymerisation of microtubules, or alternatively that microtubules depolymerise leading to excess tau in the soma of neurons that may be prone to hyperphosphorylation and aggregation (reviews: (Brandt & Bakota, 2017; Jean & Baas, 2013)). In the current study, RNA processing was annotated to genes including *Ago2, Ahcyl1, Btg2, Celf3/4/6, Cnot1/7,* and *Cpeb3* which regulate RNA splicing, RNA mediated gene silencing and mRNA deadenylation. Intracellular inclusions of RNA splicing products have been described in AD brains, accumulating in some cases around intracellular tau tangles (B. Bai et al., 2013). Moreover, aberrant pre-mRNA splicing is dysregulated in the dorsolateral prefrontal cortex of AD brains (Towfique Raj et al., 2018) (review: (Koch, 2018)).

Although gene ontology analysis was not possible for H3K4me3 marking at 6 months of age due to the low number of differentially marked sites, individual sites of H3K4me3 enrichment were at genes related to intracellular trafficking, ion channel maintenance, synaptic plasticity, and cell survival and DNA repair, which align with the previous literature (Mota et al., 2012; Potter et al., 2011). Literature suggests that impairment of axonal retrograde transporters contributes to aberrant Aβ production and clearance, possibly due to accumulation of axonal lysosomes (Gowrishankar et al., 2015). Moreover, a range of studies have implicated hyperphosphorylation of tau in AD to cause impairment of axonal transport, leading to the decay of synapses and subsequent neurodegeneration (review: (Mandelkow, Thies, Konzack, & Mandelkow, 2009)). Post-mitotic neuronal cells are particularly vulnerable to the effects of oxidative stress in the aging brain, which is further exacerbated in AD (Miquel et al., 1980; X. Wang et al., 2005) (review: (Xinkun Wang & Michaelis, 2010)). The accumulation of reactive oxygen species has been linked with subsequent DNA damage in AD and is suggested to be one of the earliest detectable events in AD (review: (Coppede & Migliore, 2009)). Recent

studies have suggested that the DNA damage response is compromised in the AD brain (review: (Wezyk & Zekanowski, 2018). Furthermore, core proteins in the DNA damage response such as BRCA1 are depleted from the AD brain, inhibiting DNA repair pathways and leading to downstream neuronal dysfunction and cell death (Suberbielle et al., 2015). Interestingly, ion channel maintenance was among the pathways enriched for H3K4me3 marking. Appropriate maintenance of synaptic ion channels is essential to proper synaptic transmission and plasticity. Dysfunction of NMDA channels have been shown to disrupt cell membrane potential and lead to cell death in AD (review: (Yan Zhang, Li, Feng, & Wu, 2016)). Post-synaptic AMPA receptor function is also reduced in hippocampal neurons of APP/PS1 mice (Chang et al., 2006). Alongside AMPA and NMDA receptors, a range of other ion channels contribute to neuronal excitability, including voltage-gated ion channels, many of which have been reported in AD literature (Boda, Hoxha, Pini, Montarolo, & Tempia, 2012; Poulopoulou et al., 2010) (review: (Cochran, Hall, & Roberson, 2014)).

It is likely that a combination of both soluble Aβ accumulation and Aβ plaque deposition and its sequelae contribute to the disruption of the neuronal epigenome at pathology onset in APP/PS1 mice.

Aβ plaque accumulation is associated with H3K4me3 enrichment that promotes inflammatory, protein refolding, and developmental pathways in neurons from pathology rich APP/PS1 mice

Aβ plaque pathology is considered one of the key pathological hallmarks of AD (review: (John Hardy & Selkoe, 2002)). 12 month old APP/PS1 mice exhibit extensive Aβ plaque deposition and recapitulate the Aβ plaque-associated neuronal pathology in human early sporadic AD cases (Garcia-Alloza et al., 2006; Jankowsky et al., 2004; Mitew et al., 2013a, 2013b; A. Woodhouse et al., 2009). The data presented in this study demonstrated enrichment of H3K4me3 marking, but minimal enrichment of H3K27ac marking in neurons from APP/PS1 mice at 12 months of age. H3K4me3 marking was enriched predominantly around TSS that contained CpG islands in APP/PS1 neurons compared to WT control neurons, but not in enhancers. Whereas there was slight enrichment for H3K27ac at the TSS, but no change at enhancers in 12 month old APP/PS1 neurons compared to WT control neurons. The enrichment of H3K4me3 in pathology rich neurons may act as a compensatory mechanism to Aβ plaque formation, soluble Aβ and synaptic loss, or as a downstream consequence of Aβ accumulation.

Gene ontology analysis further illustrated the effects of differential H3K4me3 marking from APP/PS1 neurons at 12 months of age, which were annotated to pathways including immune response, protein refolding, and antigen processing and presentation. There is strong evidence to suggest that misfolded Aβ intermediates, such as Aβ fibrils, act as precursors to core Aβ plaque pathology (review: (Fink, 1998)). Indeed, there are a number of pathways for correcting misfolded proteins with chaperones to destabilise abnormal conformations or promote refolding through heat shock protein complexes that are activated in AD (review: (Hartl, Bracher, & Hayer-Hartl, 2011; Koren et al., 2009)). H3K4me3 may be enriched to increase the activation of protein folding complexes in response to severe Aβ pathology in 12 month old APP/PS1 brains. Activation of the innate immune system and inflammation are other hallmarks of AD and have been widely implicated to be a driving force in the neurodegeneration seen in the disease (review: (Tony Wyss-Coray, 2006)). In particular, activated microglia and reactive astrocytes are observed around Aβ plaques (Ansoleaga et al., 2015; Itagaki et al., 1989). Widespread activation of microglia occurs in AD, and microglia can internalise and degrade Aβ (review: (C. Y. D. Lee & Landreth, 2010)). Studies have shown that the immune response increases between 6 and 12 months of age in APP/PS1 mice (Ansoleaga et al., 2015). Several immune response risk alleles have also been implicated in AD pathogenesis and progression (Giri et al., 2016). However, it was surprising that the current study identified immune response and antigen processing and response pathways to be differentially enriched for H3K4me3 marking in neurons from 12 month old APP/PS1 mice. It may be possible that neurons are also activating immune response pathways to further illicit an immune response as a result of Aβ accumulation in the pathology rich brain (Peltier, Simms, Farmer, & Miller, 2010) (review: (Veiga-Fernandes & Artis, 2018)).

Interestingly, there was minimal change to H3K27ac marking in neurons from 12 month old APP/PS1 mice. There was a total of 2150 differentially enriched H3K27ac marked sites in APP/PS1 neurons at 12 months of age. There was also little difference in H3K27ac marking between APP/PS1 neurons and WT control neurons at 12 months of age at enhancers and super-enhancers. Interestingly, the number of differentially enriched H3K27ac marked sites decreased in neurons across the time-course of Aβ accumulation. Meanwhile, gene ontology terms annotated by differential H3K27ac marking in 12 month old APP/PS1 neurons included pathways involved in synaptic plasticity, protein localisation, dephosphorylation, dendrite development, maintenance of location, and cerebellum development. Literature has suggested that dendritic sprouting occurs in AD (Masliah et al., 1991). Growth associated protein 43

(GAP-43) is critical to dendritic growth in developing neurons, and is associated with regenerating dendrites (review: (Benowitz & Routtenberg, 1997)). Interestingly, GAP-43 is present in coiled fibres in dystrophic neurites, pathology may be involved in synaptic pathology in AD cortex (Masliah et al., 1991). While studies have shown a reduction of GAP-43 in the frontal cortex, CA1 and CA4 regions of the hippocampus (Ansoleaga et al., 2015). Furthermore, the use of HDAC inhibitors to increase histone acetylation has resulted in increased dendritic sprouting and synaptogenesis in pathology rich CK-p25 mice (Fischer, Sananbenesi, Wang, Dobbin, & Tsai, 2007b) (review:(Arendt, 2009)).

The dense pathology burden seen in 12 month old APP/PS1 animals may cause enrichment for neuronal H3K4me3 marking at the TSS for metabolic processes such as protein refolding, and immune system responses, possibly to compensate for Aβ aggregation and its sequelae. However it is important to note that disruption of the epigenome may also contribute to the pathology onset and progression seen in AD.

A partial recapitulation of a juvenile-like epigenetic signature occurs in neurons from pathology rich APP/PS1 mice

By comparing differential enrichment of H3K27ac and H3K4me3 marking across 3, 6, and 12 months of age, this study observed sites that were shared across the time-course of Aβ pathology accumulation. Unexpectedly, the majority of differentially enriched H3K27ac and H3K4me3 marked sites in APP/PS1 neurons at 3 and 12 months of age were shared between these time-points. This posed the question of whether the shared differentially enriched sites were consistently enriched, demonstrating a recapitulation of a juvenile-like epigenetic state, or whether dysregulation in neurons from pathology rich APP/PS1 neurons was occurring at previously enriched sites of H3K27ac and H3K4me3 marking from juvenile mice. Strikingly, the majority of enriched H3K27ac marked sites (69.6%) and the vast majority of differentially enriched H3K4me3 marked sites (89.5%) that were shared between 3 and 12 month old APP/PS1 neurons were consistently enriched at both time-points. These data indicate that APP/PS1 neurons from a pathology rich environment partially recapitulate a juvenile-like histone landscape. Differentially enriched H3K27ac marked sites shared between 3 and 12 month old APP/PS1 neurons were annotated to pathways including protein localisation, synaptic plasticity, calcium ion transport, and dendrite development. Similar pathways were identified in the gene ontology analysis of all H3K27ac differentially enriched sites in APP/PS1

neurons when the 3 and 12 month old time points were analysed individually. Whereas differentially enriched H3K4me3 marked sites that were shared between APP/PS1 neurons from 3 and 12 months of age were mostly from pathways implicated in protein folding (review: (Soto & Pritzkow, 2018)), glycosylphosphatidylinositol (GPI) anchoring and autophagic pathways (review: (Uddin et al., 2018)). GPI anchoring and lipid based transport has been previously implicated in APP processing *in-vitro*, and is thought to be involved in APP and Aβ trafficking and key to the regulation of Aβ processing (Cordy, Hussain, Dingwall, Hooper, & Turner, 2003) (review:(Cordy, Hooper, & Turner, 2006)).

Interestingly, previous literature has also identified a recapitulation of juvenile pathways in AD. Several regulators for initiating and arresting the cell cycle have been implicated in AD, suggesting that reactivation of the cell cycle may occur in terminally differentiated neurons in the AD brain. For example, P16, CDK4, and hyperphosphorylated retinoblastoma protein, which are all key proteins in the regulation of cell cycle are disrupted in pyramidal neurons from human AD hippocampus and in the 3xTg mouse model of AD (Hradek et al., 2015; McShea, Harris, Webster, Wahl, & Smith, 1997). It is possible that reactivation of these pathways inhibits normal neuronal function and apoptotic pathways in impaired neurons, exacerbating AD progression (review: (Moh et al., 2011)). Studies have also shown that markers of synaptic and dendritic growth are upregulated as a result of Aβ pathology in CK-p25 mice and neurons from post-mortem AD hippocampus (Fischer et al., 2007b; McKee, Kowall, & Kosik, 1989). Growth associated proteins have also been identified to be upregulated in the AD brain and CSF of AD patients as a result of Aβ and tau accumulation (Masliah et al., 1991; Sandelius et al., 2019).

Together these data demonstrate a partial recapitulation of a juvenile-like epigenome in neurons from pathology rich APP/PS1 mice. The disruption to the normal epigenome may be driving mechanism, or occur as a downstream consequence of Aβ accumulation, or indeed may act as a compensatory mechanism against pathology accumulation.

Enrichment of H3K27ac and H3K4me3 at known AD risk variants in neurons from APP/PS1 mice

Genome-wide association studies have established a number of gene variants to be associated with AD (Harold et al., 2009; Seshadri et al., 2010). A wide array of research has identified that these AD risk loci have roles in synaptic plasticity, protein trafficking, cytoskeletal

dynamics, immune function and other neuronal processes (review: (Giri et al., 2016)). The current study demonstrated H3K27ac and H3K4me3 marking was differentially enriched in APP/PS1 neurons at 22 known AD risk loci, including *Clu, Abca7, Sorl1, Cr1, Ms4a, Bin1, Cd2ap, Picalm, Epha1, Inpp5d, Mef2c, Cass4, Ptk2b, Zcwpw1, Celf1, Fermt2, Slc24a4, Pld3, Unc5c, Akap9,* and *Adam10*. Unexpectedly, the majority of the identified AD risk variants were enriched for H3K27ac and H3K4me3 marking in APP/PS1 neurons prior to pathology onset, however there were few AD risk loci that were differentially enriched for H3K27ac and H3K4me3 marking at pathology onset in 6 month old neurons. Several AD risk variants have been differentially enriched for histone modifications in AD. Gjoneska and colleagues (2015) also observed differential enrichment of histone modifications at the *Abca1, Slc39a13, Picalm, Bin1, Inpp5d,* and *Rrbp1* AD risk loci in the CK-p25 mouse model of neurodegeneration. While Marzi, et al., (2018) determined that *APOE, CR1, APP, PS1, PS2 and MAPT* to be differentially enriched for H3K27ac marking in the post-mortem human entorhinal cortex from AD cases. Indeed, CpG islands within AD risk variants including *ANK1, BIN1, RHBDF2, ABCA7* have also been shown to be hypermethylated in AD, implicating epigenome wide alterations to AD risk alleles in the disease (P. L. De Jager et al., 2014; Lunnon et al., 2014). From the data presented here and previous literature, it is plausible that early- and late onset AD share similar pathogenic pathways, of which many are impacted by epigenetic dysregulation.

Genome-wide analysis of isolated neuronal nuclei demonstrate a distinct pattern of histone modification marking in AD

This was the first study to characterise both H3K4me3 and H3K27ac in neurons across a time-course of amyloidosis. H3K4me3 and H3K27ac are generally associated with active promoters and enhancers respectively (Creyghton et al., 2010b; Santos-Rosa et al., 2002; Z. Wang et al., 2008; Wysocka et al., 2006). There have been 5 studies to date that have performed ChIP-seq in human AD cases or animal models of AD (Benito et al., 2015; Gjoneska et al., 2015; Klein et al., 2019; Marzi et al., 2018; Nativio et al., 2018). Despite the differences in methodology, tissue source and bioinformatic analyses performed, there are several points of agreeance between this study and others in the literature.

Nativio et al. (2018) measured H4K16ac marking in the lateral temporal lobe genome-wide in young control cases, age matched control cases and AD subjects. H4K16ac marking is generally enriched at promoters and enhancers of actively transcribed genes, and displayed a

bimodal distribution at the TSS and a single peak at intergenic regions (including enhancers) (Nativio et al., 2018; Rai et al., 2014; Taylor, Eskeland, Hekimoglu-Balkan, Pradeepa, & Bickmore, 2013). Interestingly, Nativio, et al., (2018) identified depletion of H4K16ac marking in the lateral temporal lobe of AD cases, which was concentrated around the TSS. However, Nativio et al. (2018) showed no significant depletion from enhancers in AD cases. In contrast, the current study identified a slight enrichment of H3K27ac marking and widespread enrichment of H3K4me3 marking at promoters in neurons, but little change at enhancers in neurons from pathology rich APP/PS1 mice. The current study also observed that neurons from APP/PS1 mice were enriched for H3K4me3 and H3K27ac marking prior to pathology onset, with the magnitude of differential enrichment for H3K27ac marking decreased over the time-course of amyloidosis. In comparison, Nativio et al. (2018) identified age associated enrichment of H4K16ac marking, but depletion of H4K16 marking in AD cases (Nativio et al., 2018). GO analysis of H4K16ac marking demonstrated that pathways involved in myeloid differentiation, cell death, Wnt signalling, and Ras signal transduction were disrupted in the lateral temporal lobe of AD cases. Whereas the current study identified pathways associated with protein folding, GPI lipid processing and RNA modifications to be enriched for H3K4me3 marking in 12 month old APP/PS1 neurons; and synaptic plasticity, ion transport, dendrite development, and protein dephosphorylation to be enriched for H3K27ac in neurons from 12 month old APP/PS1 mice.

Another recent study has performed genome-wide assessment of H3K27ac marking in post-mortem entorhinal cortex from AD cases and age matched control cases (Marzi et al., 2018). Marzi and colleagues (2018) identified 4162 differentially enriched H3K27ac marked sites in AD cases, of which 35% were enriched for H3K27ac marking, while 65% were depleted for H3K27ac marking, however there was no report on the global levels of H3K27ac marking at promoters or enhancers in the AD cases (Marzi et al., 2018). In contrast, the current study found the vast majority of H3K27ac marking was enriched in APP/PS1 neurons, however H3K27ac marking peaked prior to pathology onset, with only 2076 significantly enriched H3K27ac marked sites in pathology rich neurons from APP/PS1 mice. Interestingly, Marzi et al. (2018) observed that H3K27ac differentially marked sites were associated with pathways for lipoprotein-particle binding, apolipoprotein binding, response to hypoxia, cardiac muscle cell development, GABA-receptor activity, synaptic plasticity, and Aβ metabolic process (Marzi et al., 2018). Several of these gene ontology terms were also present in the current study, including lipoprotein-particle binding, synaptic plasticity, and receptor activity. Interestingly,

another recently published study performed genome-wide assessment of H3K9ac marking in the post-mortem human AD prefrontal cortex has identified that tau, but not Aβ correlated with an altered H3K9ac marking in AD, and that tau regulates aspects of chromosomal and nuclear structure (Klein et al., 2019). H3K9ac is a marker of transcriptionally active chromatin and is often present around active transcriptional start sites (~41%) and enhancer elements (~27%), marking bivalently around the TSS (Klein et al., 2019). Enrichment of H3K9ac marking correlated with tau pathology at 5990 out of 26384 identified peaks, and interestingly, chromatin restructuring occurred prior to tangle formation when measured in a tau transgenic mouse model (Klein et al., 2019). Early enrichment of H3K9ac marking aligns with the findings of the current study, where H3K4me3 and H3K27ac were highly enriched in APP/PS1 neurons prior to the onset of pathology. It is possible that epigenetic dysregulation is one of the earliest changes in the pathogenesis of AD and occurs prior to both Aβ and tau pathology.

Differences between the previous literature and the current study could be due to the use of the APP/PS1 mouse model of amyloidosis, compared to the use of post-mortem human lateral temporal lobe, entorhinal cortex, and prefrontal cortex from AD cases, or different mouse models of neurodegeneration (Klein et al., 2019; Marzi et al., 2018; Nativio et al., 2018). Differences may also be due to different histone modifications measured (Klein et al., 2019; Nativio et al., 2018). Additionally, different populations of cells were measured between the studies, as the previous literature performed genome-wide ChIP-seq analysis on neurons and glia, whereas the current study used purified neurons across a time-course of amyloidosis from the forebrain of APP/PS1 mice (Klein et al., 2019; Marzi et al., 2018; Nativio et al., 2018).

There have been two studies of histone modifications in mouse models of AD. Gjoneska and colleagues (2015) provided one of the most comprehensive studies of histone modifications at two time-points in the CK-p25 mouse model of neurodegeneration; 2 weeks and 6 weeks post-induction of p25, representing low pathology, and pathology rich cases respectively. Gjoneska et al. (2015) performed ChIP-seq on several histone modifications including H3K4me1, H3K4me3, H3K27ac, H3K27me3, H3K36me3, and H4K20me1, alongside RNA-seq for transcriptomic analysis, then used ChromHMM to build a chromatin state model for active promoter and enhancer regions (Gjoneska et al., 2015). Gjoneska et al. (2015) identified chromatin states analogous with depletion of promoters and enhancers at genes associated with synaptic plasticity, but enrichment of promoters and enhancers associated with an immune response. Interestingly, the study found far fewer differentially enriched peaks compared to the current study: 3667 enriched and 5056 depleted for H3K4me3 marking, and 2456 enriched and

2154 depleted for H3K27ac marking, however, it may be due to differences in analysis (Gjoneska et al., 2015). Interestingly, gene ontology analysis revealed pathways such as immune system response, cell cycle, cell adhesion, establishment of location, neuron projection development, learning and memory, neurogenesis, which were orthologous with gene expression data from post-mortem human hippocampal grey matter (Gjoneska et al., 2015). Many of the gene ontology pathways identified in Gjoneska et al. (2015) were similar to the pathways identified by gene ontology analysis in the current study, which included protein folding, GPI lipid processing and RNA modifications, synaptic plasticity, ion transport, dendrite development, and protein dephosphorylation (Gjoneska et al., 2015). As CK-p25 mice are an inducible model that rapidly accumulate plaque pathology, widespread enrichment of immune responses is likely a consequence of the model, and differences between the two models may account for the disparity in the number of sites of enrichment of histone marks detected between the two studies, however differences may also be due the selective isolation of neuronal nuclei from the forebrain of APP/PS1 neurons in the current study (Gjoneska et al., 2015).

Benito et al. (2015) also performed genome-wide assessment of histone modifications in a mouse model of AD. To date it is the only study to isolate neuronal nuclei from the brain for genome-wide ChiP-seq analysis, characterising H4K12ac marking in neurons from the hippocampus and dentate gyrus 10 month old APP/PS1-21 AD mice (Benito et al., 2015). H4K12ac is a histone modification that generally correlates with gene expression, is a marker of active chromatin, and presents with a bimodal distribution across the TSS (Benito et al., 2015; Lopez-Atalaya et al., 2013). H4K12ac marking was depleted from the TSS in neurons and glia from AD mice (Benito et al., 2015). In contrast, the current study found enrichment of H3K27ac and H3K4me3 at the TSS in neurons from pathology rich APP/PS1 mice, however enrichment of H3K27ac decreased across disease progression in APP/PS1 neurons. H3K4me3 marking was also enriched in APP/PS1 neurons prior to pathology onset. Gene ontology analysis demonstrated that H4K12ac marking was depleted from pathways involved in protein localisation in the cell and synaptic organisation and transmission, and enriched in pathways associated with cytotoxicity, cell death, and inflammation (Benito et al., 2015). Many of the pathways implicated in Benito, et al., (2015) were similar to the pathways enriched for H3K27ac marking in neurons from APP/PS1 mice, including synaptic plasticity, inflammation, and apoptosis. Strikingly, HDAC inhibitors were able to restore neuronal H4K12ac marking in APP/PS1-21 mice to WT control levels. The differences between the current study and

previously published literature may be due to the pathology levels seen in the mouse models, or indeed different time-points analysed (Gjoneska et al., 2015). In the current study, isolating neuronal nuclei has allowed for accurate determination of the effects of Aβ accumulation on the neuronal epigenome, however future research needs to incorporate cell-type specific characterisation of the neuronal and glial epigenome in aging and AD (Mo et al., 2015).

Similar to the findings from Chapter 4, some caveats should be considered when interpreting the results of this study. NeuN labels neuronal nuclei and encodes for the transcription factor FOX-3, which is present in the vast majority of neuronal nuclei in vertebrates, with the exception of cerebellar Purkinje cells, olfactory bulb mitral cells, and retinal photoreceptor cells (K. K. Kim et al., 2009; Richard J Mullen et al., 1992). Current research shows that NeuN labels the vast majority of neuronal nuclei from adult mammalian brain, first detectable during development after neurons withdraw from the cell-cycle (Richard J Mullen et al., 1992). However, it is possible that the distribution of NeuN changes throughout aging and AD in the mammalian brain, which maintains to be an important avenue for future characterisation. Future research could incorporate independent techniques such as immunohistochemistry and single-cell sequencing to confirm the findings from the current study, and further examine inter-individual differences in H3K4me3 and H3K27ac marking in AD. Despite the advantages of using APP/PS1 neurons, the use of pseudoreplicates in the current study is another limitation to consider. The established bioinformatics pipelines are not well suited for the heterogenous samples seen in the mammalian brain. As such, the current study performed the analysis similarly to previously published studies by merging biological replicates together (Benito et al., 2015; Gjoneska et al., 2015; Nativio et al., 2018). Future research could further expand and utilise the biological replicates to identify inter-individual differences and perform more rigorous statistical analysis to further elucidate the mechanisms of epigenetic dysregulation in AD.

As a validation of the findings of the current study, an overlap analysis between genes enriched for H3K27ac and H3K4me3 marking between wild-type and APP/PS1 neurons, and neuronal RNA-seq data from human AD cases generated by Mathys and colleagues (2019) was performed. This analysis showed that approximately 88% of the genes that were differentially expressed in neurons from human control versus AD cases were differentially enriched for H3K4me3 between wild-type and APP/PS1 neurons. While approximately 47% of H3K27ac differentially marked sites between wild-type and APP/PS1 neurons were also differentially expressed between neurons from human control versus AD cases. Interestingly, this

demonstrated that APP/PS1 neurons reflect many of the changes occurring in neurons in human AD cases. Although post-mortem human tissue is a valuable resource, the inherent variability of NGS data may limit the analysis of such data. An advantage of using APP/PS1 mice in the current study is that the mice used are an inbred strain enabling the detection of differential enrichment with low background noise, which may contribute to the large number of sites identified in the current study compared to the number of differentially expressed genes detectable in the human neuron transcriptomic data (which would have heterogenous genetics).

Conclusions

In summary, this study is the first to characterise H3K4me3 and H3K27ac in neurons across a time-course of amyloidosis. Unexpectedly, this study demonstrated substantial enrichment for H3K27ac and H3K4me3 marking in neurons prior to pathology onset in APP/PS1 mice at promoters and TSS, in pathways involved in synaptic plasticity, ion channel maintenance, lipid transport and RNA modifications. This study has also identified widespread depletion of H3K27ac marking at enhancers and enrichment in cortical super enhancers in neurons prior to pathology onset in APP/PS1 mice. A major restructuring of the neuronal histone landscape occurred with dense Aβ pathology, with widespread enrichment for H3K4me3 marking, but minimal change in H3K27ac in 12 month old APP/PS1 neurons. Differential enrichment of histone marking in 12 month old APP/PS1 neurons was annotated to pathways involved in dephosphorylation, synaptic plasticity, maintenance of location and other juvenile pathways. Strikingly, this study has also demonstrated a partial recapitulation of a juvenile-like epigenome at pathology-rich time-points. Characterising the neuronal epigenome is pivotal to understanding key changes in the pathogenesis and progression of AD.

Chapter 6: Discussion

Alzheimer's disease is the most common form of dementia and is a terminal, progressive, neurodegenerative disorder. Pathological hallmarks of AD include extracellular Aβ plaques, intraneuronal NFTs of tau protein, dystrophic neurites, and neuropil threads (Braak & Braak, 1991; G. Perry et al., 1991). The cause of 90% of AD cases is unknown, and in the absence of highly penetrant risk alleles, changes to the regulatory elements controlling transcription could contribute to the pathogenesis and progression of AD. The number of published papers characterising the epigenome in AD is growing rapidly and most have identified epigenetic dysregulation present in human AD cases and in AD mouse models, which provide support for the notion of epigenetic dysregulation occurring in AD. However, it is not known whether epigenetic dysregulation is critical to the onset of AD, contributes to disease progression or acts as a downstream consequence of the disease (Benito et al., 2015; P. L. De Jager et al., 2014; Gasparoni et al., 2018; Lunnon et al., 2014). Seminal studies have demonstrated dysregulation of DNA methylation to occur at the earliest detectable stages of AD in human tissue (P. L. De Jager et al., 2014; Lunnon et al., 2014). Considering the key role of neurons in both AD and age-related cognitive decline there have been relatively few studies that have characterised the epigenome in neurons, neither in the healthy aging brain nor in AD (Benito et al., 2015; Cheung et al., 2010; Gasparoni et al., 2018; Shulha et al., 2013). To address this gap in knowledge, this thesis sought to characterise the neuronal epigenome in aging and AD, both globally and at a genome-wide level across a time-course of healthy aging and pathological progression.

Characterisation of DNA methylation was performed at a global level in a cell-type specific manner in human inferior temporal gyrus from early-AD, late-AD, and age matched control cases. Previous analyses of global DNA methylation in AD was contentious, showing global hypermethylation (Bradley-Whitman & Lovell, 2013; Coppieters et al., 2013; Lardenoije et al., 2018), global hypomethylation (Chouliaras et al., 2013; A. Fuso et al., 2005; D. Mastroeni et al., 2010; S.-C. Wang et al., 2008; West et al., 1995), or no change to global DNA methylation in AD (Lashley et al., 2014). Much of the previous literature performed qualitative analysis in all cell-types or in neurons and glia and few studies have examined epigenetic alterations in NFT-bearing neurons or in cells adjacent to Aβ plaques. To address these gaps in the literature and determine whether global dysregulation of the epigenome was occurring in NF-positive pyramidal neurons, calretinin-labelled interneurons, astrocytes and microglia in AD, this study quantitatively measured 5mC and 5hmC in human control, early-AD, and late-AD cases. This study demonstrated that astrocytes were deficient in nuclear 5mC and 5hmC in AD cases, and

a lower proportion of NF-positive pyramidal neurons displayed extranuclear 5mC in AD cases compared to controls. However, no global differences in 5mC or 5hnC were detected in calretinin-labelled interneurons and microglia in AD. Interestingly, there was also no robust alterations in 5mC and 5hmC in cells adjacent to Aβ plaques, nor any detectable change in 5mC or 5hmC in tangle-bearing neurons. These data demonstrated global dysregulation DNA methylation marks to occur in a cell-type specific manner in AD.

Although global measurements of the epigenome can provide an indication of overall changes occurring in the brain, epigenetic regulation of the genome is finely controlled at promoters and enhancers to regulate gene expression with exquisite precision. While DNA methylation alters the accessibility for transcription factors to bind to DNA and initiate transcription, other regulatory elements act in consort to alter accessibility to chromatin, including histone modifications (review: (Bannister & Kouzarides, 2011)). After identifying changes occurring to the epigenome at a global level in the AD brain, this study sought to characterise key histone modifications in neurons across a time-course of the aging and AD brain. By utilising a mouse model of AD it was possible to observe the earliest changes occurring to the epigenome in neurons due to the accumulation of Aβ (Garcia-Alloza et al., 2006; Jankowsky et al., 2004). Specifically, this enabled analysis of pre-pathology and pathology-onset time points, both of which are extremely difficult to assess in human AD cases.

To date, three studies have investigated histone modifications in neurons from the aging brain (Benito et al., 2015; Cheung et al., 2010; Shulha et al., 2013). One study has reported a loss of H4K12ac in neurons of the aging brain (Benito et al., 2015). However, the two other studies have reported developmental enrichment of H3K4me3 in neurons, that stabilise in the aging brain (Cheung et al., 2010; Shulha et al., 2013). To further expand the literature of histone modifications in the aging brain, this thesis characterised H3K27ac and H3K4me3 marking in neurons from the forebrain of C57/BL6 mice at 3, 6, 12, and 24 months of age (Chapter 4). The data from this study demonstrated a redistribution H3K4me3 and H3K27ac marking across the neuronal epigenome in juvenile, adult and aging brain. Interestingly, H3K27ac and H3K4me3 marking was enriched at promoters and enhancers in neurons from juvenile (3 month old) and aging (24 months old) mice in comparison to neurons from adult mice (6 and 12 months of age). H3K27ac and H3K4me3 marking was predominant in many synaptic and core molecular processes across life (Table 6.1). However, ontologies that were unique to juvenile neurons included developmental processes such as the centrosome cycle and spindle assembly. Ontologies that were unique to adult neurons included axonal transport, protein folding and

membrane depolarisation pathways (Table 6.1). Furthermore, pathways that were unique to aging neurons included a range of cellular functions such as apoptotic and autophagic pathways, receptor regulation pathways, and RNA processing pathways (Table 6.1).

Table 6.1: Pathways of H3K27ac and H3K4me3 enrichment in aging neurons

Shared across life	Unique to juvenile neurons	Unique to adult neurons	Unique to aging neurons
Antigen processing	Centrosome cycle	Anterograde axon transport	Apoptosis
Apoptosis	Spindle assembly	Chaperone mediated protein folding	Autophagy
Gene silencing		Dendrite development	Regulation of receptor activity
GPI anchor metabolic/biosynthetic process		Membrane depolarisation	RNA processing
Ion transport			
Mitotic spindle organisation			
Oxidative phosphorylation			
Protein localisation			
Synaptic pathways			
tRNA modifications			

This study observed a partial recapitulation of a juvenile-like epigenetic state in aged neurons. The differences in histone marking observed throughout the aging time-course demonstrated the dynamic nature of the epigenome in neurons throughout life.

As the epigenome is dynamic throughout life, it is possible that dysregulation of the epigenome contributes to the pathogenesis and progression of AD, or is a sequela of AD pathology. There have been five studies to date to investigate histone modifications in AD in a genome-wide manner (Benito et al., 2015; Gjoneska et al., 2015; Klein et al., 2019; Marzi et al., 2018; Nativio et al., 2018); however, only one study has isolated neuronal nuclei for its analysis, demonstrating genome wide loss of H4K12ac in neurons from APP/PS1-21 mice (Benito et al., 2015). To characterise the disruption of the neuronal epigenome occurring in AD, ChIP-seq was performed for H3K4me3 and H3K27ac marking on neuronal nuclei from 3, 6 and 12 month old wild-type and APP/PS1 mice, representing pre-pathology, pathology onset and pathology rich time-points in this amyloidosis model (Garcia-Alloza et al., 2006; Jankowsky et al., 2004) (Chapter 5). Interestingly, widespread differential enrichment of H3K27ac and H3K4me3 marking occurred in neurons from APP/PS1 mice across the amyloidosis time-

course. H3K4me3 marking was enriched at the TSS in APP/PS1 neurons pre-pathology compared to WT controls, however there was little difference in H3K4me3 marking between genotypes at pathology onset. By 12 months of age H3K4me3 marking was enriched again in 12 month old APP/PS1 neurons compared to WT control neurons. Whereas, H3K27ac marking was enriched at the TSS in APP/PS1 neurons prior to pathology onset, but depleted from enhancers. H3K27ac marking was enriched in APP/PS1 neurons at super-enhancers at 3 and 6 months of age, then proceeded to normalise to WT control levels in 12 month old APP/PS1 neurons. Differential enrichment for H3K27ac and H3K4me3 marking was annotated to a wide range of neuronal specific pathways and core metabolic pathways in APP/PS1 neurons that were shared across pre-pathology, pathology onset and pathology rich time-points (Table 6.2). However, there were a range of core molecular pathways that were differentially enriched in APP/PS1 neurons prior to pathology onset, such as lipid and ion transport and pathways involved in gene silencing. Furthermore, pathways unique to APP/PS1 neurons at pathology onset included cell survival pathways and protein depolymerisation and disassembly pathways. Furthermore, H3K27ac and H3K4me3 were enriched in APP/PS1 neurons from the pathology rich time-point in developmental pathways, and core molecular processes such as protein modification and protein refolding pathways, as well as dendrite and cerebellum development. Strikingly, when comparing differential enrichment from APP/PS1 neurons across 3, 6, and 12 months of age, a partial recapitulation of the epigenome from pre-pathology neurons was observed in pathology rich APP/PS1 neurons.

Table 6.2: Pathways enriched for H3K27ac and H3K4me3 marking in APP/PS1 neurons

Shared across APP/PS1 time-course	Unique to pre-pathology	Unique to pathology onset	Unique to pathology rich
Antigen processing	Gene silencing	Protein complex disassembly	Cerebellum development
ARF protein signal transduction	GPI anchor process	Protein depolymerisation	Dendrite development
Maintenance of protein location	Ion transport	Apoptosis	Mitochondrial fission
Membrane depolarisation	Neuromuscular process controlling balance	DNA repair/cell survival	Negative regulation of megakaryocyte differentiation
RNA processing	Neurotransmitter secretion		Non-ribosomal peptide biosynthetic process
Synaptic plasticity	Protein dephosphorylation		Protein acylation
			Protein acetylation
			Protein folding
			Type 1 interferon production

After characterising histone modifications in aging and AD neurons, some interesting points of comparison can be raised between the two studies. In both the aging and AD data generated in this thesis, there were distinct patterns of histone marking that were observed over the time-course. In the healthy aging brain, H3K27ac and H3K4me3 marking were enriched in juvenile neurons, depleted in young adult, then re-established with age. Similarly, in APP/PS1 neurons H3K4me3 marking was enriched in comparison to wild-type neurons at 3 months of age, with minimal difference at pathology onset, before being enriched in 12 month old APP/PS1 neurons compared to WT control neurons. In contrast, H3K27ac marking was differentially enriched in APP/PS1 neurons prior to pathology onset and was enriched in enhancers and super-enhancers in 6 month old APP/PS1 neurons compared to WT control neurons. However, differences in H3K27ac marking between APP/PS1 and WT control neurons stabilised in 12 month old neurons. Furthermore, it appeared as though amyloidosis caused a disruption to age associated enrichment of H3K27ac and H3K4me3 marking at specific regulatory elements.

This PhD thesis detailed differences in H3K4me3 and H3K27ac marking in a pairwise fashion in APP/PS1 and WT control neurons across a time-course of healthy aging and Aβ pathology accumulation. Despite there being significant differences between the APP/PS1 and WT neurons at each time-point (discussed in Chapter 5 and above), H3K27ac and H3K4me3 marking in APP/PS1 neurons followed a similar pattern of enrichment when compared to WT

neurons across the time-course of healthy aging, with the clear exception of H3K27ac marking at super-enhancers in APP/PS1 neurons. For example, when H3K27ac marking at the TSS and enhancers in aging neurons were examined across time, H3K27ac marking was enriched ("up") at 3 months of age, before being depleted at 6 months of age ("down"), then stabilised at 12 months of age ("same"; Figure 5.2). Likewise, the pattern of H3K4me3 marking over time was enriched at 3 months of age ("up"), depleted at 6 months of age ("down"), and enriched again at 12 months of age ("up"; Figure 5.7) for both APP/PS1 and WT neurons. There was one clear exception where the pattern of H3K27ac marking across the time-points differed between wild-type and APP/PS1 neurons. H3K27ac marking at super-enhancers in APP/PS1 neurons was enriched in WT control neurons at 3 months of age ("up"), then was depleted at 6 months of age ("down"), before being re-established at 12 months of age ("up"). In contrast, H3K27ac marking was enriched in APP/PS1 neurons at 3 months of age ("up"), before being reduced at 6 months of age ("down"), then further depleted at 12 months of age ("down") (Figure 5.4; Appendix 2: Supplementary Figure 3). The differential enrichment of super-enhancers was unexpected, as all other patterns of enrichment followed similar trends in marking in both the amyloidosis and aging time-course. The depletion of H3K27ac at super-enhancers in APP/PS1 neurons implies that there is a continuous loss of super-enhancer activity with the accumulation of Aβ pathology, and possible dysregulation of neuronal identity in AD in comparison to neurons from the healthy aging brain (Hnisz et al., 2013).

Next, this PhD thesis sought to determine whether the alterations in histone landscape occurred in pathways that are altered across the course of healthy aging brain that become dysregulated in AD, and/or whether epigenetic dysregulation was occurring in pathways in AD mice that were not usually altered in healthy aging. Gene ontology annotations of differential H3K4me3 and H3K27ac marking in neurons were compared between the aging and AD datasets and GO terms were categorised into: 1) Shared: pathways that were altered in the course of healthy aging and were dysregulated in AD; 2) AD specific: pathways that were present only in AD gene ontology analysis; 3) Aging specific: pathways that were altered across healthy aging and remain unperturbed in AD (Table 6.3). In the 'Shared' category H3K27ac and H3K4me3 differential marking was annotated to many pathways related to synaptic plasticity, neuronal activity, RNA processing and protein folding and localisation (Table 6.3). Gene ontology pathways that were in the 'AD specific' category included protein modification and processing and neurotransmitter pathways that were differentially enriched for H3K27ac marking and transcriptional and inflammatory-related pathways were specifically enriched for H3K4me3

marking (Table 6.3). In the unperturbed aging category H3K27ac and H3K4me3 differential marking was present in apoptotic, oxidative phosphorylation, autophagic, axon transport and oxidative phosphorylation pathways (Table 6.3). Although many of the enriched pathways observed in this PhD thesis were annotated to specific categories of 'Shared', 'Aging specific' and 'AD specific', the ontologies presented were not an exhaustive list, with only the top ten pathways being compared between the groups. However, there was a similar distribution of pathways enriched for H3K27ac and H3K4me3 marking across all three categories. Previous research has also identified 'Shared', 'AD specific' and 'Aging specific' pathways to be enriched for H4K16ac marking in human AD (Nativio et al., 2018). Nativio, et al., (2018) and this PhD thesis identified many similar "Shared" pathways for histone modifications including protein phosphorylation, synaptic pathways, and neuron development pathways (Nativio et al., 2018). There were some "Aging specific" pathways shared between the two studies, which included apoptosis, autophagy and hypoxia (which may be related to oxidative phosphorylation from the current study), however the current study was also enriched for many core molecular pathways that were not observed in previous studies (Nativio et al., 2018). "AD specific" pathways shared between the two studies included metabolic processes, however there were many pathways that were independent between the two studies such as hormone stimulus, neuron projection and signal transduction pathways (Nativio et al., 2018). The differences between the two studies may be due to the use of human brain homogenate compared to isolated neuronal nuclei in the current study, and also may due to differences as a result of tau related pathology present in human AD that does not occur in APP/PS1 mice. It has been suggested that AD results in dysregulation of chromatin restructuring that occurs as a part of normal healthy aging (Nativio et al., 2018). Indeed, some age-associated epigenetic modifications that are normally protective against disease may become dysregulated, leading to AD pathogenesis (Nativio et al., 2018).

Table 6.3: Many pathways of H3K27ac and H3K4me3 marking are shared between aging and AD

H3K27ac marking			H3K4me3 marking		
Shared	**AD specific**	**Aging specific**	**Shared**	**AD specific**	**Aging specific**
ARF protein signal transduction	Cerebellum development	Apoptosis	Antigen processing	Mitochondrial fission	Autophagy
Dephosphorylation	Neuromuscular process controlling balance	Oxidative phosphorylation	Apoptotic signalling	Negative regulation of megakaryocyte differentiation	Axon transport
Ion transport	Neurotransmitter secretion		GPI anchor metabolic/biosynthetic process	Non-ribosomal peptide biosynthetic process	Centrosome cycle
Learning	Protein complex disassembly		Protein folding (chaperone mediated)	Protein dephosphorylation	Glutathione metabolic process
Membrane depolarisation	Protein depolymerisation		Protein localisation (export from nucleus)	Protoporphyrinogen metabolic process	Mitotic spindle organisation
Protein localisation	Protein acylation & acetylation		Regulation of gene silencing	Transcription from RNA Pol III promoter	Oxidative phosphorylation
Regulation of dendrite development			RNA modifications and processing	Type 1 interferon production	Tetrapyrrole biosynthetic process
Regulation of synaptic plasticity/synaptic transmission			Synaptic plasticity		
RNA processing and modifications					

This thesis also observed a partial recapitulation of a juvenile-like state in aging neurons, and a partial recapitulation the pre-pathology epigenome in aged APP/PS1 neurons. In healthy aging more than 28% of H3K27ac and H3K4me3 differentially marked sites were shared between juvenile and aged neurons. When the direction of change of these shared sites was analysed, more than 87% of H3K4me3 and H3K27ac marked sites were consistently enriched in juvenile and aged neurons. Similarly approximately 23% of differentially H3K4me3 marked sites were shared between 3 and 12 month old APP/PS1 neurons, and more than 89% of the shared sites were consistently enriched in both time-points. In contrast, approximately 65% H3K27ac marked sites from 12 month old APP/PS1 neurons were shared with the 3 month old pre-pathology time-point, and approximately 70% of the shared sites were consistently

enriched at pre-pathology and pathology rich time-points. Due to the pairwise analysis performed for the aging data across the time-course (for example: 3 month time-point versus 6 month time-point) in comparison to time-point specific analysis in APP/PS1 neurons (for example: 3 month WT versus 3 month APP/PS1), this thesis has demonstrated that there are two independent pathways of recapitulation of juvenile-like epigenetic state in neurons; *1)* A partial recapitulation of the juvenile-like H3K27ac and H3K4me3 landscape in aging neurons from the healthy brain; and *2)* a partial recapitulation of the pre-pathology H3K4me3 neuronal signature in APP/PS1 neurons from the pathology rich environment. The data presented in this thesis support previous studies that have identified a partial recapitulation of the developmental DNA methylation profiles in the aging nervous system, and a recapitulation of the developmental cortical landscape in the aging brain when measured via structural magnetic resonance imaging (Douaud et al., 2014; Oh et al., 2016).

6.1 Strengths, limitations and future directions

There are several strengths and limitations to consider when interpreting the data from this thesis, and to take into consideration for future studies. This thesis was the first to characterise H3K27ac and H3K4me3 in neurons across a time-course of healthy aging and AD, and also quantitated cell-type specific differences in DNA methylation in AD.

The use of global measurements of DNA methylation and hydroxymethylation via immunohistochemistry allowed the current study to measure these marks in post-mortem human AD tissue in a cell-type specific manner, to analyse intracellular localization and to assess 5mC and 5hmC alterations in cells that contained or were adjacent to AD pathology. Currently, analysing neuronal and glial subtypes, intracellular localization, and spatial relationships between DNA methylation changes and AD pathology are not feasible with molecular techniques, including next-generation sequencing. While global measurements allow for cell-type specific and spatial analysis of the epigenome, they do not provide base-pair specific resolution of DNA methylation. The findings of the current study, alongside previous literature, provide compelling evidence supporting cell-type specific changes to DNA methylation in AD. However, genome-wide and cell-type specific analyses of DNA methylation and histone modifications in the same samples need to be performed to provide a comprehensive characterisation of the epigenome in AD. Recently, studies have isolated neuronal and glial nuclei in AD and demonstrated differential DNA methylation signatures

between neurons and glia in human AD (Gasparoni et al., 2018). A logical step for future research would be to develop protocols for the isolation of neuronal and glial subtypes for genome-wide analysis, however, it is currently difficult to identify markers of the nuclei from these cellular sub-types. An alternative strategy would be to use single-cell sequencing and a bioinformatics approach to cluster similar cell-types, however, such methodologies still yield low sequencing depth which may mask key aspects of differential methylation in AD (Luo et al., 2017).

To date, there have only been three previous studies of histone modifications in neurons in aging and AD (Benito et al., 2015; Cheung et al., 2010; Shulha et al., 2013). The isolation of neuronal nuclei for genome-wide analysis of H3K27ac and H3K4me3 marking was a major strength of the current study in comparison to using whole brain homogenate. It is important to note that the NeuN antibody (transcription factor FOX-3) labels a wide range of neuronal sub-types, but does not mark some subsets of neurons including Purkinje cells, Golgi cells and gamma motor neurons (Kee K. Kim et al., 2009; R. J. Mullen et al., 1992). Moreover, NeuN is not specific to excitatory or inhibitory neurons, which are known to have different epigenetic profiles (Luo et al., 2017; Mo et al., 2015), and different vulnerability to degeneration and death in AD (P. R. Hof et al., 1990; Patrick R. Hof & Morrison, 1990; Koffie et al., 2009b; Mitew et al., 2013b; Sampson et al., 1997; Thangavel et al., 2009; J. C. Vickers et al., 1994). Recent studies have demonstrated that 70-85% of neurons in the cortex are excitatory (Lake et al., 2016; Mo et al., 2015). Thus, the data presented in the current study is an approximation of the histone landscape of the vast majority of neurons, however, only four different histone modifications have been measured genome-wide in neurons in aging or AD, out of a wide range of regulatory elements that act collectively to regulate transcription (review: (M. Tan et al., 2011)). The data generated in this thesis will be a valuable resource for future research, and in conjunction with future studies of DNA methylation and nucleosome occupancy, histone modifications and RNA-seq can contribute to characterising the complete epigenetic signature of neurons in the aging and AD brain. Due to the limited number of histone modifications measured in the current study, it was not possible to confirm the putative enhancers that were identified from H3K27ac marking. It is common to identify putative enhancers by annotating H3K27ac marking outside (>2kB distal) of promoter regions, however, such a definition is limited for the accurate identification of either poised or active distal regulatory elements. Future studies should incorporate ChIP-seq for H3K4me1 marking to more accurately identify enhancers defined by H3K27ac marking, and/or incorporate functional testing of putative

enhancer regions with Hi-C and reporter assays (Jin et al., 2013; Mifsud et al., 2015). Moreover, utilising multiple histone modifications and other epigenetic readouts will allow for the creation of regulatory maps of the genome with software such as ChromHMM (Ernst & Kellis, 2017).

Another consideration when interpreting the data from this thesis is the use of the APP/PS1 mouse model of amyloidosis. Mice do not naturally develop AD related pathology. The APP/PS1 mice utilised in this thesis over-express familial AD mutations of human *APPswe* (KM670/671NL) and *PS1* (dE9) mutations under the *Pnrp* promoter (Jankowsky et al., 2004; Spanopoulou et al., 1991). These mice accumulate Aβ associated pathology, with plaque accumulation beginning at 6 months, dense plaque pathology by 12 months of age, and Aβ plaque-associated neuronal pathology similar to human early-AD cases (Garcia-Alloza et al., 2006; Jankowsky et al., 2004; Mitew et al., 2013a, 2013b; A. Woodhouse et al., 2009). APP/PS1 mice also have behavioural deficits in cognitive awareness and memory by 6 months of age (Gallagher et al., 2013; Serneels et al., 2009). However, these mice do not exhibit all aspects of human AD pathology, with no overt neuronal loss or NFT accumulation (Garcia-Alloza et al., 2006; Jankowsky et al., 2004). It is highly likely that NFT associated pathology would impact the epigenome in AD, which is not assessed in the current study. Recent studies have suggested that NFT pathology is the major contributing factor to epigenetic dysregulation in human AD (Klein et al., 2019), however, by using the APP/PS1 mouse model this thesis has clearly demonstrated that Aβ pathology also contributes to epigenetic dysregulation seen in AD in the absence of NFT pathology. It is also possible that metabolic stress would impact the epigenome in APP/PS1 mice, which over-express the familial AD mutations from birth. It would be difficult to isolate the impact of APP or the PS1 transgenes, or indeed the impact of Aβ accumulation without the associated metabolic load from over-expression (Sasaguri et al., 2017). Several new models of AD have been designed to account for the limitations of the APP/PS1 and other over-expression models. Knock-in models that express mutant human APP at the mouse *App* locus, recapitulate some aspects of AD pathology without the phenotypes of over-expression, which would be useful to incorporate into future studies of AD pathogenesis and progression (T. Saito et al., 2014) (review: (Sasaguri et al., 2017)). Despite the many advances in new model organisms it is difficult to generate models that fully recapitulate human AD. Future studies could incorporate Tau or APP/Tau transgenic models to investigate the effects of NFT pathology on the epigenome, and should also consider isolating neuronal nuclei from human tissue for genome-wide analysis of histone modifications in AD.

A range of different types of bioinformatic analyses have been performed for ChIP-seq in the AD literature. Many bioinformatic workflows for ChIP-seq analysis have focussed around the use of highly similar technical replicates, or samples with low variability such as those seen in cell lines. Biologically variable *in vivo* datasets with large sample size are difficult to analyse as there are limited tools that can accommodate for highly variable datasets (A. T. L. Lun & Smyth, 2016; M. D. Robinson et al., 2010). For example, social hierarchy and other environmental stimuli could all cause variation to the epigenome. Current ENCODE guidelines suggest peak-calling for the analysis of histone modifications in ChIP-seq, however many peak calling tools have statistical limitations as a result of the modelling, resulting in the loss of type-1 error control (Consortium, 2012; A. T. Lun & Smyth, 2014). To account for inter-individual differences and minimise technical error, the .bam files from biological replicates were merged into a single file, then reads were randomly shuffled and split into technical replicates for processing with window based differential enrichment analysis with csaw and EdgeR, which are more statistically rigorous than peak calling methods (A. T. Lun & Smyth, 2014; A. T. L. Lun & Smyth, 2016). However, as a result of the bioinformatics approach utilised in the current study and others in the field (Benito et al., 2015; Gjoneska et al., 2015; Nativio et al., 2018), it was not possible to investigate the potential inter-individual variability of the epigenome in aging or AD. New bioinformatics pipelines are needed to account for variability in biological data present both in the current study and others in the field. Characterising the inter-induvial variability in the neuronal epigenome would be fascinating to address in future studies after new bioinformatics pipelines are generated.

There are still many aspects of the epigenome that could be characterised with the data generated from this study, and indeed many questions to address in future studies. One interesting aspect of these data was that H3K27ac and H3K4me3 marked categorically different TSS, with H3K27ac marking pathways generally involved in neuronal function, while H3K4me3 marked pathways that generally were integral to core cellular function. Future work could perform peak calling for the H3K4me3 and H3K27ac data and determine whether these two histone modifications mark distinct subsets of TSS in neurons. Furthermore, the current study isolated neuronal nuclei for ChIP-seq and demonstrated a range of differential enrichment patterns in neurons of the aging and AD brain. However, literature suggests that glial cells may contribute to the pathology progression in AD (Benito et al., 2015; Gasparoni et al., 2018; Gjoneska et al., 2015) (review: (C. Y. D. Lee & Landreth, 2010)). Indeed, recent studies have demonstrated differential DNA methylation patterns exist between neurons and

glia in human aging and AD (Gasparoni et al., 2018), and ChIP-seq analysis in neurons and glia identified differential H4K12ac marking in glia, which were enriched at pathways for immune and inflammatory responses in CK-p25 mice (Benito et al., 2015). Glial nuclei were isolated from each sample via FACS and collected in the current study, but it was outside of the scope of the current project to perform ChIP-seq on these glial samples. Future work should incorporate ChIP-seq and analysis of glia to compare with the neuronal epigenome. Ideally, future studies will also incorporate post-mortem human tissue, and characterise multiple aspects of the epigenome from the same samples with experiments such as nucleosome occupancy and DNA methylation sequencing, RNA-seq, ChIP-seq and Hi-C to generate a complete reference for the neuronal and glial epigenome in the aging and AD brain. This PhD thesis has demonstrated that epigenetic dysregulation is likely occurring in the earliest stages of AD which cannot be captured in studies of human AD. It has also demonstrated the dynamic nature of the epigenome in aging, and of the impact of Aβ accumulation on the epigenome in an AD model. The data generated in this study will be a useful resource for comparison with human AD cases in future studies.

6.2 Conclusions

In summary this PhD thesis has substantially contributed to the field of neuroepigenetics in aging and AD. The key contributions of this study are:

- *There was a global loss of DNA methylation in neurofilament-positive pyramidal neurons and astrocytes in sporadic human AD.*
- *The neuronal epigenome was dynamic throughout life, with widespread changes in differential enrichment for H3K27ac and H3K4me3 marking with the greatest changes occurring in 3 month old and 24 month old neurons. Strikingly, there was a partial recapitulation of a juvenile-like epigenetic state in aging neurons.*
- *There was an increase in H3K27ac and H3K4me3 marking at promoters prior to pathology onset in APP/PS1 neurons.*
- *Enhancers and super-enhancers were differentially enriched for H3K27ac marking in APP/PS1 neurons between 3 and 6 months of age.*
- *Unlike TSS and enhancers, super-enhancers followed a different pattern of enrichment in neurons over the time-course of amyloidosis.*

- *H3K27ac marking was mostly annotated to neuron specific pathways, while H3K4me3 marking was annotated to core metabolic and cellular functions in aging and AD. There was a partial recapitulation of a pre-pathology like state of H3K4me3 and H3K27ac marking in APP/PS1 neurons from pathology rich brains.*

An improved understanding of the neuronal epigenome is crucial to understanding the pathogenesis and progression of AD, however, without understanding the nature of the neuronal epigenome in the aging brain it will not be possible to identify the dysregulation occurring in AD. This PhD thesis has substantially contributed to the growing knowledge of the neuronal epigenome in both aging and AD, by characterising H3K27ac and H3K4me3 marking in neurons across a time-course of healthy aging and AD in a mouse model, and identifying cell-type specific differences in DNA methylation in post-mortem human AD. This PhD thesis demonstrated that the epigenome is dynamic throughout life, and partially recapitulates a juvenile-like epigenetic state in aged neurons. Strikingly, this thesis has also observed wide-spread enrichment for H3K27ac and H3K4me3 in APP/PS1 neurons prior to pathology onset and at pathology rich time-points, in pathways critical for neuronal function and cellular senescence, and revealed that APP/PS1 neurons from pathology rich time-points partially recapitulated a juvenile-like epigenetic state. The data presented in this study is an important step towards developing a complete reference epigenome for neurons in aging and AD. This thesis has provided insight into the epigenetic dysregulation occurring in neurons in a milieu of amyloidosis. A better understanding of the dynamic epigenetic landscape in neurons will add to our accumulated knowledge of the molecular pathways involved in AD pathogenesis and progression, and likely contribute to the identification of novel therapeutic targets in the future.

References

Aagaard, L., Laible, G., Selenko, P., Schmid, M., Dorn, R., Schotta, G., . . . Jenuwein, T. (1999). Functional mammalian homologues of the Drosophila PEV-modifier Su(var)3-9 encode centromere-associated proteins which complex with the heterochromatin component M31. *Embo j, 18*(7), 1923-1938. doi:10.1093/emboj/18.7.1923

Achour, M., Merienne, K., Keime, C., Le Gras, S., Davidson, I., Néri, C., . . . Boutillier, A.-L. (2015). Neuronal identity genes regulated by super-enhancers are preferentially down-regulated in the striatum of Huntington's disease mice. *Human molecular genetics, 24*(12), 3481-3496. doi:10.1093/hmg/ddv099

Ahmadian, S. S., Rezvanian, A., Peterson, M., Weintraub, S., Bigio, E. H., Mesulam, M.-M., & Geula, C. (2015). Loss of calbindin-D28K is associated with the full range of tangle pathology within basal forebrain cholinergic neurons in Alzheimer's disease. *Neurobiol Aging, 36*(12), 3163-3170. doi:10.1016/j.neurobiolaging.2015.09.001

Akiyama, H., Schwab, C., Kondo, H., Mori, H., Kametani, F., Ikeda, K., & McGeer, P. L. (1996). Granules in glial cells of patients with Alzheimer's disease are immunopositive for C-terminal sequences of β-amyloid protein. *Neurosci Lett, 206*(2–3), 169-172. doi:http://dx.doi.org/10.1016/S0304-3940(96)12474-5

Aleksic, B., Kushima, I., Hashimoto, R., Ohi, K., Ikeda, M., Yoshimi, A., . . . Ozaki, N. (2013). Analysis of the VAV3 as candidate gene for schizophrenia: evidences from voxel-based morphometry and mutation screening. *Schizophr Bull, 39*(3), 720-728. doi:10.1093/schbul/sbs038

Alelú-Paz, R., Carmona, F. J., Sanchez-Mut, J. V., Cariaga-Martínez, A., González-Corpas, A., Ashour, N., . . . Ropero, S. (2016). Epigenetics in Schizophrenia: A Pilot Study of Global DNA Methylation in Different Brain Regions Associated with Higher Cognitive Functions. *Frontiers in Psychology, 7*, 1496. doi:10.3389/fpsyg.2016.01496

Allen, B., Ingram, E., Takao, M., Smith, M. J., Jakes, R., Virdee, K., . . . Goedert, M. (2002). Abundant tau filaments and nonapoptotic neurodegeneration in transgenic mice expressing human P301S tau protein. *J Neurosci, 22*(21), 9340-9351.

Allfrey, V. G., Faulkner, R., & Mirsky, A. E. (1964). ACETYLATION AND METHYLATION OF HISTONES AND THEIR POSSIBLE ROLE IN THE REGULATION OF RNA SYNTHESIS. *Proc Natl Acad Sci U S A, 51*(5), 786-794.

Allfrey, V. G., & Mirsky, A. E. (1964). Structural Modifications of Histones and their Possible Role in the Regulation of RNA Synthesis. *Science, 144*(3618), 559. doi:10.1126/science.144.3618.559

Allis, C. D., Berger, S. L., Cote, J., Dent, S., Jenuwien, T., Kouzarides, T., . . . Zhang, Y. (2007). New Nomenclature for Chromatin-Modifying Enzymes. *Cell, 131*(4), 633-636. doi:https://doi.org/10.1016/j.cell.2007.10.039

Allis, C. D., & Jenuwein, T. (2016). The molecular hallmarks of epigenetic control. *Nature Reviews Genetics, 17*, 487. doi:10.1038/nrg.2016.59

Alzheimer's Disease International. (2015). *World Alzheimer Report 2015: The Global Impact of Dementia. An Analysis of Prevalence, Incidence, Cost and Trends* Retrieved from http://www.alz.co.uk/research/WorldAlzheimerReport2015.pdf

Ambigapathy, G., Zheng, Z., & Keifer, J. (2015). Regulation of BDNF chromatin status and promoter accessibility in a neural correlate of associative learning. *Epigenetics, 10*(10), 981-993. doi:10.1080/15592294.2015.1090072

Amir, R. E., Van den Veyver, I. B., Wan, M., Tran, C. Q., Francke, U., & Zoghbi, H. Y. (1999). Rett syndrome is caused by mutations in X-linked MECP2, encoding methyl-CpG-binding protein 2. *Nat Genet, 23*, 185. doi:10.1038/13810

Andersson, R. (2015). Promoter or enhancer, what's the difference? Deconstruction of established distinctions and presentation of a unifying model. *Bioessays, 37*(3), 314-323. doi:10.1002/bies.201400162

Andorfer, C., Kress, Y., Espinoza, M., de Silva, R., Tucker, K. L., Barde, Y. A., . . . Davies, P. (2003). Hyperphosphorylation and aggregation of tau in mice expressing normal human tau isoforms. *J Neurochem, 86*(3), 582-590.

Andrews, S. (2010). FastQC: A quality control tool for high throughput sequence data. Retrieved from http://www.bioinformatics.babraham.ac.uk/projects/fastqc

Anglade, P., Vyas, S., Hirsch, E. C., & Agid, Y. (1997). Apoptosis in dopaminergic neurons of the human substantia nigra during normal aging. *Histol Histopathol, 12*(3), 603-610.

Ansoleaga, B., López-González, I., Garcia-Esparcia, P., Aso, E., LLorens, F., Moreno, J., . . . Fuso, A. (2015). Neuroinflammatory Signals in Alzheimer Disease and APP/PS1 Transgenic Mice: Correlations With Plaques, Tangles, and Oligomeric Species. *Journal of Neuropathology & Experimental Neurology, 74*(4), 319-344. doi:10.1097/nen.0000000000000176

Antequera, F., Boyes, J., & Bird, A. (1990). High levels of De Novo methylation and altered chromatin structure at CpG islands in cell lines. *Cell, 62*(3), 503-514. doi:https://doi.org/10.1016/0092-8674(90)90015-7

Anttila, T., Helkala, E. L., Viitanen, M., Kareholt, I., Fratiglioni, L., Winblad, B., . . . Kivipelto, M. (2004). Alcohol drinking in middle age and subsequent risk of mild cognitive impairment and dementia in old age: a prospective population based study. *Bmj, 329*(7465), 539. doi:10.1136/bmj.38181.418958.BE

Araque, A., Parpura, V., Sanzgiri, R. P., & Haydon, P. G. (1999). Tripartite synapses: glia, the unacknowledged partner. *Trends in Neurosciences, 22*(5), 208-215. doi:https://doi.org/10.1016/S0166-2236(98)01349-6

Arendt, T. (2009). Synaptic degeneration in Alzheimer's disease. *Acta Neuropathol, 118*(1), 167-179.

Arispe, N., Pollard, H. B., & Rojas, E. (1993). Giant multilevel cation channels formed by Alzheimer disease amyloid beta-protein [A beta P-(1-40)] in bilayer membranes. *Proc Natl Acad Sci U S A, 90*(22), 10573-10577.

Arriagada, P. V., Growdon, J. H., Hedley-Whyte, E. T., & Hyman, B. T. (1992). Neurofibrillary tangles but not senile plaques parallel duration and severity of Alzheimer's disease. *Neurology, 42*(3), 631. doi:10.1212/wnl.42.3.631

Ashford, J. W. (2004). APOE genotype effects on Alzheimer's disease onset and epidemiology. *Journal of Molecular Neuroscience, 23*(3), 157-165.

Atti, A. R., Palmer, K., Volpato, S., Winblad, B., De Ronchi, D., & Fratiglioni, L. (2008). Late-life body mass index and dementia incidence: nine-year follow-up data from the Kungsholmen Project. *J Am Geriatr Soc, 56*(1), 111-116. doi:10.1111/j.1532-5415.2007.01458.x

Avery, O. T., Macleod, C. M., & McCarty, M. (1944). STUDIES ON THE CHEMICAL NATURE OF THE SUBSTANCE INDUCING TRANSFORMATION OF PNEUMOCOCCAL TYPES : INDUCTION OF TRANSFORMATION BY A DESOXYRIBONUCLEIC ACID FRACTION ISOLATED FROM PNEUMOCOCCUS TYPE III. *J Exp Med, 79*(2), 137-158.

Azuara, V., Perry, P., Sauer, S., Spivakov, M., Jørgensen, H. F., John, R. M., . . . Fisher, A. G. (2006). Chromatin signatures of pluripotent cell lines. *Nature Cell Biology, 8*, 532. doi:10.1038/ncb1403

https://www.nature.com/articles/ncb1403#supplementary-information

Bai, B., Hales, C. M., Chen, P.-C., Gozal, Y., Dammer, E. B., Fritz, J. J., . . . Peng, J. (2013). U1 small nuclear ribonucleoprotein complex and RNA splicing alterations in Alzheimer's disease. *Proceedings of the National Academy of Sciences, 110*(41), 16562-16567. doi:10.1073/pnas.1310249110

Bai, B., Hales, C. M., Chen, P. C., Gozal, Y., Dammer, E. B., Fritz, J. J., . . . Peng, J. (2013). U1 small nuclear ribonucleoprotein complex and RNA splicing alterations in Alzheimer's disease. *Proc Natl Acad Sci U S A, 110*(41), 16562-16567. doi:10.1073/pnas.1310249110

Bakulski, K. M., Dolinoy, D. C., Sartor, M. A., Paulson, H. L., Konen, J. R., Lieberman, A. P., . . . Rozek, L. S. (2012). Genome-wide DNA methylation differences between late-onset Alzheimer's disease and cognitively normal controls in human frontal cortex. *J Alzheimers Dis, 29*(3), 571-588. doi:10.3233/JAD-2012-111223

Ballatore, C., Lee, V. M., & Trojanowski, J. Q. (2007). Tau-mediated neurodegeneration in Alzheimer's disease and related disorders. *Nat Rev Neurosci, 8*(9), 663-672. doi:10.1038/nrn2194

Bamberger, M. E., Harris, M. E., McDonald, D. R., Husemann, J., & Landreth, G. E. (2003). A cell surface receptor complex for fibrillar beta-amyloid mediates microglial activation. *J Neurosci, 23*(7), 2665-2674.

Banerjee, T., & Chakravarti, D. (2011). A Peek into the Complex Realm of Histone Phosphorylation. *Mol Cell Biol, 31*(24), 4858-4873. doi:10.1128/mcb.05631-11

Banerji, J., Olson, L., & Schaffner, W. (1983). A lymphocyte-specific cellular enhancer is located downstream of the joining region in immunoglobulin heavy chain genes. *Cell, 33*(3), 729-740.

Banerji, J., Rusconi, S., & Schaffner, W. (1981). Expression of a beta-globin gene is enhanced by remote SV40 DNA sequences. *Cell, 27*(2 Pt 1), 299-308.

Bannister, A. J., & Kouzarides, T. (2011). Regulation of chromatin by histone modifications. *Cell Research, 21*(3), 381-395. doi:10.1038/cr.2011.22

Barski, A., Cuddapah, S., Cui, K., Roh, T.-Y., Schones, D. E., Wang, Z., . . . Zhao, K. (2007). High-Resolution Profiling of Histone Methylations in the Human Genome. *Cell, 129*(4), 823-837. doi:http://dx.doi.org/10.1016/j.cell.2007.05.009

Barulli, D., & Stern, Y. (2013). Efficiency, capacity, compensation, maintenance, plasticity: emerging concepts in cognitive reserve. *Trends Cogn Sci, 17*(10), 502-509. doi:10.1016/j.tics.2013.08.012

Belikoff, E., Wong, L. J., & Alberts, B. M. (1980). Extensive purification of histone acetylase A, the major histone N-acetyl transferase activity detected in mammalian cell nuclei. *J Biol Chem, 255*(23), 11448-11453.

Benito, E., Urbanke, H., Ramachandran, B., Barth, J., Halder, R., Awasthi, A., . . . Fischer, A. (2015). HDAC inhibitor–dependent transcriptome and memory reinstatement in cognitive decline models. *J Clin Invest, 125*(9), 3572-3584. doi:10.1172/JCI79942

Benjamini, Y., & Hochberg, Y. (1995). Controlling the False Discovery Rate: A Practical and Powerful Approach to Multiple Testing. *Journal of the Royal Statistical Society. Series B (Methodological), 57*(1), 289-300.

Benowitz, L. I., & Routtenberg, A. (1997). GAP-43: an intrinsic determinant of neuronal development and plasticity. *Trends in Neurosciences, 20*(2), 84-91. doi:https://doi.org/10.1016/S0166-2236(96)10072-2

Berg, L., McKeel, D. W., Jr, Miller, J., & et al. (1998). Clinicopathologic studies in cognitively healthy aging and alzheimer disease: Relation of histologic markers to dementia severity, age, sex, and apolipoprotein e genotype. *Archives of Neurology, 55*(3), 326-335. doi:10.1001/archneur.55.3.326

Bergado, J. A., & Almaguer, W. (2002). Aging and synaptic plasticity: a review. *Neural Plast, 9*(4), 217-232. doi:10.1155/np.2002.217

Bergami, M., Masserdotti, G., Temprana, Silvio G., Motori, E., Eriksson, Therese M., Göbel, J., . . . Berninger, B. (2015). A Critical Period for Experience-Dependent Remodeling of Adult-Born Neuron Connectivity. *Neuron, 85*(4), 710-717. doi:https://doi.org/10.1016/j.neuron.2015.01.001

Bernstein, A. I., Lin, Y., Street, R. C., Lin, L., Dai, Q., Yu, L., . . . Jin, P. (2016). 5-Hydroxymethylation-associated epigenetic modifiers of Alzheimer's disease modulate Tau-induced neurotoxicity. *Hum Mol Genet, 25*(12), 2437-2450. doi:10.1093/hmg/ddw109

Bernstein, B. E., Kamal, M., Lindblad-Toh, K., Bekiranov, S., Bailey, D. K., Huebert, D. J., . . . Lander, E. S. (2005). Genomic Maps and Comparative Analysis of Histone Modifications in Human and Mouse. *Cell, 120*(2), 169-181. doi:http://dx.doi.org/10.1016/j.cell.2005.01.001

Bernstein, B. E., Mikkelsen, T. S., Xie, X., Kamal, M., Huebert, D. J., Cuff, J., . . . Lander, E. S. (2006). A Bivalent Chromatin Structure Marks Key Developmental Genes in Embryonic Stem Cells. *Cell, 125*(2), 315-326. doi:https://doi.org/10.1016/j.cell.2006.02.041

Beydoun, M. A., Lhotsky, A., Wang, Y., Dal Forno, G., An, Y., Metter, E. J., . . . Zonderman, A. B. (2008). Association of adiposity status and changes in early to mid-adulthood with incidence of Alzheimer's disease. *Am J Epidemiol, 168*(10), 1179-1189. doi:10.1093/aje/kwn229

Bihaqi, S. W., Bahmani, A., Adem, A., & Zawia, N. H. (2014). Infantile Postnatal Exposure to Lead (Pb) Enhances Tau Expression in the Cerebral Cortex of Aged Mice: Relevance to AD. *Neurotoxicology, 0*, 114-120. doi:10.1016/j.neuro.2014.06.008

Billings, L. M., Oddo, S., Green, K. N., McGaugh, J. L., & LaFerla, F. M. (2005). Intraneuronal Abeta causes the onset of early Alzheimer's disease-related cognitive deficits in transgenic mice. *Neuron, 45*(5), 675-688. doi:10.1016/j.neuron.2005.01.040

Bird, A., Taggart, M., Frommer, M., Miller, O. J., & Macleod, D. (1985). A fraction of the mouse genome that is derived from islands of nonmethylated, CpG-rich DNA. *Cell, 40*(1), 91-99.

Bishop, N. A., Lu, T., & Yankner, B. A. (2010). Neural mechanisms of ageing and cognitive decline. *Nature, 464*, 529. doi:10.1038/nature08983

Bittner, T., Burgold, S., Dorostkar, M. M., Fuhrmann, M., Wegenast-Braun, B. M., Schmidt, B., . . . Herms, J. (2012). Amyloid plaque formation precedes dendritic spine loss. *Acta Neuropathol, 124*(6), 797-807. doi:10.1007/s00401-012-1047-8

Blizzard, C. A., Chuckowree, J. A., King, A. E., Hosie, K. A., McCormack, G. H., Chapman, J. A., . . . Dickson, T. C. (2011). Focal Damage to the Adult Rat Neocortex Induces Wound Healing Accompanied by Axonal Sprouting and Dendritic Structural Plasticity. *Cerebral Cortex, 21*(2), 281-291. doi:10.1093/cercor/bhq091

Boda, E., Hoxha, E., Pini, A., Montarolo, F., & Tempia, F. (2012). Brain expression of Kv3 subunits during development, adulthood and aging and in a murine model of Alzheimer's disease. *Journal of Molecular Neuroscience, 46*(3), 606-615. doi:10.1007/s12031-011-9648-6

Bornemann, K. D., Wiederhold, K. H., Pauli, C., Ermini, F., Stalder, M., Schnell, L., . . . Staufenbiel, M. (2001). Abeta-induced inflammatory processes in microglia cells of APP23 transgenic mice. *Am J Pathol, 158*(1), 63-73.

Boukhzar, L., Hamieh, A., Cartier, D., Tanguy, Y., Alsharif, I., Castex, M., . . . Anouar, Y. (2016). Selenoprotein T Exerts an Essential Oxidoreductase Activity That Protects

Dopaminergic Neurons in Mouse Models of Parkinson's Disease. *Antioxid Redox Signal, 24*(11), 557-574. doi:10.1089/ars.2015.6478
Bourgeois, J. P., Goldman-Rakic, P. S., & Rakic, P. (1994). Synaptogenesis in the prefrontal cortex of rhesus monkeys. *Cereb Cortex, 4*(1), 78-96.
Braak, H., & Braak, E. (1985). On areas of transition between entorhinal allocortex and temporal isocortex in the human brain. Normal morphology and lamina-specific pathology in Alzheimer's disease. *Acta Neuropathol, 68*(4), 325-332. doi:10.1007/bf00690836
Braak, H., & Braak, E. (1991). Neuropathological stageing of Alzheimer-related changes. *Acta Neuropathol, 82*(4), 239-259.
Bradley-Whitman, M. A., & Lovell, M. A. (2013). Epigenetic changes in the progression of Alzheimer's disease. *Mech Ageing Dev, 134*(10), 486-495. doi:10.1016/j.mad.2013.08.005
Bramham, C. R., & Messaoudi, E. (2005). BDNF function in adult synaptic plasticity: the synaptic consolidation hypothesis. *Prog Neurobiol, 76*(2), 99-125. doi:10.1016/j.pneurobio.2005.06.003
Brandt, R., & Bakota, L. (2017). Microtubule dynamics and the neurodegenerative triad of Alzheimer's disease: The hidden connection. *Journal of Neurochemistry, 143*(4), 409-417. doi:10.1111/jnc.14011
Brayne, C., Ince, P. G., Keage, H. A., McKeith, I. G., Matthews, F. E., Polvikoski, T., & Sulkava, R. (2010). Education, the brain and dementia: neuroprotection or compensation? *Brain, 133*(Pt 8), 2210-2216. doi:10.1093/brain/awq185
Bredy, T. W., Wu, H., Crego, C., Zellhoefer, J., Sun, Y. E., & Barad, M. (2007). Histone modifications around individual BDNF gene promoters in prefrontal cortex are associated with extinction of conditioned fear. *Learn Mem, 14*(4), 268-276. doi:10.1101/lm.500907
Brier, M. R., Gordon, B., Friedrichsen, K., McCarthy, J., Stern, A., Christensen, J., . . . Ances, B. M. (2016). Tau and Aβ imaging, CSF measures, and cognition in Alzheimer's disease. *Science Translational Medicine, 8*(338), 338ra366-338ra366. doi:10.1126/scitranslmed.aaf2362
Britten, R. J., & Davidson, E. H. (1969). Gene regulation for higher cells: a theory. *Science, 165*(3891), 349-357.
Brookmeyer, R., Johnson, E., Ziegler-Graham, K., & Arrighi, H. M. (2007). Forecasting the global burden of Alzheimer’s disease. *Alzheimer's & Dementia: The Journal of the Alzheimer's Association, 3*(3), 186-191. doi:10.1016/j.jalz.2007.04.381
Brown, L., Hansnata, E., & La, H. A. (2017). Economic Cost of Dementia in Australia.
Brownell, J. E., Zhou, J., Ranalli, T., Kobayashi, R., Edmondson, D. G., Roth, S. Y., & Allis, C. D. (1996). Tetrahymena Histone Acetyltransferase A: A Homolog to Yeast Gcn5p Linking Histone Acetylation to Gene Activation. *Cell, 84*(6), 843-851. doi:https://doi.org/10.1016/S0092-8674(00)81063-6
Brun, A., & Englund, E. (1981). Regional pattern of degeneration in Alzheimer's disease: neuronal loss and histopathological grading. *Histopathology, 5*(5), 549-564. doi:10.1111/j.1365-2559.1981.tb01818.x
Buell, S., & Coleman, P. (1979). Dendritic growth in the aged human brain and failure of growth in senile dementia. *Science, 206*(4420), 854-856. doi:10.1126/science.493989
Buell, S. J., & Coleman, P. D. (1981). Quantitative evidence for selective dendritic growth in normal human aging but not in senile dementia. *Brain Research, 214*(1), 23-41.
Buenrostro, J. D., Wu, B., Litzenburger, U. M., Ruff, D., Gonzales, M. L., Snyder, M. P., . . . Greenleaf, W. J. (2015). Single-cell chromatin accessibility reveals principles of regulatory variation. *Nature, 523*(7561), 486-490. doi:10.1038/nature14590

Burke, S. N., & Barnes, C. A. (2006). Neural plasticity in the ageing brain. *Nature Reviews Neuroscience, 7*, 30. doi:10.1038/nrn1809

Caballero, B., & Coto-Montes, A. (2012). An insight into the role of autophagy in cell responses in the aging and neurodegenerative brain. *Histol Histopathol, 27*(3), 263-275. doi:10.14670/hh-27.263

Cabeza, R. (2002). Hemispheric asymmetry reduction in older adults: the HAROLD model. *Psychol Aging, 17*(1), 85-100.

Cajal, R.-y. (1909). *Histologie du système nerveux de l'homme & des vertébrés*. Paris : Maloine: Paris : Maloine.

Calderwood, S. K., Murshid, A., & Prince, T. (2009). The Shock of Aging: Molecular Chaperones and the Heat Shock Response in Longevity and Aging – A Mini-Review. *Gerontology, 55*(5), 550-558. doi:10.1159/000225957

Calfa, G., Chapleau, C. A., Campbell, S., Inoue, T., Morse, S. J., Lubin, F. D., & Pozzo-Miller, L. (2012). HDAC activity is required for BDNF to increase quantal neurotransmitter release and dendritic spine density in CA1 pyramidal neurons. *Hippocampus, 22*(7), 1493-1500. doi:10.1002/hipo.20990

Calhoun, M. E., Wiederhold, K.-H., Abramowski, D., Phinney, A. L., Probst, A., Sturchler-Pierrat, C., . . . Jucker, M. (1998). Neuron loss in APP transgenic mice. *Nature, 395*(6704), 755-756.

Cao, R., Wang, L., Wang, H., Xia, L., Erdjument-Bromage, H., Tempst, P., . . . Zhang, Y. (2002). Role of Histone H3 Lysine 27 Methylation in Polycomb-Group Silencing. *Science, 298*(5595), 1039-1043. doi:10.1126/science.1076997

Carter, C. W. (1978). Histone packing in the nucleosome core particle of chromatin. *Proc Natl Acad Sci U S A, 75*(8), 3649-3653.

Cedar, H., & Bergman, Y. (2009). Linking DNA methylation and histone modification: patterns and paradigms. *Nature Reviews Genetics, 10*(5), 295-304.

Chang, E. H., Savage, M. J., Flood, D. G., Thomas, J. M., Levy, R. B., Mahadomrongkul, V., . . . Huerta, P. T. (2006). AMPA receptor downscaling at the onset of Alzheimer's disease pathology in double knockin mice. *Proc Natl Acad Sci U S A, 103*(9), 3410-3415. doi:10.1073/pnas.0507313103

Chapuis, J., Hansmannel, F., Gistelinck, M., Mounier, A., Van Cauwenberghe, C., Kolen, K. V., . . . Lambert, J. C. (2013). Increased expression of BIN1 mediates Alzheimer genetic risk by modulating tau pathology. *Mol Psychiatry, 18*(11), 1225-1234. doi:10.1038/mp.2013.1

Charles, A. C., Merrill, J. E., Dirksen, E. R., & Sanderson, M. J. (1991). Intercellular signaling in glial cells: calcium waves and oscillations in response to mechanical stimulation and glutamate. *Neuron, 6*(6), 983-992.

Chartier-Harlin, M.-C., Crawford, F., Houlden, H., Warren, A., Hughes, D., Fidani, L., . . . Mullan, M. (1991). Early-onset Alzheimer's disease caused by mutations at codon 717 of the β-amyloid precursor protein gene. *Nature, 353*, 844. doi:10.1038/353844a0

Chen, H., Dzitoyeva, S., & Manev, H. (2012). Effect of aging on 5-hydroxymethylcytosine in the mouse hippocampus. *Restorative Neurology and Neuroscience, 30*(3), 237-245. doi:10.3233/RNN-2012-110223

Chen, L., MacMillan, A. M., Chang, W., Ezaz-Nikpay, K., Lane, W. S., & Verdine, G. L. (1991). Direct identification of the active-site nucleophile in a DNA (cytosine-5)-methyltransferase. *Biochemistry, 30*(46), 11018-11025.

Chen, W., Shieh, C., Swanger, S. A., Tankovic, A., Au, M., McGuire, M., . . . Pierson, T. M. (2017). GRIN1 mutation associated with intellectual disability alters NMDA receptor trafficking and function. *Journal of Human Genetics, 62*(6), 589-597. doi:10.1038/jhg.2017.19

Cheng, T.-L., Chen, J., Wan, H., Tang, B., Tian, W., Liao, L., & Qiu, Z. (2017). Regulation of mRNA splicing by MeCP2 via epigenetic modifications in the brain. *Scientific Reports, 7*, 42790. doi:10.1038/srep42790

Cheung, I., Shulha, H. P., Jiang, Y., Matevossian, A., Wang, J., Weng, Z., & Akbarian, S. (2010). Developmental regulation and individual differences of neuronal H3K4me3 epigenomes in the prefrontal cortex. *Proc Natl Acad Sci U S A, 107*(19), 8824-8829. doi:10.1073/pnas.1001702107

Chibnik, L. B., Yu, L., Eaton, M. L., Srivastava, G., Schneider, J. A., Kellis, M., . . . De Jager, P. L. (2015). Alzheimer's loci: epigenetic associations and interaction with genetic factors. *Annals of Clinical and Translational Neurology, 2*(6), 636-647. doi:10.1002/acn3.201

Chinta, S. J., Woods, G., Rane, A., Demaria, M., Campisi, J., & Andersen, J. K. (2015). Cellular senescence and the aging brain. *Experimental Gerontology, 68*, 3-7. doi:https://doi.org/10.1016/j.exger.2014.09.018

Chouliaras, L., Mastroeni, D., Delvaux, E., Grover, A., Kenis, G., Hof, P. R., . . . van den Hove, D. L. (2013). Consistent decrease in global DNA methylation and hydroxymethylation in the hippocampus of Alzheimer's disease patients. *Neurobiol Aging, 34*(9), 2091-2099. doi:10.1016/j.neurobiolaging.2013.02.021

Choy, J. S., Wei, S., Lee, J. Y., Tan, S., Chu, S., & Lee, T. H. (2010). DNA methylation increases nucleosome compaction and rigidity. *J Am Chem Soc, 132*(6), 1782-1783. doi:10.1021/ja910264z

Christensen, B. C., Houseman, E. A., Marsit, C. J., Zheng, S., Wrensch, M. R., Wiemels, J. L., . . . Kelsey, K. T. (2009). Aging and environmental exposures alter tissue-specific DNA methylation dependent upon CpG island context. *PLoS Genet, 5*(8), e1000602. doi:10.1371/journal.pgen.1000602

Citron, M., Oltersdorf, T., Haass, C., McConlogue, L., Hung, A. Y., Seubert, P., . . . Selkoe, D. J. (1992). Mutation of the [beta]-amyloid precursor protein in familial Alzheimer's disease increases [beta]-protein production. *Nature, 360*(6405), 672-674.

Clark, S. J., Smallwood, S. A., Lee, H. J., Krueger, F., Reik, W., & Kelsey, G. (2017). Genome-wide base-resolution mapping of DNA methylation in single cells using single-cell bisulfite sequencing (scBS-seq). *Nature Protocols, 12*, 534. doi:10.1038/nprot.2016.187

https://www.nature.com/articles/nprot.2016.187#supplementary-information

Cleary, J. P., Walsh, D. M., Hofmeister, J. J., Shankar, G. M., Kuskowski, M. A., Selkoe, D. J., & Ashe, K. H. (2004). Natural oligomers of the amyloid-β protein specifically disrupt cognitive function. *Nature neuroscience, 8*, 79. doi:10.1038/nn1372

https://www.nature.com/articles/nn1372#supplementary-information

Cleary, J. P., Walsh, D. M., Hofmeister, J. J., Shankar, G. M., Kuskowski, M. A., Selkoe, D. J., & Ashe, K. H. (2005). Natural oligomers of the amyloid-β protein specifically disrupt cognitive function. *Nature neuroscience, 8*(1), 79-84.

Cleveland, D. W., Hwo, S. Y., & Kirschner, M. W. (1977). Purification of tau, a microtubule-associated protein that induces assembly of microtubules from purified tubulin. *J Mol Biol, 116*(2), 207-225.

Cochran, J. N., Hall, A. M., & Roberson, E. D. (2014). The dendritic hypothesis for Alzheimer's disease pathophysiology. *Brain Research Bulletin, 103*, 18-28. doi:10.1016/j.brainresbull.2013.12.004

Colantuoni, C., Lipska, B. K., Ye, T., Hyde, T. M., Tao, R., Leek, J. T., . . . Kleinman, J. E. (2011). Temporal dynamics and genetic control of transcription in the human prefrontal cortex. *Nature, 478*(7370), 519-523. doi:10.1038/nature10524

Collins, J. M., King, A. E., Woodhouse, A., Kirkcaldie, M. T. K., & Vickers, J. C. (2015). The effect of focal brain injury on beta-amyloid plaque deposition, inflammation and synapses in the APP/PS1 mouse model of Alzheimer's disease. *Exp Neurol, 267*, 219-229. doi:http://dx.doi.org/10.1016/j.expneurol.2015.02.034

Connor, J. R., Menzies, S. L., St Martin, S. M., & Mufson, E. J. (1992). A histochemical study of iron, transferrin, and ferritin in Alzheimer's diseased brains. *J Neurosci Res, 31*(1), 75-83. doi:10.1002/jnr.490310111

Connor, J. R., Snyder, B. S., Beard, J. L., Fine, R. E., & Mufson, E. J. (1992). Regional distribution of iron and iron-regulatory proteins in the brain in aging and Alzheimer's disease. *J Neurosci Res, 31*(2), 327-335. doi:10.1002/jnr.490310214

Consortium, E. P. (2012). An integrated encyclopedia of DNA elements in the human genome. *Nature, 489*(7414), 57-74. doi:10.1038/nature11247

Cooke, M. S., Evans, M. D., Dizdaroglu, M., & Lunec, J. (2003). Oxidative DNA damage: mechanisms, mutation, and disease. *Faseb j, 17*(10), 1195-1214. doi:10.1096/fj.02-0752rev

Coppede, F., & Migliore, L. (2009). DNA damage and repair in Alzheimer's disease. *Curr Alzheimer Res, 6*(1), 36-47.

Coppieters, N., Dieriks, B. V., Lill, C., Faull, R. L., Curtis, M. A., & Dragunow, M. (2013). Global changes in DNA methylation and hydroxymethylation in Alzheimer's disease human brain. *Neurobiol Aging*. doi:10.1016/j.neurobiolaging.2013.11.031

Corder, E., Saunders, A., Strittmatter, W., Schmechel, D., Gaskell, P., Small, G. a., . . . Pericak-Vance, M. A. (1993). Gene dose of apolipoprotein E type 4 allele and the risk of Alzheimer's disease in late onset families. *Science, 261*(5123), 921-923.

Cordy, J. M., Hooper, N. M., & Turner, A. J. (2006). The involvement of lipid rafts in Alzheimer's disease (Review) AU - Cordy, Joanna M. *Molecular Membrane Biology, 23*(1), 111-122. doi:10.1080/09687860500496417

Cordy, J. M., Hussain, I., Dingwall, C., Hooper, N. M., & Turner, A. J. (2003). Exclusively targeting beta-secretase to lipid rafts by GPI-anchor addition up-regulates beta-site processing of the amyloid precursor protein. *Proc Natl Acad Sci U S A, 100*(20), 11735-11740. doi:10.1073/pnas.1635130100

Council, N. H. a. M. R. (2013). Australian code for the care and use of animals for scientific purposes, 8th edition. . Retrieved from

Creyghton, M. P., Cheng, A. W., Welstead, G. G., Kooistra, T., Carey, B. W., Steine, E. J., . . . Jaenisch, R. (2010a). Histone H3K27ac separates active from poised enhancers and predicts developmental state. *Proc Natl Acad Sci U S A, 107*(50), 21931-21936. doi:10.1073/pnas.1016071107

Creyghton, M. P., Cheng, A. W., Welstead, G. G., Kooistra, T., Carey, B. W., Steine, E. J., . . . Jaenisch, R. (2010b). Histone H3K27ac separates active from poised enhancers and predicts developmental state. *Proceedings of the National Academy of Sciences, 107*(50), 21931-21936. doi:10.1073/pnas.1016071107

Cruz, J. C., Tseng, H. C., Goldman, J. A., Shih, H., & Tsai, L. H. (2003). Aberrant Cdk5 activation by p25 triggers pathological events leading to neurodegeneration and neurofibrillary tangles. *Neuron, 40*(3), 471-483.

Crystal, H., Dickson, D., Fuld, P., Masur, D., Scott, R., Mehler, M., . . . Wolfson, L. (1988). Clinico-pathologic studies in dementia: nondemented subjects with pathologically confirmed Alzheimer's disease. *Neurology, 38*(11), 1682-1687.

Cummings, B. J., & Cotman, C. W. (1995). Image analysis of beta-amyloid load in Alzheimer's disease and relation to dementia severity. *Lancet, 346*(8989), 1524-1528.

Czech, C., Tremp, G., & Pradier, L. (2000). Presenilins and Alzheimer's disease: biological functions and pathogenic mechanisms. *Prog Neurobiol, 60*(4), 363-384.

Dagnas, M., Guillou, J.-L., Prévôt, T., & Mons, N. (2013). HDAC Inhibition Facilitates the Switch between Memory Systems in Young But Not Aged Mice. *The Journal of Neuroscience, 33*(5), 1954-1963. doi:10.1523/jneurosci.3453-12.2013

Danka Mohammed, C. P., Park, J. S., Nam, H. G., & Kim, K. (2017). MicroRNAs in brain aging. *Mech Ageing Dev, 168*, 3-9. doi:10.1016/j.mad.2017.01.007

Dateki, M., Horii, T., Kasuya, Y., Mochizuki, R., Nagao, Y., Ishida, J., . . . Fukamizu, A. (2005). Neurochondrin Negatively Regulates CaMKII Phosphorylation, and Nervous System-specific Gene Disruption Results in Epileptic Seizure. *Journal of Biological Chemistry, 280*(21), 20503-20508. doi:10.1074/jbc.M414033200

Davies, M. N., Volta, M., Pidsley, R., Lunnon, K., Dixit, A., Lovestone, S., . . . Mill, J. (2012). Functional annotation of the human brain methylome identifies tissue-specific epigenetic variation across brain and blood. *Genome Biol, 13*(6), R43. doi:10.1186/gb-2012-13-6-r43

Dawkins, E., & Small, D. H. (2014). Insights into the physiological function of the β-amyloid precursor protein: beyond Alzheimer's disease. *Journal of Neurochemistry, 129*(5), 756-769. doi:10.1111/jnc.12675

Day, J. J., Childs, D., Guzman-Karlsson, M. C., Kibe, M., Moulden, J., Song, E., . . . Sweatt, J. D. (2013). DNA methylation regulates associative reward learning. *Nat Neurosci, 16*(10), 1445-1452. doi:10.1038/nn.3504

de Castro, F., López-Mascaraque, L., & De Carlos, J. A. (2007). Cajal: lessons on brain development. *Brain research reviews, 55*(2), 481-489.

De Jager, P. L., Ma, Y., McCabe, C., Xu, J., Vardarajan, B. N., Felsky, D., . . . Bennett, D. A. (2018). A multi-omic atlas of the human frontal cortex for aging and Alzheimer's disease research. *Scientific Data, 5*, 180142. doi:10.1038/sdata.2018.142

De Jager, P. L., Srivastava, G., Lunnon, K., Burgess, J., Schalkwyk, L. C., Yu, L., . . . Bennett, D. A. (2014). Alzheimer's disease: early alterations in brain DNA methylation at ANK1, BIN1, RHBDF2 and other loci. *Nat Neurosci, 17*(9), 1156-1163. doi:10.1038/nn.3786

De Strooper, B., Saftig, P., Craessaerts, K., Vanderstichele, H., Guhde, G., Annaert, W., . . . Van Leuven, F. (1998). Deficiency of presenilin-1 inhibits the normal cleavage of amyloid precursor protein. *Nature, 391*, 387. doi:10.1038/34910

Deaton, A. M., & Bird, A. (2011). CpG islands and the regulation of transcription. *Genes Dev, 25*(10), 1010-1022. doi:10.1101/gad.2037511

Decressac, M., Mattsson, B., Weikop, P., Lundblad, M., Jakobsson, J., & Björklund, A. (2013). TFEB-mediated autophagy rescues midbrain dopamine neurons from α-synuclein toxicity. *Proc Natl Acad Sci U S A, 110*(19), E1817-E1826. doi:10.1073/pnas.1305623110

Demuro, A., Parker, I., & Stutzmann, G. E. (2010). Calcium signaling and amyloid toxicity in Alzheimer disease. *J Biol Chem, 285*(17), 12463-12468. doi:10.1074/jbc.R109.080895

Dhayalan, A., Rajavelu, A., Rathert, P., Tamas, R., Jurkowska, R. Z., Ragozin, S., & Jeltsch, A. (2010). The Dnmt3a PWWP domain reads histone 3 lysine 36 trimethylation and guides DNA methylation. *J Biol Chem, 285*(34), 26114-26120. doi:10.1074/jbc.M109.089433

Diaz, A., Nellore, A., & Song, J. S. (2012). CHANCE: comprehensive software for quality control and validation of ChIP-seq data. *Genome Biol, 13*(10), R98. doi:10.1186/gb-2012-13-10-r98

Dickey, C. A., Loring, J. F., Montgomery, J., Gordon, M. N., Eastman, P. S., & Morgan, D. (2003). Selectively reduced expression of synaptic plasticity-related genes in amyloid precursor protein + presenilin-1 transgenic mice. *J Neurosci, 23*(12), 5219-5226.

Dickson, T. C., King, C. E., McCormack, G. H., & Vickers, J. C. (1999). Neurochemical Diversity of Dystrophic Neurites in the Early and Late Stages of Alzheimer's Disease. *Exp Neurol, 156*(1), 100-110. doi:http://dx.doi.org/10.1006/exnr.1998.7010

Dickson, T. C., & Vickers, J. C. (2001). The morphological phenotype of β-amyloid plaques and associated neuritic changes in Alzheimer's disease. *Neuroscience, 105*(1), 99-107. doi:http://dx.doi.org/10.1016/S0306-4522(01)00169-5

Dickstein, D. L., Weaver, C. M., Luebke, J. I., & Hof, P. R. (2013). Dendritic spine changes associated with normal aging. *Neuroscience, 251*, 21-32. doi:10.1016/j.neuroscience.2012.09.077

Dion, M. F., Altschuler, S. J., Wu, L. F., & Rando, O. J. (2005). Genomic characterization reveals a simple histone H4 acetylation code. *Proc Natl Acad Sci U S A, 102*(15), 5501-5506. doi:10.1073/pnas.0500136102

Douaud, G., Groves, A. R., Tamnes, C. K., Westlye, L. T., Duff, E. P., Engvig, A., . . . Johansen-Berg, H. (2014). A common brain network links development, aging, and vulnerability to disease. *Proceedings of the National Academy of Sciences, 111*(49), 17648. doi:10.1073/pnas.1410378111

Doyle, J. P., Dougherty, J. D., Heiman, M., Schmidt, E. F., Stevens, T. R., Ma, G., . . . Heintz, N. (2008). Application of a Translational Profiling Approach for the Comparative Analysis of CNS Cell Types. *Cell, 135*(4), 749-762. doi:https://doi.org/10.1016/j.cell.2008.10.029

Driver, A. S., Kodavanti, P. R. S., & Mundy, W. R. (2000). Age-related changes in reactive oxygen species production in rat brain homogenates. *Neurotoxicology and Teratology, 22*(2), 175-181. doi:https://doi.org/10.1016/S0892-0362(99)00069-0

Du, J., Johnson, L. M., Jacobsen, S. E., & Patel, D. J. (2015). DNA methylation pathways and their crosstalk with histone methylation. *Nature reviews. Molecular cell biology, 16*(9), 519-532. doi:10.1038/nrm4043

Dyer, M., Phipps, A. J., Mitew, S., Taberlay, P. C., & Woodhouse, A. (2019). Age, but Not Amyloidosis, Induced Changes in Global Levels of Histone Modifications in Susceptible and Disease-Resistant Neurons in Alzheimer's Disease Model Mice. *Frontiers in aging neuroscience, 11*(68). doi:10.3389/fnagi.2019.00068

Eid, A., Bihaqi, S. W., Renehan, W. E., & Zawia, N. H. (2016). Developmental lead exposure and lifespan alterations in epigenetic regulators and their correspondence to biomarkers of Alzheimer's disease. *Alzheimer's & Dementia: Diagnosis, Assessment & Disease Monitoring, 2*, 123-131. doi:http://dx.doi.org/10.1016/j.dadm.2016.02.002

Elder, G. A., Gama Sosa, M. A., & De Gasperi, R. (2010). Transgenic Mouse Models of Alzheimer's Disease. *The Mount Sinai journal of medicine, New York, 77*(1), 69-81. doi:10.1002/msj.20159

Erlandsson, A., Enarsson, M., & Forsberg-Nilsson, K. (2001). Immature neurons from CNS stem cells proliferate in response to platelet-derived growth factor. *J Neurosci, 21*(10), 3483-3491.

Ernst, J., & Kellis, M. (2017). Chromatin-state discovery and genome annotation with ChromHMM. *Nature Protocols, 12*, 2478. doi:10.1038/nprot.2017.124

Ewels, P., Magnusson, M., Lundin, S., & Kaller, M. (2016). MultiQC: summarize analysis results for multiple tools and samples in a single report. *Bioinformatics, 32*(19), 3047-3048. doi:10.1093/bioinformatics/btw354

Farlik, M., Sheffield, N. C., Nuzzo, A., Datlinger, P., Schonegger, A., Klughammer, J., & Bock, C. (2015). Single-cell DNA methylome sequencing and bioinformatic inference of epigenomic cell-state dynamics. *Cell Rep, 10*(8), 1386-1397. doi:10.1016/j.celrep.2015.02.001

Fasolino, M., Liu, S., Wang, Y., & Zhou, Z. (2017). Distinct cellular and molecular environments support aging-related DNA methylation changes in the substantia nigra. *Epigenomics, 9*(1), 21-31. doi:10.2217/epi-2016-0084

Feng, J., Zhou, Y., Campbell, S. L., Le, T., Li, E., Sweatt, J. D., . . . Fan, G. (2010a). Dnmt1 and Dnmt3a maintain DNA methylation and regulate synaptic function in adult forebrain neurons. *Nature neuroscience, 13*(4), 423-430.

Feng, J., Zhou, Y., Campbell, S. L., Le, T., Li, E., Sweatt, J. D., . . . Fan, G. (2010b). Dnmt1 and Dnmt3a maintain DNA methylation and regulate synaptic function in adult forebrain neurons. *Nature neuroscience, 13*, 423. doi:10.1038/nn.2514

https://www.nature.com/articles/nn.2514#supplementary-information

Fernandez-Martos, C. M., King, A. E., Atkinson, R. A. K., Woodhouse, A., & Vickers, J. C. Neurofilament light gene deletion exacerbates amyloid, dystrophic neurite, and synaptic pathology in the APP/PS1 transgenic model of Alzheimer's disease. *Neurobiol Aging, 36*(10), 2757-2767. doi:10.1016/j.neurobiolaging.2015.07.003

Ferrándiz, M. L., Martínez, M., De Juan, E., Díez, A., Bustos, G., & Miquel, J. (1994). Impairment of mitochondrial oxidative phosphorylation in the brain of aged mice. *Brain Research, 644*(2), 335-338. doi:https://doi.org/10.1016/0006-8993(94)91699-3

Ferrari, K. J., Scelfo, A., Jammula, S., Cuomo, A., Barozzi, I., Stutzer, A., . . . Pasini, D. (2014). Polycomb-dependent H3K27me1 and H3K27me2 regulate active transcription and enhancer fidelity. *Mol Cell, 53*(1), 49-62. doi:10.1016/j.molcel.2013.10.030

Finch, J. T., & Klug, A. (1976). Solenoidal model for superstructure in chromatin. *Proc Natl Acad Sci U S A, 73*(6), 1897-1901.

Fink, A. L. (1998). Protein aggregation: folding aggregates, inclusion bodies and amyloid. *Folding and Design, 3*(1), R9-R23. doi:https://doi.org/10.1016/S1359-0278(98)00002-9

Fischer, A., Sananbenesi, F., Wang, X., Dobbin, M., & Tsai, L.-H. (2007a). Recovery of learning and memory is associated with chromatin remodelling. *Nature, 447*(7141), 178-182.

Fischer, A., Sananbenesi, F., Wang, X., Dobbin, M., & Tsai, L.-H. (2007b). Recovery of learning and memory is associated with chromatin remodelling. *Nature, 447*, 178. doi:10.1038/nature05772

https://www.nature.com/articles/nature05772#supplementary-information

Fischle, W., Tseng, B. S., Dormann, H. L., Ueberheide, B. M., Garcia, B. A., Shabanowitz, J., . . . Allis, C. D. (2005). Regulation of HP1–chromatin binding by histone H3 methylation and phosphorylation. *Nature, 438*, 1116. doi:10.1038/nature04219

https://www.nature.com/articles/nature04219#supplementary-information

Fleminger, S., Oliver, D., Lovestone, S., Rabe-Hesketh, S., & Giora, A. (2003). Head injury as a risk factor for Alzheimer's disease: the evidence 10 years on; a partial replication. *Journal of Neurology, Neurosurgery, and Psychiatry, 74*(7), 857-862. doi:10.1136/jnnp.74.7.857

Fonseca, M., & Soriano, E. (1995). Calretinin-immunoreactive neurons in the normal human temporal cortex and in Alzheimer's disease. *Brain Res, 691*(1-2), 83-91.

Ford, E. E., Grimmer, M. R., Stolzenburg, S., Bogdanovic, O., de Mendoza, A., Farnham, P. J., . . . Lister, R. (2017). Frequent lack of repressive capacity of promoter DNA methylation identified through genome-wide epigenomic manipulation. *bioRxiv*.

Förstl, H., & Kurz, A. (1999). Clinical features of Alzheimer's disease. *European Archives of Psychiatry and Clinical Neuroscience, 249*(6), 288-290. doi:10.1007/s004060050101

Fox, J. G., Barthold, S., Davisson, M., Newcomer, C. E., Quimby, F. W., & Smith, A. (2006). *The mouse in biomedical research: normative biology, husbandry, and models* (Vol. 3): Elsevier.

Francis, Y. I., Fà, M., Ashraf, H., Zhang, H., Staniszewski, A., Latchman, D. S., & Arancio, O. (2009). Dysregulation of histone acetylation in the APP/PS1 mouse model of Alzheimer's disease. *J Alzheimers Dis, 18*(1), 131-139. doi:10.3233/jad-2009-1134

Fraser, H. B., Khaitovich, P., Plotkin, J. B., Pääbo, S., & Eisen, M. B. (2005). Aging and Gene Expression in the Primate Brain. *PLoS Biology, 3*(9), e274. doi:10.1371/journal.pbio.0030274

Fu, Y., Rusznak, Z., Herculano-Houzel, S., Watson, C., & Paxinos, G. (2013). Cellular composition characterizing postnatal development and maturation of the mouse brain and spinal cord. *Brain Struct Funct, 218*(5), 1337-1354. doi:10.1007/s00429-012-0462-x

Fuks, F., Hurd, P. J., Wolf, D., Nan, X., Bird, A. P., & Kouzarides, T. (2003). The methyl-CpG-binding protein MeCP2 links DNA methylation to histone methylation. *J Biol Chem, 278*(6), 4035-4040. doi:10.1074/jbc.M210256200

Fuso, A., Nicolia, V., Cavallaro, R. A., Ricceri, L., D'Anselmi, F., Coluccia, P., . . . Scarpa, S. (2008). B-vitamin deprivation induces hyperhomocysteinemia and brain S-adenosylhomocysteine, depletes brain S-adenosylmethionine, and enhances PS1 and BACE expression and amyloid-β deposition in mice. *Molecular and Cellular Neuroscience, 37*(4), 731-746. doi:https://doi.org/10.1016/j.mcn.2007.12.018

Fuso, A., Seminara, L., Cavallaro, R. A., D'Anselmi, F., & Scarpa, S. (2005). S-adenosylmethionine/homocysteine cycle alterations modify DNA methylation status with consequent deregulation of PS1 and BACE and beta-amyloid production. *Molecular and Cellular Neuroscience, 28*(1), 195-204. doi:10.1016/j.mcn.2004.09.007

Gallagher, J. J., Minogue, A. M., & Lynch, M. A. (2013). Impaired performance of female APP/PS1 mice in the Morris water maze is coupled with increased Abeta accumulation and microglial activation. *Neurodegener Dis, 11*(1), 33-41. doi:10.1159/000337458

Garcia-Alloza, M., Robbins, E. M., Zhang-Nunes, S. X., Purcell, S. M., Betensky, R. A., Raju, S., . . . Frosch, M. P. (2006). Characterization of amyloid deposition in the APPswe/PS1dE9 mouse model of Alzheimer disease. *Neurobiol Dis, 24*(3), 516-524. doi:http://dx.doi.org/10.1016/j.nbd.2006.08.017

Gasparoni, G., Bultmann, S., Lutsik, P., Kraus, T. F. J., Sordon, S., Vlcek, J., . . . Walter, J. (2018). DNA methylation analysis on purified neurons and glia dissects age and Alzheimer's disease-specific changes in the human cortex. *Epigenetics Chromatin, 11*(1), 41. doi:10.1186/s13072-018-0211-3

Gates, L. A., Shi, J., Rohira, A. D., Feng, Q., Zhu, B., Bedford, M. T., . . . O'Malley, B. W. (2017). Acetylation on histone H3 lysine 9 mediates a switch from transcription initiation to elongation. *Journal of Biological Chemistry*. doi:10.1074/jbc.M117.802074

Ghosh, K., Agarwal, P., & Haggerty, G. (2011). Alzheimer's Disease – Not an Exaggeration of Healthy Aging. *Indian Journal of Psychological Medicine, 33*(2), 106-114. doi:10.4103/0253-7176.92047

Giri, M., Zhang, M., & Lü, Y. (2016). Genes associated with Alzheimer's disease: an overview and current status. *Clinical interventions in aging, 11*, 665-681. doi:10.2147/CIA.S105769

Gjoneska, E., Pfenning, A. R., Mathys, H., Quon, G., Kundaje, A., Tsai, L.-H., & Kellis, M. (2015). Conserved epigenomic signals in mice and humans reveal immune basis of Alzheimer/'s disease. *Nature, 518*(7539), 365-369. doi:10.1038/nature14252

http://www.nature.com/nature/journal/v518/n7539/abs/nature14252.html#supplementary-information

Goate, A., Chartier-Harlin, M.-C., Mullan, M., Brown, J., Crawford, F., Fidani, L., . . . Hardy, J. (1991). Segregation of a missense mutation in the amyloid precursor protein gene with familial Alzheimer's disease. *Nature, 349*(6311), 704-706.

Goedert, M., Spillantini, M. G., Jakes, R., Rutherford, D., & Crowther, R. A. (1989). Multiple isoforms of human microtubule-associated protein tau: sequences and localization in neurofibrillary tangles of Alzheimer's disease. *Neuron, 3*(4), 519-526.

Gomez-Arboledas, A., Davila, J. C., Sanchez-Mejias, E., Navarro, V., Nunez-Diaz, C., Sanchez-Varo, R., . . . Gutierrez, A. (2018). Phagocytic clearance of presynaptic dystrophies by reactive astrocytes in Alzheimer's disease. *Glia, 66*(3), 637-653. doi:10.1002/glia.23270

Govindarajan, N., Rao, P., Burkhardt, S., Sananbenesi, F., Schluter, O. M., Bradke, F., . . . Fischer, A. (2013). Reducing HDAC6 ameliorates cognitive deficits in a mouse model for Alzheimer's disease. *EMBO Mol Med, 5*(1), 52-63. doi:10.1002/emmm.201201923

Gowrishankar, S., Yuan, P., Wu, Y., Schrag, M., Paradise, S., Grutzendler, J., . . . Ferguson, S. M. (2015). Massive accumulation of luminal protease-deficient axonal lysosomes at Alzheimer's disease amyloid plaques. *Proceedings of the National Academy of Sciences, 112*(28), E3699-E3708. doi:10.1073/pnas.1510329112

Graff, J., Rei, D., Guan, J. S., Wang, W. Y., Seo, J., Hennig, K. M., . . . Tsai, L. H. (2012). An epigenetic blockade of cognitive functions in the neurodegenerating brain. *Nature, 483*(7388), 222-226. doi:10.1038/nature10849

Grothe, M. J., Barthel, H., Sepulcre, J., Dyrba, M., Sabri, O., & Teipel, S. J. (2017). In vivo staging of regional amyloid deposition. *Neurology, 89*(20), 2031-2038. doi:10.1212/wnl.0000000000004643

Grundke-Iqbal, I., Iqbal, K., Quinlan, M., Tung, Y. C., Zaidi, M. S., & Wisniewski, H. M. (1986). Microtubule-associated protein tau. A component of Alzheimer paired helical filaments. *J Biol Chem, 261*(13), 6084-6089.

Gu, G. J., Lund, H., Wu, D., Blokzijl, A., Classon, C., von Euler, G., . . . Kamali-Moghaddam, M. (2013). Role of individual MARK isoforms in phosphorylation of tau at Ser(2)(6)(2) in Alzheimer's disease. *Neuromolecular Med, 15*(3), 458-469. doi:10.1007/s12017-013-8232-3

Gu, X., Sun, J., Li, S., Wu, X., & Li, L. (2013). Oxidative stress induces DNA demethylation and histone acetylation in SH-SY5Y cells: potential epigenetic mechanisms in gene transcription in Aβ production. *Neurobiol Aging, 34*(4), 1069-1079. doi:https://doi.org/10.1016/j.neurobiolaging.2012.10.013

Guo, J. U., Ma, D. K., Mo, H., Ball, M. P., Jang, M.-H., Bonaguidi, M. A., . . . Song, H. (2011). Neuronal activity modifies the DNA methylation landscape in the adult brain. *Nature neuroscience, 14*, 1345. doi:10.1038/nn.2900

https://www.nature.com/articles/nn.2900#supplementary-information

Guo, J. U., Su, Y., Shin, J. H., Shin, J., Li, H., Xie, B., . . . Song, H. (2013). Distribution, recognition and regulation of non-CpG methylation in the adult mammalian brain. *Nature neuroscience, 17*, 215. doi:10.1038/nn.3607

https://www.nature.com/articles/nn.3607#supplementary-information

Hampton, D. W., Webber, D. J., Bilican, B., Goedert, M., Spillantini, M. G., & Chandran, S. (2010). Cell-mediated neuroprotection in a mouse model of human tauopathy. *J Neurosci, 30*(30), 9973-9983. doi:10.1523/jneurosci.0834-10.2010

Handley, E. E., Pitman, K. A., Dawkins, E., Young, K. M., Clark, R. M., Jiang, T. C., . . . Blizzard, C. A. (2017). Synapse Dysfunction of Layer V Pyramidal Neurons Precedes

Neurodegeneration in a Mouse Model of TDP-43 Proteinopathies. *Cereb Cortex, 27*(7), 3630-3647. doi:10.1093/cercor/bhw185

Hardy, J. (2002). The amyloid hypothesis of Alzheimer's disease: progress and problems on the road to therapeutics. *Science (New York, N.Y.), 297*(5580), 353-356. doi:10.1126/science.1072994

Hardy, J., & Selkoe, D. J. (2002). The Amyloid Hypothesis of Alzheimer's Disease: Progress and Problems on the Road to Therapeutics. *Science, 297*(5580), 353-356. doi:10.1126/science.1072994

Hardy, J. A., & Higgins, G. A. (1992). Alzheimer's disease: the amyloid cascade hypothesis. *Science, 256*(5054), 184.

Harold, D., Abraham, R., Hollingworth, P., Sims, R., Gerrish, A., Hamshere, M. L., . . . Williams, J. (2009). Genome-wide association study identifies variants at CLU and PICALM associated with Alzheimer's disease. *Nat Genet, 41*, 1088. doi:10.1038/ng.440

https://www.nature.com/articles/ng.440#supplementary-information

Hartl, F. U., Bracher, A., & Hayer-Hartl, M. (2011). Molecular chaperones in protein folding and proteostasis. *Nature, 475*, 324. doi:10.1038/nature10317

Hatanpää, K., Rapoport, S. I., Brady, D. R., Isaacs, K. R., & Shirao, T. (1999). Loss of Proteins Regulating Synaptic Plasticity in Normal Aging of the Human Brain and in Alzheimer Disease. *Journal of Neuropathology & Experimental Neurology, 58*(6), 637-643. doi:10.1097/00005072-199906000-00008

Heintzman, N. D., Hon, G. C., Hawkins, R. D., Kheradpour, P., Stark, A., Harp, L. F., . . . Ching, C. W. (2009). Histone modifications at human enhancers reflect global cell-type-specific gene expression. *Nature, 459*. doi:10.1038/nature07829

Heintzman, N. D., Stuart, R. K., Hon, G., Fu, Y., Ching, C. W., Hawkins, R. D., . . . Ren, B. (2007). Distinct and predictive chromatin signatures of transcriptional promoters and enhancers in the human genome. *Nat Genet, 39*(3), 311-318. doi:http://www.nature.com/ng/journal/v39/n3/suppinfo/ng1966_S1.html

Heitz, E. (1928). Das Heterochromatin der Moose. I. *Jahrb Wiss Bot, 1*(69), 762-818.

Henley, J. M., & Wilkinson, K. A. (2013). AMPA receptor trafficking and the mechanisms underlying synaptic plasticity and cognitive aging. *Dialogues Clin Neurosci, 15*(1), 11-27.

Hernandez, D. G., Nalls, M. A., Gibbs, J. R., Arepalli, S., van der Brug, M., Chong, S., . . . Traynor, B. J. (2011). Distinct DNA methylation changes highly correlated with chronological age in the human brain. *Human molecular genetics, 20*(6), 1164-1172.

Hirabayashi, Y., & Gotoh, Y. (2005). Stage-dependent fate determination of neural precursor cells in mouse forebrain. *Neuroscience Research, 51*(4), 331-336. doi:https://doi.org/10.1016/j.neures.2005.01.004

Hirabayashi, Y., Itoh, Y., Tabata, H., Nakajima, K., Akiyama, T., Masuyama, N., & Gotoh, Y. (2004). The Wnt/beta-catenin pathway directs neuronal differentiation of cortical neural precursor cells. *Development, 131*(12), 2791-2801. doi:10.1242/dev.01165

Hirschhorn, J. N., Brown, S. A., Clark, C. D., & Winston, F. (1992). Evidence that SNF2/SWI2 and SNF5 activate transcription in yeast by altering chromatin structure. *Genes Dev, 6*(12a), 2288-2298.

Hnisz, D., Abraham, Brian J., Lee, Tong I., Lau, A., Saint-André, V., Sigova, Alla A., . . . Young, Richard A. (2013). Super-Enhancers in the Control of Cell Identity and Disease. *Cell, 155*(4), 934-947. doi:10.1016/j.cell.2013.09.053

Ho, P. I., Ashline, D., Dhitavat, S., Ortiz, D., Collins, S. C., Shea, T. B., & Rogers, E. (2003). Folate deprivation induces neurodegeneration: roles of oxidative stress and increased homocysteine. *Neurobiol Dis, 14*(1), 32-42.

Hochberg, Z., Feil, R., Constancia, M., Fraga, M., Junien, C., Carel, J. C., . . . Albertsson-Wikland, K. (2011). Child health, developmental plasticity, and epigenetic programming. *Endocr Rev, 32*(2), 159-224. doi:10.1210/er.2009-0039

Hof, P. R., Cox, K., & Morrison, J. H. (1990). Quantitative analysis of a vulnerable subset of pyramidal neurons in Alzheimer's disease: I. Superior frontal and inferior temporal cortex. *J Comp Neurol, 301*(1), 44-54. doi:10.1002/cne.903010105

Hof, P. R., & Morrison, J. H. (1990). Quantitative analysis of a vulnerable subset of pyramidal neurons in Alzheimer's disease: II. Primary and secondary visual cortex. *J Comp Neurol, 301*(1), 55-64. doi:10.1002/cne.903010106

Hof, P. R., Nimchinsky, E. A., Celio, M. R., Bouras, C., & Morrison, J. H. (1993). Calretinin-immunoreactive neocortical interneurons are unaffected in Alzheimer's disease. *Neurosci Lett, 152*(1-2), 145-148.

Holliday, R., & Pugh, J. (1975). DNA modification mechanisms and gene activity during development. *Science, 187*(4173), 226-232. doi:10.1126/science.187.4173.226

Holtmaat, A., & Svoboda, K. (2009). Experience-dependent structural synaptic plasticity in the mammalian brain. *Nature Reviews Neuroscience, 10*, 647. doi:10.1038/nrn2699

https://www.nature.com/articles/nrn2699#supplementary-information

Hong, L., Schroth, G. P., Matthews, H. R., Yau, P., & Bradbury, E. M. (1993). Studies of the DNA binding properties of histone H4 amino terminus. Thermal denaturation studies reveal that acetylation markedly reduces the binding constant of the H4 "tail" to DNA. *J Biol Chem, 268*(1), 305-314.

Hotchkiss, R. D. (1948). The quantitative separation of purines, pyrimidines, and nucleosides by paper chromatography. *J Biol Chem, 175*(1), 315-332.

Houtman, S. H., Rutteman, M., De Zeeuw, C. I., & French, P. J. (2007). Echinoderm microtubule-associated protein like protein 4, a member of the echinoderm microtubule-associated protein family, stabilizes microtubules. *Neuroscience, 144*(4), 1373-1382. doi:10.1016/j.neuroscience.2006.11.015

Hradek, A. C., Lee, H.-P., Siedlak, S. L., Torres, S. L., Jung, W., Han, A. H., & Lee, H.-g. (2015). Distinct chronology of neuronal cell cycle re-entry and tau pathology in the 3xTg-AD mouse model and Alzheimer's disease patients. *J Alzheimers Dis, 43*(1), 57-65. doi:10.3233/JAD-141083

Hsiao, K., Chapman, P., Nilsen, S., Eckman, C., Harigaya, Y., Younkin, S., . . . Cole, G. (1996). Correlative memory deficits, Abeta elevation, and amyloid plaques in transgenic mice. *Science, 274*(5284), 99-102.

Hsu, A. L., Murphy, C. T., & Kenyon, C. (2003). Regulation of aging and age-related disease by DAF-16 and heat-shock factor. *Science, 300*(5622), 1142-1145. doi:10.1126/science.1083701

Hu, X., Pickering, E., Liu, Y. C., Hall, S., Fournier, H., Katz, E., . . . Soares, H. (2011). Meta-analysis for genome-wide association study identifies multiple variants at the BIN1 locus associated with late-onset Alzheimer's disease. *PLoS One, 6*(2), e16616. doi:10.1371/journal.pone.0016616

Huang, Y., Fang, J., Bedford, M. T., Zhang, Y., & Xu, R.-M. (2006). Recognition of Histone H3 Lysine-4 Methylation by the Double Tudor Domain of JMJD2A. *Science, 312*(5774), 748-751. doi:10.1126/science.1125162

Ikonomidou, C., Bosch, F., Miksa, M., Bittigau, P., Vöckler, J., Dikranian, K., . . . Olney, J. W. (1999). Blockade of NMDA Receptors and Apoptotic Neurodegeneration in the Developing Brain. *Science, 283*(5398), 70-74. doi:10.1126/science.283.5398.70

Ioshikhes, I. P., & Zhang, M. Q. (2000). Large-scale human promoter mapping using CpG islands. *Nat Genet, 26*, 61. doi:10.1038/79189

Irizarry, M. C., McNamara, M., Fedorchak, K., Hsiao, K., & Hyman, B. T. (1997). APPSw transgenic mice develop age-related A beta deposits and neuropil abnormalities, but no neuronal loss in CA1. *J Neuropathol Exp Neurol, 56*(9), 965-973.

Irizarry, M. C., Soriano, F., McNamara, M., Page, K. J., Schenk, D., Games, D., & Hyman, B. T. (1997). Abeta deposition is associated with neuropil changes, but not with overt neuronal loss in the human amyloid precursor protein V717F (PDAPP) transgenic mouse. *J Neurosci, 17*(18), 7053-7059.

Islam, S., Zeisel, A., Joost, S., La Manno, G., Zajac, P., Kasper, M., . . . Linnarsson, S. (2014). Quantitative single-cell RNA-seq with unique molecular identifiers. *Nat Methods, 11*(2), 163-166. doi:10.1038/nmeth.2772

Itagaki, S., McGeer, P. L., Akiyama, H., Zhu, S., & Selkoe, D. (1989). Relationship of microglia and astrocytes to amyloid deposits of Alzheimer disease. *Journal of Neuroimmunology, 24*(3), 173-182. doi:10.1016/0165-5728(89)90115-X

Ito, S., D'Alessio, A. C., Taranova, O. V., Hong, K., Sowers, L. C., & Zhang, Y. (2010). Role of Tet proteins in 5mC to 5hmC conversion, ES-cell self-renewal and inner cell mass specification. *Nature, 466*(7310), 1129-1133. doi:10.1038/nature09303

Jaenisch, R., & Bird, A. (2003). Epigenetic regulation of gene expression: how the genome integrates intrinsic and environmental signals. *Nat Genet, 33 Suppl*, 245-254. doi:10.1038/ng1089

Jaenisch, R., & Bird, A. (2003). Epigenetic regulation of gene expression: how the genome integrates intrinsic and environmental signals. *Nat Genet, 33*, 245. doi:10.1038/ng1089

Jankowsky, J. L., Fadale, D. J., Anderson, J., Xu, G. M., Gonzales, V., Jenkins, N. A., . . . Borchelt, D. R. (2004). Mutant presenilins specifically elevate the levels of the 42 residue beta-amyloid peptide in vivo: evidence for augmentation of a 42-specific gamma secretase. *Hum Mol Genet, 13*(2), 159-170. doi:10.1093/hmg/ddh019

Jean, D. C., & Baas, P. W. (2013). It cuts two ways: microtubule loss during Alzheimer disease. *Embo j, 32*(22), 2900-2902. doi:10.1038/emboj.2013.219

Jenuwein, T., & Allis, C. D. (2001). Translating the histone code. *Science, 293*(5532), 1074-1080. doi:10.1126/science.1063127

Jia, D., Jurkowska, R. Z., Zhang, X., Jeltsch, A., & Cheng, X. (2007). Structure of Dnmt3a bound to Dnmt3L suggests a model for de novo DNA methylation. *Nature, 449*(7159), 248-251. doi:10.1038/nature06146

Jiang, Y., Matevossian, A., Huang, H.-S., Straubhaar, J., & Akbarian, S. (2008). Isolation of neuronal chromatin from brain tissue. *BMC neuroscience, 9*(1), 42.

Jin, F., Li, Y., Dixon, J. R., Selvaraj, S., Ye, Z., Lee, A. Y., . . . Ren, B. (2013). A high-resolution map of the three-dimensional chromatin interactome in human cells. *Nature, 503*(7475), 290-294. doi:10.1038/nature12644

Jjingo, D., Conley, A. B., Yi, S. V., Lunyak, V. V., & Jordan, I. K. (2012). On the presence and role of human gene-body DNA methylation. *Oncotarget, 3*(4), 462-474.

Johnson, D. S., Mortazavi, A., Myers, R. M., & Wold, B. (2007). Genome-wide mapping of in vivo protein-DNA interactions. *Science, 316*(5830), 1497-1502. doi:10.1126/science.1141319

Jones, P. A. (2012). Functions of DNA methylation: islands, start sites, gene bodies and beyond. *Nat Rev Genet, 13*(7), 484-492.

Jones, P. A., & Liang, G. (2009). Rethinking how DNA Methylation Patterns are Maintained. *Nature reviews. Genetics, 10*(11), 805-811. doi:10.1038/nrg2651

Jones, P. A., & Taylor, S. M. (1980). Cellular differentiation, cytidine analogs and DNA methylation. *Cell, 20*(1), 85-93.

Jones, P. L., Jan Veenstra, G. C., Wade, P. A., Vermaak, D., Kass, S. U., Landsberger, N., . . . Wolffe, A. P. (1998). Methylated DNA and MeCP2 recruit histone deacetylase to repress transcription. *Nat Genet, 19*, 187. doi:10.1038/561

Jonsson, T., Atwal, J. K., Steinberg, S., Snaedal, J., Jonsson, P. V., Bjornsson, S., . . . Stefansson, K. (2012). A mutation in APP protects against Alzheimer's disease and age-related cognitive decline. *Nature, 488*, 96. doi:10.1038/nature11283

https://www.nature.com/articles/nature11283#supplementary-information

Kalinowska, M., Chávez, A. E., Lutzu, S., Castillo, P. E., Bukauskas, F. F., & Francesconi, A. (2015). Actinin-4 Governs Dendritic Spine Dynamics and Promotes Their Remodeling by Metabotropic Glutamate Receptors. *J Biol Chem, 290*(26), 15909-15920. doi:10.1074/jbc.M115.640136

Kalpouzos, G., Persson, J., & Nyberg, L. (2012). Local brain atrophy accounts for functional activity differences in normal aging. *Neurobiol Aging, 33*(3), 623.e621-623.e613. doi:10.1016/j.neurobiolaging.2011.02.021

Kang, J., Lemaire, H. G., Unterbeck, A., Salbaum, J. M., Masters, C. L., Grzeschik, K. H., . . . Muller-Hill, B. (1987). The precursor of Alzheimer's disease amyloid A4 protein resembles a cell-surface receptor. *Nature, 325*(6106), 733-736. doi:10.1038/325733a0

Karch, C. M., & Goate, A. M. (2015). Alzheimer's disease risk genes and mechanisms of disease pathogenesis. *Biol Psychiatry, 77*(1), 43-51. doi:10.1016/j.biopsych.2014.05.006

Karp, A., Andel, R., Parker, M. G., Wang, H. X., Winblad, B., & Fratiglioni, L. (2009). Mentally stimulating activities at work during midlife and dementia risk after age 75: follow-up study from the Kungsholmen Project. *Am J Geriatr Psychiatry, 17*(3), 227-236. doi:10.1097/JGP.0b013e318190b691

Kelly, P. H., Bondolfi, L., Hunziker, D., Schlecht, H. P., Carver, K., Maguire, E., . . . Sommer, B. (2003). Progressive age-related impairment of cognitive behavior in APP23 transgenic mice. *Neurobiol Aging, 24*(2), 365-378.

Kelly, T. K., Liu, Y., Lay, F. D., Liang, G., Berman, B. P., & Jones, P. A. (2012). Genome-wide mapping of nucleosome positioning and DNA methylation within individual DNA molecules. *Genome Res, 22*(12), 2497-2506. doi:10.1101/gr.143008.112

Keren-Shaul, H., Spinrad, A., Weiner, A., Matcovitch-Natan, O., Dvir-Szternfeld, R., Ulland, T. K., . . . Amit, I. (2017). A Unique Microglia Type Associated with Restricting Development of Alzheimer's Disease. *Cell, 169*(7), 1276-1290.e1217. doi:https://doi.org/10.1016/j.cell.2017.05.018

Khan, A., & Zhang, X. (2016). dbSUPER: a database of super-enhancers in mouse and human genome. *Nucleic Acids Res, 44*(D1), D164-171. doi:10.1093/nar/gkv1002

Khandelwal, P. J., Herman, A. M., & Moussa, C. E. H. (2011). Inflammation in the early stages of neurodegenerative pathology. *Journal of Neuroimmunology, 238*(1-2), 1-11. doi:10.1016/j.jneuroim.2011.07.002

Kidder, B. L., Hu, G., & Zhao, K. (2011). ChIP-Seq: Technical Considerations for Obtaining High Quality Data. *Nature immunology, 12*(10), 918-922. doi:10.1038/ni.2117

Kikis, E. A., Gidalevitz, T., & Morimoto, R. I. (2010). Protein homeostasis in models of aging and age-related conformational disease. *Adv Exp Med Biol, 694*, 138-159.

Kilgore, M., Miller, C. A., Fass, D. M., Hennig, K. M., Haggarty, S. J., Sweatt, J. D., & Rumbaugh, G. (2009). Inhibitors of Class 1 Histone Deacetylases Reverse Contextual

Memory Deficits in a Mouse Model of Alzheimer's Disease. *Neuropsychopharmacology, 35*(4), 870-880. doi:http://www.nature.com/npp/journal/v35/n4/suppinfo/npp2009197s1.html

Kim, K. K., Adelstein, R. S., & Kawamoto, S. (2009). Identification of neuronal nuclei (NeuN) as Fox-3, a new member of the Fox-1 gene family of splicing factors. *J Biol Chem, 284*(45), 31052-31061. doi:10.1074/jbc.M109.052969

Kim, K. K., Adelstein, R. S., & Kawamoto, S. (2009). Identification of Neuronal Nuclei (NeuN) as Fox-3, a New Member of the Fox-1 Gene Family of Splicing Factors. *J Biol Chem, 284*(45), 31052-31061. doi:10.1074/jbc.M109.052969

Kleff, S., Andrulis, E. D., Anderson, C. W., & Sternglanz, R. (1995). Identification of a gene encoding a yeast histone H4 acetyltransferase. *J Biol Chem, 270*(42), 24674-24677.

Klein, H.-U., McCabe, C., Gjoneska, E., Sullivan, S. E., Kaskow, B. J., Tang, A., . . . De Jager, P. L. (2019). Epigenome-wide study uncovers large-scale changes in histone acetylation driven by tau pathology in aging and Alzheimer's human brains. *Nature neuroscience, 22*(1), 37-46. doi:10.1038/s41593-018-0291-1

Klimasauskas, S., Kumar, S., Roberts, R. J., & Cheng, X. (1994). Hhal methyltransferase flips its target base out of the DNA helix. *Cell, 76*(2), 357-369. doi:https://doi.org/10.1016/0092-8674(94)90342-5

Koch, L. (2018). Altered splicing in Alzheimer transcriptomes. *Nature Reviews Genetics, 19*(12), 738-739. doi:10.1038/s41576-018-0064-4

Koffie, R. M., Meyer-Luehmann, M., Hashimoto, T., Adams, K. W., Mielke, M. L., Garcia-Alloza, M., . . . Spires-Jones, T. L. (2009a). Oligomeric amyloid β associates with postsynaptic densities and correlates with excitatory synapse loss near senile plaques. *Proceedings of the National Academy of Sciences, 106*(10), 4012-4017. doi:10.1073/pnas.0811698106

Koffie, R. M., Meyer-Luehmann, M., Hashimoto, T., Adams, K. W., Mielke, M. L., Garcia-Alloza, M., . . . Spires-Jones, T. L. (2009b). Oligomeric amyloid β associates with postsynaptic densities and correlates with excitatory synapse loss near senile plaques. *Proc Natl Acad Sci U S A, 106*(10), 4012-4017. doi:10.1073/pnas.0811698106

Kok, E., Haikonen, S., Luoto, T., Huhtala, H., Goebeler, S., Haapasalo, H., & Karhunen, P. J. (2009). Apolipoprotein E-dependent accumulation of Alzheimer disease-related lesions begins in middle age. *Ann Neurol, 65*(6), 650-657. doi:10.1002/ana.21696

Koldamova, R., Schug, J., Lefterova, M., Cronican, A. A., Fitz, N. F., Davenport, F. A., . . . Lefterov, I. (2014). Genome-wide approaches reveal EGR1-controlled regulatory networks associated with neurodegeneration. *Neurobiol Dis, 63*, 107-114. doi:10.1016/j.nbd.2013.11.005

Koren, J., 3rd, Jinwal, U. K., Lee, D. C., Jones, J. R., Shults, C. L., Johnson, A. G., . . . Dickey, C. A. (2009). Chaperone signalling complexes in Alzheimer's disease. *Journal of cellular and molecular medicine, 13*(4), 619-630. doi:10.1111/j.1582-4934.2008.00557.x

Kornberg, R. D. (1974). Chromatin structure: a repeating unit of histones and DNA. *Science, 184*(4139), 868-871.

Kouzarides, T. (2007). Chromatin Modifications and Their Function. *Cell, 128*(4), 693-705. doi:https://doi.org/10.1016/j.cell.2007.02.005

Kozlenkov, A., Roussos, P., Timashpolsky, A., Barbu, M., Rudchenko, S., Bibikova, M., . . . Dracheva, S. (2014). Differences in DNA methylation between human neuronal and glial cells are concentrated in enhancers and non-CpG sites. *Nucleic Acids Res, 42*(1), 109-127. doi:10.1093/nar/gkt838

Kozlenkov, A., Wang, M., Roussos, P., Rudchenko, S., Barbu, M., Bibikova, M., . . . Dracheva, S. (2016). Substantial DNA methylation differences between two major neuronal

subtypes in human brain. *Nucleic Acids Res, 44*(6), 2593-2612. doi:10.1093/nar/gkv1304

Kraus, T. F., Guibourt, V., & Kretzschmar, H. A. (2015). 5-Hydroxymethylcytosine, the "Sixth Base", during brain development and ageing. *J Neural Transm (Vienna), 122*(7), 1035-1043. doi:10.1007/s00702-014-1346-4

Kraus, T. F. J., Kilinc, S., Steinmaurer, M., Stieglitz, M., Guibourt, V., & Kretzschmar, H. A. (2016). Profiling of methylation and demethylation pathways during brain development and ageing. *Journal of Neural Transmission, 123*(3), 189-203. doi:10.1007/s00702-015-1469-2

Kuan, C. Y., Roth, K. A., Flavell, R. A., & Rakic, P. (2000). Mechanisms of programmed cell death in the developing brain. *Trends Neurosci, 23*(7), 291-297.

Kuchibhotla, K. V., Goldman, S. T., Lattarulo, C. R., Wu, H.-Y., Hyman, B. T., & Bacskai, B. J. (2008). Abeta plaques lead to aberrant regulation of calcium homeostasis in vivo resulting in structural and functional disruption of neuronal networks. *Neuron, 59*(2), 214-225. doi:10.1016/j.neuron.2008.06.008

Kwok, J. C., Warren, P., & Fawcett, J. W. (2012). Chondroitin sulfate: a key molecule in the brain matrix. *Int J Biochem Cell Biol, 44*(4), 582-586. doi:10.1016/j.biocel.2012.01.004

Lake, B. B., Ai, R., Kaeser, G. E., Salathia, N. S., Yung, Y. C., Liu, R., . . . Zhang, K. (2016). Neuronal subtypes and diversity revealed by single-nucleus RNA sequencing of the human brain. *Science, 352*(6293), 1586-1590. doi:10.1126/science.aaf1204

Lambert, J. C., Heath, S., Even, G., Campion, D., Sleegers, K., Hiltunen, M., . . . Amouyel, P. (2009). Genome-wide association study identifies variants at CLU and CR1 associated with Alzheimer's disease. *Nat Genet, 41*(10), 1094-1099. doi:10.1038/ng.439

Landt, S. G., Marinov, G. K., Kundaje, A., Kheradpour, P., Pauli, F., Batzoglou, S., . . . Snyder, M. (2012). ChIP-seq guidelines and practices of the ENCODE and modENCODE consortia. *Genome Res, 22*(9), 1813-1831. doi:10.1101/gr.136184.111

Langie, S. A. S., Cameron, K. M., Ficz, G., Oxley, D., Tomaszewski, B., Gorniak, J. P., . . . Mathers, J. C. (2017). The Ageing Brain: Effects on DNA Repair and DNA Methylation in Mice. *Genes, 8*(2), 75. doi:10.3390/genes8020075

Langmead, B., & Salzberg, S. L. (2012). Fast gapped-read alignment with Bowtie 2. *Nat Meth, 9*(4), 357-359. doi:10.1038/nmeth.1923

http://www.nature.com/nmeth/journal/v9/n4/abs/nmeth.1923.html#supplementary-information

Lardenoije, R., van den Hove, D. L. A., Havermans, M., van Casteren, A., Le, K. X., Palmour, R., . . . Rutten, B. P. F. (2018). Age-related epigenetic changes in hippocampal subregions of four animal models of Alzheimer's disease. *Molecular and Cellular Neuroscience, 86*, 1-15. doi:https://doi.org/10.1016/j.mcn.2017.11.002

Lashley, T., Gami, P., Valizadeh, N., Li, A., Revesz, T., & Balazs, R. (2014). Alterations in global DNA methylation and hydroxymethylation are not detected in Alzheimer's disease. *Neuropathol Appl Neurobiol*. doi:10.1111/nan.12183

Laurin, D., Verreault, R., Lindsay, J., MacPherson, K., & Rockwood, K. (2001). Physical activity and risk of cognitive impairment and dementia in elderly persons. *Archives of Neurology, 58*(3), 498-504. doi:10.1001/archneur.58.3.498

Lawrence, M., Gentleman, R., & Carey, V. (2009). rtracklayer: an R package for interfacing with genome browsers. *Bioinformatics, 25*(14), 1841-1842. doi:10.1093/bioinformatics/btp328

Le Gras, S., Keime, C., Anthony, A., Lotz, C., De Longprez, L., Brouillet, E., . . . Merienne, K. (2017). Altered enhancer transcription underlies Huntington's disease striatal transcriptional signature. *Scientific Reports, 7*, 42875-42875. doi:10.1038/srep42875

Lee, C. Y. D., & Landreth, G. E. (2010). The role of microglia in amyloid clearance from the AD brain. *J Neural Transm (Vienna), 117*(8), 949-960. doi:10.1007/s00702-010-0433-4

Lee, J. Y., & Lee, T.-H. (2012). Effects of DNA methylation on the structure of nucleosomes. *J Am Chem Soc, 134*(1), 173-175. doi:10.1021/ja210273w

Lee, M. K., & Cleveland, D. W. (1996). Neuronal intermediate filaments. *Annu Rev Neurosci, 19*, 187-217. doi:10.1146/annurev.ne.19.030196.001155

Lehnertz, B., Ueda, Y., Derijck, A. A. H. A., Braunschweig, U., Perez-Burgos, L., Kubicek, S., . . . Peters, A. H. F. M. (2003). Suv39h-Mediated Histone H3 Lysine 9 Methylation Directs DNA Methylation to Major Satellite Repeats at Pericentric Heterochromatin. *Current Biology, 13*(14), 1192-1200. doi:https://doi.org/10.1016/S0960-9822(03)00432-9

Leighton, L. J., Zhao, Q., Li, X., Dai, C., Marshall, P. R., Liu, S., . . . Wei, W. (2018). A Functional Role for the Epigenetic Regulator ING1 in Activity-induced Gene Expression in Primary Cortical Neurons. *Neuroscience, 369*, 248-260. doi:https://doi.org/10.1016/j.neuroscience.2017.11.018

Levenson, J. M., Roth, T. L., Lubin, F. D., Miller, C. A., Huang, I.-C., Desai, P., . . . Sweatt, J. D. (2006). Evidence that DNA (cytosine-5) methyltransferase regulates synaptic plasticity in the hippocampus. *Journal of Biological Chemistry, 281*(23), 15763-15773.

Levy-Lahad, E., Wasco, W., Poorkaj, P., Romano, D., Oshima, J., Pettingell, W., . . . al., e. (1995). Candidate gene for the chromosome 1 familial Alzheimer's disease locus. *Science, 269*(5226), 973-977. doi:10.1126/science.7638622

Lewis, J. D., Meehan, R. R., Henzel, W. J., Maurer-Fogy, I., Jeppesen, P., Klein, F., & Bird, A. (1992). Purification, sequence, and cellular localization of a novel chromosomal protein that binds to methylated DNA. *Cell, 69*(6), 905-914.

Li, H., Handsaker, B., Wysoker, A., Fennell, T., Ruan, J., Homer, N., . . . Durbin, R. (2009). The Sequence Alignment/Map format and SAMtools. *Bioinformatics, 25*(16), 2078-2079. doi:10.1093/bioinformatics/btp352

Li, X., Wei, W., Zhao, Q.-Y., Widagdo, J., Baker-Andresen, D., Flavell, C. R., . . . Bredy, T. W. (2014). Neocortical Tet3-mediated accumulation of 5-hydroxymethylcytosine promotes rapid behavioral adaptation. *Proceedings of the National Academy of Sciences, 111*(19), 7120-7125. doi:10.1073/pnas.1318906111

Li, Y., Sun, H., Chen, Z., Xu, H., Bu, G., & Zheng, H. (2016). Implications of GABAergic Neurotransmission in Alzheimer's Disease. *Frontiers in aging neuroscience, 8*, 31. doi:10.3389/fnagi.2016.00031

Liang, Y. (2019). Emerging Concepts and Functions of Autophagy as a Regulator of Synaptic Components and Plasticity. *Cells, 8*(1). doi:10.3390/cells8010034

Lindroth, A. M., Cao, X., Jackson, J. P., Zilberman, D., McCallum, C. M., Henikoff, S., & Jacobsen, S. E. (2001). Requirement of CHROMOMETHYLASE3 for maintenance of CpXpG methylation. *Science, 292*(5524), 2077-2080. doi:10.1126/science.1059745

Lipinski, M. M., Zheng, B., Lu, T., Yan, Z., Py, B. F., Ng, A., . . . Yuan, J. (2010). Genome-wide analysis reveals mechanisms modulating autophagy in normal brain aging and in Alzheimer's disease. *Proc Natl Acad Sci U S A, 107*(32), 14164-14169. doi:10.1073/pnas.1009485107

Lister, R., Mukamel, E. A., Nery, J. R., Urich, M., Puddifoot, C. A., Johnson, N. D., . . . Ecker, J. R. (2013). Global Epigenomic Reconfiguration During Mammalian Brain Development. *Science, 341*(6146). doi:10.1126/science.1237905

Lister, R., Pelizzola, M., Dowen, R. H., Hawkins, R. D., Hon, G., Tonti-Filippini, J., . . . Ecker, J. R. (2009). Human DNA methylomes at base resolution show widespread epigenomic differences. *Nature, 462*(7271), 315-322. doi:10.1038/nature08514

Liu, C. L., Kaplan, T., Kim, M., Buratowski, S., Schreiber, S. L., Friedman, N., & Rando, O. J. (2005). Single-Nucleosome Mapping of Histone Modifications in S. cerevisiae. *PLoS Biology, 3*(10), e328. doi:10.1371/journal.pbio.0030328

Liu, J., & Jia, G. (2014). Methylation modifications in eukaryotic messenger RNA. *J Genet Genomics, 41*(1), 21-33. doi:10.1016/j.jgg.2013.10.002

Local, A., Huang, H., Albuquerque, C. P., Singh, N., Lee, A. Y., Wang, W., . . . Ren, B. (2018). Identification of H3K4me1-associated proteins at mammalian enhancers. *Nat Genet, 50*(1), 73-82. doi:10.1038/s41588-017-0015-6

Loerch, P. M., Lu, T., Dakin, K. A., Vann, J. M., Isaacs, A., Geula, C., . . . Yankner, B. A. (2008). Evolution of the aging brain transcriptome and synaptic regulation. *PLoS One, 3*(10), e3329-e3329. doi:10.1371/journal.pone.0003329

Lonskaya, I., Hebron, M., Chen, W., Schachter, J., & Moussa, C. (2014). Tau deletion impairs intracellular beta-amyloid-42 clearance and leads to more extracellular plaque deposition in gene transfer models. *Mol Neurodegener, 9*, 46. doi:10.1186/1750-1326-9-46

Lopez-Atalaya, J. P., Ito, S., Valor, L. M., Benito, E., & Barco, A. (2013). Genomic targets, and histone acetylation and gene expression profiling of neural HDAC inhibition. *Nucleic Acids Res, 41*(17), 8072-8084. doi:10.1093/nar/gkt590

López-Muñoz, F., Boya, J., & Alamo, C. (2006). Neuron theory, the cornerstone of neuroscience, on the centenary of the Nobel Prize award to Santiago Ramón y Cajal. *Brain Research Bulletin, 70*(4), 391-405. doi:https://doi.org/10.1016/j.brainresbull.2006.07.010

Lopez, J. R., Lyckman, A., Oddo, S., Laferla, F. M., Querfurth, H. W., & Shtifman, A. (2008). Increased intraneuronal resting [Ca2+] in adult Alzheimer's disease mice. *J Neurochem, 105*(1), 262-271. doi:10.1111/j.1471-4159.2007.05135.x

Lord, J., & Cruchaga, C. (2014a). The epigenetic landscape of Alzheimer's disease. *Nat Neurosci, 17*(9), 1138-1140. doi:10.1038/nn.3792

Lord, J., & Cruchaga, C. (2014b). THE EPIGENETIC LANDSCAPE OF ALZHEIMER'S DISEASE. *Nature neuroscience, 17*(9), 1138-1140. doi:10.1038/nn.3792

Lovell, M. A., Robertson, J. D., Teesdale, W. J., Campbell, J. L., & Markesbery, W. R. (1998). Copper, iron and zinc in Alzheimer's disease senile plaques. *J Neurol Sci, 158*(1), 47-52.

Lu, T., Pan, Y., Kao, S.-Y., Li, C., Kohane, I., Chan, J., & Yankner, B. A. (2004). Gene regulation and DNA damage in the ageing human brain. *Nature, 429*, 883. doi:10.1038/nature02661

https://www.nature.com/articles/nature02661#supplementary-information

Lu, T., Pan, Y., Kao, S. Y., Li, C., Kohane, I., Chan, J., & Yankner, B. A. (2004). Gene regulation and DNA damage in the ageing human brain. *Nature, 429*(6994), 883-891. doi:10.1038/nature02661

Lubin, F. D., Roth, T. L., & Sweatt, J. D. (2008). EPIGENETIC REGULATION OF BDNF GENE TRANSCRIPTION IN THE CONSOLIDATION OF FEAR MEMORY. *The Journal of Neuroscience, 28*(42), 10576-10586. doi:10.1523/JNEUROSCI.1786-08.2008

Lue, L.-F., Kuo, Y.-M., Roher, A. E., Brachova, L., Shen, Y., Sue, L., . . . Rogers, J. (1999). Soluble Amyloid β Peptide Concentration as a Predictor of Synaptic Change in Alzheimer's Disease. *The American Journal of Pathology, 155*(3), 853-862. doi:10.1016/S0002-9440(10)65184-X

Lue, L. F., Brachova, L., Civin, W. H., & Rogers, J. (1996). Inflammation, A beta deposition, and neurofibrillary tangle formation as correlates of Alzheimer's disease neurodegeneration. *J Neuropathol Exp Neurol, 55*(10), 1083-1088.

Luger, K., Mader, A. W., Richmond, R. K., Sargent, D. F., & Richmond, T. J. (1997). Crystal structure of the nucleosome core particle at 2.8 A resolution. *Nature, 389*(6648), 251-260. doi:10.1038/38444

Lukas, W., & Jones, K. A. (1994). Cortical neurons containing calretinin are selectively resistant to calcium overload and excitotoxicity in vitro. *Neuroscience, 61*(2), 307-316.

Lun, A. T., & Smyth, G. K. (2014). De novo detection of differentially bound regions for ChIP-seq data using peaks and windows: controlling error rates correctly. *Nucleic Acids Res, 42*(11), e95. doi:10.1093/nar/gku351

Lun, A. T. L., & Smyth, G. K. (2016). csaw: a Bioconductor package for differential binding analysis of ChIP-seq data using sliding windows. *Nucleic Acids Res, 44*(5), e45. doi:10.1093/nar/gkv1191

Lund, H., Gustafsson, E., Svensson, A., Nilsson, M., Berg, M., Sunnemark, D., & von Euler, G. (2014). MARK4 and MARK3 associate with early tau phosphorylation in Alzheimer's disease granulovacuolar degeneration bodies. *Acta Neuropathol Commun, 2*, 22. doi:10.1186/2051-5960-2-22

Lunnon, K., Smith, R., Hannon, E., De Jager, P. L., Srivastava, G., Volta, M., . . . Mill, J. (2014). Methylomic profiling implicates cortical deregulation of ANK1 in Alzheimer's disease. *Nat Neurosci, 17*(9), 1164-1170. doi:10.1038/nn.3782

http://www.nature.com/neuro/journal/v17/n9/abs/nn.3782.html#supplementary-information

Luo, C., Keown, C. L., Kurihara, L., Zhou, J., He, Y., Li, J., . . . Ecker, J. R. (2017). Single-cell methylomes identify neuronal subtypes and regulatory elements in mammalian cortex. *Science, 357*(6351), 600.

Ma, D. K., Jang, M.-H., Guo, J. U., Kitabatake, Y., Chang, M.-l., Pow-anpongkul, N., . . . Song, H. (2009). Neuronal Activity–Induced Gadd45b Promotes Epigenetic DNA Demethylation and Adult Neurogenesis. *Science, 323*(5917), 1074-1077. doi:10.1126/science.1166859

Maeda, S., Djukic, B., Taneja, P., Yu, G. Q., Lo, I., Davis, A., . . . Mucke, L. (2016). Expression of A152T human tau causes age-dependent neuronal dysfunction and loss in transgenic mice. *EMBO Rep, 17*(4), 530-551. doi:10.15252/embr.201541438

Magi, S., Castaldo, P., Macrì, M. L., Maiolino, M., Matteucci, A., Bastioli, G., . . . Lariccia, V. (2016). Intracellular Calcium Dysregulation: Implications for Alzheimer's Disease. *BioMed Research International, 2016*, 6701324-6701324. doi:10.1155/2016/6701324

Magistri, M., Khoury, N., Mazza, E. M. C., Velmeshev, D., Lee, J. K., Bicciato, S., . . . Faghihi, M. A. (2016). A comparative transcriptomic analysis of astrocytes differentiation from human neural progenitor cells. *The European journal of neuroscience, 44*(10), 2858-2870. doi:10.1111/ejn.13382

Maia, L. F., Kaeser, S. A., Reichwald, J., Hruscha, M., Martus, P., Staufenbiel, M., & Jucker, M. (2013). Changes in amyloid-beta and Tau in the cerebrospinal fluid of transgenic mice overexpressing amyloid precursor protein. *Sci Transl Med, 5*(194), 194re192. doi:10.1126/scitranslmed.3006446

Mandelkow, E. M., Thies, E., Konzack, S., & Mandelkow, E. (2009). Tau and Intracellular Transport in Neurons. In P. H. S. George-Hyslop, W. C. C. Mobley, & Y. Christen (Eds.), *Intracellular Traffic and Neurodegenerative Disorders* (pp. 59-70). Berlin, Heidelberg: Springer Berlin Heidelberg.

Marchand, W. R., Lee, J. N., Suchy, Y., Garn, C., Johnson, S., Wood, N., & Chelune, G. (2011). Age-related changes of the functional architecture of the cortico-basal ganglia circuitry

during motor task execution. *Neuroimage, 55*(1), 194-203. doi:10.1016/j.neuroimage.2010.12.030
Martin, M. (2011). Cutadapt removes adapter sequences from high-throughput sequencing reads. *2011, 17*(1). doi:10.14806/ej.17.1.200

pp. 10-12
Martinez-Lopez, N., Athonvarangkul, D., & Singh, R. (2015). Autophagy and aging. *Adv Exp Med Biol, 847*, 73-87. doi:10.1007/978-1-4939-2404-2_3
Martinowich, K., Hattori, D., Wu, H., Fouse, S., He, F., Hu, Y., . . . Sun, Y. E. (2003). DNA Methylation-Related Chromatin Remodeling in Activity-Dependent Bdnf Gene Regulation. *Science, 302*(5646), 890-893. doi:10.1126/science.1090842
Maruyama, R., Choudhury, S., Kowalczyk, A., Bessarabova, M., Beresford-Smith, B., Conway, T., . . . Polyak, K. (2011). Epigenetic Regulation of Cell Type–Specific Expression Patterns in the Human Mammary Epithelium. *PLoS Genet, 7*(4), e1001369. doi:10.1371/journal.pgen.1001369
Marzi, S. J., Leung, S. K., Ribarska, T., Hannon, E., Smith, A. R., Pishva, E., . . . Mill, J. (2018). A histone acetylome-wide association study of Alzheimer's disease identifies disease-associated H3K27ac differences in the entorhinal cortex. *Nature neuroscience, 21*(11), 1618-1627. doi:10.1038/s41593-018-0253-7
Masliah, E., Mallory, M., Hansen, L., Alford, M., Albright, T., DeTeresa, R., . . . Saitoh, T. (1991). Patterns of aberrant sprouting in alzheimer's disease. *Neuron, 6*(5), 729-739. doi:https://doi.org/10.1016/0896-6273(91)90170-5
Masters, C. L., Simms, G., Weinman, N. A., Multhaup, G., McDonald, B. L., & Beyreuther, K. (1985). Amyloid plaque core protein in Alzheimer disease and Down syndrome. *Proceedings of the National Academy of Sciences, 82*(12), 4245.
Mastroeni, D., Chouliaras, L., Grover, A., Liang, W. S., Hauns, K., Rogers, J., & Coleman, P. D. (2013). Reduced RAN expression and disrupted transport between cytoplasm and nucleus; a key event in Alzheimer's disease pathophysiology. *PLoS One, 8*(1), e53349. doi:10.1371/journal.pone.0053349
Mastroeni, D., Delvaux, E., Nolz, J., Tan, Y., Grover, A., Oddo, S., & Coleman, P. D. (2015). Aberrant intracellular localization of H3k4me3 demonstrates an early epigenetic phenomenon in Alzheimer's disease. *Neurobiol Aging, 36*(12), 3121-3129. doi:10.1016/j.neurobiolaging.2015.08.017
Mastroeni, D., Grover, A., Delvaux, E., Whiteside, C., Coleman, P. D., & Rogers, J. (2010). Epigenetic changes in Alzheimer's disease: decrements in DNA methylation. *Neurobiol Aging, 31*(12), 2025-2037. doi:10.1016/j.neurobiolaging.2008.12.005
Mastroeni, D., McKee, A., Grover, A., Rogers, J., & Coleman, P. D. (2009). Epigenetic Differences in Cortical Neurons from a Pair of Monozygotic Twins Discordant for Alzheimer's Disease. *PLoS One, 4*(8), e6617. doi:10.1371/journal.pone.0006617
Mathys, H., Davila-Velderrain, J., Peng, Z., Gao, F., Mohammadi, S., Young, J. Z., . . . Tsai, L. H. (2019). Single-cell transcriptomic analysis of Alzheimer's disease. *Nature, 570*(7761), 332-337. doi:10.1038/s41586-019-1195-2
Mattiasson, G., Friberg, H., Hansson, M., Elmer, E., & Wieloch, T. (2003). Flow cytometric analysis of mitochondria from CA1 and CA3 regions of rat hippocampus reveals differences in permeability transition pore activation. *J Neurochem, 87*(2), 532-544.
McGhee, J. D., & Felsenfeld, G. (1980). Nucleosome structure. *Annu Rev Biochem, 49*, 1115-1156. doi:10.1146/annurev.bi.49.070180.005343
McKee, A. C., Kowall, N. W., & Kosik, K. S. (1989). Microtubular reorganization and dendritic growth response in alzheimer's disease. *Ann Neurol, 26*(5), 652-659. doi:10.1002/ana.410260511

McLean, C. A., Cherny, R. A., Fraser, F. W., Fuller, S. J., Smith, M. J., Vbeyreuther, K., . . . Masters, C. L. (1999). Soluble pool of Aβ amyloid as a determinant of severity of neurodegeneration in Alzheimer's disease. *Ann Neurol, 46*(6), 860-866.

McLean, C. Y., Bristor, D., Hiller, M., Clarke, S. L., Schaar, B. T., Lowe, C. B., . . . Bejerano, G. (2010). GREAT improves functional interpretation of cis-regulatory regions. *Nature Biotechnology, 28*, 495. doi:10.1038/nbt.1630

https://www.nature.com/articles/nbt.1630#supplementary-information

McShea, A., Harris, P. L., Webster, K. R., Wahl, A. F., & Smith, M. A. (1997). Abnormal expression of the cell cycle regulators P16 and CDK4 in Alzheimer's disease. *The American Journal of Pathology, 150*(6), 1933-1939.

Megee, P. C., Morgan, B. A., & Smith, M. M. (1995). Histone H4 and the maintenance of genome integrity. *Genes Dev, 9*(14), 1716-1727.

Meissner, A., Mikkelsen, T. S., Gu, H., Wernig, M., Hanna, J., Sivachenko, A., . . . Lander, E. S. (2008). Genome-scale DNA methylation maps of pluripotent and differentiated cells. *Nature, 454*(7205), 766-770. doi:10.1038/nature07107

Mellen, M., Ayata, P., Dewell, S., Kriaucionis, S., & Heintz, N. (2012). MeCP2 binds to 5hmC enriched within active genes and accessible chromatin in the nervous system. *Cell, 151*(7), 1417-1430. doi:10.1016/j.cell.2012.11.022

Mendizabal, I., & Yi, S. V. (2016). Whole-genome bisulfite sequencing maps from multiple human tissues reveal novel CpG islands associated with tissue-specific regulation. *Human molecular genetics, 25*(1), 69-82. doi:10.1093/hmg/ddv449

Mifsud, B., Tavares-Cadete, F., Young, A. N., Sugar, R., Schoenfelder, S., Ferreira, L., . . . Osborne, C. S. (2015). Mapping long-range promoter contacts in human cells with high-resolution capture Hi-C. *Nat Genet, 47*, 598. doi:10.1038/ng.3286

https://www.nature.com/articles/ng.3286#supplementary-information

Milde, S., Adalbert, R., Elaman, M. H., & Coleman, M. P. (2015). Axonal transport declines with age in two distinct phases separated by a period of relative stability. *Neurobiol Aging, 36*(2), 971-981. doi:10.1016/j.neurobiolaging.2014.09.018

Miquel, J., Economos, A. C., Fleming, J., & Johnson, J. E. (1980). Mitochondrial role in cell aging. *Experimental Gerontology, 15*(6), 575-591. doi:https://doi.org/10.1016/0531-5565(80)90010-8

Mirsky, A. E., & Silverman, B. (1972). Blocking by Histones of Accessibility to DNA in Chromatin. *Proc Natl Acad Sci U S A, 69*(8), 2115-2119.

Mitew, S., Kirkcaldie, M. T., Dickson, T. C., & Vickers, J. C. (2013a). Altered synapses and gliotransmission in Alzheimer's disease and AD model mice. *Neurobiol Aging, 34*(10), 2341-2351. doi:10.1016/j.neurobiolaging.2013.04.010

Mitew, S., Kirkcaldie, M. T., Dickson, T. C., & Vickers, J. C. (2013b). Neurites containing the neurofilament-triplet proteins are selectively vulnerable to cytoskeletal pathology in Alzheimer's disease and transgenic mouse models. *Front Neuroanat, 7*, 30. doi:10.3389/fnana.2013.00030

Mo, A., Mukamel, Eran A., Davis, Fred P., Luo, C., Henry, Gilbert L., Picard, S., . . . Nathans, J. (2015). Epigenomic Signatures of Neuronal Diversity in the Mammalian Brain. *Neuron, 86*(6), 1369-1384. doi:10.1016/j.neuron.2015.05.018

Moh, C., Kubiak, J. Z., Bajic, V. P., Zhu, X., Smith, M. A., & Lee, H.-G. (2011). Cell cycle deregulation in the neurons of Alzheimer's disease. *Results and problems in cell differentiation, 53*, 565-576. doi:10.1007/978-3-642-19065-0_23

Molyneaux, B. J., Arlotta, P., Menezes, J. R., & Macklis, J. D. (2007). Neuronal subtype specification in the cerebral cortex. *Nat Rev Neurosci, 8*(6), 427-437. doi:10.1038/nrn2151

Moms, J. C., Heyman, A., Mohs, R. C., Hughes, J. P., van Belle, G., Fillenbaum, G., . . . Clark, C. (1989). The Consortium to Establish a Registry for Alzheimer's Disease (CERAD). Part I. Clinical and neuropsychological assesment of Alzheimer's disease. *Neurology, 39*(9), 1159. doi:10.1212/wnl.39.9.1159

Morris, M. C., Tangney, C. C., Wang, Y., Sacks, F. M., Bennett, D. A., & Aggarwal, N. T. (2015). MIND diet associated with reduced incidence of Alzheimer's disease. *Alzheimers Dement, 11*(9), 1007-1014. doi:10.1016/j.jalz.2014.11.009

Morris, S. A., Rao, B., Garcia, B. A., Hake, S. B., Diaz, R. L., Shabanowitz, J., . . . Strahl, B. D. (2007). Identification of histone H3 lysine 36 acetylation as a highly conserved histone modification. *J Biol Chem, 282*(10), 7632-7640. doi:10.1074/jbc.M607909200

Morrison, J. H., Lewis, D. A., Campbell, M. J., Huntley, G. W., Benson, D. L., & Bouras, C. (1987). A monoclonal antibody to non-phosphorylated neurofilament protein marks the vulnerable cortical neurons in Alzheimer's disease. *Brain Research, 416*(2), 331-336.

Mortimer, J., Van Duijn, C., Chandra, V., Fratiglioni, L., Graves, A., Heyman, A., . . . Rocca, W. A. (1991). Head trauma as a risk factor for Alzheimer's disease: a collaborative re-analysis of case-control studies. *International Journal of Epidemiology, 20*(Supplement_2), S28-S35.

Mosher, K. I., & Wyss-Coray, T. (2014). Microglial Dysfunction in Brain Aging and Alzheimer's Disease. *Biochemical pharmacology, 88*(4), 594-604. doi:10.1016/j.bcp.2014.01.008

Mota, S. I., Ferreira, I. L., Pereira, C., Oliveira, C. R., & Rego, A. C. (2012). Amyloid-beta peptide 1-42 causes microtubule deregulation through N-methyl-D-aspartate receptors in mature hippocampal cultures. *Curr Alzheimer Res, 9*(7), 844-856.

Mullen, R. J., Buck, C. R., & Smith, A. M. (1992). NeuN, a neuronal specific nuclear protein in vertebrates. *Development, 116*(1), 201-211.

Mullen, R. J., Buck, C. R., & Smith, A. M. (1992). NeuN, a neuronal specific nuclear protein in vertebrates. *Development, 116*(1), 201-211.

Murayama, S., & Saito, Y. (2004). Neuropathological diagnostic criteria for Alzheimer's disease. *Neuropathology, 24*(3), 254-260.

Murgatroyd, C., & Spengler, D. (2011). Epigenetics of early child development. *Frontiers in psychiatry, 2*, 16-16. doi:10.3389/fpsyt.2011.00016

Murray, A. J., Sauer, J. F., Riedel, G., McClure, C., Ansel, L., Cheyne, L., . . . Wulff, P. (2011). Parvalbumin-positive CA1 interneurons are required for spatial working but not for reference memory. *Nat Neurosci, 14*(3), 297-299. doi:10.1038/nn.2751

Murray, M. E., Lowe, V. J., Graff-Radford, N. R., Liesinger, A. M., Cannon, A., Przybelski, S. A., . . . Dickson, D. W. (2015). Clinicopathologic and 11C-Pittsburgh compound B implications of Thal amyloid phase across the Alzheimer's disease spectrum. *Brain, 138*(5), 1370-1381. doi:10.1093/brain/awv050

Nan, X., Ng, H.-H., Johnson, C. A., Laherty, C. D., Turner, B. M., Eisenman, R. N., & Bird, A. (1998). Transcriptional repression by the methyl-CpG-binding protein MeCP2 involves a histone deacetylase complex. *Nature, 393*, 386. doi:10.1038/30764

Nan, X., Ng, H. H., Johnson, C. A., Laherty, C. D., Turner, B. M., Eisenman, R. N., & Bird, A. (1998). Transcriptional repression by the methyl-CpG-binding protein MeCP2 involves a histone deacetylase complex. *Nature, 393*(6683), 386-389. doi:10.1038/30764

Narayan, P. J., Lill, C., Faull, R., Curtis, M. A., & Dragunow, M. (2015). Increased acetyl and total histone levels in post-mortem Alzheimer's disease brain. *Neurobiol Dis, 74*, 281-294. doi:10.1016/j.nbd.2014.11.023

Näslund, J., Haroutunian, V., Mohs, R., & et al. (2000). COrrelation between elevated levels of amyloid β-peptide in the brain and cognitive decline. *JAMA, 283*(12), 1571-1577. doi:10.1001/jama.283.12.1571

Nativio, R., Donahue, G., Berson, A., Lan, Y., Amlie-Wolf, A., Tuzer, F., . . . Berger, S. L. (2018). Dysregulation of the epigenetic landscape of normal aging in Alzheimer's disease. *Nature neuroscience*. doi:10.1038/s41593-018-0101-9

Nimmerjahn, A., Kirchhoff, F., & Helmchen, F. (2005). Resting Microglial Cells Are Highly Dynamic Surveillants of Brain Parenchyma in Vivo. *Science, 308*(5726), 1314-1318. doi:10.1126/science.1110647

Numata, S., Ye, T., Hyde, T. M., Guitart-Navarro, X., Tao, R., Wininger, M., . . . Lipska, B. K. (2012). DNA methylation signatures in development and aging of the human prefrontal cortex. *Am J Hum Genet, 90*(2), 260-272. doi:10.1016/j.ajhg.2011.12.020

O'Carroll, D., Scherthan, H., Peters, A. H., Opravil, S., Haynes, A. R., Laible, G., . . . Jenuwein, T. (2000). Isolation and characterization of Suv39h2, a second histone H3 methyltransferase gene that displays testis-specific expression. *Mol Cell Biol, 20*(24), 9423-9433.

Oakford, P. C., James, S. R., Qadi, A., West, A. C., Ray, S. N., Bert, A. G., . . . Holloway, A. F. (2010). Transcriptional and epigenetic regulation of the GM-CSF promoter by RUNX1. *Leuk Res, 34*(9), 1203-1213. doi:10.1016/j.leukres.2010.03.029

Oakley, H., Cole, S. L., Logan, S., Maus, E., Shao, P., Craft, J., . . . Vassar, R. (2006). Intraneuronal beta-amyloid aggregates, neurodegeneration, and neuron loss in transgenic mice with five familial Alzheimer's disease mutations: potential factors in amyloid plaque formation. *J Neurosci, 26*(40), 10129-10140. doi:10.1523/jneurosci.1202-06.2006

Oddo, S., Caccamo, A., Shepherd, J. D., Murphy, M. P., Golde, T. E., Kayed, R., . . . LaFerla, F. M. (2003). Triple-transgenic model of Alzheimer's disease with plaques and tangles: intracellular Abeta and synaptic dysfunction. *Neuron, 39*(3), 409-421.

Oh, G., Ebrahimi, S., Wang, S.-C., Cortese, R., Kaminsky, Z. A., Gottesman, I. I., . . . Petronis, A. (2016). Epigenetic assimilation in the aging human brain. *Genome Biol, 17*(1), 76. doi:10.1186/s13059-016-0946-8

Okano, M., Bell, D. W., Haber, D. A., & Li, E. (1999). DNA methyltransferases Dnmt3a and Dnmt3b are essential for de novo methylation and mammalian development. *Cell, 99*(3), 247-257.

Olins, A. L., & Olins, D. E. (1974). Spheroid Chromatin Units (ν Bodies). *Science, 183*(4122), 330-332. doi:10.1126/science.183.4122.330

Ooi, S. K., Qiu, C., Bernstein, E., Li, K., Jia, D., Yang, Z., . . . Bestor, T. H. (2007). DNMT3L connects unmethylated lysine 4 of histone H3 to de novo methylation of DNA. *Nature, 448*(7154), 714-717. doi:10.1038/nature05987

Outchkourov, N. S., Muino, J. M., Kaufmann, K., van Ijcken, W. F., Groot Koerkamp, M. J., van Leenen, D., . . . Timmers, H. T. (2013). Balancing of histone H3K4 methylation states by the Kdm5c/SMCX histone demethylase modulates promoter and enhancer function. *Cell Rep, 3*(4), 1071-1079. doi:10.1016/j.celrep.2013.02.030

Palmer, A., & Klein, R. (2003). Multiple roles of ephrins in morphogenesis, neuronal networking, and brain function. *Genes Dev, 17*(12), 1429-1450. doi:10.1101/gad.1093703

Parodi, J., Sepulveda, F. J., Roa, J., Opazo, C., Inestrosa, N. C., & Aguayo, L. G. (2010). Beta-amyloid causes depletion of synaptic vesicles leading to neurotransmission failure. *J Biol Chem, 285*(4), 2506-2514. doi:10.1074/jbc.M109.030023

Pavlopoulos, E., Jones, S., Kosmidis, S., Close, M., Kim, C., Kovalerchik, O., . . . Kandel, E. R. (2013). Molecular Mechanism for Age-Related Memory Loss: The Histone-Binding

Protein RbAp48. *Science Translational Medicine, 5*(200), 200ra115. doi:10.1126/scitranslmed.3006373

Peleg, S., Sananbenesi, F., Zovoilis, A., Burkhardt, S., Bahari-Javan, S., Agis-Balboa, R. C., . . . Fischer, A. (2010). Altered histone acetylation is associated with age-dependent memory impairment in mice. *Science, 328*(5979), 753-756. doi:10.1126/science.1186088

Peltier, D. C., Simms, A., Farmer, J. R., & Miller, D. J. (2010). Human neuronal cells possess functional cytoplasmic and TLR-mediated innate immune pathways influenced by phosphatidylinositol-3 kinase signaling. *J Immunol, 184*(12), 7010-7021. doi:10.4049/jimmunol.0904133

Peng, S., Garzon, D. J., Marchese, M., Klein, W., Ginsberg, S. D., Francis, B. M., . . . Fahnestock, M. (2009). Decreased Brain-Derived Neurotrophic Factor Depends on Amyloid Aggregation State in Transgenic Mouse Models of Alzheimer's Disease. *The Journal of Neuroscience, 29*(29), 9321.

Penner, M. R., Roth, T. L., Chawla, M. K., Hoang, L. T., Roth, E. D., Lubin, F. D., . . . Barnes, C. A. (2011). Age-related changes in Arc transcription and DNA methylation within the hippocampus. *Neurobiol Aging, 32*(12), 2198-2210. doi:https://doi.org/10.1016/j.neurobiolaging.2010.01.009

Perea, G., Navarrete, M., & Araque, A. (2009). Tripartite synapses: astrocytes process and control synaptic information. *Trends Neurosci, 32*(8), 421-431. doi:10.1016/j.tins.2009.05.001

Perry, G., Cash, A. D., Srinivas, R., & Smith, M. A. (2002). Metals and oxidative homeostasis in Alzheimer's disease. *Drug Development Research, 56*(3), 293-299. doi:10.1002/ddr.10099

Perry, G., Kawai, M., Tabaton, M., Onorato, M., Mulvihill, P., Richey, P., . . . Gambetti, P. (1991). Neuropil threads of Alzheimer's disease show a marked alteration of the normal cytoskeleton. *J Neurosci, 11*(6), 1748-1755.

Peters, D. G., Connor, J. R., & Meadowcroft, M. D. (2015). The Relationship between Iron Dyshomeostasis and Amyloidogenesis in Alzheimer's Disease: Two Sides of the Same Coin. *Neurobiol Dis, 81*, 49-65. doi:10.1016/j.nbd.2015.08.007

Phillips, H. S., Hains, J. M., Armanini, M., Laramee, G. R., Johnson, S. A., & Winslow, J. W. (1991). BDNF mRNA is decreased in the hippocampus of individuals with Alzheimer's disease. *Neuron, 7*(5), 695-702.

Pike, C. J., & Cotman, C. W. (1995). Calretinin-immunoreactive neurons are resistant to β-amyloid toxicity in vitro. *Brain Research, 671*(2), 293-298. doi:https://doi.org/10.1016/0006-8993(94)01354-K

Plassman, B. L., Havlik, R., Steffens, D., Helms, M., Newman, T., Drosdick, D., . . . Burke, J. (2000). Documented head injury in early adulthood and risk of Alzheimer's disease and other dementias. *Neurology, 55*(8), 1158-1166.

Polydoro, M., Acker, C. M., Duff, K., Castillo, P. E., & Davies, P. (2009). Age-dependent impairment of cognitive and synaptic function in the htau mouse model of tau pathology. *J Neurosci, 29*(34), 10741-10749. doi:10.1523/jneurosci.1065-09.2009

Pott, S. (2017). Simultaneous measurement of chromatin accessibility, DNA methylation, and nucleosome phasing in single cells. *eLife, 6*, e23203. doi:10.7554/eLife.23203

Pott, S., & Lieb, J. D. (2014). What are super-enhancers? *Nat Genet, 47*, 8. doi:10.1038/ng.3167

Potter, P. E., Rauschkolb, P. K., Pandya, Y., Sue, L. I., Sabbagh, M. N., Walker, D. G., & Beach, T. G. (2011). Pre- and post-synaptic cortical cholinergic deficits are proportional to amyloid plaque presence and density at preclinical stages of Alzheimer's disease. *Acta Neuropathol, 122*(1), 49-60. doi:10.1007/s00401-011-0831-1

Poulopoulou, C., Markakis, I., Davaki, P., Tsaltas, E., Rombos, A., Hatzimanolis, A., & Vassilopoulos, D. (2010). Aberrant modulation of a delayed rectifier potassium channel by glutamate in Alzheimer's disease. *Neurobiol Dis, 37*(2), 339-348. doi:10.1016/j.nbd.2009.10.012

Puzzo, D., Vitolo, O., Trinchese, F., Jacob, J. P., Palmeri, A., & Arancio, O. (2005). Amyloid-β Peptide Inhibits Activation of the Nitric Oxide/cGMP/cAMP-Responsive Element-Binding Protein Pathway during Hippocampal Synaptic Plasticity. *The Journal of Neuroscience, 25*(29), 6887-6897. doi:10.1523/jneurosci.5291-04.2005

Quinlan, A. R. (2014). BEDTools: The Swiss-Army Tool for Genome Feature Analysis. *Current protocols in bioinformatics, 47*, 11.12.11-11.12.34. doi:10.1002/0471250953.bi1112s47

Rada-Iglesias, A., Bajpai, R., Swigut, T., Brugmann, S. A., Flynn, R. A., & Wysocka, J. (2011). A unique chromatin signature uncovers early developmental enhancers in humans. *Nature, 470*(7333), 279-283. doi:10.1038/nature09692

Radde, R., Bolmont, T., Kaeser, S. A., Coomaraswamy, J., Lindau, D., Stoltze, L., . . . Jucker, M. (2006). Abeta42-driven cerebral amyloidosis in transgenic mice reveals early and robust pathology. *EMBO Rep, 7*(9), 940-946. doi:10.1038/sj.embor.7400784

Raff, M. C., Miller, R. H., & Noble, M. (1983). A glial progenitor cell that develops in vitro into an astrocyte or an oligodendrocyte depending on culture medium. *Nature, 303*, 390. doi:10.1038/303390a0

Rai, T. S., Cole, J. J., Nelson, D. M., Dikovskaya, D., Faller, W. J., Vizioli, M. G., . . . Adams, P. D. (2014). HIRA orchestrates a dynamic chromatin landscape in senescence and is required for suppression of neoplasia. *Genes Dev, 28*(24), 2712-2725. doi:10.1101/gad.247528.114

Raj, T., Li, Y. I., Wong, G., Humphrey, J., Wang, M., Ramdhani, S., . . . De Jager, P. L. (2018). Integrative transcriptome analyses of the aging brain implicate altered splicing in Alzheimer's disease susceptibility. *Nat Genet, 50*(11), 1584-1592. doi:10.1038/s41588-018-0238-1

Raj, T., Li, Y. I., Wong, G., Humphrey, J., Wang, M., Ramdhani, S., . . . De Jager, P. L. (2018). Integrative transcriptome analyses of the aging brain implicate altered splicing in Alzheimer's disease susceptibility. *Nat Genet, 50*(11), 1584-1592. doi:10.1038/s41588-018-0238-1

Rajendran, L., & Annaert, W. (2012). Membrane trafficking pathways in Alzheimer's disease. *Traffic, 13*(6), 759-770.

Ramírez, F., Ryan, D. P., Grüning, B., Bhardwaj, V., Kilpert, F., Richter, A. S., . . . Manke, T. (2016). deepTools2: a next generation web server for deep-sequencing data analysis. *Nucleic Acids Res, 44*(Web Server issue), W160-W165. doi:10.1093/nar/gkw257

Ramsahoye, B. H., Biniszkiewicz, D., Lyko, F., Clark, V., Bird, A. P., & Jaenisch, R. (2000). Non-CpG methylation is prevalent in embryonic stem cells and may be mediated by DNA methyltransferase 3a. *Proceedings of the National Academy of Sciences, 97*(10), 5237-5242. doi:10.1073/pnas.97.10.5237

Rao, J. S., Keleshian, V. L., Klein, S., & Rapoport, S. I. (2012). Epigenetic modifications in frontal cortex from Alzheimer's disease and bipolar disorder patients. *Transl Psychiatry, 2*, e132. doi:10.1038/tp.2012.55

Razin, A., & Riggs, A. (1980). DNA methylation and gene function. *Science, 210*(4470), 604-610. doi:10.1126/science.6254144

Reed-Geaghan, E. G., Savage, J. C., Hise, A. G., & Landreth, G. E. (2009). CD14 and toll-like receptors 2 and 4 are required for fibrillar A{beta}-stimulated microglial activation. *J Neurosci, 29*(38), 11982-11992. doi:10.1523/jneurosci.3158-09.2009

Ridge, P. G., Ebbert, M. T. W., & Kauwe, J. S. K. (2013). Genetics of Alzheimer's Disease. *BioMed Research International, 2013*, 254954. doi:10.1155/2013/254954

Rizzardi, L., Hickey, P., Rodriguez, V., Tryggvadottir, R., Callahan, C., Idrizi, A., . . . Feinberg, A. P. (2017). Neuronal brain region-specific DNA methylation and chromatin accessibility are associated with neuropsychiatric disease heritability. *bioRxiv*.

Roberson, E. D., Scearce-Levie, K., Palop, J. J., Yan, F., Cheng, I. H., Wu, T., . . . Mucke, L. (2007). Reducing endogenous tau ameliorates amyloid beta-induced deficits in an Alzheimer's disease mouse model. *Science, 316*(5825), 750-754. doi:10.1126/science.1141736

Robertson, G., Hirst, M., Bainbridge, M., Bilenky, M., Zhao, Y., Zeng, T., . . . Jones, S. (2007). Genome-wide profiles of STAT1 DNA association using chromatin immunoprecipitation and massively parallel sequencing. *Nature Methods, 4*, 651. doi:10.1038/nmeth1068

https://www.nature.com/articles/nmeth1068#supplementary-information

Robinson, M. D., McCarthy, D. J., & Smyth, G. K. (2010). edgeR: a Bioconductor package for differential expression analysis of digital gene expression data. *Bioinformatics, 26*(1), 139-140. doi:10.1093/bioinformatics/btp616

Robinson, M. D., & Oshlack, A. (2010). A scaling normalization method for differential expression analysis of RNA-seq data. *Genome Biol, 11*(3), R25. doi:10.1186/gb-2010-11-3-r25

Rodrigues, H. F., Souza, T. A., Ghiraldini, F. G., Mello, M. L., & Moraes, A. S. (2014). Increased age is associated with epigenetic and structural changes in chromatin from neuronal nuclei. *J Cell Biochem, 115*(4), 659-665. doi:10.1002/jcb.24705

Rodriguez-Vieitez, E., Saint-Aubert, L., Carter, S. F., Almkvist, O., Farid, K., Schöll, M., . . . Nordberg, A. (2016). Diverging longitudinal changes in astrocytosis and amyloid PET in autosomal dominant Alzheimer's disease. *Brain, 139*(3), 922-936. doi:10.1093/brain/awv404

Rossetto, D., Avvakumov, N., & Côté, J. (2012). Histone phosphorylation: a chromatin modification involved in diverse nuclear events. *Epigenetics, 7*(10), 1098-1108. doi:10.4161/epi.21975

Rotem, A., Ram, O., Shoresh, N., Sperling, R. A., Goren, A., Weitz, D. A., & Bernstein, B. E. (2015). Single-cell ChIP-seq reveals cell subpopulations defined by chromatin state. *Nature Biotechnology, 33*, 1165. doi:10.1038/nbt.3383

https://www.nature.com/articles/nbt.3383#supplementary-information

Saito, T., Matsuba, Y., Mihira, N., Takano, J., Nilsson, P., Itohara, S., . . . Saido, T. C. (2014). Single App knock-in mouse models of Alzheimer's disease. *Nat Neurosci, 17*(5), 661-663. doi:10.1038/nn.3697

Saito, T., Matsuba, Y., Mihira, N., Takano, J., Nilsson, P., Itohara, S., . . . Saido, T. C. (2014). Single App knock-in mouse models of Alzheimer's disease. *Nature neuroscience, 17*, 661. doi:10.1038/nn.3697

https://www.nature.com/articles/nn.3697#supplementary-information

Saito, T., Matsuba, Y., Yamazaki, N., Hashimoto, S., & Saido, T. C. (2016). Calpain Activation in Alzheimer's Model Mice Is an Artifact of APP and Presenilin Overexpression. *J Neurosci, 36*(38), 9933-9936. doi:10.1523/jneurosci.1907-16.2016

Sala, C., Rudolph-Correia, S., & Sheng, M. (2000). Developmentally Regulated NMDA Receptor-Dependent Dephosphorylation of cAMP Response Element-Binding Protein (CREB) in Hippocampal Neurons. *The Journal of Neuroscience, 20*(10), 3529-3536. doi:10.1523/jneurosci.20-10-03529.2000

Sambrook, J., & Russell, D. W. (2006). Purification of Nucleic Acids by Extraction with Phenol:Chloroform. *Cold Spring Harbor Protocols, 2006*(1), pdb.prot4455. doi:10.1101/pdb.prot4455

Sample, V., Ramamurthy, S., Gorshkov, K., Ronnett, G. V., & Zhang, J. (2015). Polarized activities of AMPK and BRSK in primary hippocampal neurons. *Mol Biol Cell, 26*(10), 1935-1946. doi:10.1091/mbc.E14-02-0764

Sampson, V. L., Morrison, J. H., & Vickers, J. C. (1997). The cellular basis for the relative resistance of parvalbumin and calretinin immunoreactive neocortical neurons to the pathology of Alzheimer's disease. *Exp Neurol, 145*(1), 295-302. doi:10.1006/exnr.1997.6433

Sanchez-Mut, J. V., Aso, E., Heyn, H., Matsuda, T., Bock, C., Ferrer, I., & Esteller, M. (2014). Promoter hypermethylation of the phosphatase DUSP22 mediates PKA-dependent TAU phosphorylation and CREB activation in Alzheimer's disease. *Hippocampus*. doi:10.1002/hipo.22245

Sanchez-Mut, J. V., Aso, E., Panayotis, N., Lott, I., Dierssen, M., Rabano, A., . . . Esteller, M. (2013). DNA methylation map of mouse and human brain identifies target genes in Alzheimer's disease. *Brain, 136*(Pt 10), 3018-3027. doi:10.1093/brain/awt237

Sanchez-Mut, J. V., Heyn, H., Vidal, E., Moran, S., Sayols, S., Delgado-Morales, R., . . . Esteller, M. (2016). Human DNA methylomes of neurodegenerative diseases show common epigenomic patterns. *Translational psychiatry, 6*(1), e718. doi:10.1038/tp.2015.214

Sandelius, A., Portelius, E., Kallen, A., Zetterberg, H., Rot, U., Olsson, B., . . . Blennow, K. (2019). Elevated CSF GAP-43 is Alzheimer's disease specific and associated with tau and amyloid pathology. *Alzheimers Dement, 15*(1), 55-64. doi:10.1016/j.jalz.2018.08.006

Santos-Rosa, H., Schneider, R., Bannister, A. J., Sherriff, J., Bernstein, B. E., Emre, N. C., . . . Kouzarides, T. (2002). Active genes are tri-methylated at K4 of histone H3. *Nature, 419*(6905), 407-411. doi:10.1038/nature01080

Sasaguri, H., Nilsson, P., Hashimoto, S., Nagata, K., Saito, T., De Strooper, B., . . . Saido, T. C. (2017). APP mouse models for Alzheimer's disease preclinical studies. *Embo j, 36*(17), 2473-2487. doi:10.15252/embj.201797397

Sasaki, A., Yamaguchi, H., Ogawa, A., Sugihara, S., & Nakazato, Y. (1997). Microglial activation in early stages of amyloid beta protein deposition. *Acta Neuropathol, 94*(4), 316-322.

Sauzeau, V., Horta-Junior, J. A., Riolobos, A. S., Fernandez, G., Sevilla, M. A., Lopez, D. E., . . . Bustelo, X. R. (2010). Vav3 is involved in GABAergic axon guidance events important for the proper function of brainstem neurons controlling cardiovascular, respiratory, and renal parameters. *Mol Biol Cell, 21*(23), 4251-4263. doi:10.1091/mbc.E10-07-0639

Scarmeas, N., Stern, Y., Tang, M.-X., Mayeux, R., & Luchsinger, J. A. (2006). Mediterranean Diet and Risk for Alzheimer's Disease. *Ann Neurol, 59*(6), 912-921. doi:10.1002/ana.20854

Scarpa, S., Fuso, A., D'Anselmi, F., & Cavallaro, R. A. (2003). Presenilin 1 gene silencing by S-adenosylmethionine: a treatment for Alzheimer disease? *FEBS Letters, 541*(1-3), 145-148. doi:doi:10.1016/S0014-5793(03)00277-1

Scheuner, D., Eckman, C., Jensen, M., Song, X., Citron, M., Suzuki, N., . . . Younkin, S. (1996). Secreted amyloid β–protein similar to that in the senile plaques of Alzheimer's disease is increased in vivo by the presenilin 1 and 2 and APP mutations linked to familial Alzheimer's disease. *Nature medicine, 2*, 864. doi:10.1038/nm0896-864

Schmid, C. D., & Bucher, P. (2007). ChIP-Seq Data Reveal Nucleosome Architecture of Human Promoters. *Cell, 131*(5), 831-832. doi:https://doi.org/10.1016/j.cell.2007.11.017

Selemon, L. D. (2013). A role for synaptic plasticity in the adolescent development of executive function. *Translational psychiatry, 3*, e238. doi:10.1038/tp.2013.7

Selkoe, D. J. (2008). Soluble oligomers of the amyloid β-protein impair synaptic plasticity and behavior. *Behav Brain Res, 192*(1), 106-113. doi:http://dx.doi.org/10.1016/j.bbr.2008.02.016

Semple, B. D., Blomgren, K., Gimlin, K., Ferriero, D. M., & Noble-Haeusslein, L. J. (2013). Brain development in rodents and humans: Identifying benchmarks of maturation and vulnerability to injury across species. *Prog Neurobiol, 106-107*, 1-16. doi:10.1016/j.pneurobio.2013.04.001

Sen, A., Nelson, T. J., & Alkon, D. L. (2015). ApoE4 and Aβ Oligomers Reduce BDNF Expression via HDAC Nuclear Translocation. *The Journal of Neuroscience, 35*(19), 7538-7551. doi:10.1523/jneurosci.0260-15.2015

Sen, A., Nelson, T. J., & Alkon, D. L. (2017). ApoE isoforms differentially regulates cleavage and secretion of BDNF. *Molecular Brain, 10*, 19. doi:10.1186/s13041-017-0301-3

Serneels, L., Van Biervliet, J., Craessaerts, K., Dejaegere, T., Horre, K., Van Houtvin, T., . . . De Strooper, B. (2009). gamma-Secretase heterogeneity in the Aph1 subunit: relevance for Alzheimer's disease. *Science, 324*(5927), 639-642. doi:10.1126/science.1171176

Serrano, F., & Klann, E. (2004). Reactive oxygen species and synaptic plasticity in the aging hippocampus. *Ageing Research Reviews, 3*(4), 431-443. doi:https://doi.org/10.1016/j.arr.2004.05.002

Seshadri, S., Fitzpatrick, A. L., Ikram, M. A., DeStefano, A. L., Gudnason, V., Boada, M., . . . EADI1 Consortia, f. t. (2010). Genome-wide Analysis of Genetic Loci Associated With Alzheimer Disease. *JAMA, 303*(18), 1832-1840. doi:10.1001/jama.2010.574

Shankar, G. M., Li, S., Mehta, T. H., Garcia-Munoz, A., Shepardson, N. E., Smith, I., . . . Selkoe, D. J. (2008). Amyloid-β protein dimers isolated directly from Alzheimer's brains impair synaptic plasticity and memory. *Nature medicine, 14*, 837. doi:10.1038/nm1782

https://www.nature.com/articles/nm1782#supplementary-information

Sherrington, R., Rogaev, E. I., Liang, Y., Rogaeva, E. A., Levesque, G., Ikeda, M., . . . St George-Hyslop, P. H. (1995). Cloning of a gene bearing missense mutations in early-onset familial Alzheimer's disease. *Nature, 375*(6534), 754-760.

Shogren-Knaak, M., Ishii, H., Sun, J.-M., Pazin, M. J., Davie, J. R., & Peterson, C. L. (2006a). Histone H4-K16 Acetylation Controls Chromatin Structure and Protein Interactions. *Science, 311*(5762), 844.

Shogren-Knaak, M., Ishii, H., Sun, J.-M., Pazin, M. J., Davie, J. R., & Peterson, C. L. (2006b). Histone H4-K16 Acetylation Controls Chromatin Structure and Protein Interactions. *Science, 311*(5762), 844-847. doi:10.1126/science.1124000

Shoji, H., Takao, K., Hattori, S., & Miyakawa, T. (2016). Age-related changes in behavior in C57BL/6J mice from young adulthood to middle age. *Molecular Brain, 9*, 11-11. doi:10.1186/s13041-016-0191-9

Shulha, H. P., Cheung, I., Guo, Y., Akbarian, S., & Weng, Z. (2013). Coordinated cell type-specific epigenetic remodeling in prefrontal cortex begins before birth and continues into early adulthood. *PLoS Genet, 9*(4), e1003433-e1003433. doi:10.1371/journal.pgen.1003433

Siegmund, K. D., Connor, C. M., Campan, M., Long, T. I., Weisenberger, D. J., Biniszkiewicz, D., . . . Akbarian, S. (2007). DNA methylation in the human cerebral cortex is dynamically regulated throughout the life span and involves differentiated neurons. *PLoS One, 2*(9), e895. doi:10.1371/journal.pone.0000895

Singh, R. P., Shiue, K., Schomberg, D., & Zhou, F. C. (2009). Cellular epigenetic modifications of neural stem cell differentiation. *Cell Transplant, 18*(10), 1197-1211. doi:10.3727/096368909x12483162197204

Skene, P. J., Illingworth, R. S., Webb, S., Kerr, A., James, K. D., Turner, D. J., . . . Bird, A. P. (2010). Neuronal MeCP2 is expressed at near histone-octamer levels and globally alters the chromatin state. *Mol Cell, 37*(4), 457-468. doi:10.1016/j.molcel.2010.01.030

Smallwood, S. A., Lee, H. J., Angermueller, C., Krueger, F., Saadeh, H., Peat, J., . . . Kelsey, G. (2014). Single-cell genome-wide bisulfite sequencing for assessing epigenetic heterogeneity. *Nat Methods, 11*(8), 817-820. doi:10.1038/nmeth.3035

Smith, A. R., Smith, R. G., Condliffe, D., Hannon, E., Schalkwyk, L., Mill, J., & Lunnon, K. (2016). Increased DNA methylation near TREM2 is consistently seen in the superior temporal gyrus in Alzheimer's disease brain. *Neurobiol Aging, 47*, 35-40. doi:https://doi.org/10.1016/j.neurobiolaging.2016.07.008

Soreq, L., Rose, J., Soreq, E., Hardy, J., Trabzuni, D., Cookson, M. R., . . . Ule, J. (2017). Major Shifts in Glial Regional Identity Are a Transcriptional Hallmark of Human Brain Aging. *Cell Rep, 18*(2), 557-570. doi:10.1016/j.celrep.2016.12.011

Soto, C., & Pritzkow, S. (2018). Protein misfolding, aggregation, and conformational strains in neurodegenerative diseases. *Nat Neurosci, 21*(10), 1332-1340. doi:10.1038/s41593-018-0235-9

Spanopoulou, E., Giguere, V., & Grosveld, F. (1991). The functional domains of the murine Thy-1 gene promoter. *Mol Cell Biol, 11*(4), 2216-2228.

Squires, J. E., Patel, H. R., Nousch, M., Sibbritt, T., Humphreys, D. T., Parker, B. J., . . . Preiss, T. (2012). Widespread occurrence of 5-methylcytosine in human coding and non-coding RNA. *Nucleic Acids Res, 40*(11), 5023-5033. doi:10.1093/nar/gks144

St George-Hyslop, P. H., Tanzi, R. E., Polinsky, R. J., Haines, J. L., Nee, L., Watkins, P. C., . . . et al. (1987). The genetic defect causing familial Alzheimer's disease maps on chromosome 21. *Science, 235*(4791), 885-890.

Stadler, M. B., Murr, R., Burger, L., Ivanek, R., Lienert, F., Schöler, A., . . . Schübeler, D. (2011). DNA-binding factors shape the mouse methylome at distal regulatory regions. *Nature, 480*, 490. doi:10.1038/nature10716

https://www.nature.com/articles/nature10716#supplementary-information

Stedman, E., & Stedman, E. (1950). Cell Specificity of Histones. *Nature, 166*, 780. doi:10.1038/166780a0

Stempor, P., & Ahringer, J. (2016). SeqPlots - Interactive software for exploratory data analyses, pattern discovery and visualization in genomics. *Wellcome Open Research, 1*, 14. doi:10.12688/wellcomeopenres.10004.1

Stern, Y., Gurland, B., Tatemichi, T. K., Tang, M. X., Wilder, D., & Mayeux, R. (1994). Influence of education and occupation on the incidence of Alzheimer's disease. *JAMA, 271*(13), 1004-1010.

Strittmatter, W. J., Saunders, A. M., Schmechel, D., Pericak-Vance, M., Enghild, J., Salvesen, G. S., & Roses, A. D. (1993). Apolipoprotein E: high-avidity binding to beta-amyloid and increased frequency of type 4 allele in late-onset familial Alzheimer disease. *Proceedings of the National Academy of Sciences, 90*(5), 1977-1981. doi:10.1073/pnas.90.5.1977

Sturchler-Pierrat, C., Abramowski, D., Duke, M., Wiederhold, K.-H., Mistl, C., Rothacher, S., . . . Sommer, B. (1997). Two amyloid precursor protein transgenic mouse models with Alzheimer disease-like pathology. *Proc Natl Acad Sci U S A, 94*(24), 13287-13292.

Suberbielle, E., Djukic, B., Evans, M., Kim, D. H., Taneja, P., Wang, X., . . . Mucke, L. (2015). DNA repair factor BRCA1 depletion occurs in Alzheimer brains and impairs cognitive function in mice. *Nature Communications, 6*, 8897. doi:10.1038/ncomms9897

https://www.nature.com/articles/ncomms9897#supplementary-information

Suzuki, M. M., & Bird, A. (2008). DNA methylation landscapes: provocative insights from epigenomics. *Nature Reviews Genetics, 9*, 465. doi:10.1038/nrg2341

Swank, M. W., & Sweatt, J. D. (2001). Increased histone acetyltransferase and lysine acetyltransferase activity and biphasic activation of the ERK/RSK cascade in insular cortex during novel taste learning. *J Neurosci, 21*(10), 3383-3391.

Szulwach, K. E., Li, X., Li, Y., Song, C.-X., Wu, H., Dai, Q., . . . Levey, A. I. (2011). 5-hmC-mediated epigenetic dynamics during postnatal neurodevelopment and aging. *Nature neuroscience, 14*(12), 1607-1616.

Taberlay, P. C., Kelly, T. K., Liu, C. C., You, J. S., De Carvalho, D. D., Miranda, T. B., . . . Jones, P. A. (2011). Polycomb-repressed genes have permissive enhancers that initiate reprogramming. *Cell, 147*(6), 1283-1294. doi:10.1016/j.cell.2011.10.040

Taberlay, P. C., Statham, A. L., Kelly, T. K., Clark, S. J., & Jones, P. A. (2014). Reconfiguration of nucleosome-depleted regions at distal regulatory elements accompanies DNA methylation of enhancers and insulators in cancer. *Genome Res, 24*(9), 1421-1432. doi:10.1101/gr.163485.113

Tahiliani, M., Koh, K. P., Shen, Y., Pastor, W. A., Bandukwala, H., Brudno, Y., . . . Rao, A. (2009). Conversion of 5-methylcytosine to 5-hydroxymethylcytosine in mammalian DNA by MLL partner TET1. *Science, 324*(5929), 930-935. doi:10.1126/science.1170116

Takahashi, H., Brasnjevic, I., Rutten, B. P., Van Der Kolk, N., Perl, D. P., Bouras, C., . . . Dickstein, D. L. (2010). Hippocampal interneuron loss in an APP/PS1 double mutant mouse and in Alzheimer's disease. *Brain Struct Funct, 214*(2-3), 145-160. doi:10.1007/s00429-010-0242-4

Takihara, Y., Inatani, M., Eto, K., Inoue, T., Kreymerman, A., Miyake, S., . . . Tanihara, H. (2015). In vivo imaging of axonal transport of mitochondria in the diseased and aged mammalian CNS. *Proc Natl Acad Sci U S A, 112*(33), 10515-10520. doi:10.1073/pnas.1509879112

Takizawa, T., Nakashima, K., Namihira, M., Ochiai, W., Uemura, A., Yanagisawa, M., . . . Taga, T. (2001). DNA methylation is a critical cell-intrinsic determinant of astrocyte differentiation in the fetal brain. *Dev Cell, 1*(6), 749-758.

Tamaru, H., & Selker, E. U. (2001). A histone H3 methyltransferase controls DNA methylation in Neurospora crassa. *Nature, 414*, 277. doi:10.1038/35104508

https://www.nature.com/articles/35104508#supplementary-information

Tamaru, H., Zhang, X., McMillen, D., Singh, P. B., Nakayama, J., Grewal, S. I., . . . Selker, E. U. (2003). Trimethylated lysine 9 of histone H3 is a mark for DNA methylation in Neurospora crassa. *Nat Genet, 34*(1), 75-79. doi:10.1038/ng1143

Tan, M., Luo, H., Lee, S., Jin, F., Yang, J. S., Montellier, E., . . . Zhao, Y. (2011). Identification of 67 histone marks and histone lysine crotonylation as a new type of histone modification. *Cell, 146*(6), 1016-1028. doi:10.1016/j.cell.2011.08.008

Tan, S.-L., Nishi, M., Ohtsuka, T., Matsui, T., Takemoto, K., Kamio-Miura, A., . . . Kageyama, R. (2012). Essential roles of the histone methyltransferase ESET in the epigenetic control of neural progenitor cells during development. *Development, 139*(20), 3806.

Taunton, J., Hassig, C. A., & Schreiber, S. L. (1996). A mammalian histone deacetylase related to the yeast transcriptional regulator Rpd3p. *Science, 272*(5260), 408-411.

Taylor, G. C., Eskeland, R., Hekimoglu-Balkan, B., Pradeepa, M. M., & Bickmore, W. A. (2013). H4K16 acetylation marks active genes and enhancers of embryonic stem cells, but does not alter chromatin compaction. *Genome Res, 23*(12), 2053-2065. doi:10.1101/gr.155028.113

Terry, R. D., Masliah, E., Salmon, D. P., Butters, N., DeTeresa, R., Hill, R., . . . Katzman, R. (1991). Physical basis of cognitive alterations in Alzheimer's disease: synapse loss is the major correlate of cognitive impairment. *Ann Neurol, 30*(4), 572-580. doi:10.1002/ana.410300410

Thangavel, R., Sahu, S. K., Van Hoesen, G. W., & Zaheer, A. (2009). Loss of nonphosphorylated neurofilament immunoreactivity in temporal cortical areas in Alzheimer's disease. *Neuroscience, 160*(2), 427-433. doi:10.1016/j.neuroscience.2009.02.037

The, E. P. C. (2012). An integrated encyclopedia of DNA elements in the human genome. *Nature, 489*, 57. doi:10.1038/nature11247

https://www.nature.com/articles/nature11247#supplementary-information

Thinakaran, G., & Koo, E. H. (2008). Amyloid Precursor Protein Trafficking, Processing, and Function. *Journal of Biological Chemistry, 283*(44), 29615-29619. doi:10.1074/jbc.R800019200

Thoma, F., & Koller, T. (1977). Influence of histone H1 on chromatin structure. *Cell, 12*(1), 101-107.

Tohgi, H., Utsugisawa, K., Nagane, Y., Yoshimura, M., Ukitsu, M., & Genda, Y. (1999). The methylation status of cytosines in a tau gene promoter region alters with age to downregulate transcriptional activity in human cerebral cortex. *Neurosci Lett, 275*(2), 89-92.

Tokuda, T., Calero, M., Matsubara, E., Vidal, R., Kumar, A., Permanne, B., . . . Ghiso, J. (2000). Lipidation of apolipoprotein E influences its isoform-specific interaction with Alzheimer's amyloid beta peptides. *Biochemical Journal, 348*(Pt 2), 359-365.

Tolias, K. F., Duman, J. G., & Um, K. (2011). Control of synapse development and plasticity by Rho GTPase regulatory proteins. *Prog Neurobiol, 94*(2), 133-148. doi:https://doi.org/10.1016/j.pneurobio.2011.04.011

Tollervey, J. R., Wang, Z., Hortobágyi, T., Witten, J. T., Zarnack, K., Kayikci, M., . . . Ule, J. (2011). Analysis of alternative splicing associated with aging and neurodegeneration in the human brain. *Genome Res, 21*(10), 1572-1582. doi:10.1101/gr.122226.111

Toth, M. L., Melentijevic, I., Shah, L., Bhatia, A., Lu, K., Talwar, A., . . . Driscoll, M. (2012). Neurite Sprouting and Synapse Deterioration in the Aging Caenorhabditis elegans Nervous System. *The Journal of Neuroscience, 32*(26), 8778. doi:10.1523/JNEUROSCI.1494-11.2012

Trachtenberg, J. T., Chen, B. E., Knott, G. W., Feng, G., Sanes, J. R., Welker, E., & Svoboda, K. (2002). Long-term in vivo imaging of experience-dependent synaptic plasticity in adult cortex. *Nature, 420*, 788. doi:10.1038/nature01273

https://www.nature.com/articles/nature01273#supplementary-information

Trinchese, F., Liu, S., Battaglia, F., Walter, S., Mathews, P. M., & Arancio, O. (2004). Progressive age-related development of Alzheimer-like pathology in APP/PS1 mice. *Ann Neurol, 55*(6), 801-814. doi:10.1002/ana.20101

Turrigiano, G. (2011). Too Many Cooks? Intrinsic and Synaptic Homeostatic Mechanisms in Cortical Circuit Refinement. *Annu Rev Neurosci, 34*(1), 89-103. doi:10.1146/annurev-neuro-060909-153238

Uddin, M. S., Stachowiak, A., Mamun, A. A., Tzvetkov, N. T., Takeda, S., Atanasov, A. G., . . . Stankiewicz, A. M. (2018). Autophagy and Alzheimer's Disease: From Molecular Mechanisms to Therapeutic Implications. *Frontiers in aging neuroscience, 10*, 04-04. doi:10.3389/fnagi.2018.00004

Unger, M. S., Marschallinger, J., Kaindl, J., Höfling, C., Rossner, S., Heneka, M. T., . . . Aigner, L. (2016). Early Changes in Hippocampal Neurogenesis in Transgenic Mouse Models for Alzheimer's Disease. *Molecular neurobiology, 53*(8), 5796-5806. doi:10.1007/s12035-016-0018-9

Van Dam, D., D'Hooge, R., Staufenbiel, M., Van Ginneken, C., Van Meir, F., & De Deyn, P. P. (2003). Age-dependent cognitive decline in the APP23 model precedes amyloid deposition. *European Journal of Neuroscience, 17*(2), 388-396. doi:10.1046/j.1460-9568.2003.02444.x

van Duijn, C. M., de Knijff, P., Cruts, M., Wehnert, A., Havekes, L. M., Hofman, A., & Broeckhoven, C. V. (1994). Apolipoprotein E4 allele in a population–based study of early–onset Alzheimer's disease. *Nat Genet, 7*, 74. doi:10.1038/ng0594-74

van Galen, P., Viny, A. D., Ram, O., Ryan, R. J. H., Cotton, M. J., Donohue, L., . . . Bernstein, B. E. (2015). A Multiplexed System for Quantitative Comparisons of Chromatin Landscapes. *Mol Cell, 61*(1), 170-180. doi:10.1016/j.molcel.2015.11.003

Vassar, R., Bennett, B. D., Babu-Khan, S., Kahn, S., Mendiaz, E. A., Denis, P., . . . Citron, M. (1999). β-Secretase Cleavage of Alzheimer's Amyloid Precursor Protein by the Transmembrane Aspartic Protease BACE. *Science, 286*(5440), 735-741. doi:10.1126/science.286.5440.735

Vecsey, C. G., Hawk, J. D., Lattal, K. M., Stein, J. M., Fabian, S. A., Attner, M. A., . . . Wood, M. A. (2007). Histone Deacetylase Inhibitors Enhance Memory and Synaptic Plasticity via CREB: CBP-Dependent Transcriptional Activation. *The Journal of Neuroscience, 27*(23), 6128-6140. doi:10.1523/jneurosci.0296-07.2007

Veiga-Fernandes, H., & Artis, D. (2018). Neuronal–immune system cross-talk in homeostasis. *Science, 359*(6383), 1465. doi:10.1126/science.aap9598

Viana, J., Hannon, E., Dempster, E., Pidsley, R., Macdonald, R., Knox, O., . . . Turecki, G. (2016). Schizophrenia-associated methylomic variation: molecular signatures of disease and polygenic risk burden across multiple brain regions. *Human molecular genetics, 26*(1), 210-225.

Vickers, J. C., Chin, D., Edwards, A. M., Sampson, V., Harper, C., & Morrison, J. (1996). Dystrophic neurite formation associated with age-related beta amyloid deposition in the neocortex: clues to the genesis of neurofibrillary pathology. *Exp Neurol, 141*(1), 1-11. doi:10.1006/exnr.1996.0133

Vickers, J. C., Kirkcaldie, M. T., Phipps, A., & King, A. E. (2016). Alterations in neurofilaments and the transformation of the cytoskeleton in axons may provide insight into the aberrant neuronal changes of Alzheimer's disease. *Brain Res Bull, 126*(Pt 3), 324-333. doi:10.1016/j.brainresbull.2016.07.012

Vickers, J. C., Riederer, B. M., Marugg, R. A., Buee-Scherrer, V., Buee, L., Delacourte, A., & Morrison, J. H. (1994). Alterations in neurofilament protein immunoreactivity in human hippocampal neurons related to normal aging and Alzheimer's disease. *Neuroscience, 62*(1), 1-13.

Vickers, J. C., Tan, A., & Dickson, T. C. (2003). Direct determination of the proportion of intra- and extra-cellular neocortical neurofibrillary tangles in Alzheimer's disease. *Brain Research, 971*(1), 135-137. doi:http://dx.doi.org/10.1016/S0006-8993(03)02429-6

Waddington, C. H. (1942a). CANALIZATION OF DEVELOPMENT AND THE INHERITANCE OF ACQUIRED CHARACTERS. *Nature, 150*, 563. doi:10.1038/150563a0

Waddington, C. H. (1942b). The Epigenotype. *Endeavour, 1*, 18-20.

Wagner, M., Steinbacher, J., Kraus, T. F. J., Michalakis, S., Hackner, B., Pfaffeneder, T., . . . Carell, T. (2015). Age-Dependent Levels of 5-Methyl-, 5-Hydroxymethyl-, and 5-Formylcytosine in Human and Mouse Brain Tissues. *Angewandte Chemie International Edition, 54*(42), 12511-12514. doi:10.1002/anie.201502722

Walker, M., LaFerla, F., Oddo, S., & Brewer, G. (2013). Reversible epigenetic histone modifications and Bdnf expression in neurons with aging and from a mouse model of Alzheimer's disease. *AGE, 35*(3), 519-531. doi:10.1007/s11357-011-9375-5

Walsh, D. M., Klyubin, I., Fadeeva, J. V., Cullen, W. K., Anwyl, R., Wolfe, M. S., . . . Selkoe, D. J. (2002). Naturally secreted oligomers of amyloid β protein potently inhibit hippocampal long-term potentiation in vivo. *Nature, 416*, 535. doi:10.1038/416535a

Wang, C., JeBailey, L., & Ridgway, N. D. (2002). Oxysterol-binding-protein (OSBP)-related protein 4 binds 25-hydroxycholesterol and interacts with vimentin intermediate filaments. *Biochem J, 361*(Pt 3), 461-472.

Wang, H. W., Pasternak, J. F., Kuo, H., Ristic, H., Lambert, M. P., Chromy, B., . . . Trommer, B. L. (2002). Soluble oligomers of beta amyloid (1-42) inhibit long-term potentiation but not long-term depression in rat dentate gyrus. *Brain Res, 924*(2), 133-140.

Wang, H. X., Wahlin, Å., Basun, H., Fastbom, J., Winblad, B., & Fratiglioni, L. (2001). Vitamin B₁₂ and folate in relation to the development of Alzheimer's disease. *Neurology, 56*(9), 1188.

Wang, S.-C., Oelze, B., & Schumacher, A. (2008). Age-Specific Epigenetic Drift in Late-Onset Alzheimer's Disease. *PLoS One, 3*(7), e2698. doi:10.1371/journal.pone.0002698

Wang, X., & Michaelis, E. K. (2010). Selective neuronal vulnerability to oxidative stress in the brain. *Frontiers in aging neuroscience, 2*, 12-12. doi:10.3389/fnagi.2010.00012

Wang, X., Pal, R., Chen, X. W., Limpeanchob, N., Kumar, K. N., & Michaelis, E. K. (2005). High intrinsic oxidative stress may underlie selective vulnerability of the hippocampal CA1 region. *Brain Res Mol Brain Res, 140*(1-2), 120-126. doi:10.1016/j.molbrainres.2005.07.018

Wang, Z., Zang, C., Cui, K., Schones, D. E., Barski, A., Peng, W., & Zhao, K. (2009). Genome-wide mapping of HATs and HDACs reveals distinct functions in active and inactive genes. *Cell, 138*(5), 1019-1031. doi:10.1016/j.cell.2009.06.049

Wang, Z., Zang, C., Rosenfeld, J. A., Schones, D. E., Barski, A., Cuddapah, S., . . . Zhao, K. (2008). Combinatorial patterns of histone acetylations and methylations in the human genome. *Nat Genet, 40*(7), 897-903. doi:10.1038/ng.154

Ward, D. D., Andel, R., Saunders, N. L., Thow, M. E., Klekociuk, S. Z., Bindoff, A. D., & Vickers, J. C. (2017). The BDNF Val66Met polymorphism moderates the effect of cognitive reserve on 36-month cognitive change in healthy older adults. *Alzheimer's & Dementia : Translational Research & Clinical Interventions, 3*(3), 323-331. doi:10.1016/j.trci.2017.04.006

Waterston, R. H., Lindblad-Toh, K., Birney, E., Rogers, J., Abril, J. F., Agarwal, P., . . . Lander, E. S. (2002). Initial sequencing and comparative analysis of the mouse genome. *Nature, 420*(6915), 520-562. doi:10.1038/nature01262

Watson, C. T., Roussos, P., Garg, P., Ho, D. J., Azam, N., Katsel, P. L., . . . Sharp, A. J. (2016). Genome-wide DNA methylation profiling in the superior temporal gyrus reveals epigenetic signatures associated with Alzheimer's disease. *Genome Med, 8*(1), 5. doi:10.1186/s13073-015-0258-8

Watt, F., & Molloy, P. L. (1988). Cytosine methylation prevents binding to DNA of a HeLa cell transcription factor required for optimal expression of the adenovirus major late promoter. *Genes Dev, 2*(9), 1136-1143.
Weingarten, M. D., Lockwood, A. H., Hwo, S. Y., & Kirschner, M. W. (1975). A protein factor essential for microtubule assembly. *Proc Natl Acad Sci U S A, 72*(5), 1858-1862.
West, R., Lee, J., & Maroun, L. (1995). Hypomethylation of the amyloid precursor protein gene in the brain of an alzheimer's disease patient. *Journal of Molecular Neuroscience, 6*(2), 141-146. doi:10.1007/BF02736773
Wezyk, M., & Zekanowski, C. (2018). Role of BRCA1 in Neuronal Death in Alzheimer's Disease. *ACS Chem Neurosci, 9*(5), 870-872. doi:10.1021/acschemneuro.8b00149
Whitehouse, I., Flaus, A., Cairns, B. R., White, M. F., Workman, J. L., & Owen-Hughes, T. (1999). Nucleosome mobilization catalysed by the yeast SWI/SNF complex. *Nature, 400*, 784. doi:10.1038/23506
Whyte, Warren A., Orlando, David A., Hnisz, D., Abraham, Brian J., Lin, Charles Y., Kagey, Michael H., . . . Young, Richard A. (2013). Master Transcription Factors and Mediator Establish Super-Enhancers at Key Cell Identity Genes. *Cell, 153*(2), 307-319. doi:10.1016/j.cell.2013.03.035
Widagdo, J., Zhao, Q.-Y., Kempen, M.-J., Tan, M. C., Ratnu, V. S., Wei, W., . . . Bredy, T. W. (2016). Experience-Dependent Accumulation of N⁶-Methyladenosine in the Prefrontal Cortex Is Associated with Memory Processes in Mice. *The Journal of Neuroscience, 36*(25), 6771-6777. doi:10.1523/jneurosci.4053-15.2016
Woodhouse, A., Vickers, J. C., Adlard, P. A., & Dickson, T. C. (2009). Dystrophic neurites in TgCRND8 and Tg2576 mice mimic human pathological brain aging. *Neurobiol Aging, 30*(6), 864-874. doi:10.1016/j.neurobiolaging.2007.09.003
Woodhouse, A., Vickers, J. C., Adlard, P. A., & Dickson, T. C. (2009). Dystrophic neurites in TgCRND8 and Tg2576 mice mimic human pathological brain aging. *Neurobiol Aging, 30*(6), 864-874. doi:http://dx.doi.org/10.1016/j.neurobiolaging.2007.09.003
Wysocka, J., Swigut, T., Xiao, H., Milne, T. A., Kwon, S. Y., Landry, J., . . . Allis, C. D. (2006). A PHD finger of NURF couples histone H3 lysine 4 trimethylation with chromatin remodelling. *Nature, 442*, 86. doi:10.1038/nature04815

https://www.nature.com/articles/nature04815#supplementary-information
Wyss-Coray, T. (2006). Inflammation in Alzheimer disease: driving force, bystander or beneficial response? *Nature medicine, 12*, 1005. doi:10.1038/nm1484
Wyss-Coray, T., Loike, J. D., Brionne, T. C., Lu, E., Anankov, R., Yan, F., . . . Husemann, J. (2003). Adult mouse astrocytes degrade amyloid-beta in vitro and in situ. *Nat Med, 9*(4), 453-457. doi:10.1038/nm838
Xu, T., Yu, X., Perlik, A. J., Tobin, W. F., Zweig, J. A., Tennant, K., . . . Zuo, Y. (2009). Rapid formation and selective stabilization of synapses for enduring motor memories. *Nature, 462*, 915. doi:10.1038/nature08389

https://www.nature.com/articles/nature08389#supplementary-information
Xu, W. L., Atti, A. R., Gatz, M., Pedersen, N. L., Johansson, B., & Fratiglioni, L. (2011). Midlife overweight and obesity increase late-life dementia risk: a population-based twin study. *Neurology, 76*(18), 1568-1574. doi:10.1212/WNL.0b013e3182190d09
Yanagisawa, M., Nakashima, K., Arakawa, H., Ikenaka, K., Yoshida, K., Kishimoto, T., . . . Taga, T. (2000). Astrocyte differentiation of fetal neuroepithelial cells by interleukin-11 via activation of a common cytokine signal transducer, gp130, and a transcription factor, STAT3. *J Neurochem, 74*(4), 1498-1504.

Yankner, B. A. (2000). A century of cognitive decline. *Nature, 404*, 125. doi:10.1038/35004673

Yaron, A., & Schuldiner, O. (2016). Common and Divergent Mechanisms in Developmental Neuronal Remodeling and Dying Back Neurodegeneration. *Curr Biol, 26*(13), R628-R639. doi:10.1016/j.cub.2016.05.025

Yoshiyama, Y., Higuchi, M., Zhang, B., Huang, S. M., Iwata, N., Saido, T. C., . . . Lee, V. M. (2007). Synapse loss and microglial activation precede tangles in a P301S tauopathy mouse model. *Neuron, 53*(3), 337-351. doi:10.1016/j.neuron.2007.01.010

Yoshizawa, M., Sone, M., Matsuo, N., Nagase, T., Ohara, O., Nabeshima, Y.-i., & Hoshino, M. (2003). Dynamic and coordinated expression profile of dbl-family guanine nucleotide exchange factors in the developing mouse brain. *Gene Expression Patterns, 3*(3), 375-381. doi:https://doi.org/10.1016/S1567-133X(03)00002-4

Young, M. D., Willson, T. A., Wakefield, M. J., Trounson, E., Hilton, D. J., Blewitt, M. E., . . . Majewski, I. J. (2011). ChIP-seq analysis reveals distinct H3K27me3 profiles that correlate with transcriptional activity. *Nucleic Acids Res, 39*(17), 7415-7427. doi:10.1093/nar/gkr416

Yu, M., Hon, G. C., Szulwach, K. E., Song, C. X., Zhang, L., Kim, A., . . . He, C. (2012). Base-resolution analysis of 5-hydroxymethylcytosine in the mammalian genome. *Cell, 149*(6), 1368-1380. doi:10.1016/j.cell.2012.04.027

Zamanian, J. L., Xu, L., Foo, L. C., Nouri, N., Zhou, L., Giffard, R. G., & Barres, B. A. (2012). Genomic Analysis of Reactive Astrogliosis. *J Neurosci, 32*(18), 6391-6410. doi:10.1523/JNEUROSCI.6221-11.2012

Zecevic, N., Bourgeois, J.-P., & Rakic, P. (1989). Changes in synaptic density in motor cortex of rhesus monkey during fetal and postnatal life. *Developmental Brain Research, 50*(1), 11-32. doi:https://doi.org/10.1016/0165-3806(89)90124-7

Zeisel, A., Muñoz-Manchado, A. B., Codeluppi, S., Lönnerberg, P., La Manno, G., Juréus, A., . . . Linnarsson, S. (2015). Cell types in the mouse cortex and hippocampus revealed by single-cell RNA-seq. *Science, 347*(6226), 1138-1142. doi:10.1126/science.aaa1934

Zentner, G. E., & Henikoff, S. (2013). Regulation of nucleosome dynamics by histone modifications. *Nature Structural &Amp; Molecular Biology, 20*, 259. doi:10.1038/nsmb.2470

Zhang, B., Carroll, J., Trojanowski, J. Q., Yao, Y., Iba, M., Potuzak, J. S., . . . Brunden, K. R. (2012). The Microtubule-Stabilizing Agent, Epothilone D, Reduces Axonal Dysfunction, Neurotoxicity, Cognitive Deficits, and Alzheimer-Like Pathology in an Interventional Study with Aged Tau Transgenic Mice. *The Journal of Neuroscience, 32*(11), 3601.

Zhang, Y., Iratni, R., Erdjument-Bromage, H., Tempst, P., & Reinberg, D. (1997). Histone Deacetylases and SAP18, a Novel Polypeptide, Are Components of a Human Sin3 Complex. *Cell, 89*(3), 357-364. doi:https://doi.org/10.1016/S0092-8674(00)80216-0

Zhang, Y., Li, P., Feng, J., & Wu, M. (2016). Dysfunction of NMDA receptors in Alzheimer's disease. *Neurological sciences : official journal of the Italian Neurological Society and of the Italian Society of Clinical Neurophysiology, 37*(7), 1039-1047. doi:10.1007/s10072-016-2546-5

Zhang, Y., Liu, T., Meyer, C. A., Eeckhoute, J., Johnson, D. S., Bernstein, B. E., . . . Liu, X. S. (2008). Model-based Analysis of ChIP-Seq (MACS). *Genome Biol, 9*(9), R137-R137. doi:10.1186/gb-2008-9-9-r137

Zhao, J., Zhu, Y., Yang, J., Li, L., Wu, H., De Jager, P. L., . . . Bennett, D. A. (2017). A genome-wide profiling of brain DNA hydroxymethylation in Alzheimer's disease. *Alzheimers Dement, 13*(6), 674-688. doi:10.1016/j.jalz.2016.10.004

Zhao, Q., Zhang, J., Chen, R., Wang, L., Li, B., Cheng, H., . . . Wong, J. (2016). Dissecting the precise role of H3K9 methylation in crosstalk with DNA maintenance methylation in mammals. *Nature Communications, 7*, 12464. doi:10.1038/ncomms12464

https://www.nature.com/articles/ncomms12464#supplementary-information

Zhou, Y., & Grummt, I. (2005). The PHD finger/bromodomain of NoRC interacts with acetylated histone H4K16 and is sufficient for rDNA silencing. *Curr Biol, 15*(15), 1434-1438. doi:10.1016/j.cub.2005.06.057

Ziller, M. J., Gu, H., Müller, F., Donaghey, J., Tsai, L. T.-Y., Kohlbacher, O., . . . Bernstein, B. E. (2013). Charting a dynamic DNA methylation landscape of the human genome. *Nature, 500*(7463), 477-481.

Ziller, M. J., Gu, H., Muller, F., Donaghey, J., Tsai, L. T., Kohlbacher, O., . . . Meissner, A. (2013). Charting a dynamic DNA methylation landscape of the human genome. *Nature, 500*(7463), 477-481. doi:10.1038/nature12433

Appendix 1

General solutions

Stock solutions

90.0g sodium chloride (NaCl) (BDH, USA) was dissolved in 1L milliQ water

28.0g di-sodium hydrogen orthophosphate (Na2HPO) (BDH, USA) was dissolved in 1L milliQ water

31.2g sodium di-hydrogen orthophosphate (NaH2PO4.2H2O) (Ajax, Australia) was dissolved in 1L milliQ water.

Stock solutions were prepared by dissolving reagents in one litre of milliQ water using a magnetic stirrer. All stock solutions were stored at RT.

0.01 M Phosphate buffered saline (PBS):
10mL $NaH_2PO4.2H_2O$ stock solution
40mL Na_2HPO stock solution
100mL NaCl stock solution
850mL milliQ water
0.01M PBS solution was mixed briefly then stored at RT.

For molecular and flow cytometry-based experiments, fresh 0.01M PBS was sterilised with 0.22um filters and stored at 4°C.

Immunohistochemistry solutions

PBS-X

600µL Triton-X-100 (0.3%) (Sigma-Aldrich, Missouri, USA) was dissolved in 199.4mL 0.01M PBS.

Solutions were dissolved together with a magnetic stirrer then stored at 4°C.

0.01M Citrate Buffer

2.94g trisodium citrate (Sigma-Aldrich, Missouri, USA) was dissolved in 800mL MilliQ® water

Solutions were dissolved and adjusted to pH 6 with 0.1M citric acid, then made up to 1L with MilliQ® water.

18.0% Sucrose Solution

180g sucrose (Sigma-Aldrich, Missouri, USA) was dissolved in 1L 0.01M PBS-0.01% Sodium azide (Sigma)

18% sucrose solution was stored at 4°C.

30.0% Sucrose Solution

300g sucrose (Sigma-Aldrich, Missouri, USA) was dissolved in 1L 0.01M PBS with 0.01% Sodium azide (Sigma-Aldrich, Missouri, USA)

30% sucrose solution was stored at 4°C.

Tissue Storage Solution

0.1% sodium azide (Sigma-Aldrich, Missouri, USA)

500mL 0.01M PBS

0.5g sodium azide was dissolved in 500mL 0.01M PBS

Tissue storage solution was stored at 4°C

4% paraformaldehyde (PFA)

40g granulated paraformaldehyde (PFA)

500mL MilliQ® water

400mL 28.0g/L Na_2HPO

100mL 31.2g/L $NaH_2PO_4.2H_2O$

1.0M NaOH & 1.0M HCl to pH

MilliQ water was heated to 80°C, then granulated PFA was added with 5 drops of NaOH with heat until dissolved. $NaH_2PO_4.H_2O$ and Na_2HPO was added then filtered and pH to 7.4. Stored at -20°C

Nuclei extraction solutions

All stock solutions are kept at 4°C unless otherwise stated.

Stock solutions

1M glycine 25mL

1.8765g glycine (Sigma-Aldrich, Missouri, USA) was dissolved in 25mL MilliQ water.

0.5M EDTA pH8 10mL

1.461g EDTA (Sigma-Aldrich, Missouri, USA) was dissolved in 8mL MilliQ water, then pH adjusted to 8.0 with sodium hydroxide then made up to 10mL with MilliQ water.

100mM Mg(Ac).4H2O 10mL

0.2145g $Mg(Ac).{}_4H_2O$ (Sigma-Aldrich, Missouri, USA) was dissolved in 10mL MilliQ water.

1M Tris-HCl pH8 10mL

1.576g Tris HCl (Sigma-Aldrich, Missouri, USA) was dissolved in 8mL MilliQ water, then pH adjusted to 8.0 with sodium hydroxide and made to 10mL with MilliQ water.

100mM PMSF 10mL

0.1742g PMSF (Sigma-Aldrich, Missouri, USA) was dissolved in 10mL 2-Propanol, then aliquoted into 100µL and frozen at -80°C.

10% Triton-X100

1000µL Triton-X100 (Sigma-Aldrich, Missouri, USA) was dissolved in 10mL MilliQ water.

1M CaCl2 10mL

1.1098g $CaCl_2$ (Sigma-Aldrich, Missouri, USA) was dissolved in 10mL MilliQ water.

Nuclei Extraction Buffer (NEB):

Nuclei extraction buffer was made fresh for each experiment performed. Approximately 5mL was required per sample, however a minimum 10mL was made up to ensure accuracy of measurements.

Appendix table 1: Nuclei extraction buffer solution

Total	**10mL volume**	**Final conc**
Sucrose	1.095g	0.32M
1M CaCl	50uL	5mM
100mM Mg(Ac).4H2O	300uL	3mM
0.5M EDTA pH8	2uL	0.1mM
1M Tris-HCl pH8	100uL	10mM
Roche mini protease inhibitor	1 tablet per 10mL	
100mM PMSF	10uL	0.1mM
Trion-X100 (if Immunostaining)	100uL	0.10%
MilliQ	make up to 10mL	

Chromatin Immunoprecipitation buffers

Stock solutions were made up and stored at room temperature apart from Low Salt, High Salt LiCl and TE buffers.

Appendix table 2: Chromatin immunoprecipitation buffers

Stock Solutions	**Final Concentration**						
	IP dilution	*Low Salt*	*High Salt*	*LiCl*	*TE*	*SDS Lysis Buffer*	*Elution Buffer*
0.5M EDTA, pH8.0	1.2mM	2mM	2mM	1mM	1mM	10mM	-
10% SDS	0.01%	0.1%	0.1%	-	-	1%	1%
10% Triton-X-100	1%	1%	1%	-	-	-	-
1M Tris-HCl pH8.1	16.7mM	20mM	20mM	10mM	10mM	50mM	-
5M NaCl	167mM	150mM	500mM	-	-	-	-
5M LiCl	-	-	-	250mM	-	-	-
10% IgePal	-	-	-	1%	-	-	-
10% Sodium Deoxycholate	-	-	-	1%	-	-	-
1M Sodium bicarbonate[1]	-	-	-	-	-	-	100mM

Stock Solutions	**Volumes for 50mL stocks**						
	IP dilution 50mL	*Low Salt 50mL*	*High Salt 50mL*	*LiCl 50mL*	*TE 50mL*	[1]*SDS lysis buffer 10mL*	[2]*Elution Buffer 3mL*
0.5M EDTA, pH8.0	120µl	200µl	200µl	100µl	100µl	200µl	-
10% SDS	50µl	500µl	500µl	-	-	1000µl	300µl
10% Triton-X-100	5000µl	5000µl	5000µl	-	-	-	-
1M Tris-HCl pH8.1	835µl	1000µl	1000µl	500µl	500µl	500µl	-
5M NaCl	1670µl	1500µl	5000µl	-	-	-	-
5M LiCl	-	-	-	2500µl	-	-	-
10% IgePal	-	-	-	5000µl	-	-	-
10% Sodium deoxycholate	-	-	-	5000µl	-	-	-
1M Sodium bicarbonate[2]	-	-	-		-	-	300µl
dH_2O	41907.5µl	41800µl	38300µl	36900µl	49400µl	8300µl	2400µl

[1]To be made fresh each time

Appendix 2

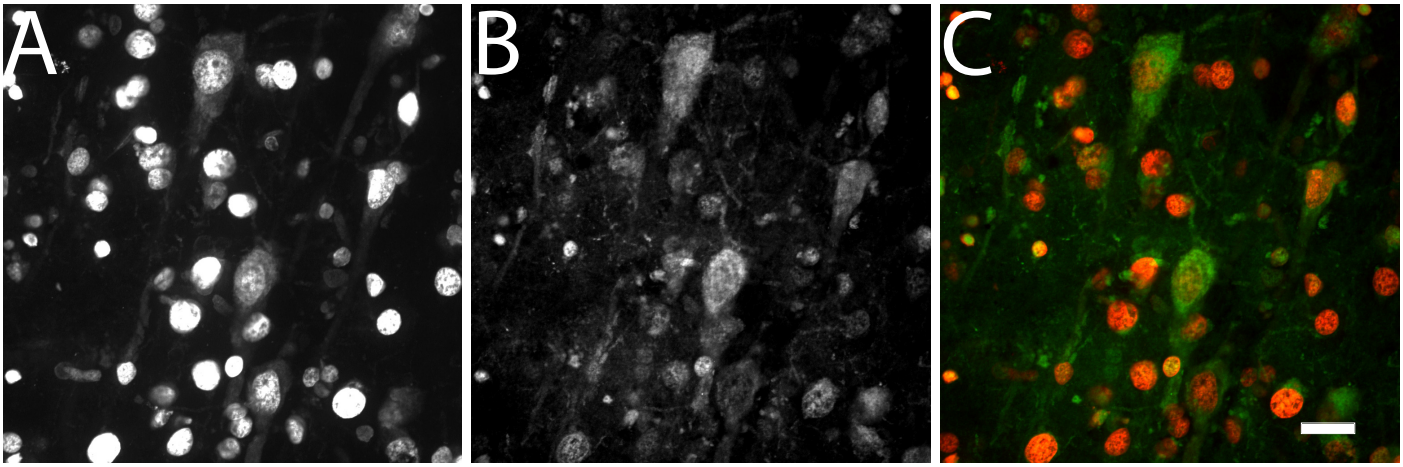
A
B
C

Appendix 2: Supplementary Figure 1: Polyclonal 5hmC antibody versus mouse monoclonal 5hmC antibody labelling

Representative flattened image stacks of rabbit polyclonal 5hmC (A), and mouse monoclonal 5hmC (B), demonstrating analogous extranuclear immunoreactivity (C) in human post-mortem AD tissue. Scale bar: 20μm

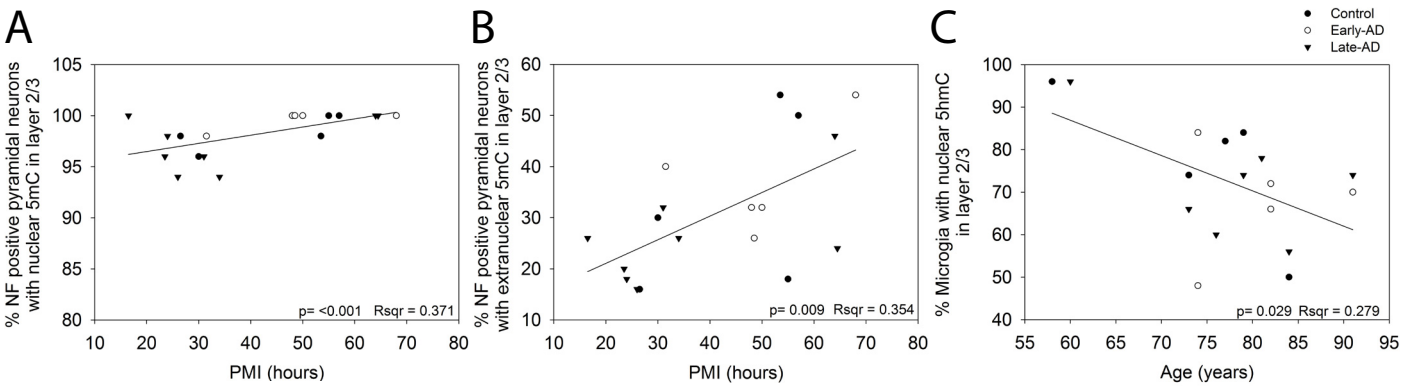
A
% NF positive pyramidal neurons with nuclear 5mC in layer 2/3
105
100
95
90
85
80
10 20 30 40 50 60 70 80
PMI (hours)
p= <0.001 Rsqr = 0.371
B
% NF positive pyramidal neurons with extranuclear 5mC in layer 2/3
60
50
40
30
20
10
10 20 30 40 50 60 70 80
PMI (hours)
p= 0.009 Rsqr = 0.354
C
Control
Early-AD
Late-AD
% Microgia with nuclear 5hmC in layer 2/3
100
90
80
70
60
50
40
55 60 65 70 75 80 85 90 95
Age (years)
p= 0.029 Rsqr = 0.279

Appendix 2: Supplementary Figure 2: Correlations detected between cell-type specific DNA methylation data and PMI or Age

Scatter plot of the percentage NF-positive pyramidal neurons with nuclear 5mC in layer 2/3 versus PMI (A). Scatter plot of the percentage NF-positive pyramidal neurons with extranuclear 5mC in layer 2/3 versus PMI (B). Scatter plot of the percentage microglia with nuclear 5hmC in layer 2/3 versus Age (C). Filled circles represent control cases, open circles represent Early-AD cases, and filled triangles represent Late-AD cases. Lines represent linear regression of plot.

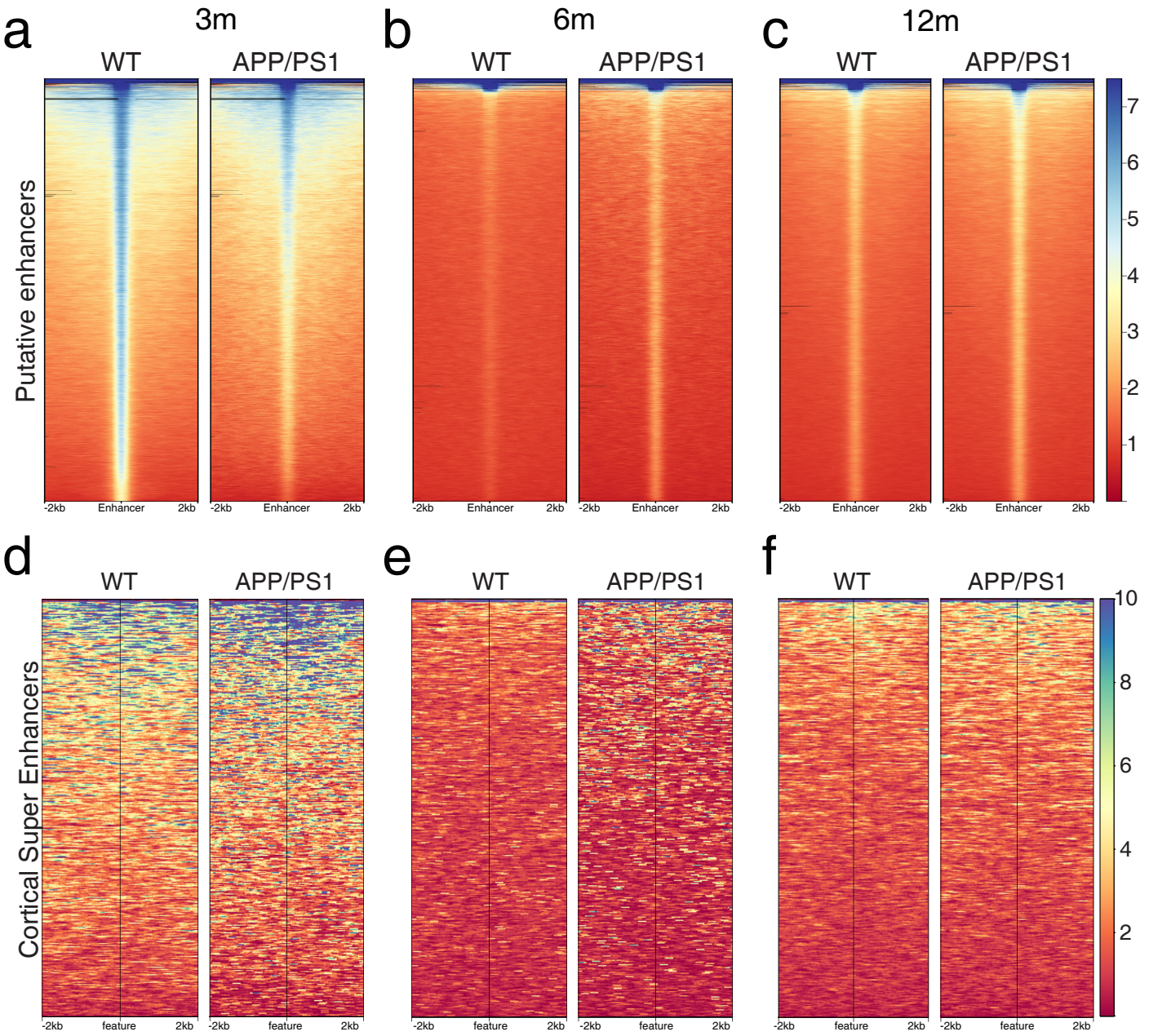
a
3m
WT
APP/PS1
b
6m
WT
APP/PS1
c
12m
WT
APP/PS1
Putative enhancers
-2kb
Enhancer
2kb
7
6
5
4
3
2
1
d
WT
APP/PS1
e
WT
APP/PS1
f
WT
APP/PS1
Cortical Super Enhancers
-2kb
feature
2kb
10
8
6
4
2

Appendix 2: Supplementary Figure 3: Dysregulation of H3K27ac marking at enhancers and super-enhancers in APP/PS1 neurons

(a-c) Heatmaps for H3K27ac signal at enhancers sorted by strongest (blue) to weakest (red) signal in WT (left) and APP/PS1 (right) at (a) 3 months, (b) 6 months and (c) 12 months of age. (d-f) Heatmaps for the Super-Enhancer Database (dbSUPER) track were sorted by strongest (blue) to weakest (red) signal in WT (left) and APP/PS1 (right) mice at (d) 3 months, (e) 6 months and (f) 12 months of age.